Role of innate lymphoid cells in type 1-dominated experimental *Plasmodium berghei* ANKA and type 2-dominated *Litomosoides sigmodontis* infection

Dissertation

zur Erlangung des Doktorgrades (Dr. rer. nat.)
der Mathematisch-Naturwissenschaftlichen Fakultät
der Rheinischen Friedrich-Wilhelms-Universität Bonn

Fach Molekulare Biomedizin

vorgelegt von

Julia Jennifer Reichwald
aus Freilassing in Oberbayern

Bonn, Mai 2021

Angefertigt mit Genehmigung der Mathematisch-Naturwissenschaftlichen Fakultät der Rheinischen Friedrich-Wilhelms-Universität Bonn

Prof. Dr. med. Achim Hörauf

Erster Gutachter

Prof. Dr. rer. nat. Sven Burgdorf

Zweiter Gutachter

Tag der Promotion: 13.10.2021

Erscheinungsjahr: 2021

Diese Arbeit wurde von Februar 2018 bis Mai 2021 am Institut für Medizinische Mikrobiologie, Immunologie und Parasitologie unter der Leitung von Prof. Dr. Achim Hörauf angefertigt.

Ich versichere an Eides statt, dass die vorgelegte Arbeit persönlich, selbstständig und ohne Benutzung anderer als der ausdrücklich angegebenen Hilfsmittel angefertigt wurde. Die aus anderen Quellen direkt oder indirekt übernommenen Daten und Konzepte wurden unter Angabe der Quelle kenntlich gemacht. Ich habe die vorgelegte Arbeit oder ähnliche Arbeiten an keiner anderen Universität als Dissertation eingereicht und habe für die Erstellung der vorgelegten Arbeit keine fremde Hilfe, insbesondere keine entgeltliche Hilfe von Vermittlungs- bzw. Beratungsdiensten (Promotionsberatern/-vermittlern oder anderen Personen) in Anspruch genommen.

Ort, Datum	Julia Reichwald	Unterschrift

Auszüge dieser Arbeit wurden auf verschiedenen Konferenzen als Vortrag oder Poster präsentiert und sind bisher nicht publiziert worden.

Contents

Summary

Parasitic infectious diseases such as malaria and filariasis are still among the biggest health problems in the tropics and subtropics, especially in Africa, and in the case of malaria among the ten most frequent causes of death. They not only represent a health risk for the population, but also have a considerable impact on the socioeconomic status of those affected. The microbes that cause malaria and filariasis, plasmodia and helminths, respectively, trigger completely differently directed immune responses in their host. In the case of a *Plasmodium* infection, this can lead to considerable complications as a result of a strong systemic inflammation and to the clinical picture of cerebral malaria, which is a life-threatening condition that particularly endangers children. Helminths, on the other hand, regulate the immune system of their host in order to achieve an immune tolerance that ensures their survival and limits morbidities in most patients if immune modulation is successful. Recently, a new cell population within the innate immune system has been characterized: innate lymphoid cells (ILCs), whose role is currently being investigated in different infection models. First indications for the involvement of these cells in various infectious diseases were already demonstrated. However, for cerebral malaria and filariasis there are only a few studies that have not yet assessed the influence of these cells on infection. Therefore, the role and function of ILCs in these diseases was investigated. For this purpose, the experimental infection models established in the lab for CM and filariasis in mice with *Plasmodium berghei* ANKA and *Litomosoides sigmodontis* were used.

Establishment of staining procedures for flow cytometry was followed by experiments with *Plasmodium berghei* ANKA (PbA)-infected wild-type (WT) C57BL/6 mice, which develop experimental cerebral malaria (ECM) after infection, and PbA-infected *Ifnar1*$^{-/-}$ mice, which are protected from ECM. These experiments provided evidence for the involvement of ILC1s and NK cells in the immune response to PbA, since these cells increased in numbers during infection, infiltrated the brain and NK cells isolated from the spleens of *Ifnar1*$^{-/-}$ mice were significantly less activated and produced fewer effector molecules (e.g. IFN-γ). This suggested that in *Ifnar1*$^{-/-}$ mice the NK cells might have an influence on the protective mechanism. Therefore, NK cells were depleted in PbA-infected WT and *Ifnar1*$^{-/-}$ mice to analyze ECM development in both mouse strains. The WT mice continued to develop ECM, which precludes a dominant role of NK cells in the development of ECM. Interestingly, the NK cell-depleted *Ifnar1*$^{-/-}$ mice

were still protected and also showed a strong regulatory and type 2 immune response characterized by an increase of eosinophils as well as IL-13 levels in the spleen. The depletion of eosinophils finally led to ECM development in *Ifnar1*$^{-/-}$ mice suggesting an important role of these cells in the protection of *Ifnar1*$^{-/-}$ from PbA-induced ECM. Thus, although a direct role of NK cells and also ILC1s in the protection mechanism could be excluded, those cells are important mediators in the immune response to *Plasmodium berghei* ANKA in general, since they produced both GzmB and IFN-γ, which are known to be involved in ECM development, and infiltrate the brain of ECM-positive mice. NK cells and ILC1s showed a significantly higher GzmB expression than CD8^{+} T cells, suggesting their involvement in mediating ECM.

In addition, experiments were performed with *L. sigmodontis*-infected animals, comparing WT BALB/c mice that develop a chronic infection and WT C57BL/6 mice that eliminate the infection right after moulting of L4 to the adult worm. Kinetics were performed to analyze the occurrence of ILC populations during the course of infection in both strains. A significantly higher number of ILC2s in the pleural cavity in infected C57BL/6 mice was found compared to BALB/c animals and a strong type 2 immune response was observed with very high IL-5 levels in infected WT C57BL/6 mice. ILC2s were the main producers of IL-5 and had a higher IL-5 expression compared to CD4^{+} T cells. In the absence of T cells (*Rag2*$^{-/-}$ mice), ILC2s remained one of the dominant sources of IL-5, together with eosinophils. Depletion of ILC2s in T and B cell-deficient and susceptible *Rag2*$^{-/-}$ mice did not lead to a further increase in adult worm burden, suggesting that ILC2s are not essential for the elimination of adult *L. sigmodontis* in C57BL/6 mice. However, an enhanced microfilarial load was observed in ILC2-depleted *Rag2*$^{-/-}$ mice compared to isotype controls accompanied by a strong type 1 inflammatory immune response in *Rag2*$^{-/-}$ mice in general. Thus, ILC2s do not have a decisive impact on the adult worm burden at least on day 63 but do control the microfilarial load in the absence of T and B cells in C57BL/6 mice.

In summary, the project makes a decisive contribution to the detailed characterization of ILCs in the immune response to parasitic infections. By using two immunologically completely different models, it was shown that depending on the model, different ILC populations were in focus. Furthermore, the data underline the heterogeneity of ILCs subsets and contribute, despite their small proportion among all immune cells, to protective immune responses.

Zusammenfassung

Parasitäre Infektionskrankheiten wie Malaria und Filariose gehören nach wie vor zu den größten Gesundheitsproblemen in den Tropen und Subtropen, vor allem in Afrika, und im Fall von Malaria zu den zehn häufigsten Todesursachen. Sie stellen nicht nur ein Gesundheitsrisiko für die Bevölkerung dar, sondern haben auch einen erheblichen Einfluss auf den sozioökonomischen Status der Betroffenen. Die für die Erkrankungen verantwortlichen Parasiten - Plasmodien und Helminthen - lösen in ihrem Wirt völlig unterschiedlich gerichtete Immunantworten aus. Im Falle einer Plasmodien-Infektion kann dies zu erheblichen Komplikationen durch eine starke systemische Entzündung und zum Krankheitsbild der zerebralen Malaria führen, einer lebensbedrohlichen Erkrankung, die besonders Kinder gefährdet. Helminthen hingegen regulieren das Immunsystem ihres Wirts, um eine Immuntoleranz zu erreichen, die ihr Überleben sichert und bei erfolgreicher Immunmodulation bei den meisten Patienten keine Symptome verursacht. Kürzlich wurde eine neue Zellpopulation innerhalb des angeborenen Immunsystems charakterisiert: die angeborenen lymphoiden Zellen (ILCs), deren Rolle derzeit in verschiedenen Infektionsmodellen untersucht wird. Erste Hinweise auf eine Beteiligung dieser Zellen an verschiedenen Infektionskrankheiten konnten bereits gefunden werden. Für die zerebrale Malaria und die Filariose gibt es jedoch nur wenige Studien und in diesen wurde der Einfluss dieser Zellen auf die Infektion noch nicht untersucht. Daher wurde in dieser Dissertation die Rolle und Funktion von ILCs in beiden Erkrankungen analysiert. Dazu wurden die etablierten Mausmodelle *Plasmodium berghei* ANKA und *Litomosoides sigmodontis* verwendet.

Nach der Etablierung durchflusszytometrischer Färbungen folgten Experimente mit *Plasmodium berghei* ANKA (PbA)-infizierten Wildtyp (WT) C57BL/6-Mäusen, die nach der Infektion experimentelle zerebrale Malaria (ECM) entwickeln, und PbA-infizierten *Ifnar1*$^{-/-}$ Mäusen, die vor ECM geschützt sind. Diese Experimente lieferten Hinweise für die Beteiligung von ILC1s und NK Zellen an der Immunantwort auf PbA, da diese Zellen während der Infektion vermehrt das Gehirn infiltrierten und NK-Zellen, die aus der Milz von *Ifnar1*$^{-/-}$ Mäusen isoliert wurden, signifikant weniger aktiviert waren und weniger Effektormoleküle (z.B. IFN-γ) produzierten. Dies legte nahe, dass die NK-Zellen in *Ifnar1*$^{-/-}$ Mäusen einen Einfluss auf den Schutzmechanismus haben könnten. Daher wurden NK-Zellen in PbA-infizierten WT- und *Ifnar1*$^{-/-}$ Mäusen depletiert, um die ECM-Entwicklung in beiden Mausstämmen zu analysieren. Die WT Mäuse

entwickelten weiterhin ECM, was eine dominante Rolle der NK-Zellen bei der Entwicklung der ECM ausschließt. Interessanterweise waren die NK-Zell-depletierten *Ifnar1*$^{-/-}$ Mäuse immer noch geschützt und zeigten auch eine starke regulatorische und Typ-2-Immunantwort, die durch einen Anstieg der Eosinophilen sowie der IL-13-Level in der Milz gekennzeichnet war. Die Depletion der Eosinophilen führte schließlich zur ECM-Entwicklung in *Ifnar1*$^{-/-}$ Mäusen, was auf eine wichtige Rolle dieser Zellen beim Schutz von *Ifnar1*$^{-/-}$ Mäusen vor PbA-induzierter ECM hinweist. Obwohl also eine direkte Rolle von NK-Zellen und auch ILC1s in dem Schutzmechanismus ausgeschlossen werden konnte, sind diese Zellen wichtige Mediatoren in der Immunantwort auf *Plasmodium berghei* ANKA im Allgemeinen, da sie sowohl GzmB als auch IFN-γ produzierten und das Gehirn von ECM-positiven Mäusen infiltrierten. NK-Zellen und ILC1s zeigten eine signifikant höhere GzmB-Expression als CD8^{+} T-Zellen, was auf ihre Beteiligung an der Vermittlung von ECM hindeutet.

Zusätzlich wurden Experimente mit *L. sigmodontis*-infizierten Tieren durchgeführt, wobei WT BALB/c-Mäuse, die eine chronische Infektion entwickeln, und WT C57BL/6-Mäuse, die die Infektion direkt nach der Häutung von L4 zum adulten Wurm eliminieren, verglichen wurden. Es wurden kinetische Untersuchungen durchgeführt, um das Auftreten von ILC-Populationen im Verlauf der Infektion in beiden Mausstämmen zu analysieren. In diesen Experimenten wurde eine signifikant höhere Anzahl von ILC2s in der Pleurahöhle in infizierten C57BL/6-Mäusen im Vergleich zu BALB/c-Tieren festgestellt und eine starke Typ-2-Immunantwort mit sehr hohen IL-5 Leveln in infizierten WT C57BL/6-Mäusen beobachtet. ILC2s waren die Hauptproduzenten von IL-5 und hatten eine höhere IL-5-Expression im Vergleich zu CD4^{+} T-Zellen. In Abwesenheit von T-Zellen (*Rag2*$^{-/-}$ Mäuse) blieben ILC2s zusammen mit Eosinophilen eine der dominierenden Quellen von IL-5. Die Depletion von ILC2s in T- und B-Zell-defizienten *Rag2*$^{-/-}$ Mäusen führte nicht zu einem weiteren Anstieg der Adultwurmlast, was darauf hindeutet, dass ILC2s für die Eliminierung von adulten *L. sigmodontis* Würmern in C57BL/6-Mäusen nicht essentiell sind. Allerdings wurde in ILC2-depletierten *Rag2*$^{-/-}$ Mäusen im Vergleich zu den Isotyp-Kontrollen eine erhöhte Mikrofilarienlast beobachtet, begleitet von einer starken entzündlichen Typ-1-Immunantwort in *Rag2*$^{-/-}$ Mäusen im Allgemeinen. Somit hat die Depletion von ILC2s zumindest zum Zeitpunkt der Häutung zum Adultwurm keinen entscheidenden Einfluss

auf die spätere adulte Wurmlast, kontrolliert aber die Mikrofilarienlast in Abwesenheit von T- und B-Zellen in C57BL/6-Mäusen.

Zusammenfassend leistet das Projekt einen entscheidenden Beitrag zur detaillierten Charakterisierung der ILCs bei der Immunantwort auf parasitäre Infektionen. Durch die Verwendung zweier immunologisch völlig unterschiedlicher experimenteller Modelle wurde gezeigt, dass je nach Modell unterschiedliche ILC-Populationen im Fokus stehen. Darüber hinaus unterstreichen die Daten die Heterogenität der ILCs-Subsets, die trotz ihres geringen Anteils an allen Immunzellen zur protektiven Immunantwort beitragen.

List of Figures

List of Abbreviations

ACT ..... *Artemisinin-based combination therapy*
APCs ..... *Antigen-presenting cells*
ARDS ..... *Acute respiratory distress syndrome*
BBB ..... *Blood-brain-barrier*
BMDC ..... *Bone marrow-derived cells*
BSA ..... *Bovine serum albumin*
CCL5 ..... *CC-chemokine ligand 5*
CD ..... *Cluster of differentiation*
CILCPs ..... *Common ILC precursor*
CLP ..... *Common lymphoid progenitor*
CM ..... *Cerebral malaria*
CXCR3 ..... *CXC-motif chemokine receptor 3*
DCs ..... *Dendritic cells*
DEC ..... *Diethylcarbamazine citrate*
dpi ..... *Days post infection*
ECM ..... *Experimental cerebral malaria*
EDTA ..... *Ethylenediaminetetraacetic acid*
ELISA ..... *Enzyme linked immunosorbent assay*
EPEC ..... *Enteropathogenic Escherichia coli*
FACS ..... *Fluorescence activated cell sorting*
FBS ..... *Fetal bovine serum*
Fc ..... *Fragment crystallizable*
FMO ..... *Fluorescence minus one*
GMFI ..... *Geometric mean of fluorescence intensity*
GPELF ..... *Global Programme to Eliminate Lymphatic Filariasis*
GPI ..... *Glycophosphatidylinositol*
GzmB ..... *Granzyme B*
hi ..... *Heat inactivated*
i. p. ..... *Intraperitoneally*
i. v. ..... *Intravenously*
ICAM-1 ..... *Intracellular adhesion molecule 1*
IFNAR ..... *Type I Interferon receptor*

IgG ..... *Immunoglobulin G*
IL ..... *Interleukin*
ILC1s ..... *Group 1 innate lymphoid cells*
ILC2s ..... *Group 2 innate lymphoid cells*
ILC3s ..... *Group 3 innate lymphoid cells*
ILCP ..... *ILC precursor*
ILCs ..... *Innate lymphoid cells*
iRBCs ..... *Infected red blood cells*
IRF ..... *IFN-regulatory factor*
LE ..... *Lymphedema*
LF ..... *Lymphatic filariasis*
LPS ..... *Lipopolysaccharide*
LTi ..... *Lymphoid tissue inducer cells*
LTα ..... *Lymphotoxin alpha*
Ly6C ..... *Lymphocyte antigen 6 complex locus C*
MAb ..... *Monoclonal antibody*
MACS ..... *Magnetic cell separation*
MDA ..... *Mass drug administration*
Mf ..... *Microfilariae*
MHC ..... *Major histocompatibility complex*
mLNs ..... *Mesenteric lymph nodes*
NCR ..... *Natural cytotoxicity receptor*
NFκB ..... *Nuclear factor kB*
NK ..... *Natural killer*
NK cells ..... *Natural killer cells*
NTDs ..... *Neglected tropical diseases*
OVA ..... *Ovalbumin*
PAMPs ..... *Pathogen-associated molecular patterns*
PbA ..... *Plasmodium berghei ANKA*
PBS ..... *Phosphate buffered saline*
PfEMP-1 ..... *P. falciparum erythrocyte membrane protein-1*
PMA *Phorbol-12-myristat-13-acetat*
PRRs ..... *Pattern recognition receptors*
Rag1 ..... *Recombination-activating gene 1*

Rag2 ..... *Recombination-activating gene 2*
RBCs ..... *Red blood cells*
RMCBS ..... *Rapid Murine Coma and Behavior Scale*
RORγt ..... *Retinoic-acid-receptor-related orphan nuclear receptor gamma*
RT ..... *Room temperature*
Sca-1 ..... *Stem cells antigen 1*
SN ..... *Supernatant*
spp. ..... *Species pluralis*
T-bet ..... *T-box transcription factor*
TCR ..... *T cell receptor*
Th1 ..... *Type 1 T helper cells*
Th17 ..... *Type 17 T helper cells*
Th2 ..... *Type 2 T helper cells*
TLRs ..... *Toll-like receptors*
TMB ..... *Tetramethylbenzidine*
TNF ..... *Tumor necrosis factor*
TSLP ..... *Thymic stromal lymphopoietin*
VCAM1 ..... *Vascular cell adhesion molecule 1*
WT ..... *Wildtype*

1. Introduction

1.1 Malaria

Malaria is one of the top 10 causes of death in sub-Saharan Africa (World Health Organization 2020b) and is transmitted by a vector, the female *Anopheles* mosquito, which releases *Plasmodium* parasites into the host's bloodstream through its bite (World Health Organization 2020a). Currently, five human pathogenic *Plasmodium* species are known: *P. falciparum*, *P. vivax*, *P. ovale*, *P. malariae*, and *P. knowlesi* (Centers for Disease Control and Prevention 2020a), with *P. falciparum* being responsible for the majority of malaria cases, e. g. for 99.7% of the cases in the African Region in 2018 (World Health Organization 2020a).

In 2019, there were 228 million malaria cases worldwide, including 409,000 deaths (World Health Organization 2019). 94% of these malaria cases occurred in 2019 in the WHO African Region, which therefore carries the highest malaria burden worldwide. The occurrence of malaria depends mainly on climatic conditions, such as temperature, humidity and also rainfall. Therefore, malaria is particularly prevalent in tropical and subtropical areas, where the *Anopheles* mosquito can reproduce and the parasite can complete its life cycle (Centers for Disease Control and Prevention 2020f). Accordingly, an intensive spread can be observed especially in Sub-Saharan Africa (Centers for Disease Control and Prevention 2020f), but also in the Eastern Mediterranean and Western Pacific regions as well as parts of the Americas (World Health Organization 2020a). However, there are also regional differences within the endemic areas, as malaria does not occur at high altitudes, during cold seasons or in desert regions (World Health Organization 2020a).

The WHO aims to reduce the malaria incidence and the mortality rates by at least 90% by 2030 (World Health Organization 2015). Moreover, the aim is to eliminate malaria in 35 countries by 2030. In order to achieve this goal, various options exist that, taken together, should lead to success in this regard. On the one hand, vector control is of central importance to stop the transmission of malaria (World Health Organization 2020a). Insecticide-treated mosquito nets are used for this purpose; in 2019, 46% of all people at risk of malaria in Africa already had such a net. Indoor spraying of insecticides is also used to control the vectors. It is also effective to remove the larvae of the mosquitoes, which are mainly found in small water pools (Centers for Disease

Control and Prevention 2018a). Antimalarial drugs are used as well, especially for travellers but also in Mass Drug Administration (MDA) programs, to prevent infection. Furthermore, early diagnosis and treatment helps to reduce transmission, here the best currently available therapy especially for *P. falciparum* is the artemisinin-based combination therapy (ACT) (World Health Organization 2020a). However, resistance of mosquitoes to insecticides and resistance of parasites to drugs are also increasingly emerging, so new agents need to be found to ensure the effectiveness of interventions in the long term. Last but not least, tracking and recording of all malaria cases is also of great importance to monitor transmission trends and take action based on them.

1.1.1 Life cycle of *Plasmodium* spp.

The life cycle of human pathogenic *Plasmodium* spp. (Fig. 1) requires two hosts: the human, where the asexual part of the cycle occurs, and the female mosquito, where the sporogonic cycle and sexual reproduction occurs (Centers for Disease Control and Prevention 2020a). The cycle is further divided into the exo-erythrocytic and the erythrocytic cycle, which occurs in humans (Fig. 1).

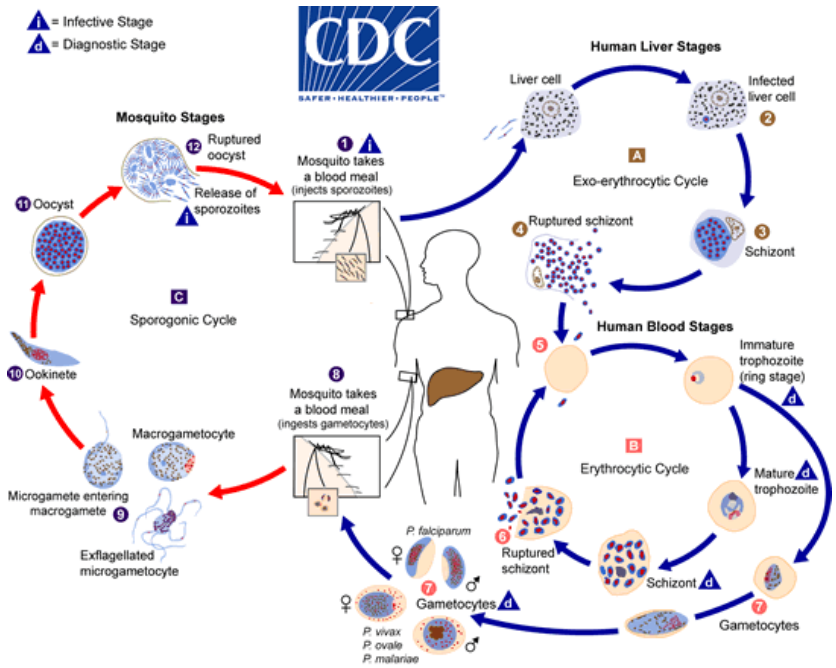

Figure 1: Life cycle of *Plasmodium* spp. (Centers for Disease Control and Prevention 2020a). By taking a blood meal the mosquito transmits sporozoites into the host, where asexual reproduction occurs. The parasites first migrate into the liver cells, where they develop into liver schizonts that burst and release merozoites into the blood stream, which then infect erythrocytes. Here they develop from immature trophozoites to mature trophozoites and then to schizonts, which in turn release new merozoites when the erythrocytes rupture. These merozoites infect new erythrocytes and the erythrocytic cycle starts again. However, some of the trophozoites develop into gametocytes, which are ingested by the blood meal of a mosquito. In the mosquito, the parasite undergoes sexual reproduction, producing oocysts with sporozoites that can be transmitted to new hosts with another bite. Image courtesy of DPDx, Centers for Disease Control and Prevention (https://www.cdc.gov/dpdx).

The cycle begins when the mosquito transfers infectious sporozoites to the host during a blood meal (Centers for Disease Control and Prevention 2020a). The parasites first migrate to the liver, where liver cells become infected and the parasites develop into schizonts within 7 to 10 days (PATH's Malaria Vaccine Initiative 2015). These liver schizonts rupture and release merozoites into the blood stream, which infect erythrocytes. Here, immature trophozoites develop into mature trophozoites and finally into schizonts (Centers for Disease Control and Prevention 2020a). These schizonts rupture and release new merozoites that can infect other erythrocytes and the blood cycle is closed. However, some of the trophozoites develop into female and male gametocytes, which are taken up by a mosquito during another blood meal. The sporogonic cycle then takes place in the mosquito, as sexual reproduction occurs in the gut and oocysts are produced, which contain infectious sporozoites. These oocyts rupture and allow the sporozoites to be transmitted from the salivary gland of the mosquito to a host by another bite. This completes the life cycle of *Plasmodium* spp. The stage that leads to symptoms in humans is the erythrocytic stage, which is also the stage that allows diagnosis of malaria.

1.1.2 Symptoms and complications of malaria

Malaria disease can be divided into two categories in terms of its symptoms: uncomplicated and complicated or severe malaria (Centers for Disease Control and Prevention 2020b). In a non-immune person, the first symptoms can be observed 10 to 15 days after infection (World Health Organization 2020a). Symptoms usually occur in the form of attacks that appear at different intervals depending on the *Plasmodium* spp. For example, in the case of *P. falciparum*, in irregular intervals (Centers for Disease Control and Prevention 2020b). Symptoms range from fever, chills, sweating and headache to nausea and vomiting. If malaria is diagnosed and treated quickly and properly, it can be cured without complications.

However, severe courses of malaria with various complications often occur as well, in particular, following infection with *P. falciparum* (Centers for Disease Control and Prevention 2020b). Possible complications caused amongst others by serious organ failure include cerebral malaria (CM), severe anaemia due to constant haemolysis, acute respiratory distress syndrome (ARDS), hyperparasitemia and metabolic acidosis (Centers for Disease Control and Prevention 2020b). Particularly at risk of developing

such complications are children under five years of age who have not yet developed an adequate immunity to malaria, pregnant women whose immune system is downregulated, and travellers who did not come into contact with *Plasmodium* spp. before (Centers for Disease Control and Prevention 2020c). These severe courses can be life-threatening and bear the risk of leading finally to high numbers of deaths as a result of a *Plasmodium* infection.

1.2 Cerebral malaria (CM)

Cerebral malaria is one of the most severe complications of *P. falciparum* infection and is characterized as an encephalopathy, which can lead to coma and in consequence to death (Ghazanfari *et al.* 2018). The WHO defines CM as a syndrome characterized by coma with the presence of asexual forms of *P. falciparum* in the peripheral blood and in which other causes of unconsciousness have been excluded (World Health Organization 2000). As mentioned earlier, *P. falciparum* is thus responsible for most malaria-associated deaths. The mortality rate of CM is between 15 and 25% especially when brain edema is present (Gad *et al.* 2018).

The neurological symptoms of CM include seizures, psychosis, agitation, impaired consciousness, and coma, with the last two symptoms defined as characteristic for CM (Mishra & Newton 2009). Other specific clinical features of CM include retinopathy and brain stem alterations due to increased intracranial pressure and swelling of the brain as well as a break-down of the blood-brain-barrier (BBB), which leads to hemorrhages and finally neurological manifestations (Rénia *et al.* 2012).

In malaria endemic areas, such neurological symptoms appear in nearly half of all children hospitalized with *P. falciparum* malaria (Mishra & Newton 2009). The proportion of children and adult patients who develop CM is comparable in areas where severe courses occur. In travelers, CM occurs in 2.4% of *P. falciparum*-infected patients.

Due to the high mortality rate in case of CM, the obvious vulnerability especially of children under five years, and the high prevalence of *P. falciparum* in many areas, it is of great importance to understand the underlying pathological mechanisms of CM and to develop appropriate prevention strategies and treatments based on this. This would lead to a significant reduction in malaria-related deaths.

1.2.1 Mouse model of cerebral malaria – *Plasmodium berghei* ANKA

Research on human CM depends mainly on the availability of tissue samples, especially brains, *post mortem*, as it is not possible to perform studies on CM patients for ethical reasons. Therefore, a well-established mouse model of experimental cerebral malaria (ECM) is often used as surrogate model. The rodent parasite *Plasmodium berghei* ANKA (PbA) (Fig. 2) is utilized for infection of various susceptible mouse strains including C57BL/6 mice (Montes de Oca *et al.* 2013; Ghazanfari *et al.* 2018). More than 90% of C57BL/6 mice develop ECM after approximately 6-10 days of infection (Montes de Oca *et al.* 2013).

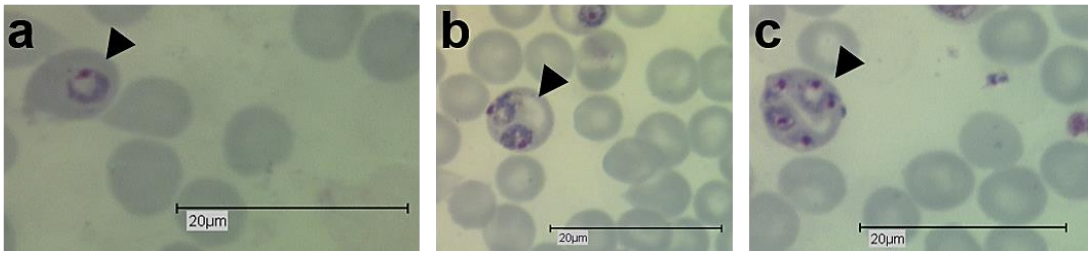

Figure 2: *Plasmodium berghei* ANKA parasites in the blood of a C57BL/6 mouse. C57BL/6 mice were infected with 5e+04 PbA iRBCs i. v.. After 6 days blood was taken from the tail and a blood smear was performed, airdried and stained with Giemsa solution. The arrows indicate parasitized erythrocytes in the peripheral blood. **(a)** Ring stage of *P. berghei* ANKA in the peripheral blood (magnification: 1000x). **(b)** 2 later ring stages of *P. berghei* ANKA. **(c)** Erythrocyte with multiple parasites.

At this timepoint PbA-infected C57BL/6 mice develop neurological symptoms similar to humans, whereas the exact onset is dependent on the infectious dose as well as the genetic background of the mice (de Souza *et al.* 2010). Symptoms include paralysis, ataxia, convulsion, and similar to the human situation coma (de Souza & Riley 2002; de Souza *et al.* 2010; Ghazanfari *et al.* 2018). ECM development in mice can be determined using a specific scoring system: the Rapid Murine Coma and Behavior Scale (RMCBS) (Carroll *et al.* 2010). This health score assesses a total of 10 parameters in five categories (coordination, exploratory behavior, strength and tone, reflexes and self-preservation and hygiene-related behavior), of which each parameter can be rated from zero (lowest score) to two (highest score). Therefore, the maximum score is 20 for a healthy (naive) mouse. Mice with a score of six or lower are considered ECM-positive.

However, there are mouse strains that do not develop ECM, including BALB/c mice (de Souza & Riley 2002), and *Ifnar1*$^{-/-}$ C57BL/6 mice lacking the type I interferon receptor (IFNAR1) (Palomo *et al.* 2013). The majority of these different mouse strains

that are protected from ECM, develop ECM-like symptoms later during the course of infection or die later from hyperparasitemia (Ball *et al.* 2013).

1.2.2 Immunological characteristics of malaria in general

The immune system can be divided into two central parts: the innate immune system and the adaptive immune system. The cellular innate immune response includes in particular antigen-presenting cells (APCs) such as dendritic cells (DCs) or macrophages and granulocytes (eosinophils, neutrophils, basophils), but also innate lymphoid cells (ILCs). Central players of the adaptive immune system are T and B cells (Chaplin 2010).

In the case of malaria, the host immune system first encounters the sporozoite form of the parasite. These remain in the skin for up to 6h, where a local immune response takes place that includes in particular the presentation of antigens by DCs (López *et al.* 2017). Approximately 50% of sporozoites do not leave the injection site, which is particularly important for vaccine design (Belachew 2018). These first line of defense cells recognize the pathogen-associated molecular patterns (PAMPs) of the parasite through pattern recognition receptors (PRRs), resulting in an intracellular signaling cascade that drives the maturation of DCs and further immune responses. This innate immune response starts already before the onset of symptoms. At that timepoint, the genes for PRRs such as toll-like receptors (TLRs) and many inflammatory cytokines are already upregulated and the immune response is mainly directed against free sporozoites and infected hepatocytes (Belachew 2018; Kalantari 2018). The immune response to the liver stage of *Plasmodium* is further characterized in particular by interferon (IFN)-γ producing $CD8^+$ T cells, which eliminate intrahepatic parasites (Belachew 2018). Other cells such as natural killer (NK) cells also contribute to the killing of intrahepatic parasites by secreting type I interferons and IFN-γ (Belachew 2018). The immune response during the erythrocytic and symptomatic phase of *Plasmodium* spp. Infection is mainly characterized by adaptive immune responses (T and B cells), but also NK cells and the production of antibodies (López *et al.* 2017). This immune response is directed against the merozoites and intraerythrocytic parasites, with T cell responses and antibodies being of particular importance in controlling these stages (Belachew 2018).

PAMPs of *Plasmodium* spp., in particular of the erythrocytic stage, and their immunomodulatory function during malaria are extensively studied and include hemozoin, plasmodial DNA and glycophosphatidylinositol (GPI) anchors (López *et al.* 2017). GPI anchors lead to the synthesis of proinflammatory cytokines such as tumor necrosis factor (TNF) and interleukin (IL)-1β by macrophages through binding to TLRs (Kalantari 2018). However, GPIs of plasmodia are also thought to act as toxins that upregulate the expression of cell adhesion molecules, thereby contributing to increased adherence of parasites and also immune cells to endothelial cells (Kalantari 2018). This is particularly central in the pathogenesis of CM.

Hemozoin is a waste product of the heme detoxification process of the parasite, as plasmodia use the hemoglobin of erythrocytes as a source of amino acids, resulting in high levels of free heme metabolites, which are toxic to the parasite and also to the host (Kalantari 2018). These metabolites are consequently released in the form of insoluble crystalline structures that are no longer dangerous for the parasite. The release of hemozoin causes an increase in proinflammatory cytokines such as IL-1β and TNF, contributing to the characteristic periodic episodes of fever during malaria (Kalantari 2018).

With erythrocytes as its habitat *Plasmodium* parasites have chosen an immunologically well protected cell type, as erythrocytes have no nucleus and no possibility to present intracellular antigens to effector T cells on their surface, because they lack major histocompatibility complex (MHC) molecules (Deroost *et al.* 2016; Belachew 2018). But the host still has the possibility to eliminate parasitized erythrocytes, e.g. by antibody-opsonization (Del Portillo *et al.* 2012). This elimination process occurs in particular in the spleen. Here, mechanical trapping of infected erythrocytes occurs, because these parasitized erythrocytes are deformed compared to non-infected erythrocytes, they are less flexible and thus can be filtered out in the spleen (Del Portillo *et al.* 2012). This physiological process is also known for the recycling of old erythrocytes in the spleen.

However, *Plasmodium* possess even more strategies to evade the host's immune system and thus remain in the host as long as possible. These can be roughly divided into antigenic diversity and sequestration (Belachew 2018). Here, the antigenic diversity is particularly present in regard to the surface proteins and arises from

multicopy gene families and polymorphic alleles, making it very difficult for the host to elicit an specific immune response directed against these proteins (Belachew 2018). One of these proteins is the *P. falciparum* erythrocyte membrane protein-1 (PfEMP-1), which is not only highly polymorphic but also mediates among others the second important immune evasion strategy of *P. falciparum*: the sequestration or cytoadherence (Pasternak & Dzikowski 2009; Deroost *et al.* 2016; Belachew 2018). This protein allows parasitized erythrocytes to bind to various receptors, such as intracellular adhesion molecule 1 (ICAM-1), vascular cell-adhesion molecule 1 (VCAM-1), cluster of differentiation (CD) 36, E-selectin and others (Schofield & Grau 2005; Belachew 2018). These molecules are expressed by vascular endothelial cells, thus infected erythrocytes can attach to them, remain in the corresponding organ e.g. in the brain, are withdrawn from the circulation and can consequently not be eliminated in the spleen (Belachew 2018). This process is called sequestration (Schofield & Grau 2005).

The immunological balance is of special importance during a *Plasmodium* infection (Deroost *et al.* 2016). When the immune response and immune evasion of the parasite are in balance, clearance of the parasite or asymptomatic chronic infection often occurs (Deroost *et al.* 2016; Alvar *et al.* 2020), which is mostly observed in many malaria endemic areas where people are in constant exposition to the parasite and develop semi-immunity (Autino *et al.* 2012). However, if the immune responses are insufficient or the parasite is able to take excessive advantage of its evasion strategies, high parasitaemia, metabolic problems, and death will result (Deroost *et al.* 2016). An excessive inflammatory immune response can also lead to problems. Although it contributes to low parasitemia, it leads to tissue damage and pathology in the human host. In the worst case, both an exaggerated immune response and excessive parasite evasion occur, which then leads to immunopathology and simultaneously high parasitic loads creating a positive feedback mechanism that damages the host even further (Deroost *et al.* 2016). Such an imbalance leads to immunopathology and to the already described complications of malaria such as CM.

1.2.3 Pathogenesis of cerebral malaria in human and mouse

P. falciparum is commonly known as the only *Plasmodium* species leading to CM (Rénia *et al.* 2012). However, there are rare reports of CM following *P. vivax* infection

(Sarkar & Bhattacharya 2008). Erythrocytes parasitized with *P. falciparum* disappear from the peripheral circulation and are then found in the microvessels of the brain and other organs mediated by PfEMP-1 and the mediated upregulation of cell adhesion proteins on endothelial cells (Ghazanfari *et al.* 2018). Interestingly, almost all patients with *P. falciparum* malaria show parasites in the brain, with only 1% developing CM (Schofield & Grau 2005). While parasites in the brain are to some extent essential for the development of this complication, they do not appear to be the sole trigger of CM. It is known that this is a very complex immunological process, including the additional presence of immune cells in the brain (Ghazanfari *et al.* 2018). Indeed, in autopsy studies of children with fatal course of CM, intravascular accumulations of monocytes, platelets, and other leukocytes were detected as well as a strong upregulation of ICAM-1, VCAM-1 and E-selectin on brain endothelial cells, suggesting the importance of sequestration for CM development (Ghazanfari *et al.* 2018). Accumulation of infected red blood cells (iRBCs) in capillaries is thought to lead to reduction of blood flow, hypoxia, and consequent coma and death. Also, blood-brain barrier (BBB) alterations have been investigated in such studies and it has been shown that BBB permeabilization occurs in patients with CM. In particular, axonal damage, edema, breakdown of BBB and glial responses were observed (Ghazanfari *et al.* 2018). Brain swelling was also shown to be a key component of CM pathology, as it occurs as a result of cerebral edema and leads to cerebral herniation, resulting in severe brain damage and thus the characteristic neurological CM symptoms (Rénia *et al.* 2012). It was also shown that, in particular, the expression of endothelial tight-junction-associated proteins, which are of great importance for the integrity of the BBB, was decreased in the vessels of CM brains (Brown *et al.* 2001).

From these observations the question arises which specific processes lead to these pathophysiological features of CM. Human studies are limited to *post mortem* analyses of CM patients due to ethical reasons, which makes it difficult to understand the whole process in detail. Although significant numbers of cytotoxic T cells have been found in the capillaries of CM-positive brains in human studies (Barrera *et al.* 2019), suggesting a role of these cells in pathology, it is only an observation which does not explain where these cells come from and how they exactly mediate the pathology. Therefore, to study the pathophysiological mechanisms of CM, experimental models are used that allow to closely follow the processes during a *Plasmodium* infection and, in particular, to

demonstrate the importance of specific cell types, receptors or effector molecules in the development of pathology. One of these models is *Plasmodium berghei* ANKA using C57BL/6 mice that develop ECM after six to ten days (Montes de Oca *et al.* 2013).

Similar to humans, various pathological changes were detected in the brains of PbA-infected mice, including edema, enlarged perivascular lacunae, BBB collapse, and vascular lacuna (Ghazanfari *et al.* 2018). Also, decreased expression of endothelial tight junction proteins in the region of collapse in the brain was observed for mice just as it was in humans (Swanson *et al.* 2016).

Regarding the specific pathology of ECM, there are two main theories: the mechanical hypothesis and the cytokine storm hypothesis (Schiess *et al.* 2020). The mechanical hypothesis is based on the fact that sequestration of iRBCs leads to various consequences in particular vascular congestion, hypoperfusion and local hypoxia (Schiess *et al.* 2020). These differences in blood flow in the brain can lead to increased intracranial pressure and to certain areas of the brain being less well supplied. Together, this ultimately leads to BBB breakdown and edema. For this process, sequestration of infected erythrocytes seems to be necessary (Ghazanfari *et al.* 2018). The iRBCs bind directly to the endothelial cells in the brain and accumulate more platelets and further interact with the endothelial cells, losing control over the movement of solutes along the BBB (Ghazanfari *et al.* 2018). The cytokine storm hypothesis focuses on the importance of peripheral inflammation and high levels of circulating cytokines such as TNF, IFN-γ, IL-2 and IL-6 in pathology (Schiess *et al.* 2020). Proinflammatory cytokines were indeed found to be responsible for the overexpression of adhesion molecules on brain endothelial cells, thus contributing to the development of ECM (Kalantari 2018). Due to that effect of cytokines, iRBCs can effectively sequestrate in the host's brain and cause vascular leakage and perfusion abnormalities (Gazzinelli *et al.* 2014). This allows the infiltration of immune cells into the host brain and leads to tissue inflammation which further enhances the pathological processes.

Various cell types, effector molecules and receptors were already shown to be crucial for ECM development in mice. Depletion of $CD8^+$ T cells in PbA-infected C57BL/6 mice for example prevented vascular hemorrhages, breakdown of the BBB, and

consequently development of ECM (Howland *et al.* 2015), suggesting that $CD8^+$ T cells play an important role in mediating ECM. Furthermore, B and T cell-deficient *Rag2*$^{-/-}$ mice were also no longer protected from ECM after transfer of C57BL/6 $CD8^+$ T cells (Ghazanfari *et al.* 2018). However, not only T cells seem to be important in mediating pathology, as depletion of inflammatory monocytes could also prevent ECM (Schumak *et al.* 2015). It was further determined which effector molecules play a central role. Granzyme B (GzmB)-deficient mice not only had a significantly lower parasitemia, but were also fully protected from ECM, but still exhibited infiltration of $CD8^+$ T cells into the brain (Haque *et al.* 2011b). IFN-γ also appears to play a key role, as both IFN-γ-deficient mice and mice lacking the IFN-γ receptor were protected from ECM (Amani *et al.* 2000; Belnoue *et al.* 2008). However, not only effector molecules were investigated, but also the importance of adhesion molecules and chemokine receptors was of interest. It was shown that *Icam-1*$^{-/-}$ and a large proportion of CXC-motif chemokine receptor 3 (CXCR3)-deficient mice do not develop ECM (Favre *et al.* 1999; Miu *et al.* 2008). This suggests, that adhesion is a central aspect of ECM pathology but also the ability of cells to sense chemokines – effector molecules guiding cells to a target organ – seems to be an important feature.

Taken together, ECM appears to be a very complex process that requires the involvement of several factors. Although these individual factors have a major influence alone, their elimination has far-reaching consequences for the whole immune response to PbA. For example, although $CD8^+$ T cells are central to the pathology, it appears that the absence of GzmB expression is sufficient to prevent ECM. On the other hand, the absence of adhesion molecules also has a major impact, suggesting that sequestration is a central aspect of ECM.

1.2.4 Type I interferons in *Plasmodium* infection and (E)CM

By far not all cell populations, receptors and effector molecules have been investigated with regard to their involvement in ECM development, yet type I interferons and their receptors are coming into focus.

Interferons in general are very central components of the cytokine environment, which are divided into three families: type I, type II and type III interferons (McNab *et al.* 2015). In the type I interferon family, 13 partly very homologous IFNα subtypes are found in humans, as well as one IFNβ and a few poorly defined single gene products. The type

II family consists of only one cytokine, IFN-γ, and the type III family includes IFNλ cytokines, also known as IL-28A and IL-28B (Capobianchi *et al.* 2015).

Type I interferons are recognized by the type I Interferon receptor IFNAR (encoded by the *Ifnar* gene) (Capobianchi *et al.* 2015) and are capable of establishing an anti-viral response by inducing a transcriptional program that interferes with the viral replication cycle (McNab *et al.* 2015). However, they also have many other functions and have a major impact on many innate and adaptive immune responses, not only to viruses but also to other pathogens. The extent to which a type I interferon response influences the outcome of an infection always depends on the pathogen and on the exact signaling pathway which is induced, since the pathogen influences when and where type I interferon signals are delivered and which pathway is then triggered downstream of the IFNAR. Therefore, these cytokines can have both protective and detrimental effects on infections.

Nearly all cells are able to produce IFNα/β in response to stimulation of surface (e. g. TLR4) or intracellular PRRs by microbial products, especially products of nucleic origin or lipopolysaccharide (LPS) of bacteria (McNab *et al.* 2015). After stimulation, various pathways can be activated downstream of these receptors, with IFN-regulatory factors (IRF) in particular activating transcription of IFNα/β at the end of signal transduction, together with nuclear factor-κB (NFκB) as a cofactor. The IFNα/β molecules are then recognized by the IFNAR on other cells. This receptor consists of two different subunits, the *IFNAR1* (encoded by the *Ifnar1* gene) and the IFNAR2, which together form the receptor (Capobianchi *et al.* 2015). The recognition of IFNα/β by the IFNAR in turn triggers a signaling cascade which leads to the transcription of specific IFN-stimulated genes, depending on the signaling molecules involved. These genes encode for example cytokines, chemokines, antibacterial effectors, or apoptotic molecules that strongly influence the immune response to pathogens and the outcome of an infection (McNab *et al.* 2015).

As already mentioned, the innate immune response plays a crucial role in the disease malaria (Belachew 2018). Various *Plasmodium*-derived molecules like GPI anchors, hemozoin and nucleic acids are recognized by PRRs on innate immune cells and therefore induce a signalling cascade leading to type I Interferon production by these cells (Sebina & Haque 2018). In various studies, exogenous type I IFN was shown to

be protective during the liver phase of *Plasmodium*, whereas it showed little effect in the blood phase, suggesting that the site of the immune response has a crucial role in the effect of type I IFNs. However, administration of human IFNα modified to be recognized by the mouse IFNAR was able to help reduce parasitemia during *P. yoelii* infection, whereas it was barely affected in the liver phase (Vigário *et al.* 2001). Using mice lacking the type I IFN receptor (*Ifnar1*$^{-/-}$), it was further shown that type I IFN signaling via *IFNAR1*, together with IRF3 but not IRF7, impairs early parasite control, both in the *P. chabaudi chabaudi* model and during *P. yoelii* infection (Edwards *et al.* 2015; Sebina *et al.* 2016). Depending on the genetic background of the host and the model chosen, type I IFN signaling plays a somehow protective role during non-lethal *Plasmodium* infection or appears to impair control of primary blood-stage infection (Sebina & Haque 2018).

However, type I IFN signaling seems to play a special role not only during non-lethal *Plasmodium* infection. Also during ECM, type I IFN and the associated signaling pathways and molecules influence the outcome of the infection (Sebina & Haque 2018). First, *Ifnar1*$^{-/-}$ mice were found to be almost completely protected from ECM development, suggesting a detrimental role of type I IFN signaling in the ECM model (Haque *et al.* 2011a). Mice lacking only the downstream signaling molecules IRF3 and IRF7 were also protected from ECM (Sharma *et al.* 2011). Interestingly, regarding the influence of type I IFN signaling on parasite burden in the brain, known to be crucial for CM development at least in humans, different observations were made (Sebina & Haque 2018). While some detected fewer parasites in the brain, others detected levels similar to those in WT controls (Haque *et al.* 2011a; Ball *et al.* 2013). The mechanisms by which type I IFN signaling leads to ECM have not been clearly elucidated. While some studies have shown that *IFNAR1* expression on CD8^{+} T cells alone is sufficient to induce ECM, others show that this is also true for DCs (Ball *et al.* 2013; Haque *et al.* 2014). Last but not least, in human malaria, children with a specific genetic variant of the *Ifnar1* gene showed protection against CM (Ball *et al.* 2013). Thus, type I IFNs and their signaling pathways play a central role in the development of cerebral malaria in mice and in humans. The mechanisms behind this phenomenon need to be further investigated to better understand this serious complication of *Plasmodium* infection.

1.3 Filariasis

Filariasis is caused by helminths, relatively large multicellular organisms that are divided into 3 distinct groups: the platyhelminths (flatworms), the acanthocephala, and the nematodes (round worms), which include the family of filariae (Centers for Disease Control and Prevention 2020e). Filariae can lead to severe diseases, including onchoceriasis and lymphatic filariasis (LF), which represent a major health problem in the affected regions (Taylor *et al.* 2010).

1.3.1 Onchocerciasis

Onchocerciasis belongs to the neglected tropical diseases (NTDs) and is caused by the filarial nematode *Onchocerca volvulus* (Centers for Disease Control and Prevention 2019c). This parasite is transmitted by infected blackflies of the genus *Simulium*, which breed especially at rivers, which is why onchocerciasis is also called river blindness (World Health Organization 2021d).

In 2017, it was estimated that 20.9 million people were infected with *O. volvulus*, 1.15 million of whom experienced vision loss or complete blindness (World Health Organization 2021d). Infections with *O. volvulus* occur in the tropics, with the main burden in 31 countries in sub-Saharan Africa, where 99% of all infected people live (Centers for Disease Control and Prevention 2019e; World Health Organization 2021d). People living along rivers are particularly at risk due to the breeding behavior of the flies. However, since it takes many bites to become infected, travelers are not at great risk (Centers for Disease Control and Prevention 2019e).

Since 1974, there have been various programs aiming to bring onchocerciasis under control (World Health Organization 2021d). These programs mainly focus on the distribution and administration of large quantities of ivermectin and vector control in endemic areas. In 2017, 145 million people in Africa have already been treated, representing 70% of people worldwide in need of treatment against onchocerciasis.

The WHO recommends ivermectin for the treatment of onchocerciasis at least once a year for 10 to 15 years (World Health Organization 2021d), as it does not kill the adult worms and only temporarily inhibits the transmission of the disease by clearing the microfilarial offspring of the filariae. However, it must first be ruled out that a co-infection with *Loa loa* exists, otherwise severe side effects of the medication may occur

(Centers for Disease Control and Prevention 2018d). Prevention is mainly achieved through personal protection measures from the bites of the vectors by using repellents applied to the skin or by wearing long clothing (Centers for Disease Control and Prevention 2019f).

1.3.2 Lymphatic Filariasis (LF)

Lymphatic filariasis (LF) belongs to the NTDs as well (Centers for Disease Control and Prevention 2018b) and is caused by filarial nematodes (World Health Organization 2021c). Three different filariae cause LF: *Wuchereria bancrofti*, *Brugia malayi*, and *B. timori*, with 90% of all LF cases being caused by *W. bancrofti* (Centers for Disease Control and Prevention 2019a). These parasites are transmitted by mosquitoes of various genera, including *Aedes* spp., *Anopheles* spp. and *Culex* spp.

Worldwide around 68 million people in 72 countries are affected by LF, mainly in the tropics and subtropics in Asia, Africa and the West Pacific, but also parts of the Caribbean and South America are affected (Simonsen *et al.* 2013; World Health Organization 2021a). People who live in endemic regions for a long time are particularly at risk, as it takes many mosquito bites over several months to get LF (Centers for Disease Control and Prevention 2019b). Travelers who spend only a short time in such areas have a very low risk of contracting the disease.

The WHO launched its Global Programme to Eliminate Lymphatic Filariasis (GPELF) in 2000 with the goal of eliminating LF by 2020 (World Health Organization 2021c). While this goal has not been met, 597 million people who were at risk for LF no longer need preventive chemotherapy. These strategies consist of 2 components: i) MDA programs, under which people in affected regions are treated preventively with drugs in large quantities to prevent transmission, and ii) morbidity management, under which affected people receive medical care, such as surgery, to alleviate their suffering (World Health Organization 2021b).

Currently there are 3 different drug regimens used in MDA programs (World Health Organization 2021b): the combination of diethylcarbamazine citrate (DEC) with albendazole, the combination of ivermectin with albendazole which is used in areas where onchocerciasis is also prevalent, because DEC is contraindicated (Bryceson *et al.* 1977) and administration of albendazole alone in areas where *Loa loa* cases occur, as neither ivermectin nor DEC can be used here (Twum-Danso 2003). These MDA

programs should run for at least 5 years and include 65% of individuals in an at-risk population to be successful (World Health Organization 2021b). Currently, the WHO recommends a triple therapy with ivermectin, DEC and albendazole (IDA) in countries where neither onchocerciasis nor *Loa loa* are endemic, as this regimen has been shown to be much more efficient in reducing the microfilarial load compared with a two-drug regimen (World Health Organization 2017; King *et al.* 2018).

In addition, vector control measures are also useful to interfere with the mosquito-borne transmission (Centers for Disease Control and Prevention 2020d). Since most vectors of the mentioned parasites bite especially at dusk and at night, it is advisable to sleep under mosquito nets and wear long clothing when outdoors at dusk.

1.3.3 Life cycle of filariae

During the life cycle of filariae (Fig. 3) infective L3 larvae first enter the skin of humans during a bloodmeal of an infected mosquito or blackfly (Centers for Disease Control and Prevention 2019a, 2019d). The L3 larvae enter the lymphatics of the host in case of LF and the subcutaneous tissues in onchocerciasis and there develop into adult worms. Sexual reproduction further occurs, producing so-called microfilariae (Mf). Mf of *W. bancrofti* are found in the peripheral blood, whereas *O. volvulus* Mf are mainly seen in the skin and lymphatics, but also sometimes in the peripheral blood. The Mfs are then taken up by another vector during a bloodmeal.

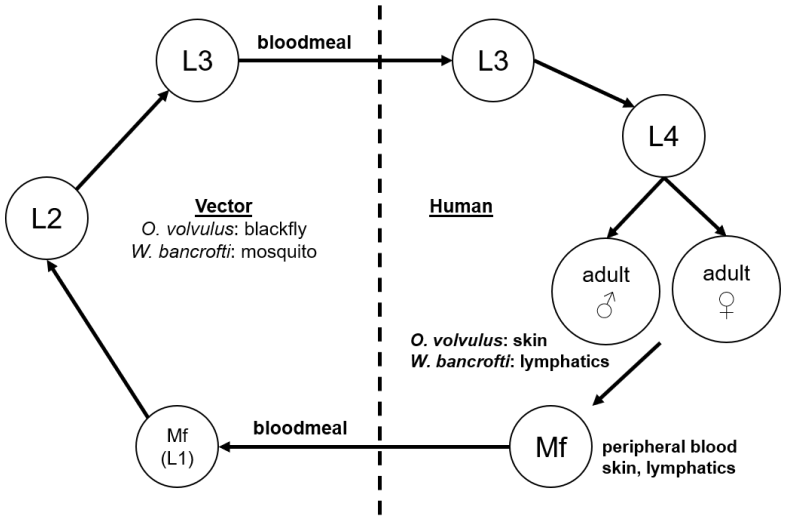

Figure 3: Life cycle of filarial nematodes. Infective L3 larvae enter the skin via the bite of the vector and migrate to the filarial species-specific locations like the skin for *O. volvulus* and the lymphatics for *W. bancrofti*, where they develop into adult worms. Sexual reproduction occurs between males and females, resulting in the production of microfilariae (Mf), which are found mainly in the peripheral blood of the host. There they can be taken up by a vector by another bite. In the vector, the microfilariae develop again into L3 larvae that can be transmitted to the next host. Adapted after (Mackenzie *et al.* 2017).

In the vector, the Mf then develop into L3 larvae, which migrate into the head of the vector and are transmitted to another human host via another bite (Centers for Disease Control and Prevention 2019a, 2019d).

Treatment of filariasis strongly focuses on the Mf, which are affected by administration of the drugs currently used in MDA programs (Taylor *et al.* 2010; Hoerauf *et al.* 2011). Against the adult worms, whose existence have a great influence on the morbidity of especially LF, there is so far only doxycycline as an effective and well tolerated drug (Risch *et al.* 2021). It targets the endosymbiotic *Wolbachia* bacteria of filariae worms, limiting their reproductive capacity and viability (Hoerauf *et al.* 2003; Debrah *et al.* 2007; Hoerauf 2008; Mand *et al.* 2008). Doxycycline treatment also lessens lymphedema pathology caused by infection with for example *W. bancrofti* (Mand *et al.* 2012).

1.3.4 Symptoms and complications of LF and onchocerciasis

Lymphatic filariasis

The majority of infections with LF-causing filariae are asymptomatic, these patients show no outward signs of infection, yet contribute to the spread of the parasites and also present damage of the lymphatic system as well as alterations of the immune system (Alvar *et al.* 2020; World Health Organization 2021c).

Chronically infected patients often do develop a clinical manifestation after years of being infected and then characteristically show lymphedema (LE) of the extremities or genital area (hydrocele in men), which is accompanied by severe swelling of the affected areas (Centers for Disease Control and Prevention 2019a). This is caused by an impaired functionality of the lymphatic system due to immunological changes induced by the adult worms in the lymphatics (Centers for Disease Control and Prevention 2018c). Patients with such clinical manifestations are also more vulnerable to secondary infections with for example bacteria due to the skin abnormalities affecting the barrier immunity as well as the malfunction of the lymphatics.

In addition to the chronic manifestations, acute symptoms may also occur simultaneously, especially local inflammatory processes of the skin, lymph nodes or lymphatic vessels (World Health Organization 2021c). These are triggered on the one hand by the immune response to the parasite and on the other hand by the secondary

infections already mentioned. The severe physical changes as well as the acute episodes mostly lasting for weeks also have other significant effects on the patients, as they are stigmatized, restricted in their work, and thus at increased risk of poverty (World Health Organization 2021c).

Onchocerciasis

Infection with *O. volvulus* initially results in nodules under the skin where the adult worms live (Taylor *et al.* 2010). These nodules usually cause no symptoms except for visible nodules and sometimes local swelling of lymph nodes. The symptoms of onchocerciasis are triggered by the Mf, which migrate subcutaneously through the host's body and cause strong inflammatory immune responses when they die (Saint André *et al.* 2002). These inflammatory immune responses are induced by the release of the endosymbiotic *Wolbachia* bacteria (Tamarozzi *et al.* 2011). Itching and skin lesions occur, which in turn can promote secondary infections. However, the Mf can also migrate to the eyes, and due to the strong immune response, the host suffers from eye lesions which impair their vision and can lead to blindness (Hoerauf *et al.* 2011).

It has also been shown that in areas with a high prevalence of onchocerciasis, there is an increased prevalence of nodding syndrome, an epileptic encephalopathy, the cause of which has not yet been determined (Kakooza-Mwesige 2017). This syndrome is also prevalent in villages located along blackfly-breeding rivers, suggesting an association with onchocerciasis (Colebunders *et al.* 2016).

1.3.5 Mouse model of filariasis – *Litomosoides sigmodontis*

To study the immune response to filarial nematodes, researchers use a well-established experimental model: *Litomosoides sigmodontis*, a rodent parasite that undergoes a complete life cycle in both jirds (*Meriones unguiculatus*) and mice, depending on the strain, comparable to that of filarial nematodes in humans (Hübner *et al.* 2009; Risch *et al.* 2021). The life cycle of *L. sigmodontis* (Fig. 4) requires the tropical rat mite *Ornithonyssus bacoti* as a vector that transmits infective L3 larvae to mice or jirds via its bite. There, L3 larvae migrate into the pleural cavity where they molt into L4 larvae and then into adult female and male worms 28 to 30 days after infection. After 50 days, females begin to produce Mf that can be detected in the peripheral blood and can be taken up by the tropical rat mite through another bite.

BALB/c mice show chronic infection with *L. sigmodontis* with adult worms in the pleural cavity and circulating Mf from day 50 after infection (Hübner *et al.* 2009). However, C57BL/6 mice are only semi-susceptible to *L. sigmodontis* infection because they eliminate adult worms by day 40, thus do not develop a patent infection and no Mf are detectable (Babayan *et al.* 2003; Layland *et al.* 2015; Finlay & Allen 2020).

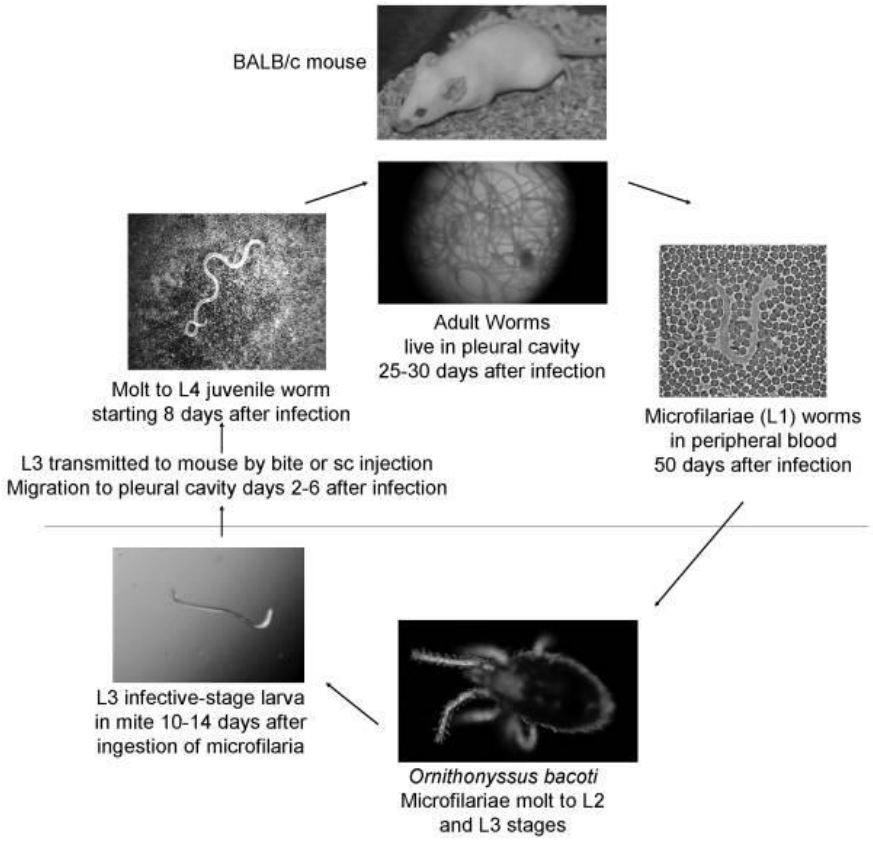

Figure 4: Life cycle of *Litomosoides sigmodontis*. The *L. sigmodontis*-infected tropical rat mite takes a bloodmeal on mice or jirds and injects infectious L3 larvae. L3 migrate into the pleural cavity and molt into L4 larvae of mice or jirds and molt into adult worms. After 50 days the female adult worms start to produce microfilariae which are detectable in the peripheral blood and can be taken up by another bite of a tropical rate mite (Hübner *et al.* 2009).

That the susceptibility to *L. sigmodontis* infection is strongly dependent on the immune response and the specific presence of certain immune cells is shown by the fact that both *Rag2*$^{-/-}$ mice lacking T and B cells and *Rag2IL-2Rγ*$^{-/-}$ additionally lacking NK cells are completeley susceptible to *L. sigmodontis* infection, although they have the genetic background of a C57BL/6 mouse (Layland *et al.* 2015; Finlay & Allen 2020).

The immune response to *L. sigmodontis* is comparable in many aspects to the immune response in humans, making this model a good tool for analyzing immune responses to filarial nematodes in general and allowing to demonstrate the importance of specific immune cells and effector molecules (Frohberger *et al.* 2019).

1.3.6 Immune response to helminth infections in human and mouse

The immune response to helminths is the result of a long co-evolution between host and parasite (Allen & Maizels 2011). Helminths are able to modulate the immune system of their host to create a favorable environment, in which they can reproduce and survive in the long-term (Anthony *et al.* 2007). The resulting immune response must be beneficial to the parasite but not harmful to the host. Thus, the worms are often found in places inside of the host that are poorly accessible to the immune system, which further promotes parasite survival. However, the host aims to trigger a protective immune response that eliminates the parasite.

The characteristic and to some extent protective immune response to filarial nematodes in humans and mice is a strong type 2 response, defined by an increase in especially type 2 T helper cells (Th2) and the corresponding type 2 and regulatory cytokines IL-4, IL-5, IL-9, IL-10, and IL-13 (Babu & Nutman 2014). Also, certain antibody isotypes are produced e.g. immunoglobulin G1 (IgG1) in mice and IgG4 in humans as well as IgE and there is an increase in eosinophils and alternatively activated macrophages upon infection with filarial nematodes. In the early induction of the host immune response, dendritic cells (DCs), macrophages, basophils and also innate lymphoid cells (ILCs) play a role (Allen & Maizels 2011; Risch *et al.* 2021) . DCs in particular were identified as important mediators of filarial antigen presentation to T cells in human filarial infections.

Furthermore, the susceptibility of BALB/c mice to *L. sigmodontis* infection was shown to be mediated by the recruitment of regulatory T cells that downregulate the immune response of the host (Taylor *et al.* 2009). Also, IL-10-producing macrophages appear to play an important role, as overexpression of IL-10 on these cells promotes patency of infection by decreasing the number of IL-5-producing T cells (Specht *et al.* 2012). In addition, eosinophils in particular have been shown to play an important role in the protective immune responses to filarial nematodes, and the eosinophil-inducing cytokine IL-5 has also been shown to be a critical factor in the outcome of infection (Frohberger *et al.* 2019).

Interestingly, the initial often pro-inflammatory and to some extent also protective (Babayan *et al.* 2003; Muhsin *et al.* 2018) host immune response to filarial infection is actively down-regulated by the parasites themselves, as they are strongly able to

manipulate the hosts immune system (Maizels & McSorley 2016). This involves, among other things, reducing the cytotoxic activity of T cells and establishing a T cell anergy (Nutman *et al.* 1987; Kolbaum *et al.* 2012; Knipper *et al.* 2019). This occurs through the establishment of a regulatory, anti-inflammatory immune response during the course of chronic helminth infection, which is accompanied by the expansion of regulatory T and B cells, alternatively activated macrophages, the expression of immunosuppressive molecules (CTLA-4, PD-1), and the production of anti-inflammatory cytokines such as IL-10 and TGFβ (Taylor *et al.* 2006; Taylor *et al.* 2012; Buerfent *et al.* 2015). This phenomenon of immune regulation/tolerance induction is in the best interest of the host, as it is not observed in patients with pathologies of filarial infection. Thus, regulation of the immune response after initial infection appears to contribute significantly to the prevention of severe complications and favors chronic courses of filarial infections. However, it is also a survival strategy of the parasite, as it ensures microfilaremia and its own survival within its host. Furthermore, immune regulation by helminths also leads to the reduction of parasite-independent immune responses, such as autoimmune responses or the reaction to allergens and has an impact on the outcome of co-infections, e. g. malaria or *Escherichia coli*-induced sepsis (Maizels *et al.* 2004; Specht *et al.* 2010; Hübner *et al.* 2013; Ajendra *et al.* 2014; Berbudi *et al.* 2016) .This fact is used, among other things, to develop new treatments for allergies and autoimmune diseases (McSorley *et al.* 2013).

1.4 Innate lymphoid cells (ILCs)

Innate lymphoid cells (ILCs) have only recently been identified as a distinct immune cell population and are part of the innate immune system (Artis & Spits 2015). They have a classic lymphoid morphology, but can be distinguished from T and B cells of the adaptive immune system by the absence of clonotypic antigen receptors and their development in the absence of recombination-activating gene 1 (*Rag1*) or *Rag2* (Serafini *et al.* 2015). ILCs are early effector cells and respond within a few hours after activation (Huang *et al.* 2017), which clearly distinguishes them from T and B cells. However, they develop from the common lymphoid progenitor (CLP) and their surface receptor expression and characteristic cytokines are under the control of specific transcription factors which are mainly typical for T cells, which emphasizes their similarity to T cells (Burg *et al.* 2015). ILCs share many functions and cytokines with T cells (Eberl *et al.* 2015) and are found in many tissues, including both lymphoid and

non-lymphoid tissues, while exhibiting tissue-specific characteristics (Artis & Spits 2015; Huang *et al.* 2017).

ILCs are thought to be the evolutionary precursors of T cells which means that ILCs existed in evolution before the establishment of an adaptive immune system in vertebrates (Eberl *et al.* 2015). The development of ILCs from CLPs is divided into three phases: I) the generation of common ILC precursors (CILCPs), II) the diversification of ILC precursors (ILCPs) into the three major groups of ILCs, and III) the maintenance of the ILC pool and regulation in peripheral tissues (Serafini *et al.* 2015). Through various intermediate steps, during which the expression of surface molecules changes and temporarily also the expression of transcription factors, mature ILCs develop at the end (Huang *et al.* 2017).

In general, depending on the subset, ILCs are strategically located in specific tissues and function there as tissue-resident cells. This on the one hand ensures normal tissue function and on the other hand plays an important role in the barrier-immunity, as they can respond very quickly to local signals and mediate effector functions and provide help for tissue repair (Huang *et al.* 2018).

1.4.1 ILC subsets, their characteristic markers and general functions

ILCs are broadly divided into three groups (Fig. 5) based on their cytokine profile and transcription factor expression: group 1, 2 and 3 (Jiao *et al.* 2016). Group 1 ILCs include NK cells, and helper ILC1s, group 2 contains the ILC2s, and group 3 has the greatest heterogeneity of subpopulations, as it consist of natural cytotoxicity receptor (NCR)-positive, NCR-negative, and lymphoid tissue inducer (LTi) cells (Burg *et al.* 2015). All ILCs have in common that they lack the expression of certain lineage markers (Elemam *et al.* 2017). These include the T cell marker CD3, the granulocyte marker lymphocyte antigen 6 complex locus C (Ly6C)/Ly6G, CD11b for myeloid cells, CD45R for B cells and TER119 for erythroid cells (Biolegend 2018b). Furthermore, ILCs also lack expression of the T cell receptor (TCR) (Palomo *et al.* 2017).

However, this classification is relatively conservative and does not take into account the fact that, similar to T cells, ILCs exhibit a certain plasticity that allows them to generate properties of other subtypes depending on environmental influences in the tissue (Krabbendam *et al.* 2018). For example, it is possible for ILC2s to become IL-17-producing cells or for ILC2s to become exILC2s capable of producing IFN-γ under the

influence of IL-1β and IL-12. It is important to note, however, that ILCs generated by this plasticity are not fully comparable to *bona fide* ILCs; rather, it is an additional way for the immune system to increase the pool of required ILCs without the need to expensively generate ILCs (Bal *et al.* 2020).

1.4.1.1 ILC1s and NK cells

The group of ILC1s resembles type 1 T helper cells (Th1) and consists of the helper ILC1s, which have no cytotoxic activity, and cytotoxic NK cells (Spits *et al.* 2013). NK cells can be further subdivided into subpopulations, as there are different stages of mature NK cells based on CD27 and CD11b expression, with CD11b$^+$ NK cells having the greatest effector potential among all NK cell subpopulations (Guimont-Desrochers & Lesage 2013). ILC1s are found in steady state in almost all tissues, but are particularly enriched in the liver, uterus, skin, and intestine (Jiao *et al.* 2016).

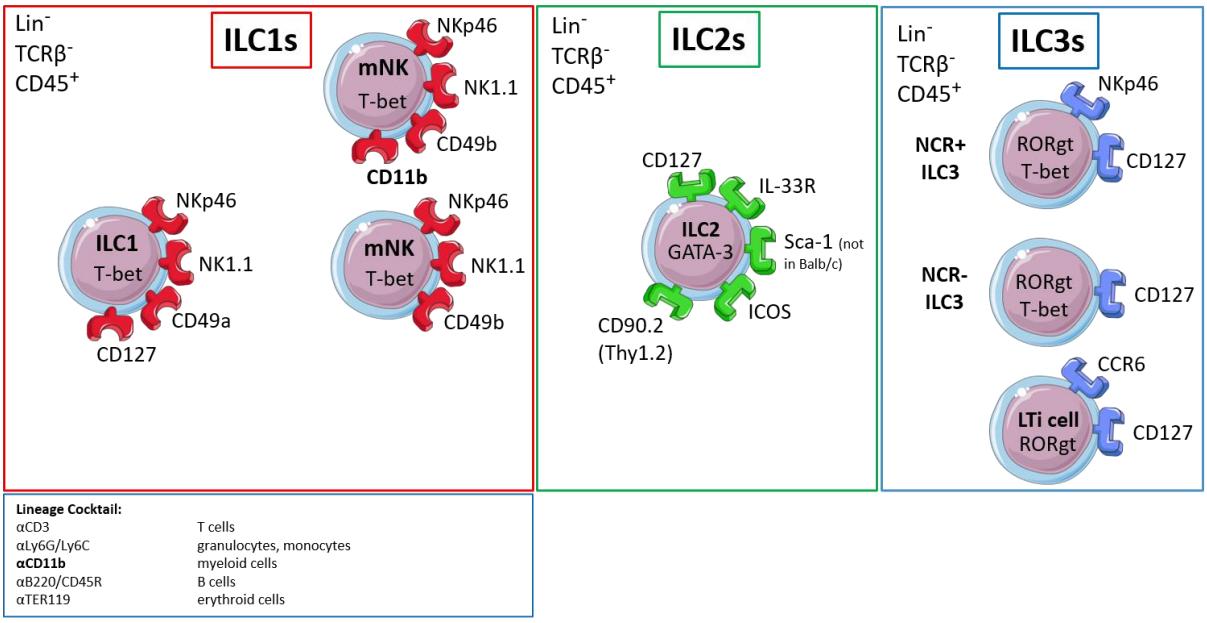

Figure 5: Overview of ILC subsets and their characteristic markers. ILCs are divided into 3 groups: ILC1s, ILC2s and ILC3s. All ILCs are CD45$^+$, lineage$^-$ and TCR$^-$, whereas CD11b$^+$ NK cells are lineage$^+$. In group 1, NK cells are found together with helper ILC1s. Characteristically, NK cells express CD49b, NKp46, and NK1.1 (in C57BL/6 mice), ILC1s express CD49a along with NKp46 and NK1.1, and all ILC1s are T-bet$^+$. ILC2s are defined as CD90.2$^+$, IL-33R$^+$, Sca-1$^+$, GATA-3$^+$. The group of ILC3s includes NCR$^+$ ILC3s with NKp46, RORγt, and T-bet expression, NCR$^-$ ILC3s lacking NKp46, and LTi cells showing no co-expression of the transcription factors T-bet and RORγt. Adapted after (Serafini *et al.* 2015).

The different subsets of ILC1s can be distinguished from each other by characteristic surface markers. NK cells are characterized by their expression of α2 integrin (CD49b), show expression of CD11b depending on the stage or are negative for CD11b, are positive for NKp46 and NK1.1, the latter being the case in C57BL/6 mice (Spits *et al.*

2013; Cuff & Male 2017). ILC1s, on the other hand, are negative for CD49b (Besnard *et al.* 2015), but express the α1 integrin (CD49a) (Ng *et al.* 2018) and like NK cells are positive for NKp46 and depending on the mouse strain for NK1.1 as well (Kim *et al.* 2017). All ILC1s and NK cells show expression of the characteristic transcription factor T-box transcription factor (T-bet) which plays a crucial role for the development of ILC1s (Bal *et al.* 2020).

NK cells and ILC1s produce mainly type 1 cytokines such as IFN-γ and TNF after activation by IL-12, IL-15, and IL-18, whereas NK cells additionally produce cytotoxic GzmB and perforin and can eliminate infected cells by cytolytic granules (Artis & Spits 2015; Serafini *et al.* 2015). In general, ILC1s contribute to the immune response to viruses, intracellular bacteria, parasites, and fungi, are able to regulate and shape the adaptive immune response, and play a role in macrophage activation (Gasteiger & Rudensky 2014; Artis & Spits 2015; Flores-Borja *et al.* 2016). It has also been shown that during pregnancy, vascular changes are mediated by ILC1s that contribute to the unrestricted flow of nutrients between the fetus and placenta (Bando & Colonna 2016). A role in cancer has also already been identified (Germain & Huang 2018).

1.4.1.2 ILC2s

ILC2s resemble Th2 cells and are defined by the characteristic markers CD90.2 (Thy1.2), the IL-33 receptor (IL-33R), stem cells antigen 1 (Sca-1 or Ly-6A/E), and the transcription factor GATA-3, with Sca-1 being expressed by all ILC2s in C57BL/6 mice (Serafini *et al.* 2015; Biolegend 2018a). In BALB/c mice, resting ILC2s are negative for Sca-1 and begin to express Sca-1 upon activation. ILC2s are localized in many barrier tissues, for example in the intestine, in the lung and in the skin (Germain & Huang 2018). In WT C57BL/6 mice, they account for 0.25-1% of all living cells in the lung and are found here predominantly in the collagen-rich regions adjacent to blood vessels, but not in the alveoli (Drake *et al.* 2014).

These cells can be activated by IL-25, IL-33 and thymic stromal lymphopoietin (TSLP), produced by epithelial cells, and in turn produce typical type 2 cytokines such as IL-4, IL-5, IL-9, and IL-13 (Spits *et al.* 2013; Serafini *et al.* 2015). ILC2s interact with the adaptive immune system to indirectly elicit a protective immune response (Artis & Spits 2015). Thus, ILC2s express MHC II molecules and are able to activate T cells to promote IL-2 production, which in turn drives their own proliferation and thus the

production of type 2 cytokines. They are also involved in tissue repair as they produce amphiregulin, an epidermal growth factor that can rebuild the bronchial epithelium after tissue damage (Monticelli *et al.* 2011). Involvement of ILC2s in metabolic homeostasis was also demonstrated, as immune responses through ILC2s limited high-fat diet-induced obesity and insulin resistance (Elemam *et al.* 2017). In the arthritis model, ILC2s are critically involved in the activation of regulatory T cells through their production of IL-9 and lead to the limitation of the inflammatory response (Symowski & Voehringer 2017). However, ILC2s do not always play a protective role in the immune response. ILC2s are also associated with many chronic and autoimmune diseases, such as atopic dermatitis and hepatic fibrosis (Serafini *et al.* 2015). They are thought to be crucially involved in the development of allergic asthma and chronic rhinosinusitis (Spits *et al.* 2013; Artis & Spits 2015; Ebbo *et al.* 2017).

1.4.1.3 ILC3s

The group of ILC3s is comparable to type 17 T helper (Th17) cells and is the most heterogeneous group of ILCs (Ignacio *et al.* 2017). It includes NCR^+ ILC3s that express the NCR NKp46 and the transcription factors T-bet and retinoic-acid-receptor-related orphan nuclear receptor gamma (RORγt), NCR^- ILC3s that do not express NKp46 but are also positive for T-bet and RORγt, and LTi cells that lack T-bet expression (Artis & Spits 2015). They are enriched in the intestinal tract and in mesenteric lymph nodes (mLNs) (Chu *et al.* 2018).

ILC3s produce mainly IL-17, IL-22, lymphotoxin alpha (LTα) and LTβ after activation by IL-1β and IL-23 (Serafini *et al.* 2015). Due to their strong heterogeneity, their functions are also directed very differently. For example, they are important for the regulation of the host-commensal bacteria relationship, developing an important immunotolerogenic status (Ignacio *et al.* 2017). In this context, ILC3s can activate B cells and stimulate them to produce IgA, which is important for this interaction (Artis & Spits 2015). LTi cells are among the first cells to colonize the lymph nodes after birth and regulate the formation of secondary lymphoid tissue such as Peyer's patches (Burg *et al.* 2015; Elemam *et al.* 2017). They also influence the adaptive immune response by mediating the recruitment of $CD4^+$ T cells to mucosal sites and by playing an important role in maintaining the memory function of T cells (Burg *et al.* 2015). Regeneration of intestinal epithelial cells after damage is also mediated by ILC3s,

mainly through the production of IL-22, which acts specifically on intestinal stem cells (Ignacio *et al.* 2017). However, detrimental roles have also been demonstrated. During colitis, NCR^+ ILC3s differentiate into RORγt-negative IFN-γ-producing ILC1s and also contribute to the immunopathology during psoriasis by producing their characteristic cytokines (Ebbo *et al.* 2017). Patients with recurrent relapses of multiple sclerosis also showed abnormally high levels of ILC3s in the blood, especially those with cerebral lesions had abnormally high proportions of these cells in the blood.

1.4.2 ILCs in infectious diseases and interactions with other cell types

Although ILCs have not long been known as a distinct immune cell population, their importance during various infectious diseases in mouse models and in humans has already been investigated, as their localization at barrier sites in particular suggests that they are involved precisely when pathogens enter the body.

IFN-γ-producing ILC1s and also ILC3s have been shown to be important for resistance to *Salmonella* infection leading to typhoid fever and for protection against *Toxoplasma gondii* infection (Artis & Spits 2015; Huang *et al.* 2018). In the case of ILC3s, their IL-22 production in particular plays a crucial role in the protection from *Salmonella* infection (Ignacio *et al.* 2017). However, other studies show that although ILC1s are involved in innate barrier protective function, they may later mediate immunopathology during *Salmonella* infection (Diefenbach 2013). ILC1s prevent *T. gondii* infection by recruiting myeloid cells and by producing IFN-γ and TNF (Ng & Engwerda 2018). An ILC response to *Listeria monocytogenes* has also been previously identified (Ebbo *et al.* 2017). In addition, the innate immune response to infection with *Citrobacter rodentium*, a murine pathogen that bears similarity to enteropathogenic *Escherichia coli* (EPEC) (Collins *et al.* 2014), is strongly dependent on IL-22 produced by ILC3s, which is critical for maintaining intestinal barrier function (Artis & Spits 2015). Since ILC2s can produce amphiregulin, they contribute critically to lung tissue repair after influenza infection (Ebbo *et al.* 2017). Thus, ILCs are often important mediators of the innate and initial immune response to a pathogen that penetrates the barrier function of various tissues and contribute to the restoration of the functionality of tissues after successfully eliminated infection. This applies not only to bacterial diseases, but also to viral and parasitic infections.

Immune responses must always be considered in a complex network, since immune cells always interact with other immune cells, influencing them directly or indirectly and thereby favouring their functions in a certain direction. This network is composed differently depending on the tissue or organ, as many cells are enriched in some organs, while in others they represent only a small proportion. ILCs in general constitute a relatively small proportion in all organs compared with other immune cell populations (Flores-Borja *et al.* 2016). Nevertheless, they appear to be important mediators of the immune response, as they have already been shown to have crucial functions in many diseases.

ILCs interact with other immune cells in several ways. ILC2s and ILC3s express MHC II molecules and can both process antigens and present them to T cells, leading to their activation, despite the fact that they lack co-stimulatory molecules such as those possessed by professional APCs (Artis & Spits 2015). ILC2s influence the T cell response either through cytokines, indirect effects on accessor cells, or through direct cell-cell contact as is the case with antigen presentation (Symowski & Voehringer 2017). They actively contribute to the recruitment of eosinophils through the production of IL-5, their IL-9 production leads to the proliferation of T cells (Artis & Spits 2015; Symowski & Voehringer 2017) and IL-13 produced by ILC2s leads to migration of DCs into lymph nodes to prime Th2 responses there (Serafini *et al.* 2015). Furthermore, ILC2s are responsible for an increase in alternatively activated macrophages in different disease models (Symowski & Voehringer 2017). With respect to ILC1s, it has been shown that they do not possess an MHC molecule and thus do not interact in an antigen-dependent manner, however, NK cells have a role in the control of the T cell-dependent immune response in various models, as they can exhibit direct cytotoxic activity against $CD4^+$ and $CD8^+$ T cells, as well as against APCs, which are important for T cell priming (Burg *et al.* 2015). Interestingly, there seems to be some kind of competition between T cells and ILCs for activating cytokines from DCs, so that ILCs in turn may also be regulated (Eberl *et al.* 2015; Vivier *et al.* 2018). Thus, the interaction is always reciprocal and in particular the crosstalk between T cells and ILCs determines the outcome of CD4 T cell responses (Dutton *et al.* 2017). However, recent studies have now also shown that ILCs not only interact with immune cells, but ILCs also have receptors for neural peptides and thus could interact with the peripheral nervous system as well (Barrow & Colonna 2018).

Thus, ILCs are part of a very complex network of immune and tissue cells and influence the immune response by direct cell-cell contact, but also by specific production of cytokines and effector molecules. Although they represent only a small fraction of all immune cells in the body, they appear to contribute significantly to the outcome of certain diseases and are therefore of great interest for the understanding of these.

1.4.3 ILCs in *Plasmodium* and helminth infections

ILCs in *Plasmodium* infection

The first ILCs to be associated with an immune response to *P. falciparum* are NK cells, as these ILCs have been known longest and were only later classified into the group of ILCs (Ng & Engwerda 2018). To date, there are conflicting results on the importance of NK cells and ILC1s during malaria and especially CM (Burrack *et al.* 2019).

In mouse models that do not lead to ECM development, it was shown that NK cells mediate protection mainly through their ability to produce IFN-γ and TNF in response to interaction with APCs (Ng & Engwerda 2018). NK cells are also involved in the immune response against *Plasmodium* in the liver and are important for vaccine-induced protection against *P. yoelii* infection (Burrack *et al.* 2019). *In vitro* experiments showed that IFN-γ production by NK cells in response to plasmodia requires direct cell-cell contact of NK cells with iRBCs and a source of IL-12 and IL-18 such as DCs or monocytes. *In vivo*, NK cells are important for the control of parasitemia in a humanized mouse model (Chen *et al.* 2014) and it was shown that the cytotoxicity receptors of NK cells recognize the PfEMP-1 protein on RBCs and thus contribute to the lysis of infected RBCs (Mavoungou *et al.* 2007). Depletion of NK cells with anti-NK1.1 or anti-asialo GM1 in mice led to increased mortality, lower IFN-γ levels, and either increased or unchanged parasitemia during *P. chabaudi* malaria (Burrack *et al.* 2019). However, both antibodies are known to affect other cell populations (e. g. NKT cells, basophils and some T cells) as well, making it difficult to draw a definitive conclusion about the sole significance of NK cells. From studies with another protozoan parasite, *T. gondii*, it is known that helper ILC1s as well protect the host from infection with this parasite by producing IFN-γ and TNF. It is hypothesized that there may be a similar mechanism in malaria with regard to these cells due to the similarity of *T. gondii* to plasmodia, as they may help to clear infected erythrocytes by activating phagocytic cells (Ng & Engwerda 2018).

In the ECM model, NK cells were shown to be important for the induction of ECM and control of parasitemia, but the outcome here was highly dependent on the antibody used and on the mouse strain (Palomo *et al.* 2017). NK cells, like $CD8^+$ T cells, infiltrate the brain of ECM-positive mice and depletion of these cells via anti-asialo GM1 could limit T cell recruitment by reducing CXCR3 expression on T cells (Hansen *et al.* 2007). However, other studies show that depletion with anti-NK1.1 does not protect against ECM (Yañez *et al.* 1996). Therefore, it is not clear whether and to what extent NK cells are responsible for the development of ECM. Because there are no specific depletion antibodies for helper ILC1s to date, involvement of these cells in pathology is difficult to demonstrate and therefore there are no data on the role of ILC1s during ECM. Nevertheless, T-bet-deficient mice have higher parasitemia and are also partially resistant to ECM (Oakley *et al.* 2013). However, these mice are deficient in both ILC1s and Th1 cells.

Regarding ILC2s, there is preliminary evidence for their involvement in protection against ECM, as exogenous IL-33 led to the expansion of ILC2s, which in turn produced increased type 2 cytokines, preventing the development of ECM (Besnard *et al.* 2015). This mechanism is thought to be mediated mainly by a marked increase in alternatively activated macrophages and regulatory T cells following ILC2 expansion, suggesting rather an indirect influence of ILC2s on a protective immune response than a direct effect. Here, ILC2s apparently act in a complex network of immune cells. No critical role in pathology or protection against ECM has yet been demonstrated for ILC3s.

ILCs in helminth infections

The importance of ILCs during helminth infection is being investigated in several mouse models, although these are mainly models for intestinal nematodes and not extraintestinal filarial nematodes. However, general hypothesis for the involvement of ILCs in the immune response to filariae can be generated from these models.

In general, ILC2s have been identified as the most important mediators of resistance to nematodes due to their production of IL-5, IL-13, and also IL-9 (Diefenbach 2013; Spits *et al.* 2013; Elemam *et al.* 2017). During *Nippostrongylus brasiliensis* infection, ILC2s were dominant sources of IL-13, which is important for specific control of the worm (Artis & Spits 2015; Elemam *et al.* 2017; Symowski & Voehringer 2017). ILC2s

expressing the IL-25R were identified as important mediators of resistance prior to infection with *N. brasiliensis* (Spits *et al.* 2013). Also, in this model, ILC2s cooperate with $CD4^+$ T cells to mediate larvae killing in the small intestine during primary infection and also later in the lung (Symowski & Voehringer 2017). Interestingly, transfer of ILC2s into *N. brasiliensis*-infected IL-13-deficient mice resulted in partial expulsion of the worm, but not in T cell-deficient mice, suggesting that ILC2s are sufficient for primary infection, but $CD4^+$ T cells are still required for complete clearance. An important feature of the immune response to helminths is the recruitment of eosinophils (Diefenbach 2013). ILC2s are essential for this infiltration of eosinophils into the site of infection. The expression of amphiregulin by ILC2s is important during the immune response to *Trichuris muris* infection and IL-33 produced by epithelial cells during *Strongyloides venezuelensis* leads to the expansion of ILC2s (Yasuda *et al.* 2012; Zaiss *et al.* 2015) . In the *Heligmosomoides polygyrus* model, IL-4 produced by ILC2s was shown to lead to early differentiation of Th2 cells without the need for direct cell-cell contact (Symowski & Voehringer 2017). In the *Litomosoides sigmodontis* model, there are first hints that ILC2s expand during the pre-patent infection (Boyd *et al.* 2015; Neill & Fallon 2017) .

There are few studies to date on the other subpopulations of ILCs that suggest or investigate a role during helminth infections. ILC2s appear to be the most important ILCs in the immune response to helminths because they influence the type 2 immune response, interact strongly with eosinophils and alternatively activated macrophages, immune cells that have already been identified as central mediators of the immune response to helminths. Studies in the *L. sigmodontis* filarial model are few to date that address the importance of ILCs and would allow insights for human filariasis.

1.5 Aim

Malaria, including CM, and filariasis are both major health problems. Better understanding of the development of complications of both diseases represents an important factor in combating them. In particular, the immunological characteristics are of great interest, as the immune response has been shown to influence the outcome of such infections.

ILCs have only recently been identified as a distinct immune cell population. Accordingly, their role in many infectious diseases has not yet been analyzed in detail,

including malaria and filariasis. Although there is initial evidence of cell involvement in the immune response, this is contradictory in the case of malaria and very limited in the case of filariasis.

Thus, the aim of this study was to examine each ILC subpopulation during the course of a *Plasmodium* and *L. sigmodontis* infection in both susceptible and resistant/semi-susceptible mouse strains in terms of number and proportion in order to obtain hints for the involvement of these cells in the respective immune response. These data are so far lacking for various ILC subsets. To address this, various functional analyses of the respective ILC population were done concerning their activation status and their ability to produce effector molecules (IFN-γ, GzmB, IL-5) to reveal differences between mice being susceptible to infection or being protected from infection. Based on this, depletion experiments were performed that should clearly demonstrate the importance of the respective population in each model.

2. Materials & Methods

2.1 Materials

Software for analysis

Software	Company
CytExpert 6	Beckman Coulter, Brea, California, USA
Excel 2016	Microsoft, Redmond, USA
FlowJo v10	TreeStar Software
Prism 8	GraphPad, La Jolla, USA
SoftMax Pro 6.5	Molecular Devices, Sunnyvale, USA

Machines

Machine	Company
CytoFLEX S Flow Cytometer	Beckman Coulter, Brea, California, USA
Casy® TT Cell Counter + Analyser System	Schärfe Systems, Reutlingen, Germany
Centrifuge Eppendorf 5810R	Eppendorf AG, Hamburg, Germany
Centrifuge Hettich type 2004	Hettich, Tuttlingen, Germany
Clean bench HERAsafe	Kendro, Langenselbold, Germany
Ice Machine MF26	Scotsman Industries Inc., Vernon Hills, Illinois, USA
Incubator	Binder GmbH, Tuttlingen, Germany
Microplate Shaker Duomax 1030	Heidolph Instruments GmbH & Co. KG, Schwabach, Germany
Microscope Zeiss Axioskop 50	Zeiss, Göttingen, Germany
Multi-pipette (30-300 µl)	Sartorius, Göttingen, Germany
Peristaltic pump	Ismatec, Wertheim, Germany
pH meter (SevenEasy™)	Mettler Toledo, Columbus, Ohio, USA
Pipetteboy	Integra Biosciences, Zizers, Switzerland
Pipettes (0.1 – 1000 µl)	Eppendorf AG, Hamburg, Germany
Scale PCB200-2	Kern & Sohn GmbH, Balingen-Frommern, Germany
Shaker Certomat RM	Sartorius, Göttingen, Germany
Spectramax 190	Molecular Devices, Sunnyvale, USA
Vortex RS-VA10	Phoenix Instrument, Garbsen, Germany
Waterbath TW8	Julabo GmbH, Seelbach, Germany
EasyEights™ EasySep™ Magnet	STEMCELL Technologies, Vancouver, Canada

Mice

Mouse strain	Description
BALB/c	white wild type
C57BL/6	black wild type
Rag2$^{-/-}$	lack T and B cells
Ifnar1$^{-/-}$	Knock out for IFN-α receptor on all cells (Ortego *et al.* 2014)
Sigmodon hispidus	cotton rat for *L. sigmodontis* maintenance

Parasites

Parasite Strain	Date/provided by
Plasmodium berghei ANKA (PbA) Ama1 OVA clone 2.2	08.06.2016 (Heidelberg)
Litomosoides sigmodontis	IMMIP Bonn
Ornithonyssus bacoti (mite)	IMMIP Bonn

Consumables

Material	Company
BD Discardit syringes (5 & 10 ml)	BD Biosciences, Franklin Lakes, USA
CASY® cups	Omni Life Science GmbH & Co. KG, Bremen, Germany
Cell culture plates 24 wells	Greiner bio-one GmbH, Kremsmüster, Austria
Cell culture plates 6 wells	Greiner bio-one GmbH, Kremsmüster, Austria
Cell culture plates 96 wells (U-bottom)	Greiner bio-one GmbH, Kremsmüster, Austria
Cell gaze 41 µm, 1020 mm, Polyamid (PA 6.6)	Labomedic, Bonn, Germany
Centrifuge tubes 15 ml/50ml	Greiner bio-one GmbH, Kremsmüster, Austria
Deep well plates	VWR, Radnor, USA
EDTA Tubes	SARSTEDT AG & Co. KG, Nümbrecht, Germany
FACS tubes (5 ml polystyrene tubes)	Falcon by Corning Incorporated, Corning, USA
Goldenrot Animal Lancet (4 mm)	Braintree Scientific, Braintree, USA
MACS SmartStrainers	Miltenyi Biotec, Bergisch Gladbach, Germany
Microtiter plates 96 well (F-bottom, clear)	Greiner bio-one GmbH, Kremsmüster, Austria
Microtiter plates 96 well (F-bottom, high-binding)	Greiner bio-one GmbH, Kremsmüster, Austria

Object slides	Engelbrecht Medizin- und Labortechnik GmbH, Edermünde, Germany
Omnican®-F, 0,30 x 12 mm / G 30 x 1/2"", 1 ml	B. Braun, Melsungen, Germany
Parafilm®	American National Can™, Chicago, USA
Pasteur pipette (3 ml)	Ratiolab GmbH, Dreieich, Germany
Petri dishes	Greiner bio-one GmbH, Kremsmüster, Austria
Pipette tips (10 - 1000 µl)	Starlab Group, Hamburg, Germany
Reaction tubes (0.5 – 5 ml)	Eppendorf AG, Hamburg, Germany
Serological pipettes (50 ml)	Falcon by Corning Incorporated, Corning, USA
Serological pipettes (5-25 ml)	Costar by Corning Incorporated, Corning, USA
T25 cell culture flask	Greiner bio-one GmbH, Kremsmüster, Austria

Chemicals, reagents and kits

Chemical/Reagent/Kit	**Company**
Advanced RPMI 1640 medium	Gibco by life technologies Corporation, Carlsbad, USA
BSA	PAA Laboratories GmbH & Co. KG, Bremen, Germany
Buffer tablets pH 7.2 (0.63 g/l Na_2HPO_4 x 2 H_2O + 0.31 g/l KH_2PO_4)	Merck KGaA, Darmstadt, Germany
CASY TT solution	OLS OMNI Life Science GmbH & Co. KG, Bremen, Germany
Collagenase type VIII (*Clostridium histolyticum*)	Sigma Aldrich, St. Louis, USA
ConcanavalinA (ConA)	InvivoGen, San Diego, USA
DuoSet ELISA kit	R&D Systems, Minneapolis, USA
EasySep™ Mouse NK Cell Isolation Kit	StemCell Technologies, Vancouver, Canada
eBioscience™ Cell Stimulation Cocktail (plus protein transport inhibitors) (500X)	Invitrogen, Carlsbad, USA
EDTA	Roth, Karlsruhe, Germany
Ethanol 96%	Merck KGaA, Darmstadt, Germany
FBS	PAN Biotech, Aidenbach, Germany
Formaldehyde	Sigma-Aldrich, St. Louis, USA
Foxp3 Transcription Factor Staining Buffer Kit	Invitrogen by Thermo Fisher Scientific, Waltham, USA
Giemsa´s azur-eosin methylene blue solution	Merck KGaA, Darmstadt, Germany

Golgi Plug Protein Transport Inhibitor (Brefeldin A)	BD Biosciences, Franklin Lakes, USA
Golgi Stop Protein Transport Inhibitor (Monensin)	BD Biosciences, Franklin Lakes, USA
H_2SO_4	Merck KGaA, Darmstadt, Germany
IMDM medium	Gibco by life technologies Corporation, Carlsbad, USA
Ionomycin	Sigma Aldrich, St. Louis, USA
Isoflurane	Piramal Health Care, Mumbai, India
Ketamine (10%)	bela-pharm GmbH, Vechta, Germany
L-Glutamine (L-Glut) 200 mM	Gibco by life technologies Corporation, Carlsbad, USA
Methanol 100%	Merck KGaA, Darmstadt, Germany
OneComp eBeads™ Compensation Beads	invitrogen by Thermo Fisher Scientific, Waltham, USA
Ovalbumin$^{254-264}$ (SIINFEKL, S8L-peptide)	Pineda, Berlin, Germany
PBS powder	Gibco by life technologies Corporation, Carlsbad, USA
Penicillin/Streptomycin (Pen/Strep) 10.000 Units/ml, 10.000 µg/ml	Gibco by life technologies Corporation, Carlsbad, USA
Percoll	GE Healthcare Life Sciences, Chalfont St Giles, GB
Phorbol-12-myristat-13-acetat (PMA)	InvivoGen, San Diego, USA
Rat IgG from rat serum	Sigma-Aldrich, St. Louis, USA
RBC lysis buffer multispecies (10 x)	eBioscience by Thermo Fisher Scientific, Waltham, USA
Ready-Set-Go! ELISA kits	eBioscience by Thermo Fisher Scientific, Waltham, USA
Recombinant Murine IL-15	Peprotech, Rocky Hill, USA
Rompun/Xylazine (2%)	Bayer AG, Leverkusen, Germany
Tween20	Sigma-Aldrich, München, Germany

Buffers and solutions

Buffer/solution	**Preparation**
1x PBS	47.75 g PBS powder in 5 l dH_2O
30/70% Percoll solution	1x PBS + required % Percoll
4% Formaldehyde in PBS	1x PBS, 4% Formaldehyde, stored at RT
60% Ethanol	96% Ethanol diluted in dH_2O
Blocking solution	1x PBS + 1% BSA + Rat IgG (1:1000 diluted)
Cell culture medium	Advanced RPMI 1640 medium + 10% FBS + 1% L-Glut + 1% Pen/Strep
Collagenase buffer	300 µl collagenase stock + 30 ml 1x PBS

Collagenase stock	50 mg/ml collagenase type VIII diluted 1:125 in 1x PBS, stored at -20 °C
Complete IMDM medium	IMDM medium + 10% FBS + 1% L-Glut + 1% Pen/Strep
Digestion medium	RPMI 1640 + 0.5 mg/ml collagenase
EasySep™ buffer	PBS + 2% FBS + 1 mM EDTA
EDTA stock solution	200 mM EDTA in dH_2O
ELISA wash buffer	0.05% Tween 20 in 1x PBS, pH 7.2
FACS buffer	1x PBS, 1% FCS
Fc block	FACS buffer + Rat IgG (1:1000 diluted)
Fix/Perm (FoxP3 Transcription factor staining buffer kit)	1 part reagent A + 3 parts reagent B
Giemsa buffer	1 buffer tablet in 1 l H_2O
Hinkelmann solution	0.5% eosin Y, 0.5% phenol, 0.185% formaldehyde in distilled water
Ketamine/Xylazine (4:1)	4 parts Ketamine, 1 part Rompun/Xylazine
MACS buffer	1x PBS, 1% FCS, 2 mM EDTA
Ovalbumin$^{254-264}$ (SIINFEKL, S8L-peptide) stock solution	5 mM/20 mM in DMSO, stored at -20 °C
Perm buffer	1 part wash buffer concentrate + 9 parts PBS/1% BSA
RBC lysis buffer 1x	1:10 diluted in sterile ddH2O, stored at 4 °C
Stop solution for ELISA	1 M H_2SO_4 in dH2O, stored at RT

FACS antibodies

Fluorochrome	**Antigen**	**Clone**	**Company**
BV510	CD11b	M1/70	Biolegend
APC	CD19	eBio1D3	invitrogen
APC-Cy7	CD3	15A2	Biolegend
BV605	CD4	RM4-5	Biolegend
FITC	CD45	30-F11	Biolegend
PerCP-Cy5.5	CD45	30-F11	Biolegend
PE	CD49a (a1 integrin)	HMa1	Biolegend
Alexa Fluor 488	CD49b (a2 integrin)	HMa2	Biolegend
PE	CD8	53-6.7	Biolegend
PE	CD90.2 (Thy1.2)	53-2.1	Biolegend
PE-Cy7	GATA-3	L50-823	BD Biosciences
BV605	IFN-γ	XMG1.2	Biolegend
APC	IL-33R (ST2)	DIH9	Biolegend
PE	IL-5	TRFK5	invitrogen
Pacific Blue	Lineage Cocktail	various	Biolegend
APC-Cy7	Ly6C	HK1.4	Biolegend
BV421	Ly6G	1A8	Biolegend
APC-Cy7	NK1.1	PK136	Biolegend

PE-Cy7	NKp46 (CD335)	29A1.4	Biolegend
PE	RORγt	AFKJS-9	invitrogen
BV510	Sca-1 (Ly6A/E)	D7	Biolegend
APC-Cy7	Siglec-F	E50-2440	BD Biosciences
PE	Siglec-F	E50-2440	Biolegend
APC	T-bet	4B10	Biolegend
Alexa Fluor 700	TCRβ	H57-597	Biolegend

Depletion antibodies

Antibody	**Company**	**Dose per injection**
*InVivo*MAb mouse IgG2a isotype control; unknown specificity, clone C1.18.4	BioXCell	600 µg
*InVivo*MAb anti-mouse NK1.1, clone PK136	BioXCell	600 µg
*InVivo*MAb rat IgG2b isotype control, anti-keyhole limpet hemocyanin, clone LTF-2	BioXCell	500 µg
*InVivo*MAb anti-mouse Thy1.2 (CD90.2), clone 30H12	BioXCell	500 µg
Mouse Siglec-F Antibody, AF1706	R&D Systems	1.5 µg/g body weight

2.2 Methods

Animals and ethical statement

Experiments were conducted according to the Directive 2010/63/EU and animal protocols were approved by the local authorities (Landesamt für Natur, Umwelt und Verbraucherschutz Nordrhein-Westfalen).

C57BL/6 wildtype (WT) and BALB/c WT mice were ordered from Janvier (Le Genest-Saint-Isle, France). Genetically modified mouse strains (*Ifnar1*$^{-/-}$, *Rag2*$^{-/-}$) and cotton rats (*Sigmodon hispidus*) were bred in the House of Experimental Therapy (HET) of the University Hospital Bonn or in case of *Rag2*$^{-/-}$ and cotton rats in the animal houses of the Institute of Medical Microbiology, Immunology and Parasitology (IMMIP) of the University Hospital Bonn. All mouse strains were kept in the animal houses of the Institute of Medical Microbiology, Immunology and Parasitology (IMMIP). Water and food were provided *ad libitum*. Nestlets and wooden sticks were given into the cages to create an enriched environment.

Plasmodium strain source and storage

The parasite stocks were kindly provided by Dr. Ann-Kristin Müller from Heidelberg. The experimental animals and stock mice were infected with the *Plasmodium berghei* ANKA (PbA) Ama1 OVA clone 2.2 strain with surface expression of OVA antigen presented before (Scheunemann, Reichwald *et al.* submitted). The blood stocks were stored in liquid nitrogen until using them for experimental infection.

Infection procedure *Plasmodium berghei* ANKA

Two C57BL/6 mice (stock mice) were intraperitoneally (i. p.) infected with 200 µl of thawed *Plasmodium* stock (PbA Ama1 OVA clone 2.2). 4 days post infection (4 dpi) the parasitemia was determined by performing a blood smear and staining it with Giemsa solution (see below). The red blood cells (RBCs) were counted in a total dilution of 1:40,000 in 10 ml CASY TT solution with the CASY TT. The infectious dose was prepared by taking fresh blood from the tail of the stock mouse with the highest parasitemia and diluting it in 1 x phosphate buffered saline (PBS) to 5e+04 infected red blood cells (iRBCs) in 100 µl injection volume per mouse. The dose was injected intravenously (i. v.) into the tail vein of experimental animals after disinfection with ethanol and exposure of the tail to a heat lamp.

Rapid Murine Coma and Behaviour Scale (RMCBS)

3, 5 and 6 dpi the PbA-infected mice were scored according to the Rapid Murine Coma and Behaviour Scale (RMCBS) (Carroll *et al.* 2010). Ten parameters in the categories coordination, exploratory behaviour, strength and tone, reflexes and self-preservation and hygiene-related behaviour were determined for each mouse separately and valued with 0 (lowest score) to 2 (highest score). The maximal score of 20 indicates a healthy mouse (naive mice). Mice with scores below 8 were considered to suffer from ECM as they show first neurological symptoms. Mice reaching a total score of 5 and below before the analysis were sacrificed before the experiment due to ethical reasons.

Determination of parasitemia

A small piece of the tail was cut off and one drop of blood (~ 5 µl) was given onto a glass slide. With a second glass slide the blood smear was performed and was airdried. The blood smear was fixed with 100% methanol. 1 ml Giemsa solution was diluted in 19 ml Giemsa buffer and the slides were stained for 22 min with the diluted Giemsa solution. The slides were then rinsed with tap water and dried with a hairdryer. Using the Microscope Zeiss Axioskop 50 (magnification: 1000x) the total number of RBCs was counted in six sections as well as the number of iRBCs among them to calculate the percentage of parasitaemia according to the formula:

$$\frac{iRBCs}{RBCs}\ x\ 100 = parasitemia\ in\ \%$$

Extracellular parasites were excluded in the calculation of the parasitemia.

Infection procedure *Litomosoides sigmodontis*

L. sigmodontis was passed through the cotton rat *Sigmodon hispidus* (bred at the Institute of Medical Microbiology, Immunology and Parasitology, University Hospital Bonn, Germany, originally obtained from The Jackson Laboratories, US) for maintenance as previously described (Hübner *et al.* 2009). Prior to infection of the experimental mice, *Ornithonyssus bacoti* mites were fed overnight on microfilaremic (~1000 Mf/µl blood) cotton rats. The bedding including the mites was collected, given to an Erlenmeyer flask and placed in an incubator for 12 to 14 days at 27 °C and 80% humidity. The experimental mice were then infected by exposure to infectious L3 larvae via the bite of these mites. All mice of one experiment were exposed to the same

population of mites to ensure equal infection levels. The infected animals were scored once per week by measuring the body weight and analysing their behaviour and appearance. Scores were assigned from A to C. A score of “A” requires daily observations and represents an animal with minor abnormalities, e. g. loss of fur. A score of “B” refers to an animal that shows more severe signs of weight loss, abnormalities in social behaviours or injuries. These animals have to be presented to the supervisor of the animal experiments. Animals with a “C” score present severe injuries, lost more than 20% of weight or do show pain signs and thus have to be eliminated immediately. Experimental mice were euthanized and analysed at 9, 30, 63 and 70 dpi.

Determination of worm burden and worm length

Worms were collected during pleura lavage (described below) and given into a 6-well plate with 1x PBS. The worm count of male and female worms for each mouse was determined by checking for the vulva of female worms or spiculae of male worms using a light microscope (magnification: 250x). The length of the worms was determined with a ruler.

Determination of microfilarial load

To determine the number of microfilariae in the peripheral blood of *L. sigmodontis* infected mice, 50 µl blood were taken from the *Vena facialis* on day 50, 57, 63 and 70 pi using an animal lancet and given into an EDTA tube. 50 µl blood were then mixed with 1 ml RBC lysis buffer and centrifuged for 5 min at 400xg and RT. The supernatant (SN) was discarded and 10 µl of the pellet were given onto a glass slide. The microfilariae were counted in the whole slide. The procedure was repeated until the whole pellet was counted.

Analysis of female embryogenesis

The female worms from C57BL/6 and *Rag2*$^{-/-}$ mice were separated from the males and 5 female worms, if present, per mouse were placed in 4% formaldehyde (diluted in 1x PBS) for 24h. The formaldehyde was removed from the tube and replaced with 60% Ethanol. The worms were stored at room temperature (RT) until determination of the embryonic stages (egg, morula, pretzel, stretched Mf). The worms were homogenized in 80 µl PBS and 20 µl of Hinkelmann solution (0.5% eosin Y, 0.5% phenol, 0.185%

formaldehyde in dH_2O). If necessary 1:10 and 1:100 dilutions were prepared in Hinkelmann solution. Embryonic stages were determined and counted in 10 µl under a light microscope (100x magnification).

Depletion of NK cells in PbA-infected mice

C57BL/6 WT and *Ifnar1*$^{-/-}$ mice received 600 µg anti-NK1.1 (*InVivo*MAb anti-mouse NK1.1, clone PK136 by BioXCell) or Isotype control (*InVivo*MAb mouse IgG2a isotype control; unknown specificity, clone C1.18.4 by BioXCell) in 200 µl PBS i. p. on day -2, +1 and +4 around PbA infection (d0). Mice were infected with PbA on day 0 as described above and ECM development was determined on day 6. *Ex vivo* analyses, i. e. spleen and brain cell isolation, flow cytometry and enzyme-linked immunosorbent assay (ELISA) analyses were subsequently performed on day 6 pi.

Depletion of eosinophils in PbA-infected *Ifnar1*$^{-/-}$ mice

C57BL/6 WT and *Ifnar1*$^{-/-}$ mice were infected with PbA as described above. *Ifnar1*$^{-/-}$ mice received 1.5 µg/g body weight anti-siglecF (R&D System AF1706) in 100 to 150 µl PBS i. p. on day +3, +4 and +5 after PbA infection. ECM development was determined on day 6. *Ex vivo* analyses were also performed on day 6 pi.

Depletion of ILC2s in *L. sigmodontis* infected *Rag2*$^{-/-}$ mice

C57BL/6 and *Rag2*$^{-/-}$ mice were naturally infected with *L. sigmodontis* as it was already described. On day 26, 27 and 28 pi, the timepoint where larvae moult into adult worms, *Rag2*$^{-/-}$ mice received 500 µg anti-CD90.2 (*InVivo*MAb anti-mouse Thy1.2 (CD90.2), clone 30H12 by BioXCell) or isotype control (*InVivo*MAb rat IgG2b isotype control, anti-keyhole limpet hemocyanin, clone LTF-2 by BioXCell) in 200 µl PBS i. p.. C57BL/6 mice served as WT and untreated controls and thus did not receive depletion antibodies. *Ex vivo* analyses, i. e. pleura lavage, lung and worm isolation, flow cytometry and ELISA analyses, were performed on day 63 pi.

Anaesthesia and killing of mice

In experiments where a perfusion of mice was required for brain dissection (6 dpi PbA experiments), the experimental mice were anaesthetized i. p. with a 4:1 Ketamine-Rompun mixture (0.01ml/10g body weight) and checked for pain recognition with a tweezer. They were fixated for dissection with a canula, were opened to the heart and perfused for 5 min with PBS through the left ventricle.

In PbA experiments where no perfusion was required, the mice were anaesthetized with isoflurane and killed with cervical dislocation after anaesthesia. Then the mice were fixated for dissection with a canula and were opened for organ dissection.

In experiments where pleura lavage was performed (all *L. sigmodontis* experiments) the mice were killed with an overdose of isoflurane as cervical dislocation would lead to bleeding into the pleural cavity which contaminates infiltrated pleural cells with blood cells.

Preparation of tissues and blood

Blood and serum

The blood of the experimental mice was taken from the *Vena fascialis* by using an animal lancet. The blood was stored for at least 2h at RT to allow clotting. The samples were then centrifuged for 10 min at RT and 6000xg, the serum was carefully collected and frozen at -20 °C until usage for ELISA analysis.

Lymphocyte preparation from spleen

The spleens were isolated and given into a 15-ml-falcon with 3 ml collagenase buffer. They were put into a petri dish and perfused *in vitro* with collagenase buffer to distribute the enzyme in the whole tissue by using a syringe. Then the organs were cut into pieces and incubated in collagenase buffer for 20 min at 37 °C on a shaker. 10 ml magnetic cell separation (MACS) buffer were added to the digested cells and a single cell suspension was prepared by filtering the cells through a SmartStrainer. The suspensions were centrifuged for 5 min at 4 °C and 400xg. The pellet was taken up in 500 µl RBC lysis buffer, the cells were incubated at RT for 5 min, washed with 5 ml MACS buffer (add MACS buffer and centrifuge 5 min at 4 °C and 400xg) before taking the cells up in cell culture medium (RPMI 1640 + 10% FCS + 1% L-Glutamin + 1% Pen/Strep). The cell suspensions were counted with CASY TT as described below and adjusted to a cell concentration of 1e+07 cells/ml with cell culture medium.

Lymphocyte preparation from mesenteric lymph nodes (mLN)

The gut of each mouse was separated in order to find the mesenteric lymph nodes (mLNs). The LNs were isolated with a scissor and collected in a petri dish with cell culture medium. Then the tissue was put into a 15 ml tube with 3 ml collagenase buffer and in a petri dish the mLNs were cut into pieces. Afterwards the mLNs were incubated

on a shaker at 37 °C and 200 rpm for 20 min. 10 ml MACS buffer were added and a single cell suspension was prepared by filtering the cells through a metal sieve. The cells were centrifuged at 4 °C and 400xg for 5 min, 0.5 to 1 ml cell culture medium was added and the cells were counted with CASY TT. The cell concentration was adjusted to 1e+07/ml using cell culture medium.

Enrichment of brain leukocytes/lymphocytes

The mouse head was removed and the brains of 6 days PbA-infected animals were collected in 3 ml collagenase buffer. The organ was cut into pieces and incubated for 20 min at 37 °C and 200 rpm on a shaker. 10 ml MACS buffer were added to the cells and a single cell suspension was prepared by using a metal sieve. The cells were then centrifuged for 5 min at 4°C and 400xg. The pellet was resuspended in 30% Percoll (RT) and underlaid with 70% Percoll (RT). The samples were centrifuged for 20 min at RT and 530xg (without brake). The upper phase was discarded and the interphase collected into a fresh tube. The cells were washed with 30 ml MACS buffer and the SN was discarded until 200 µl were remaining. Cells were counted with CASY TT.

Pleura lavage, worm isolation and collection of pleura samples for ELISA

Mice were opened without destroying the diaphragm. A little hole was cut in the upper right part of the diaphragm and the pleural cavity was washed with 1 ml cold, sterile PBS and a Pasteur pipette (pleura lavage). The fluid was passed through cell gaze (41 µm) to hold back the worms and the first 1 ml was given into a 1.5 ml tube. The used gaze was transferred onto a 15 ml tube and the procedure was repeated until a final volume of at least 5 ml of cell suspension.

The collected worms on the gaze were given into a 6-well plate with PBS and characterized as described above.

The 1.5 ml tubes were centrifuged for 5 min at 4 °C and 400xg. The SNs were given into new 1.5 ml tubes and frozen at -20 °C until ELISA analysis. The cell pellets were transferred into their corresponding 15 ml tubes.

The isolated cells were centrifuged for 5 min at 4 °C and 400xg, the SNs were discarded and the pellets were resuspended in 500 µl RBC lysis buffer. After 5 min incubation at RT the reaction was stopped with 10 ml MACS buffer and the cells were

centrifuged again. Then the pellets were taken up in 2 ml PBS and counted with CASY TT.

Lymphocyte preparation from lung

The thorax was completely opened, the lungs were carefully removed and given into a petri dish with PBS to remove the blood. The organs were cut in two pieces. The lung was put into a 15 ml tube with 3 ml digestion medium (RPMI 1640 + collagenase), given into a petri dish and cut into small pieces. The organs were incubated on a shaker at 37 °C and 200 rpm for 45 min. The enzymatic reaction was stopped by adding 1 ml fetal bovine serum (FBS) heat-inactivated (hi). After adding 3 ml of cell culture medium a single cell suspension was prepared by filtering the cells through a SmartStrainer. The cells were centrifuged for 5 min at 4 °C and 400xg. The pellet was taken up in 1 ml RBC lysis buffer and incubated at RT for 5 min. The reaction was stopped with 10 ml MACS buffer and the cells were centrifuged at 4 °C and 400xg for 5 min. The supernatant was discarded, the pellet was resuspended in 5 ml cell culture medium and the cells were counted with CASY TT.

Isolation and *in vitro* stimulation of NK cells from spleens

For the isolation of NK cells from spleens of naive and PbA-infected mice the StemCell EasySep™ NK cell isolation kit, 5 ml polystyrene tubes and the EasyEights magnet were used. After anaesthesia of mice with Ketamin/Xylazin as described above the spleen was removed before perfusion procedure as the isolation of NK cells still requires the RBCs. The spleen was taken out with a scissor, given into 3 ml PBS and cut into pieces. 10 ml of MACS buffer were added and a single cell suspension was prepared by passing the organ through SmartStrainers. The cells were centrifuged for 5 min at 4 °C and 400xg. 5 ml of MACS buffer were added and the cells were counted with CASY TT as described below. The suspension was adjusted to 1e+07 cells/ml with MACS buffer and used for isolation. 5e+07 splenocytes per mouse were used and the isolation was performed according to the manufacturer's protocol (STEMCELL Technologies Inc. 2020). The isolated cells were centrifuged and adjusted to a concentration of 2e+06 cells/ml. 2e+05 cells (= 100 µl of cell suspension) of each sample were plated in dublicates into a 96-well U-bottom cell culture plate, centrifuged for 5 min at 4 °C and 400xg. The pellets were resuspended in 150 µl complete IMDM medium with 200 ng/ml IL-15 or in complete IMDM medium without stimulus

(unstimulated controls). The cells were incubated for 24 h at 37 °C and 5% CO_2. The next day the SNs were harvested by centrifuging the plate for 5 min at 400xg and transferring the SNs into a 96-well non-binding plate. SNs were analysed for IFN-γ, GzmB and IL-10 via ELISA as described below. The cells were given into a new plate and stained for FACS analysis of their activation status (NKp46 and NK1.1 expression) as described below.

Counting of cells

All cell suspensions were counted using the Casy® TT Cell Counter. 10 µl of every cell suspension were mixed with 10 ml CASYton solution (1:1000 dilution) in a CASY cup. For all tissue cells (splenocytes, mLNs and lung) the spleen program was used and the TML value was taken as the value of cells/ml. For pleura cells the BMDC program was used and the TML value was taken as the value of cells/ml. For blood cells, the blood program was used and CML as well as TML were recorded as they were subtracted for the calculation of the RBCs/ml.

Generation of splenocyte supernatants

For ELISAs, cell culture SNs of splenocytes were prepared. 1e+06 splenocytes were plated in triplicates in 200 µl cell culture medium (RPMI 1640, 10% FCS, 1% Pen/Strep, 1% L-Glutamine) into a 96-well cell culture plate and cultured at 37 °C and 5% CO_2 for 24 h.

After 24 h the cell culture plates were centrifuged at 400xg for 5 min, the SNs were transferred into a 96-well F-bottom plate (clear surface) and frozen at -20 °C until analysis.

Enzyme-linked immunosorbent assay (ELISA)

The generated SNs as well as the pleura samples (1^{st} ml of pleura lavage) were taken for cytokine detection via ELISA. Splenocyte samples had to be diluted 1:3 for IFN-γ ELISA in ELISA diluent. The Ready-SET-Go!™ kits (for detection of IFN-γ, IL-5, IL-10 and IL-13 levels) by eBioscience (Fisher Scientific 2017) and the DuoSet Kit (for detection of GzmB levels) by R&D Systems (R&D Systems 2017) were used, whereas flat-bottom, high-binding microtiter plates 96-well by Greiner GmbH served as ELISA plates.

For the eBioscience ELISAs all provided solutions as well as the recommended dilutions in the corresponding kits were used, 1M H_2SO_4 served as stopping solution and 1x PBS + 0.05% Tween20 was used as wash buffer. The protocol was followed as the manufacturers recommend.

For the GzmB DuoSet ELISA the coating antibody was diluted according to the R&D protocol in 1x PBS and incubated on the plate at 4 °C overnight (ON). All other steps of the assay procedure as well as the reagents except for the Avidin-HRP were adapted from the eBioscience Ready-SET-Go! ELISA protocol including also the washing steps, the washing solution as well as all incubation times. For blocking and dilution of standards, detection antibodies and Avidin-HRP 1x ELISA diluent provided by the Ready-SET-Go! ELISA kits by eBioscience were used. Tetramethylbenzidine (TMB) substrate (50 µl/well) was also taken from eBioscience kits. 1M H_2SO_4 served as stopping solution as well.

All plates were read at 450 nm and 570 nm with Spectramax 190 by subtracting the values of the latter wavelength from the first.

Flow cytometry

Surface staining procedure

A mastermix of all surface antibodies was prepared in fragment crystallizable (Fc) block (FACS buffer + Rat IgG 1:1000 diluted) according to the dilutions 1:100, 1:200 or 1:300. The fluorescence minus one (FMO) controls were also prepared as master-mixes in Fc Block according to the same dilutions. A part of the cells of each sample and organ was pooled into one tube for FMOs and unstained controls. 1e+06 cells (for brains all cells available were used) were pipetted into a 96-well U-bottom plate. The cells were centrifuged 5 min at 4 °C and 400xg. The SN was discarded and the prepared master-mixes were added in a total volume of 50 µl/well. The unstained controls were resuspended in 50 µl Fc block. The FMO controls received their corresponding FMO master-mix (50 µl/well). The samples were incubated for 20 min in the dark in the fridge. They were washed twice with 150 µl FACS buffer and resuspended in 150 µl MACS, filtered through gaze and stored in the fridge until measurement.

Intracellular staining procedure – transcription factors

In case of intracellular staining of transcription factors (T-bet, GATA-3, RORγt), in addition to surface staining, 1e+06 cells (for brains all cells available were used) per sample were given into a 96-well U-bottom plate. For FMOs and unstained controls a part of the cells of each sample and organ was pooled into one tube. The cells were centrifuged for 5 min at 400xg and 4 °C. 200 µl Fixation/Permeabilization (Fix/Perm) were given to each sample and the cells were fixed for 20 min at RT. The cells were centrifuged again and resuspended in 200 µl of blocking buffer (PBS/1% bovine serum albumin (BSA) + 1:1000 Rat IgG). The next day the cells were centrifuged and permeabilized with 200 µl/sample Perm buffer for 20 min at RT. In the meantime, the antibody master-mixes (for samples and FMOs) were prepared in Perm buffer (surface and intracellular antibodies together) according to the desired dilutions. After centrifugation 50 µl master mix per sample were added to the cells. For unstained controls 50 µl Perm buffer were added and the FMO controls received their corresponding FMO master-mix. The cells were incubated for 45 min at 4 °C in the dark. Afterwards the cells were washed twice with 150 µl Perm buffer (add Perm buffer and centrifuge for 5 min at 400xg and 4 °C), resuspended in 150 µl MACS buffer, filtered through gaze and stored in the fridge until measurement.

Intracellular staining procedure - cytokines

In case of intracellular staining of cytokines (IFN-γ and IL-5), in addition to surface and transcription factor staining, 1e+06 cells (for brains all cells available were used) per sample were given into a 96-well U-bottom plate. For FMOs and unstained controls a part of the cells of each sample and organ was pooled into one tube. The cells were centrifuged for 5 min at 400xg and 4 °C. For IFN-γ staining in PbA experiments the cells were restimulated with 1 µM SIINFEKL peptide (peptide of Ovalbumin which is expressed by the PbA strain) and treated with Golgi Plug/Stop (0.8 µl/ml medium) in 200 µl cell culture medium/well for 4 h at 37 °C before the staining procedure. For GzmB staining in PbA experiments the cells were treated with only Golgi Plug/Stop (0.8 µl/ml medium) in 200 µl cell culture medium/well for 4h at 37 °C. For IFN-γ and IL-5 staining in *L. sigmodontis* experiments the cells were restimulated with 1x eBioscience Cell Stimulation Cocktail plus protein transport inhibitors (containing PMA, Ionomycin, Brefeldin and Monensin) in 200 µl/well complete IMDM medium or only

received Brefeldin A and Monensin (Golgi Plug/Stop) for 3 h at 37 °C. As a further control two more plates were prepared with cells restimulated for 3 h and 72 h with 50 ng/ml PMA and 1 µg/ml Ionomycin alone but without protein transport inhibitors in order to see whether the cells are actively secreting IL-5 and IFN-γ upon restimulation. The SNs were taken for ELISA analysis. After the restimulation the cells prepared for flow cytometric analysis were centrifuged and 200 µl Fix/Perm were given to each sample and the cells were fixed for 20 min at RT. The cells were centrifuged again, the SN was discarded, 200 µl of blocking (PBS/1% BSA + 1:1000 Rat IgG) were added to the pellet and the cells were incubated overnight at 4 °C. The cells were centrifuged and permeabilized with 200 µl/sample Perm buffer for 20 min at RT. In the meantime, the antibody master-mixes (for samples and FMOs) were prepared in Perm buffer (surface and intracellular antibodies together) according to the desired dilutions. After centrifugation 50 µl master-mix per sample were added to the cells. For unstained controls 50 µl Perm buffer were added and the FMO controls received their corresponding FMO master-mix. The cells were incubated for 45 min at 4 °C in the dark. Afterwards the cells were washed twice with 150 µl Perm buffer (add Perm buffer and centrifuge for 5 min at 400xg and 4 °C), resuspended in 150 µl MACS buffer, filtered through gaze and stored in the fridge until measurement.

Measurement and analysis

The samples were measured with the Beckman Coulter CytoFLEX S by using the plate reader. For the automatic compensation the oneComp Beads by Thermo Fisher Scientific were used. For 3 samples one drop of these beads were mixed with 300 µl FACS buffer. 100 µl of this mixture were given into one FACS tube and the corresponding antibody was added in the desired dilution. After an incubation of 5 min at RT in the dark 100 µl FACS buffer were added to the beads and they were measured with Beckman Coulter CytoFLEX S. FACS data were analysed with FlowJo version 10 by Treestar Software. Expression levels of cytokines, transcription factors and activation markers (NK1.1 and NKp46 for NK cells) were analysed by calculating the geometric mean of fluorescence intensity (GMFI).

Statistical analysis

Data were organised with Microsoft Excel 2016. Cell counts and frequencies were calculated with Microsoft Excel 2016. Data analysis was performed by using GraphPad

Prism 8. For comparison of 3 or more groups non-parametric Kruskal-Wallis-Test was used as well as the Dunn's post-test. For comparison of 2 groups non-parametric Mann-Whitney-Test was used. For correlation analysis non-parametric Spearman correlation was used. Spearman test for heteroscedasticity was performed, only data failing the test for heteroscedasticity were pooled. For the analysis of microfilariae over time Mixed-effects analysis or Two-Way ANOVA with Bonferroni multiple comparison test was performed. Error bars represent the median with interquartile ranges. A p-value of <0.05 was considered to be significant.

License for Servier Medical Art material

For the creation of the experimental setup graphs, the spleen, brain, lung and lymphocyte pictures material from Servier Medical Art (https://smart.servier.com/) was used according to their following license: Creative Commons License (https://creativecommons.org/licenses/by/3.0/), Attribution 3.0 Unported (CC BY 3.0). Changes of the pictures were indicated under the figures if necessary.

3. Results

3.1 Identification of ILC subsets via flow cytometry

Although ILCs can be found in almost every lymphoid and non-lymphoid organ (Artis & Spits 2015; Gasteiger *et al.* 2015), there is a tissue-specific distribution of the individual ILC subsets (Flores-Borja *et al.* 2016). For example, ILC1s are found primarily in the liver (Jiao *et al.* 2016), ILC2s are particularly enriched in the lung (Ignacio *et al.* 2017), and ILC3s are found in the intestinal tract and mesenteric lymph nodes (Chu *et al.* 2018). Nevertheless, compared with other immune cell populations, ILCs are a cell population which accounts for a small proportion of the total number of all immune cells in an organ (Flores-Borja *et al.* 2016). Therefore, it is not straightforward to reliably find and characterize these cells in a flow cytometric analysis. After each gate, significant amounts of cells that can be further analyzed are lost, so that the resolution loss increases with deep gating, leading to the risk that the few remaining cells due to low ILC numbers in general can no longer be unambiguously identified. It is therefore of great importance to establish a functional staining panel including a reliable gating strategy to ensure an unambiguous identification of each ILC population in the subsequent analyses.

3.1.1 ILC1s and NK cells

Usually a gating strategy is established in such a way that all subsets can be identified with a single staining panel. This saves antibodies and it allows parallel analysis of multiple subsets. However, since the loss of resolution is particularly pronounced in the case of ILCs, due to their small number, it was decided to use one staining panel per subset in order to identify them unambiguously by using multiple markers.

For the characterization of ILC1s and NK cells (Fig. 6), the larger immune cells (granulocytes and monocytes) were initially excluded in the first gate and only the lymphocytes were used for further analysis. This was found to minimize the loss of resolution in further analysis. Subsequently, the $CD45^+$ cells were gated and these were analyzed for their lineage marker (CD3, Ly6C/Ly6G, CD11b, B220/CD45R, TER119) and NKp46 expression. In the gate of the Lin^+ $NKp46^+$ cells, CD49b and T-bet were used to identify the Lin^+ ($CD11b^+$) NK cells. In the gate of Lin^- $NKp46^+$ cells, $CD49b^+$ $CD49a^-$ $T\text{-}bet^+$ Lin^- ($CD11b^-$) NK cells were found as well as $CD49b^-$ $CD49a^+$

T-bet⁺ ILC1s. The gates were set by using an appropriate FMO to ensure that there were indeed positive signals in each case.

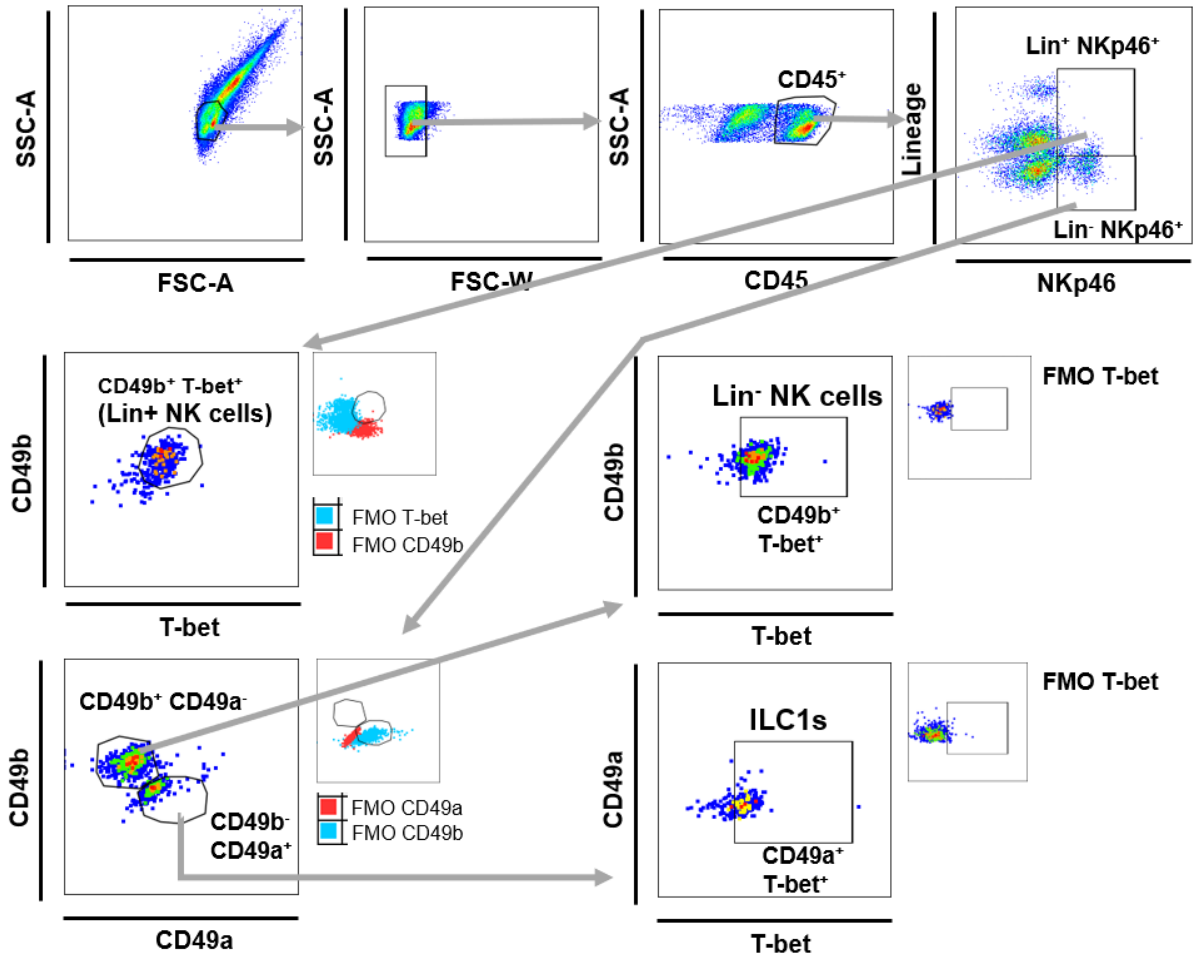

Figure 6: Gating strategy for the identification of ILC1s and NK cell subsets. The gating strategy is shown exemplarily in the lung of a *L. sigmodontis*-infected BALB/c mouse. The cells were gated on CD45⁺ lymphocytes whereas granulocytes and monocytes were excluded in the first gate to increase resolution. ILC1s were identified as CD45⁺ Lin⁻ NKp46⁺ CD49b⁻ CD49a⁺ T-bet⁺, Lin⁺ NK cells were identified as CD45⁺ Lin⁺ NKp46⁺ CD49b⁺ T-bet⁺ and Lin⁻ NK cells were identified as CD45⁺ Lin⁻ NKp46⁺ CD49b⁺ CD49a⁻ T-bet⁺. The gates were set by using FMOs. The gating strategy was adapted for every organ which was analysed later on.

It was useful to distinguish between the two NK cell subsets, as the Lin⁺ NK cells in particular became interesting in the later analyses. They are the NK cells with the highest effector potential (Walzer & Vivier 2011).

The gating strategy shown could be used in all further analyses and was adapted for every organ which was analyzed in the experiments with PbA and *L. sigmodontis*. The respective subsets could be identified reliably and even further expression analyses were possible by using the staining panel and adding for example antibodies against cytokines such as IFN-γ.

3.1.2 ILC2s

For the identification of ILC2s (Fig. 7), the larger cells (granulocytes and monocytes) were again initially excluded in the first gate and only the lymphocytes were further analyzed, as this minimized the loss of resolution. Subsequently, the ILC2s were identified in the CD45$^+$ gate.

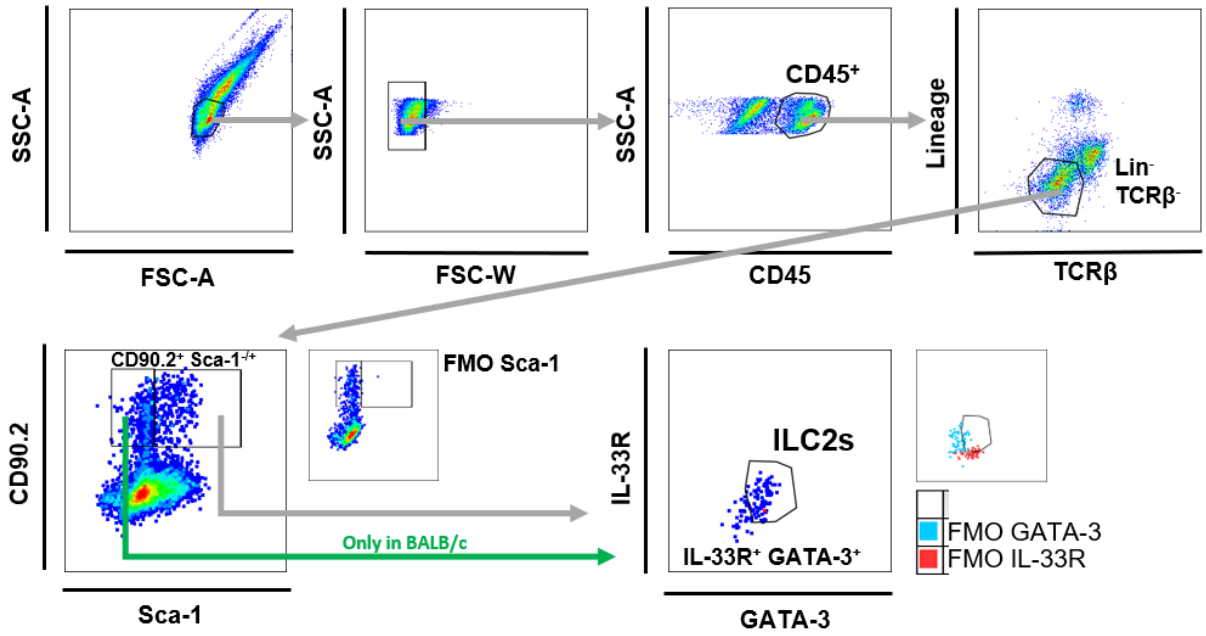

Figure 7: Gating strategy for the identification of ILC2s. The gating strategy is shown exemplarily in the lung of a *L. sigmodontis*-infected C57BL/6 mouse. The cells were gated on CD45$^+$ lymphocytes whereas granulocytes and monocytes were excluded in the first gate to increase resolution. ILC2s of BALB/c mice were identified as CD45$^+$ Lin$^-$ TCRβ$^-$ CD90.2$^+$ Sca-1$^{+/-}$ IL-33R$^+$ GATA-3$^+$, ILC2s of C57BL/6 mice were identified as CD45$^+$ Lin$^-$ TCRβ$^-$ CD90.2$^+$ Sca-1$^+$ IL-33R$^+$ GATA-3$^+$. The gates were set by using FMOs. The gating strategy was adapted for every organ which was analysed later on.

Lin$^-$ TCRβ$^-$ cells were gated first excluding the T cells (Lin$^+$ TCRβ$^+$). Within the Lin$^-$ TCRβ$^-$ cells, CD90.2$^+$ (Thy1.2$^+$) Sca-1$^+$ cells were further analyzed for C57BL/6 mice and CD90.2$^+$ Sca-1$^{+/-}$ cells for BALB/c mice, as these mice have low Sca-1 expression on resting peripheral lymphocytes (Biolegend 2018a) and therefore ILC2s, if resting and not activated, must be found in the Sca-1$^-$ gate as well. Upon activation, Sca-1 expression is upregulated on peripheral lymphocytes and ILC2s are then also found in the Sca-1$^+$ gate of samples from BALB/c mice. In contrast, C57BL/6 mice show clear Sca-1 expression on resting peripheral lymphocytes even without previous activation, so their ILC2s are only found in the Sca-1$^+$ gate. For quantification later on, the "resting" (Sca-1$^-$) and "activated" (Sca-1$^+$) ILC2s were added for the BALB/c mice to get the numbers of the entire ILC2 population. The gates were set by using an appropriate FMO to ensure that there were indeed positive signals in each case.

The gating strategy shown was again used for all upcoming experiments and organs as for the ILC1s and NK cells and was supplemented with the appropriate antibody for further analysis of cytokine expression (here IL-5).

3.1.3 ILC3s

The gating strategy for the ILC3 subsets was established in the mesenteric lymph nodes (mLN) (Fig. 8) and adopted for all upcoming experiments and organs. Again, the CD45$^+$ immune cells were first identified. Subsequently, Lin$^-$ TCRβ$^-$ cells were further analyzed, excluding T cells in advance.

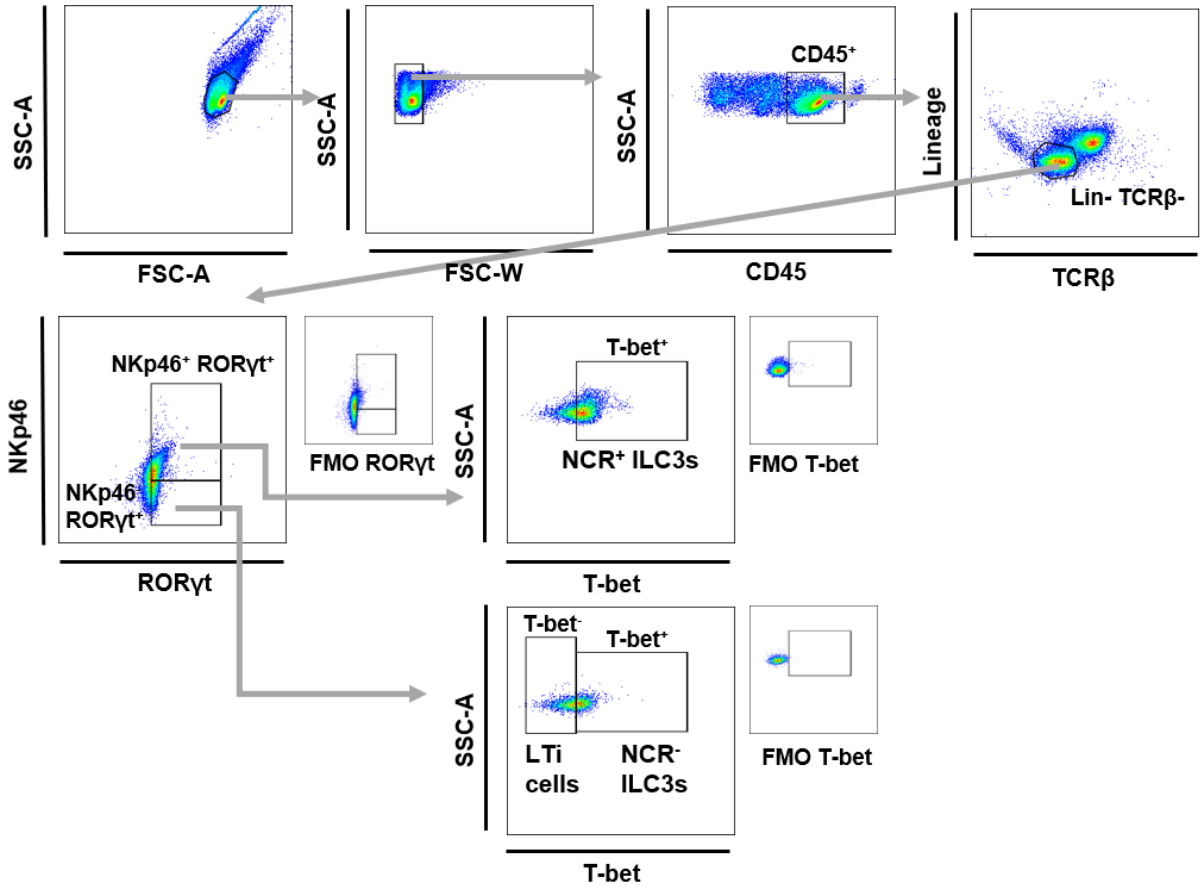

Figure 8: Gating strategy for the identification of ILC3 subsets. The gating strategy is shown exemplarily in the mesenteric lymph node (mLN) of a naive C57BL/6 mouse. The cells were gated on CD45$^+$ lymphocytes whereas granulocytes and monocytes were excluded in the first gate to increase resolution. NCR$^+$ ILC3s were identified as CD45$^+$ Lin$^-$ TCRβ$^-$ NKp46$^+$ RORγt$^+$ T-bet$^+$, NCR$^-$ ILC3s were identified as CD45$^+$ Lin$^-$ TCRβ$^-$ NKp46$^-$ RORγt$^+$ T-bet$^+$ and LTi cells were identified as CD45$^+$ Lin$^-$ TCRβ$^-$ NKp46$^-$ RORγt$^+$ T-bet$^-$. The gates were set by using FMOs. The gating strategy was adapted for every organ which was analysed later on.

Within the Lin$^-$ TCRβ$^-$ cells, it was possible to identify NKp46$^+$ RORγt$^+$ and NKp46$^-$ RORγt$^+$ cells. Within the NKp46$^+$ RORγt$^+$ cells, T-bet$^+$ NCR$^+$ ILC3s could be characterized. NCR$^-$ ILC3s were distinguished from T-bet$^-$ LTi cells within NKp46$^-$ RORγt$^+$ cells based on their T-bet expression. The identification of the LTi cells took

place by exclusion principle, since within the RORγt$^+$ cells these cells remain, provided that the NCR$^+$ and NCR$^-$ ILC3s are identified beforehand. The gates were set by using an appropriate FMO to ensure that there were indeed positive signals in each case. Again, the gating strategy was adopted in all upcoming experiments and for all organs.

3.2 *Plasmodium berghei* ANKA – experimental cerebral malaria (ECM)

It is already known from previous experiments in our lab and from others that *Ifnar1*$^{-/-}$ mice lacking the type I interferon receptor on all immune cells are protected from ECM in contrast to C57BL/6 wildtype (WT) mice, which develop ECM within 6-10 days post infection with *Plasmodium berghei* ANKA (PbA) accompanied by a strong inflammatory immune response (Ball *et al.* 2013; Palomo *et al.* 2013). This protection in *Ifnar1*$^{-/-}$ mice was mainly explained by the strong accumulation of CD8$^+$ T cells in the spleen of *Ifnar1*$^{-/-}$ mice because these cells infiltrate the brain in WT mice, where they contribute largely to pathology development by production of IFN-γ and GzmB (Schiess *et al.* 2020) and the recruitment of other immune cells into the brain (Sierro & Grau 2019). This central role was determined by specific depletion of CD8$^+$ cells in the ECM model (Ghazanfari *et al.* 2018). In *Ifnar1*$^{-/-}$ mice, this infiltration of immune cells into the brain does not occur, protecting them from ECM. The underlying mechanisms had to be elucidated (Scheunemann, Reichwald *et al.* submitted) and in the context of this project, an involvement of ILCs and NK cells in the pathology or in the protection from ECM had to be investigated, since there are hardly any studies on this, especially with regard to ILCs.

For that purpose, the established ECM model was used. The ILC populations in the brain were analysed 6 dpi, the day of ECM development in WT mice, and the various ILC populations in the spleen were examined at different time points after infection followed by a specific NK cell depletion in PbA-infected mice.

3.2.1 ILC1s and NK cells infiltrate the brain of PbA-infected WT mice 6 dpi

Ifnar1$^{-/-}$ mice, in contrast to WT mice, were protected from ECM, as their median RMCBS score at day 6 after infection was higher than that of WT mice (Fig. 9a). The WT mice showed a significant reduction of the score at day 6 compared to naive controls and had a median score of less than 5, indicating severe neurological symptoms, breakdown of the blood brain barrier (BBB), and thus ECM development. *Ifnar1*$^{-/-}$ mice were protected from PbA-induced ECM with a median score of over 10,

while neurological symptoms such as the loss of reflexes do not occur until a score of 5. Furthermore, the protection of *Ifnar1*$^{-/-}$ mice could not be explained by a lower parasitemia of these animals, as the parasitemia of WT mice was comparable to that of *Ifnar1*$^{-/-}$ mice (Fig. 9b).

Analysis of immune cells isolated from the brain from perfused animals revealed a significant increase in the total cell number of CD45^{+} immune cells in WT mice 6 dpi PbA infection compared to naive controls, whereas this was not the case in *Ifnar1*$^{-/-}$ mice (Fig. 9c). The total cell number of immune cells isolated from the brain of WT mice was higher than that of *Ifnar1*$^{-/-}$ mice upon PbA infection (p=0.0679). Thus, infiltration of immune cells into the brain following PbA infection occurred in WT mice but not in *Ifnar1*$^{-/-}$ mice. This confirms previous findings from our lab (Scheunemann, Reichwald *et al.* submitted). Detailed analysis of immune cells infiltrated into the brain revealed a significant increase in the total cell number of T cells in the brain of WT mice upon PbA infection (Fig. 9d). Although this was also found for *Ifnar1*$^{-/-}$ mice, the total cell number of T cells isolated from the brain of PbA-infected *Ifnar1*$^{-/-}$ mice was lower than that of PbA-infected WT mice. The increase of T cells upon PbA infection in *Ifnar1*$^{-/-}$ mice could be explained by the fact that these cells were located upstream of the blood brain barrier but have not yet actively infiltrated the brain, as at day 6 their blood brain barrier was still intact (Scheunemann, Reichwald *et al.* submitted). This hypothesis is supported by the higher score of *Ifnar1*$^{-/-}$ mice 6 dpi compared to the score of WT mice (p=0.0981) which was also not decreased in comparison to their naive controls as it was observed for WT mice.

Interestingly, among those cells infiltrated into the brain ILC1s and NK cells were present as well (Fig. 9e-h). Regarding ILC1s, there was a significant increase in total cell number and also in the proportion among all CD45^{+} lymphocytes in WT and *Ifnar*$^{-/-}$ mice upon PbA infection (Figs. 9e, 9f) whereas the proportion of ILC1s among the immune cells in the brain or upstream of the blood brain barrier in case of *Ifnar1*$^{-/-}$ mice did not differ between PbA-infected WT and *Ifnar1*$^{-/-}$ mice (Fig. 9f). This was different for NK cells. Here, a significant increase in the total cell number was detected in WT and *Ifnar1*$^{-/-}$ mice upon PbA infection (Fig. 9g), but the total NK cell number that infiltrated into the brain of PbA-infected WT mice was higher than in PbA-infected *Ifnar1*$^{-/-}$ mice (p=0.0695).

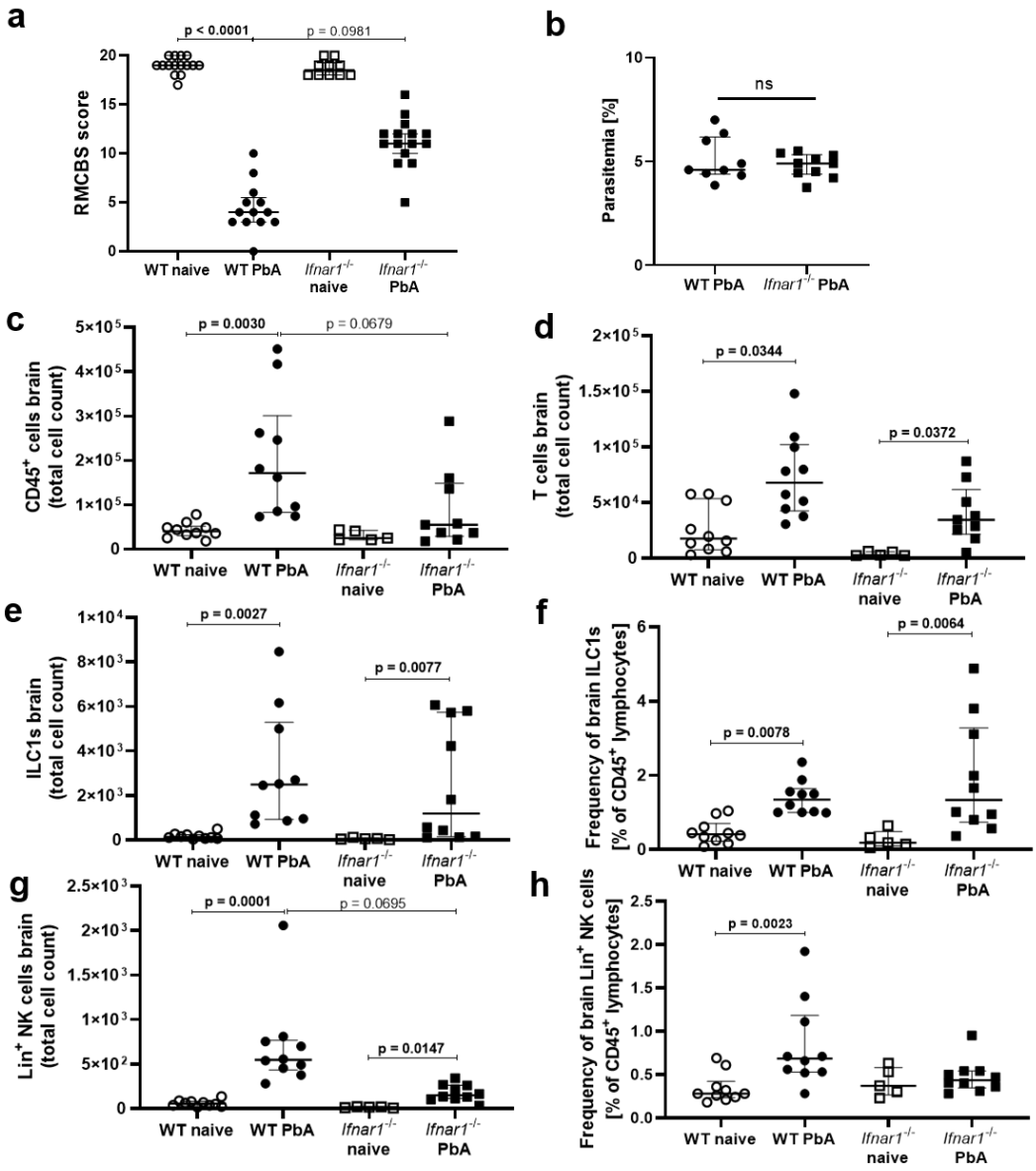

Figure 9: ILC1s and NK cells infiltrate the brain of PbA-infected WT mice 6 dpi. C57BL/6 and *Ifnar1*$^{-/-}$ mice were infected with 5e+04 PbA iRBCs i. v., naive mice were left untreated. After 6 days RMCBS score of each mouse as well as the parasitemia was determined. Brain-derived T cells were identified as Lin$^+$ TCRβ$^+$, brain-derived ILC1s were identified as CD45$^+$ Lin$^-$ NKp46$^+$ CD49b$^-$ CD49a$^+$ T-bet$^+$ and brain-derived Lin$^+$ NK cells as CD45$^+$ Lin$^+$ NKp46$^+$ CD49b$^+$ T-bet$^+$ **(a)** RMCBS score 6 dpi. **(b)** Parasitemia 6 dpi. **(c)** Total cell count of CD45$^+$ immune cells isolated from the brains 6 dpi. **(d)** Total cell count of T cells isolated from the brains 6 dpi. **(e)** Total cell count of ILC1s isolated from the brains 6 dpi. **(f)** Frequency [% of CD45$^+$ lymphocytes] of ILC1s isolated from the brains 6 dpi. **(g)** Total cell count of Lin$^+$ NK cells isolated from the brains 6 dpi. **(h)** Frequency [% of CD45$^+$ lymphocytes] of Lin$^+$ NK cells isolated from the brains 6 dpi. Bars represent the median with interquartile ranges. Data shown in (a) n = 10 for naive *Ifnar1*$^{-/-}$ mice and n = 15 for all other groups, pooled data from 3 independent experiments. (b) n = 10, pooled data from 2 independent experiment. (c) n = 5 for naive *Ifnar1*$^{-/-}$ mice and n = 10 for all other groups, pooled data from 2 independent experiments. (d) n = 5 for naive *Ifnar1*$^{-/-}$ mice and n = 10 for all other groups, pooled data from 2 independent experiments. (e) n = 5 for naive *Ifnar1*$^{-/-}$ mice and n = 10 for all other groups, pooled data from 2 independent experiments. (f) n = 5 for naive *Ifnar1*$^{-/-}$ mice and n = 10 for all other groups, pooled data from 2 independent experiments. (g) n=5 for naive *Ifnar1*$^{-/-}$ mice and n = 10 for all other groups, pooled data from 2 independent experiments. (h) n = 5 for naive *Ifnar1*$^{-/-}$ mice and n = 10 for all other groups, pooled data from 2 independent experiments. Spearman's rank correlation test for heteroscedasticity was performed and only data failing the heteroscedasticity were pooled. Data were analysed with Kruskal-Wallis test and Dunn's post-test. A p-value below 0.05 was considered to be significant.

The percentage of NK cells among the immune cells isolated from the brain increased significantly only in the WT mice and remained constant in *Ifnar1*$^{-/-}$ mice upon PbA infection (Fig. 9h).

It was concluded that WT and *Ifnar1*$^{-/-}$ mice differ in terms of immune cells isolated from the brain, particularly with regard to NK cells, and that there was a marked infiltration of NK cells into the brains of WT mice in addition to an obvious and previously reported infiltration of T cells. For the first time, ILC1s were also observed among the immune cells in the brain. Both cell types are capable of IFN-γ production, NK cells are moreover also able to produce Granzyme B (GzmB) (Serafini *et al.* 2015). Both effector molecules were identified as important mediators of ECM pathology (Ghazanfari *et al.* 2018, 2018). Here, the expression of GzmB of NK cells isolated from the brain was found to be significantly higher than the GzmB expression of CD8$^+$ T cells isolated from the brain (Fig. 10).

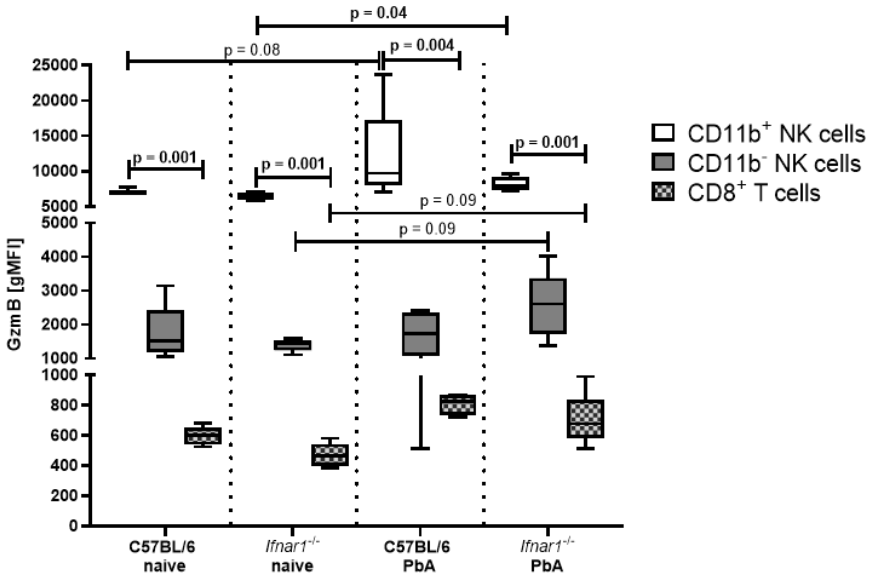

Figure 10: Higher GzmB expression of NK cells compared to CD8$^+$ T cells isolated from the brain 5 days after PbA infection. C57BL/6 and *Ifnar1*$^{-/-}$ mice were infected with 5e+04 PbA iRBCs i.v.. After 5 days brain-derived CD8$^+$ T cells were characterized as CD45$^+$ CD11b$^-$ CD3$^+$ CD8$^+$, brain-derived CD11b$^+$ NK cells as CD45$^+$ CD11b$^+$ NK1.1$^+$ and brain-derived CD11b$^-$ NK cells as CD45$^+$ CD11b$^-$ NK1.1$^+$. The GMFI of GzmB was determined for every cell population.

Although WT and *Ifnar1*$^{-/-}$ NK cells did not differ here, these observations nevertheless suggested that NK cells may make a critical contribution to pathology development in the brain. Although NK cells were underrepresented compared to T cells in terms of total cell count, they exhibited an over 10-fold higher GzmB expression.

3.2.2 PbA-infected *Ifnar1*$^{-/-}$ and WT mice differ mainly in terms of NK cells but not ILC1s, ILC2s and ILC3s on day 6 post infection

The spleen is an important organ that plays a central role especially during *Plasmodium* infection (Engwerda *et al.* 2005). Infected erythrocytes are filtered and recycled here, which brings the immune cells in the spleen into contact with high concentrations of parasitic antigens and leads to corresponding immune reactions. The spleen is an important immunological organ, as many cell populations are found here in high quantities and central immunological processes are mediated.

In addition, previous studies have shown that there is an accumulation of CD8$^+$ T cells in the spleens of *Ifnar1*$^{-/-}$ mice, whereas these cells migrate from the spleen to the brain in WT mice 6 dpi. Accordingly, the spleen is of great interest for the analysis of the ILC populations as well to determine whether WT and *Ifnar1*$^{-/-}$ mice also differ in this regard possibly giving hints at a role of ILCs in the protective phenotype of *Ifnar1*$^{-/-}$ mice. Based on this, kinetics of all ILC subsets were generated. An early time point after infection (3 dpi) was chosen to represent the situation shortly after infection. The time point shortly before ECM development (5 dpi) was chosen, since at this time point the CD8$^+$ T cells have not yet left the spleen of the WT mice and it is thus possible to see whether any differences might already exist shortly before ECM development. In addition, the ILC populations were also analyzed on day 6, the timepoint of ECM development.

With regard to ILC1s, no significant differences were detected between PbA-infected WT and *Ifnar1*$^{-/-}$ mice on day 3 after PbA infection, neither in terms of total cell count nor in terms of the proportion among all CD45$^+$ lymphocytes (Figs. 11a, 11b). However, on day 5 after infection, there was an increase in the total cell count of ILC1s in the spleens of *Ifnar1*$^{-/-}$ mice compared with naive controls ($p=0.1188$) with the total cell count of ILC1s in the spleens being significantly higher in the PbA-infected *Ifnar1*$^{-/-}$ mice than in PbA-infected WT mice ($p=0.0394$) (Fig. 11a). Regarding the percentage of ILC1s, there was only a slight increase at 5 dpi in *Ifnar1*$^{-/-}$ mice compared with their naive controls ($p=0.2369$) (Fig. 11b). In both groups of mice, there was a significant increase in the total cell count and the proportion of ILC1s in the spleen on 6 dpi compared with the corresponding naive controls (Figs. 11a, 11b), yet PbA-infected WT mice did not differ from PbA-infected *Ifnar1*$^{-/-}$ mice in this regard.

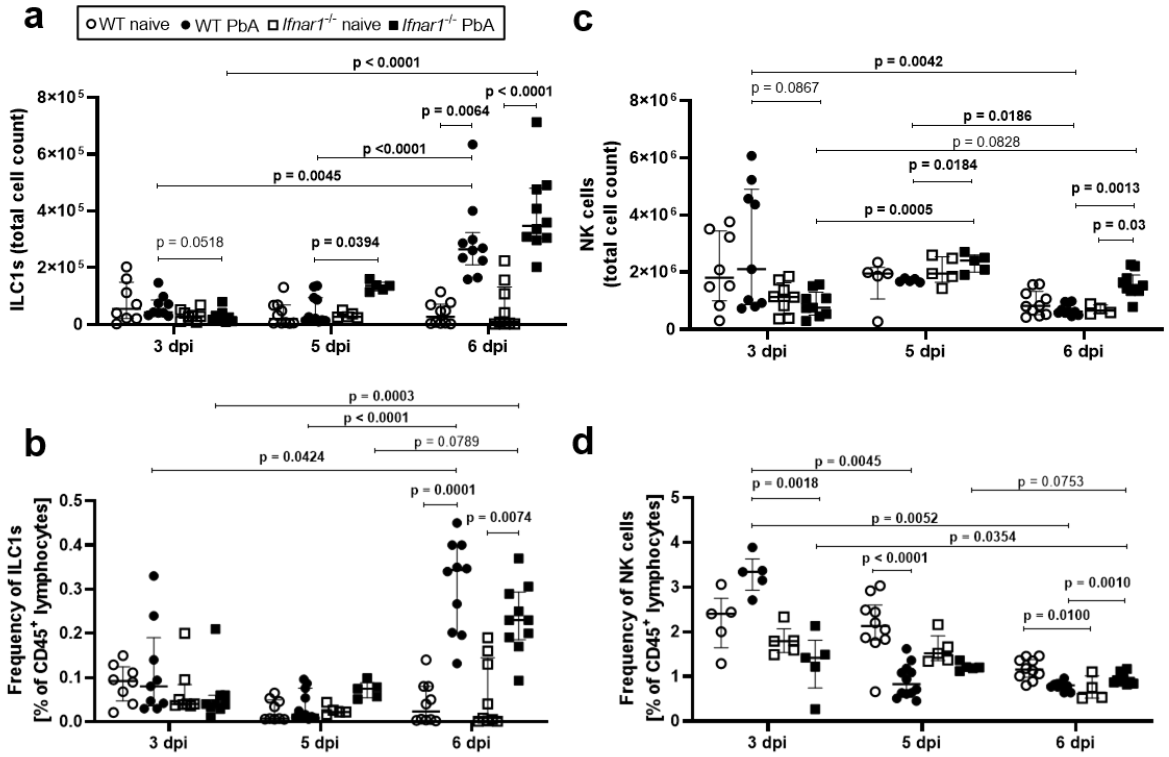

Figure 11: *Ifnar1*$^{-/-}$ mice show significantly higher splenic NK cell counts and frequencies on day 6 post PbA infection than WT mice. C57BL/6 and *Ifnar1*$^{-/-}$ mice were infected with 5e+04 PbA iRBCs i. v.. After 3, 5 or 6 days the spleens were isolated and used for flow cytometric analysis. ILC1s were identified as CD45$^+$ Lin$^-$ NKp46$^+$ CD49b$^-$ CD49a$^+$ T-bet$^+$ and NK cells were identified as CD45$^+$ Lin$^{+/-}$ NKp46$^+$ CD49b$^+$ CD49a$^-$ T-bet$^+$. **(a)** Total cell count of ILC1s in the spleen 3, 5 and 6 dpi. **(b)** Frequency [% of CD45$^+$ lymphocytes] of ILC1s in the spleen 3, 5 and 6 dpi. **(c)** Total cell count of NK cells in the spleen 3, 5 and 6 dpi. **(d)** Frequency [% of CD45$^+$ lymphocytes] of NK cells in the spleen 3, 5 and 6 dpi. Bars represent the median with interquartile ranges. Data shown in (a) n = 5 for naive and PbA-infected *Ifnar1*$^{-/-}$ mice 5 dpi; n = 8-10 for all other groups and timepoints, pooled data from 2 independent experiments per timepoint. (b) n = 5 for naive and PbA-infected *Ifnar1*$^{-/-}$ mice 5 dpi, n = 8-10 for all other groups and timepoints, pooled data from 2 independent experiments per timepoint. (c) n = 5 for 5 dpi, data show 1 representative experiment from 2 independent experiments; n = 4 for naive *Ifnar1*$^{-/-}$ mice 6 dpi; n = 10 for all other groups 6 dpi and n = 8 for all groups 3 dpi, pooled data from 2 independent experiments respectively. (d) n = 5 for 3 dpi, data show 1 representative experiment from 2 independent experiments, n = 4-5 for naive *Ifnar1*$^{-/-}$ mice 5 and 6 dpi; n = 5 for PbA-infected *Ifnar1*$^{-/-}$ mice 5 dpi; n = 10-12 for all other groups 5 dpi and 6 dpi, pooled data from 2 independent experiments respectively. Spearman's for heteroscedasticity was performed and only data failing the heteroscedasticity were pooled. Data were analysed with Kruskal-Wallis test and Dunn's post-test. A p-value below 0.05 was considered to be significant.

PbA-infected WT and *Ifnar1*$^{-/-}$ mice both showed a significant increase in the total cell count and the proportion of ILC1s over the course of infection (from 3 dpi to 6 dpi) (Fig. 11a, 11b). At least regarding the total cell count, this can be explained by a general increase in splenocyte numbers, since splenomegaly occurred as a consequence of PbA infection, especially in *Ifnar1*$^{-/-}$ mice (data not shown). Of interest at this point is the markedly increased proportion of ILC1s among all CD45$^+$ lymphocytes in the spleen 6 dpi compared with the early time point after infection (Fig. 11b). Their proportion increased threefold from day 3 to day 6 in the PbA-infected WT mice and

also in the PbA-infected *Ifnar1*$^{-/-}$ during the same period. This suggests a shift in the immune cell composition in the spleen, particularly at day 6 after infection in both types of mice, and also suggests that ILC1s are involved in the immune response to PbA in the spleen.

Analysis of the total cell count of NK cells in the spleen revealed no differences between WT and *Ifnar1*$^{-/-}$ mice on day 3 or day 5, both in the naive state and after PbA infection (Fig. 11c). However, PbA-infected WT mice had significantly higher proportions of NK cells among all CD45^{+} lymphocytes than PbA-infected *Ifnar1*$^{-/-}$ mice 3 dpi (Fig. 11d). At day 5, the proportion of NK cells among all lymphocytes decreased significantly in the spleens of WT mice ($p<0.0001$) after PbA infection, whereas it remained constant in *Ifnar1*$^{-/-}$ mice. The proportions of NK cells in both PbA-infected groups were then comparable. On day 6, only *Ifnar1*$^{-/-}$ mice showed a significant increase in the total cell count of NK cells in the spleen upon PbA infection ($p=0.03$) (Fig. 11c), the total cell count of NK cells was then also significantly higher in the PbA-infected *Ifnar1*$^{-/-}$ mice compared to PbA-infected WT mice ($p=0.0013$). Although the proportion of NK cells among all CD45^{+} lymphocytes in the spleen did not change with PbA infection in both mouse strains 6 dpi (Fig. 11d), the proportion of NK cells in PbA-infected *Ifnar1*$^{-/-}$ mice was still significantly higher than their proportion in PbA-infected WT mice ($p=0.001$).

Since there were already differences in the total cell count and the proportion of NK cells among all CD45^{+} lymphocytes in the naive controls, the analysis of the development of NK cells over the course of infection (3 dpi to 6 dpi) has to be treated with caution. Nevertheless, PbA-infected WT mice showed a significant reduction in the total cell count of NK cells from 5 dpi to 6 dpi ($p=0.0186$) (Fig. 11c). In contrast, in PbA-infected *Ifnar1*$^{-/-}$ mice, an increase in NK cell counts was observed from 3 dpi to 6 dpi ($p=0.0828$), which was detectable already from 3 dpi to 5 dpi. The proportion of NK cells among all CD45^{+} lymphocytes decreased significantly in PbA-infected WT mice from 3 dpi to 6 dpi (Fig. 11d), this reduction was already observable from 3 dpi to 5 dpi. In PbA-infected *Ifnar1*$^{-/-}$ mice, the proportion of NK cells also decreased significantly from 3 dpi to 6 dpi.

Thus, kinetic analysis showed that PbA-infected WT and *Ifnar1*$^{-/-}$ mice differed during the course of infection, particularly with regard to NK cells. These differences were

particularly pronounced on 6 dpi, the timepoint of ECM development in WT mice. Looking again at the data from the brain (Fig. 9), it was reasonable to assume that the PbA-infected *Ifnar1*$^{-/-}$ mice possess more NK cells in the spleen than PbA-infected WT mice, because 6 dpi the NK cells infiltrated the brain in WT mice which was not the case in *Ifnar1*$^{-/-}$ mice. This phenomenon has already been observed for CD8^{+} T cells (Scheunemann, Reichwald *et al.* submitted).

Besides ILC1s and NK cells, ILC2s and ILC3s were also of interest, since to date there have been only few studies determining the possible involvement of these cells in the immune response to PbA.

At the early time point of infection (3 dpi), there were no differences between naive and PbA-infected WT and *Ifnar1*$^{-/-}$ mice in either total cell count or the proportion of ILC2s among all CD45^{+} lymphocytes in the spleen (Figs. 12a, 12b). In contrast, on day 5, there was a significant increase in the ILC2 total cell count in PbA-infected WT mice compared with naive controls (p=0.0178), whereas the total cell count of ILC2s did not change in the *Ifnar1*$^{-/-}$ mice (Fig. 12a). The percentage of ILC2s only slightly increased in WT mice upon PbA infection at day 5 (p=0.1711), which was not observed for *Ifnar1*$^{-/-}$ mice (Fig. 12b). In contrast to day 5, a significant increase in ILC2 cell counts was observed 6 dpi in the spleen of PbA-infected *Ifnar1*$^{-/-}$ mice compared to naive controls (p=0.0019) as well as compared to PbA-infected WT mice (p=0.0108) (Fig. 12a). With regard to the percentage of ILC2s on 6 dpi the analysis did not reveal any significant differences between the mouse strains (Fig. 12b). The increase in ILC2 cell numbers in the spleens of 6-day PbA-infected *Ifnar1*$^{-/-}$ could be explained mainly by the general splenomegaly that accompanied PbA infection and was also significantly more pronounced in *Ifnar1*$^{-/-}$ mice than in WT mice (data not shown).

Over the course of infection, ILC2s increased tendentially in total cell count from 3 dpi to 5 dpi in PbA-infected WT mice (p=0.0791) and significantly from 3 dpi to 6 dpi in PbA-infected *Ifnar1*$^{-/-}$ mice (p=0.0044) (Fig. 12a). Regarding the proportion of ILC2s, a tendential increase in ILC2s in PbA-infected WT (p=0.0696) and *Ifnar1*$^{-/-}$ mice (p=0.0999) from 3 dpi to 5 dpi was observed, whereas a tendential increase was additionally observed from 3 dpi to 6 dpi in PbA-infected *Ifnar1*$^{-/-}$ mice (p=0.0587) (Fig. 12b). Nevertheless, the observed changes in the proportions of ILC2s during the course of infection did not reach statistical significance.

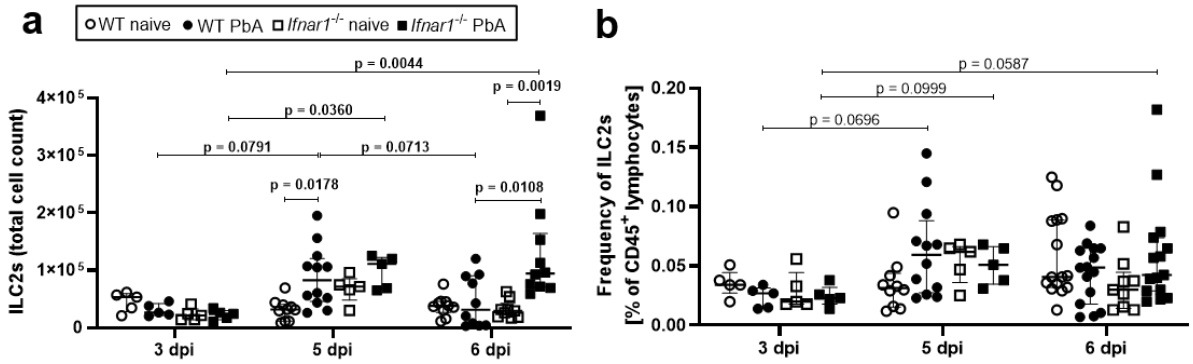

Figure 12: *Ifnar1*$^{-/-}$ mice show increased ILC2 cell counts but not frequencies upon PbA infection. C57BL/6 and *Ifnar1*$^{-/-}$ mice were infected with 5e+04 PbA iRBCs i. v.. After 3, 5 or 6 days the spleens were isolated and used for flow cytometric analysis. ILC2s were characterized as CD45^{+} Lin^{-} TCRβ^{-} CD90.2^{+} Sca-1^{+} IL-33R^{+} GATA-3^{+}. **(a)** Total cell count of ILC2s in the spleen 3, 5 and 6 dpi. **(b)** Frequency [% of CD45^{+} lymphocytes] of ILC2s in the spleen 3, 5 and 6 dpi. Bars represent the median with interquartile ranges. Data shown in (a) n = 5 for 3 dpi, data show 1 representative experiment from 2 independent experiments, n = 5 for naive and PbA-infected *Ifnar1*$^{-/-}$ mice 5 dpi, n = 10-12 for all other groups 5 dpi and all groups 6 dpi, pooled data from 2 independent experiments respectively. Spearman's test for heteroscedasticity was performed and only data failing the heteroscedasticity were pooled. Data were analysed with Kruskal-Wallis test and Dunn's post-test. A p-value below 0.05 was considered to be significant.

The analysis of the ILC3 subsets (NCR^{+} ILC3s, NCR^{-} ILC3s, and LTi cells) revealed no major differences between WT and *Ifnar1*$^{-/-}$ mice at either 3 dpi or 5 dpi, neither in total cell count nor in the proportion of these cells among all CD45^{+} lymphocytes (Fig. 13a-f). Also, infection with PbA did not result in a change in cell counts and proportions in either mouse strain. In the day 6 experiments, differences in the ILC3 populations in the naive state occurred, which prevented the comparison to PbA-infected mice.

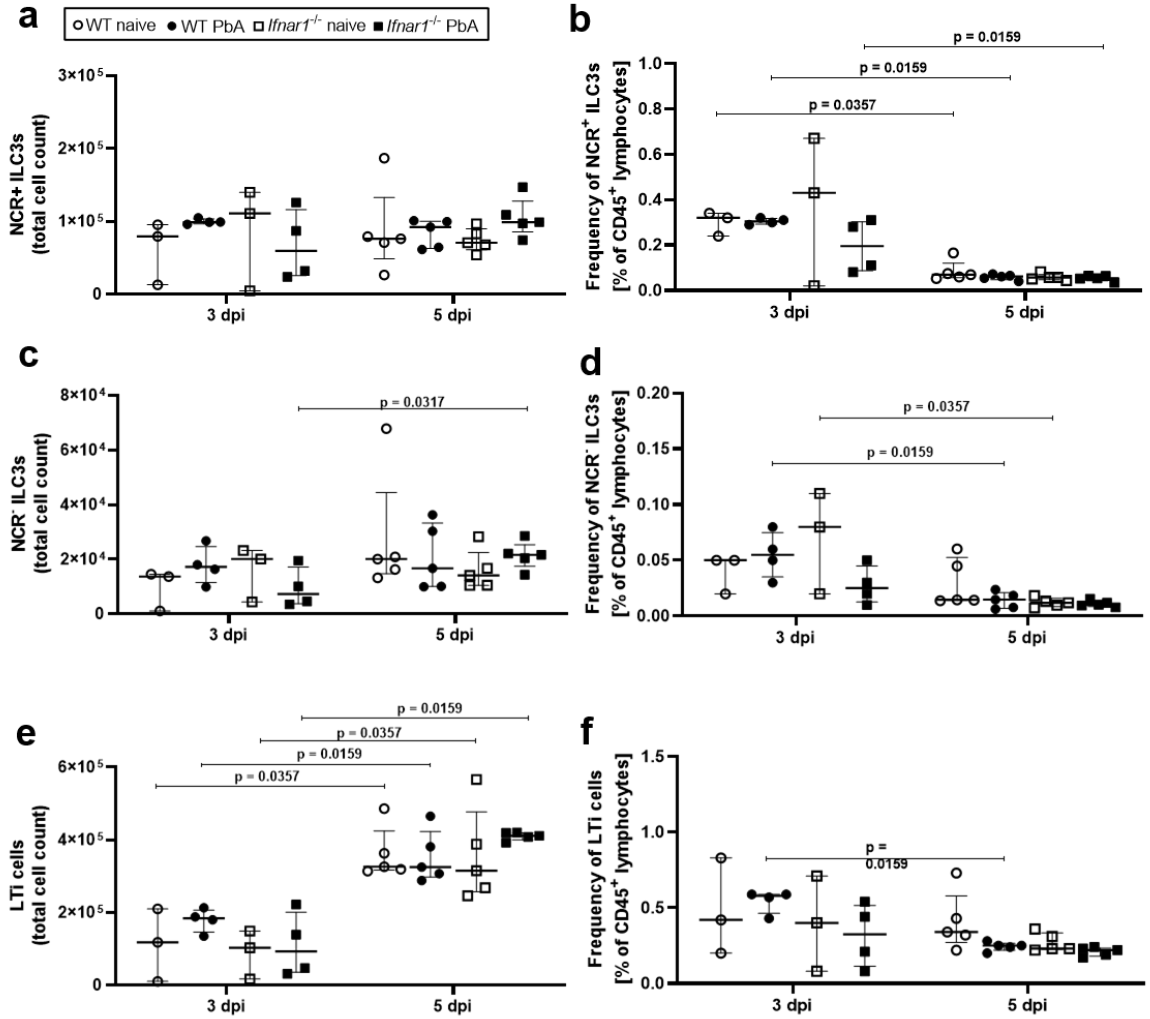

Figure 13: PbA-infected C57BL/6 and *Ifnar1*$^{-/-}$ do not significantly differ with regard to ILC3 populations. C57BL/6 and *Ifnar1*$^{-/-}$ mice were infected with 5e+04 PbA iRBCs i. v.. After 3 and 5 days the spleens were isolated and used for flow cytometric analysis. NCR^{+} ILC3s were identified as CD45^{+} Lin^{-} TCRβ^{-} NKp46^{+} RORγt^{+} T-bet^{+}, NCR^{-} ILC3s as CD45^{+} Lin^{-} TCRβ^{-} NKp46^{-} RORγt^{+} T-bet^{+} and LTi cells as CD45^{+} Lin^{-} TCRβ^{-} NKp46^{-} RORγt^{+} T-bet^{-}**. (a)** Total cell count of NCR+ ILC3s in the spleen 3 and 5 dpi. **(b)** Frequency [% of CD45^{+} lymphocytes] of NCR+ ILC3s in the spleen 3 and 5 dpi. **(c)** Total cell count of NCR- ILC3s in the spleen 3 and 5 dpi. **(d)** Frequency [% of CD45^{+} lymphocytes] of NCR- ILC3s in the spleen 3 and 5 dpi. **(e)** Total cell count of LTi cells in the spleen 3 and 5 dpi. **(f)** Frequency [% of CD45^{+} lymphocytes] of LTi cells in the spleen 3 and 5 dpi. Bars represent the median with interquartile ranges. Data shown in (a-f) n = 3 for naive mice 3 dpi; n = 4-5 for all other groups and timepoints, data from 1 experiment. Data were analysed with Kruskal-Wallis test and Dunn's post-test. A p-value below 0.05 was considered to be significant.

The summary of the results provides an overview of the main findings from the kinetic analyses of ILC populations during PbA infection in the spleen and the brain of WT and *Ifnar1*$^{-/-}$ mice on 5 and 6 dpi, where the most prominent differences were observed (Fig. 14).

a

	Cell counts of…	5 dpi C57BL/6	5 dpi *Ifnar1*$^{-/-}$	6 dpi C57BL/6	6 dpi *Ifnar1*$^{-/-}$
Brain	ILC1s			++	+
	NK cells			++	→
Spleen	ILC1s	→	+	++	++
	NK cells	→	→	→	+
	ILC2s	+	→	→	+
	NCR+ ILC3s	→	→		
	NCR- ILC3s	→	→		
	LTi cells	→	→		

b

Frequency of…	5 dpi C57BL/6	5 dpi *Ifnar1*$^{-/-}$	6 dpi C57BL/6	6 dpi *Ifnar1*$^{-/-}$
ILC1s			+	+
NK cells			++	→
ILC1s	→	+	++	++
NK cells	-	→	→	→
ILC2s	→	→	→	→
NCR+ ILC3s	→	→		
NCR- ILC3s	→	→		
LTi cells	→	→		

++ = strongly increased compared to naive control
\+ = increased compared to naive control
\- = decreased compared to naive control
→ = no difference to naïve control
□ = most important differences

Figure 14: Summary of results from 5 and 6 days PbA-infected C57BL/6 and *Ifnar1*$^{-/-}$ mice. Cell counts as well as frequencies of ILC1s, NK cells, ILC2s and ILC3s of 5 and 6 days PbA-infected C57BL/6 and *Ifnar1*$^{-/-}$ were compared to their naive controls. ++ = strongly increased compared to naive control, + = increased compared to naive control, - = decreased compared to naive control, → = no differences to naive control. Red square = most important differences. Day 3 is not shown as the differences were minor. **(a)** Summary of the changes of ILC1, NK cell, ILC2 and ILC3 total cell counts in the brain and spleen of PbA-infected WT and *Ifnar1*$^{-/-}$ mice. **(b)** Summary of the changes of ILC1, NK cell, ILC2 and ILC3 frequencies in the brain and spleen of PbA-infected WT and *Ifnar1*$^{-/-}$ mice. Pictures of spleen and brain were taken from Servier Medical Art.

Among the tested ILC subsets, differences between C57BL/6 WT mice and *Ifnar1*$^{-/-}$ mice upon PbA infection were most prominent in terms of ILC1s and especially NK cells. Therefore, the upcoming analyses focused on NK cells and their immunological characteristics.

3.2.3 NK cells from PbA-infected *Ifnar1*$^{-/-}$ mice are less activated and produce less effector molecules than WT NK cells on 3 and 6 dpi

The kinetic analysis of NK cells and the fact that the type I interferon receptor on NK cells negatively regulates their IFN-γ production (Lee *et al.* 2019) suggested that there might also be distinct differences in the phenotype and functionality of NK cells when comparing WT and *Ifnar1*$^{-/-}$ mice, which in turn might have an impact on the protection of *Ifnar1*$^{-/-}$ mice from ECM or on the pathology development in WT mice. Therefore, in the next steps, NK cells from WT and *Ifnar1*$^{-/-}$ mice were analyzed in more detail with regard to their activation status and their ability to produce effector molecules like IFN-γ and GzmB.

For this purpose, NK cells were isolated from the spleens of naive and PbA-infected WT and *Ifnar1*$^{-/-}$ mice at two different time points (Fig. 15). Day 3 was chosen to determine whether any differences existed early in infection and day 6 was intended to represent the situation on the day of ECM development in WT mice.

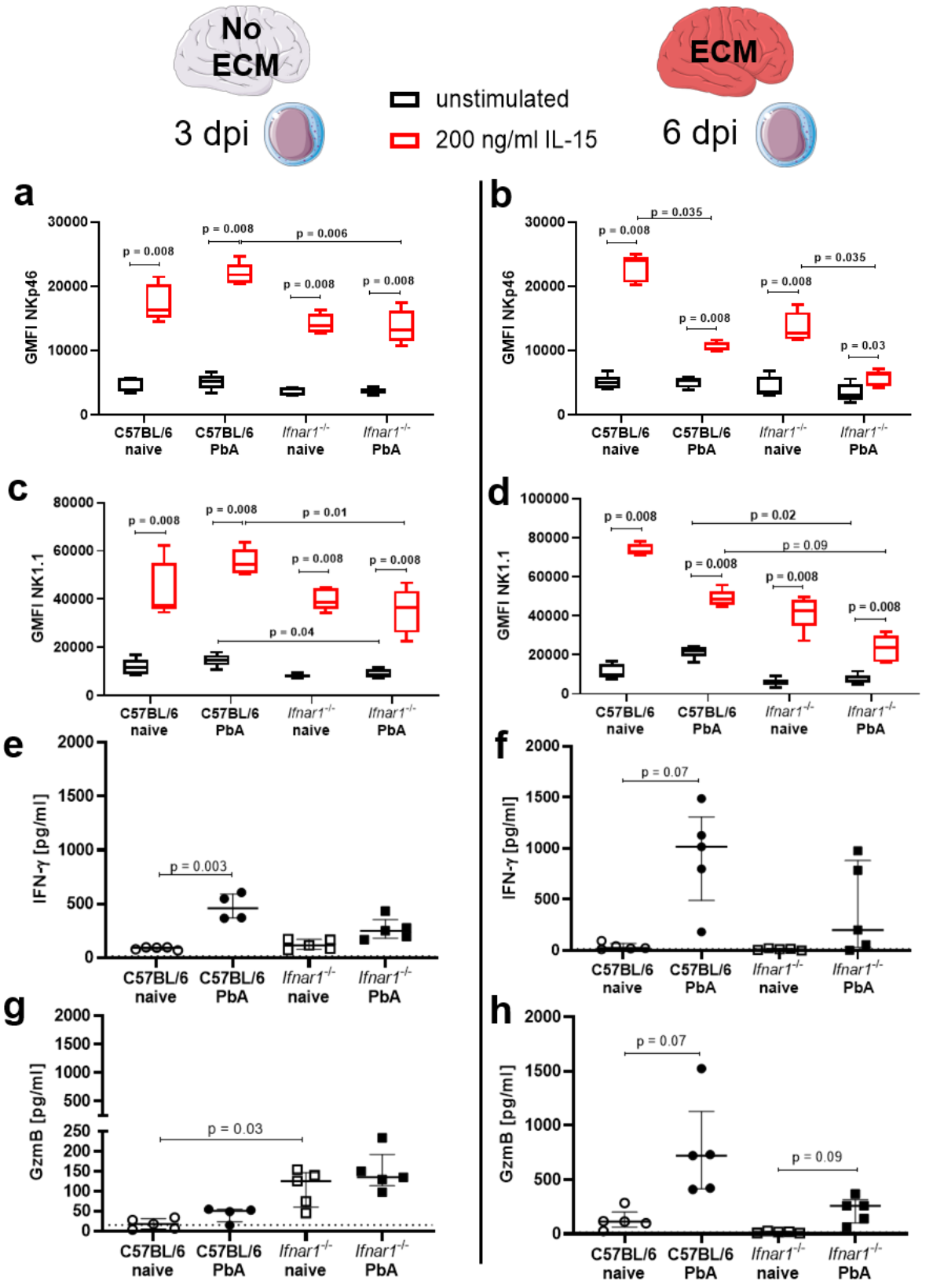
No ECM
3 dpi
unstimulated
200 ng/ml IL-15
ECM
6 dpi
a
GMFI NKp46
b
GMFI NKp46
c
GMFI NK1.1
d
GMFI NK1.1
e
IFN-γ [pg/ml]
f
IFN-γ [pg/ml]
g
GzmB [pg/ml]
h
GzmB [pg/ml]
C57BL/6 naive
C57BL/6 PbA
Ifnar1-/- naive
Ifnar1-/- PbA

Figure 15: NK cells from PbA-infected *Ifnar1*$^{-/-}$ are less activated and produce less IFN-γ and GzmB than WT NK cells. C57BL/6 and *Ifnar1*$^{-/-}$ mice were infected with 5e+04 PbA iRBCs i. v.. After 3 and 6 days the spleens were isolated and purified NK cells stimulated with IL-15 were analyzed. NK cells were characterized as CD49b^{+} Lin^{+} and analysed for expression level (GMFI) of NKp46 and NK1.1. (a-d) show box and whiskers with Tukey. (e-h) show the median with interquartile range. **(a)** Expression level (GMFI) of NKp46 of unstimulated and IL-15 stimulated NK cells from naive and 3 days PbA-infected mice. **(b)** Expression level (GMFI) of NKp46 of unstimulated and IL-15 stimulated NK cells from naive and 6 days PbA-infected mice. **(c)** Expression level (GMFI) of NK1.1 of unstimulated and IL-15 stimulated NK cells from naive and 3 days PbA-infected mice. **(d)** Expression level (GMFI) of NK1.1 of unstimulated and IL-15 stimulated NK cells from naive and 6 days PbA-infected mice. **(e)** IFN-γ production by NK cells of 3 days PbA-infected mice stimulated with IL-15 for 24 h. **(f)** IFN-γ production by NK cells of 6 days PbA-infected mice stimulated with IL-15 for 24 h. **(g)** GzmB production by NK cells of 3 days PbA-infected mice stimulated with IL-15 for 24 h. **(h)** GzmB production by NK cells of 6 days PbA-infected mice stimulated with IL-15 for 24 h. Data shown in (a-h) n = 5 per group, data from 1 experiment. Data were analysed with Kruskal-Wallis test and Dunn's post-test. A p-value below 0.05 was considered to be significant.

The cells were analyzed in unstimulated condition and under stimulation with IL-15, a cytokine that is essential for the development, activation and functionality of NK cells (Artis & Spits 2015; Eberl *et al.* 2015; Geiger & Sun 2016). The activation status was assessed by expression analysis of the two activating NK cell receptors NKp46 and NK1.1 (Joshi & Lang 2013; Glasner *et al.* 2018).

Stimulation of NK cells with IL-15 resulted in a significant increase in the NKp46 expression in all groups of mice (naive and PbA-infected), although the increase was more pronounced in the WT groups than in the *Ifnar1*$^{-/-}$ groups (Fig. 15a). The NKp46 expression levels of stimulated NK cells from PbA-infected animals were comparable with their corresponding naive controls. The NKp46 expression of NK cells stimulated with IL-15 at day 3 after PbA infection was significantly lower in *Ifnar1*$^{-/-}$ mice than in WT mice (p=0.006). At day 6, the picture was different (Fig. 15b). Here, although there was also a significant increase in NKp46 expression on NK cells in all groups due to IL-15 stimulation, the NKp46 expression of stimulated NK cells from PbA-infected mice was significantly lower than that of NK cells from naive controls. Also, WT and *Ifnar1*$^{-/-}$ no longer differed significantly with regard to NKp46 expression by stimulated NK cells.

NK1.1 expression of NK cells stimulated with IL-15 at day 3 after PbA infection was significantly lower in *Ifnar1*$^{-/-}$ mice than in WT mice (p=0.01) (Fig. 15c). Interestingly, even in the unstimulated state, lower NK1.1 expression was observed here on NK cells from PbA-infected *Ifnar1*$^{-/-}$ mice compared with NK cells from PbA-infected WT mice (p=0.04). Again, IL-15 stimulation resulted in a significant increase in NK1.1 expression on NK cells in all mouse groups (naive and PbA-infected) although the increase was more pronounced in the WT groups than in the *Ifnar1*$^{-/-}$ groups. The NK1.1 expression

levels of stimulated NK cells from PbA-infected animals were comparable with their corresponding naive controls. On day 6, a similar picture was observed (Fig. 15d). Already in the unstimulated condition, NK1.1 expression of NK cells from PbA-infected *Ifnar1*$^{-/-}$ mice was significantly lower than the expression of NK cells from PbA-infected WT mice (p=0.02). This was also the case by trend for the stimulated NK cells (p=0.09). Here, IL-15 stimulation also significantly increased NK1.1 expression in all mouse groups, with NK cells from naive WT mice responding the strongest to IL-15 stimulation.

In addition to the activation status, the production of IFN-γ and GzmB of the isolated NK cells was determined. NK cells stimulated with IL-15 from 3 and 6 day PbA-infected *Ifnar1*$^{-/-}$ mice produced slightly less IFN-γ than NK cells from PbA-infected WT mice (p=0.5958 for d6) (Figs. 15e, 15f). Furthermore, 3 dpi (p=0.003) and 6 dpi (p=0.07) the NK cells isolated from PbA-infected WT mice showed a higher IFN-γ production than their naive controls. For *Ifnar1*$^{-/-}$ mice, no differences could be detected in this regard at least on day 3 compared with the corresponding naive controls; only 6 dpi, PbA-infected *Ifnar1*$^{-/-}$ mice showed a detectable IFN-γ level in some of the samples (Fig. 15f). Regarding the GzmB production by NK cells isolated from the spleen and stimulated with IL-15, a significantly higher level was detected in naive *Ifnar1*$^{-/-}$ mice compared with naive WT mice at day 3 (p=0.03) (Fig. 15g). The PbA-infected mice only tended to differ here (p=0.1455). The picture was clearer on day 6 (Fig. 15h). Here, a higher GzmB production by NK cells isolated from PbA-infected WT (p=0.07) and *Ifnar1*$^{-/-}$ mice (p=0.09) compared to naive controls was detected, with levels of PbA-infected *Ifnar1*$^{-/-}$ NK cells tending to be lower than those of PbA-infected WT mice (p=0.3487), similar to the IFN-γ results.

It was concluded that NK cells of *Ifnar1*$^{-/-}$ mice are in general less activated than those of WT mice, in the unstimulated and stimulated states, and that they also produce lower levels of effector molecules. Accordingly, they differ in their phenotype and functionality.

3.2.4 NK cells are not responsible for the protection of *Ifnar1*$^{-/-}$ mice from PbA-induced ECM

The results regarding the altered phenotype and reduced functionality of the NK cells in *Ifnar1*$^{-/-}$ mice raised the question whether NK cells are involved in the protection of

Ifnar1$^{-/-}$ mice and/or pathogenesis in WT mice. In depletion experiments NK cells were indicated to be important for the induction of ECM and control of parasitemia, but the outcome was highly dependent on the antibody used and on the mouse strain (Palomo *et al.* 2017). For example the use of anti-asialo GM1 limited the recruitment of T cells to the brain leading to protection from ECM in WT mice, but the use of anti-NK1.1 did not protect these mice against ECM (Yañez *et al.* 1996; Hansen *et al.* 2007; Burrack *et al.* 2019). Moreover, the impact of NK cell depletion on PbA-infected *Ifnar1*$^{-/-}$ has not been demonstrated so far in the ECM model. Therefore, the next step was to deplete NK cells in both PbA-infected WT and *Ifnar1*$^{-/-}$ mice (Fig. 16a), and the corresponding immunological analyses in the brain and spleen were examined at day 6.

Depletion of NK cells in PbA-infected WT mice did not protect these mice from ECM (Fig. 16b). There was a significant reduction in RMCBS score 6 dpi of PbA-infected WT mice compared with naive controls that was comparable for both isotype control and NK cell depleted WT mice. Therefore, NK cell depletion did not cause improvement of ECM symptoms in WT mice. *Ifnar1*$^{-/-}$ mice were still protected after NK cell depletion, the score of the depleted mice was comparable to that of the isotype controls and the median score was above 10, so there was no ECM development. Parasitemia was comparable among all PbA-infected groups (Fig. 16c), so it can be concluded that NK cells are not responsible for parasite control at least in WT and *Ifnar1*$^{-/-}$ mice.

The analysis of cells isolated from the brain revealed a significant increase in the total cell count of CD45^{+} immune cells only in PbA-infected WT mice that received the isotype control compared with naive controls ($p=0.02$) (Fig. 16d). The depleted PbA-infected WT mice also had a slight increase in the cell count of immune cells isolated from the brain compared to naive controls ($p=0.388$). In *Ifnar1*$^{-/-}$ mice, there was no infiltration of immune cells into the brain, as for the isotype controls, the total cell number of immune cells was significantly lower than in the isotype controls of WT mice ($p=0.02$). The depleted *Ifnar1*$^{-/-}$ had similar cell numbers to their corresponding isotype controls ($p>0.9999$).

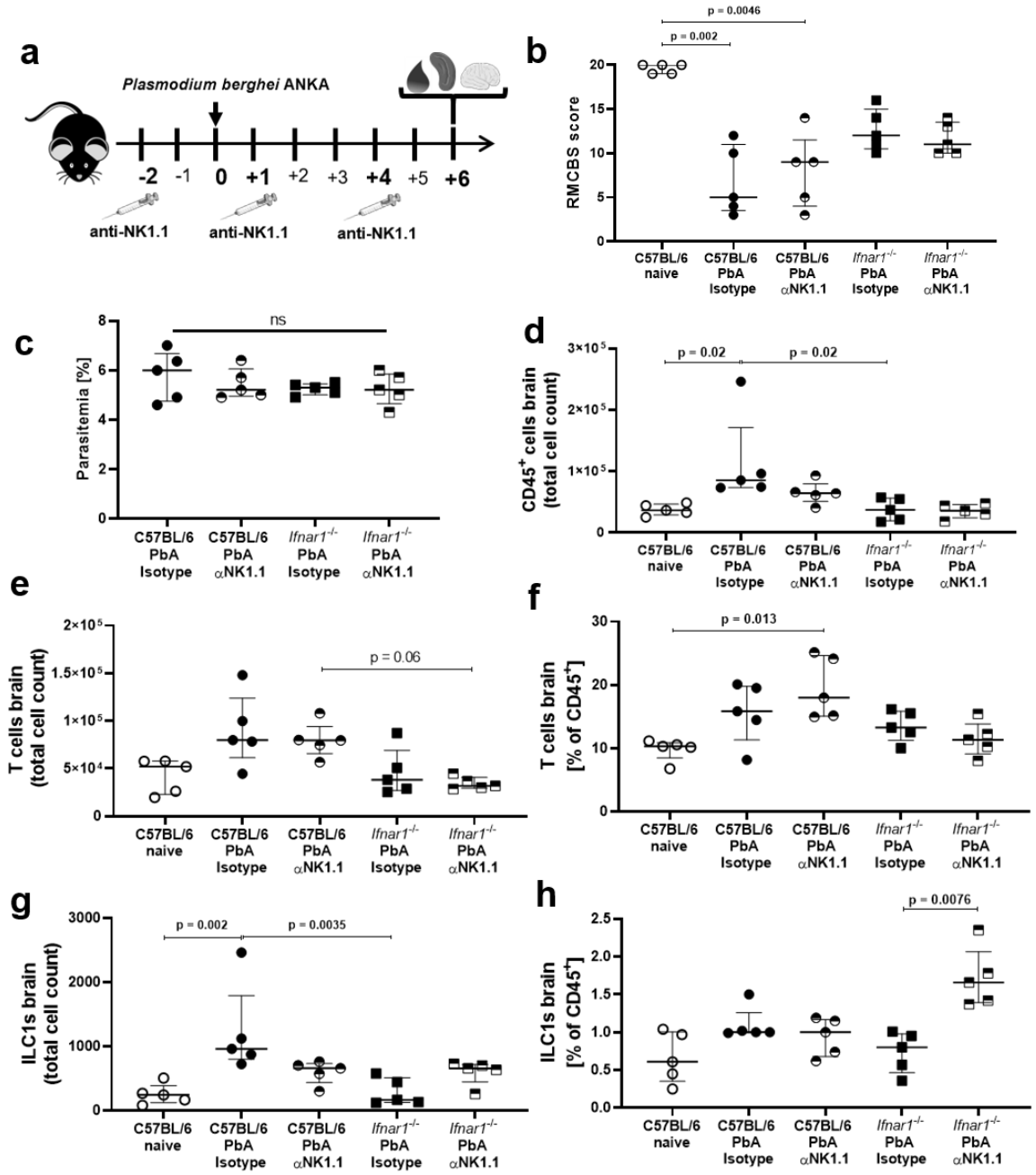

Figure 16: NK cell depletion does neither alter ECM development in WT mice nor protection of *Ifnar1*$^{-/-}$ mice. C57BL/6 and *Ifnar1*$^{-/-}$ mice received 600 µg anti-NK1.1 or Isotype control on day -2, +1 and +4 around PbA infection (d0) that was performed by administering 5e+04 PbA iRBCs i. v. to the animals. After 6 days RMCBS score of each mouse as well as the parasitemia was determined. Brain-derived T cells were identified as Lin$^+$ TCRβ$^+$, ILC1s as CD45$^+$ Lin$^-$ NKp46$^+$ CD49b$^-$ CD49a$^+$ T-bet$^+$. **(a)** Experimental setup. **(b)** RMCBS score 6 dpi. **(c)** Parasitemia [%] 6 dpi. **(d)** Total cell count of CD45$^+$ immune cells isolated from the brain 6 dpi. **(e)** Total cell count of T cells isolated from the brain 6 dpi. **(f)** Frequency [% of CD45$^+$ cells] of T cells isolated from the brain 6 dpi. **(g)** Total cell count of ILC1s isolated from the brain 6 dpi. **(h)** Frequency [% of CD45+ cells] isolated from the brain 6 dpi. Bars represent the median with interquartile ranges. Data in (a-h) n = 5 per group, data from 1 experiment. Data were analysed with Kruskal-Wallis test and Dunn's post-test. A p-value below 0.05 was considered to be significant.

T cells and ILC1s were analyzed among all cells isolated from the brain as well. The total cell count of T cells in the brain increased only in the WT mice (p=0.2350) (Fig.

16e). Moreover, the total cell count of T cells tended to be higher in the depleted WT mice than in the depleted *Ifnar1*$^{-/-}$ mice (p=0.06), supporting the data of the RMCBS scores, according to which ECM development does not occur in *Ifnar1*$^{-/-}$ mice. Isotype controls of PbA-infected *Ifnar1*$^{-/-}$ mice also had slightly lower cell numbers of T cells in the brain than WT mice (p=0.2886). The proportion of T cells among all CD45^{+} lymphocytes purified from the brain increased only in WT mice compared with naive controls, and in the case of the depleted WT mice, it increased significantly (p=0.013) (Fig. 16f). Infiltration of ILC1s into the brain occurred only in WT mice, especially in the isotype controls, as the total cell count of ILC1s was significantly higher in the isotype controls of WT mice than in the naive WT mice (p=0.002) (Fig. 16g). Furthermore, the total cell count of these cells was significantly lower than in the isotype controls of *Ifnar1*$^{-/-}$ mice compared to the isotype controls of WT mice (p=0.0035). In depleted *Ifnar1*$^{-/-}$ mice hardly any ILC1s could be detected in the brain. Interestingly, however, unlike for other cells, the total cell number of ILC1s in depleted WT mice was not as high as the cell number of ILC1s in the WT isotype controls. This could be explained by the fact that ILC1s also partially express NK1.1 and thus could be affected by the NK cell depletion. The proportion of ILC1s among all immune cells isolated from the brain was not different among the WT groups and the isotype control of *Ifnar1*$^{-/-}$ mice (Fig. 16h). Only the depleted *Ifnar1*$^{-/-}$ mice showed a markedly increased proportion of these cells which was significantly higher than in the corresponding isotype controls (p=0.0076). This indicates that in *Ifnar1*$^{-/-}$ mice a significant change in the composition of the immune cells has taken place, according to which ILC1s account for a higher percentage.

Although there were no significant differences observed between isotype controls and depleted mice in the brain, the next step was to analyze the immune response in the spleen to determine whether depletion of NK cells still led to the accumulation of CD8^{+} T cells in *Ifnar1*$^{-/-}$ mice.

NK cells were effectively depleted in the spleen (Fig. 17a, 17b) as NK cells were no longer detectable in the CD49b^{+} NKp46^{+} gate and their proportion among all CD45^{+} cells in the spleen was also strongly reduced in depleted WT and *Ifnar1*$^{-/-}$ mice (Fig. 17b). Analysis of CD8^{+} T cells in the spleen revealed a significantly higher total cell count of these cells in the spleen of NK-cell depleted PbA-infected *Ifnar1*$^{-/-}$ mice than in WT mice (p=0.03) (Fig. 17c). This was also observed for the proportion of CD8^{+} T

cells among all spleen cells, which was significantly higher in both depleted groups than in the corresponding isotype controls (p=0.015 for WT, p=0.046 for *Ifnar1*$^{-/-}$). This suggests that even after NK cell depletion, there is an accumulation of CD8^{+} T cells in the spleens of *Ifnar1*$^{-/-}$ mice, whereas in the WT mice they infiltrate into the brain.

To address whether NK cell depletion affected the cytokine milieu in the spleen, IFN-γ and GzmB levels were determined in the spleen of each group; both effector molecules are produced by NK cells.

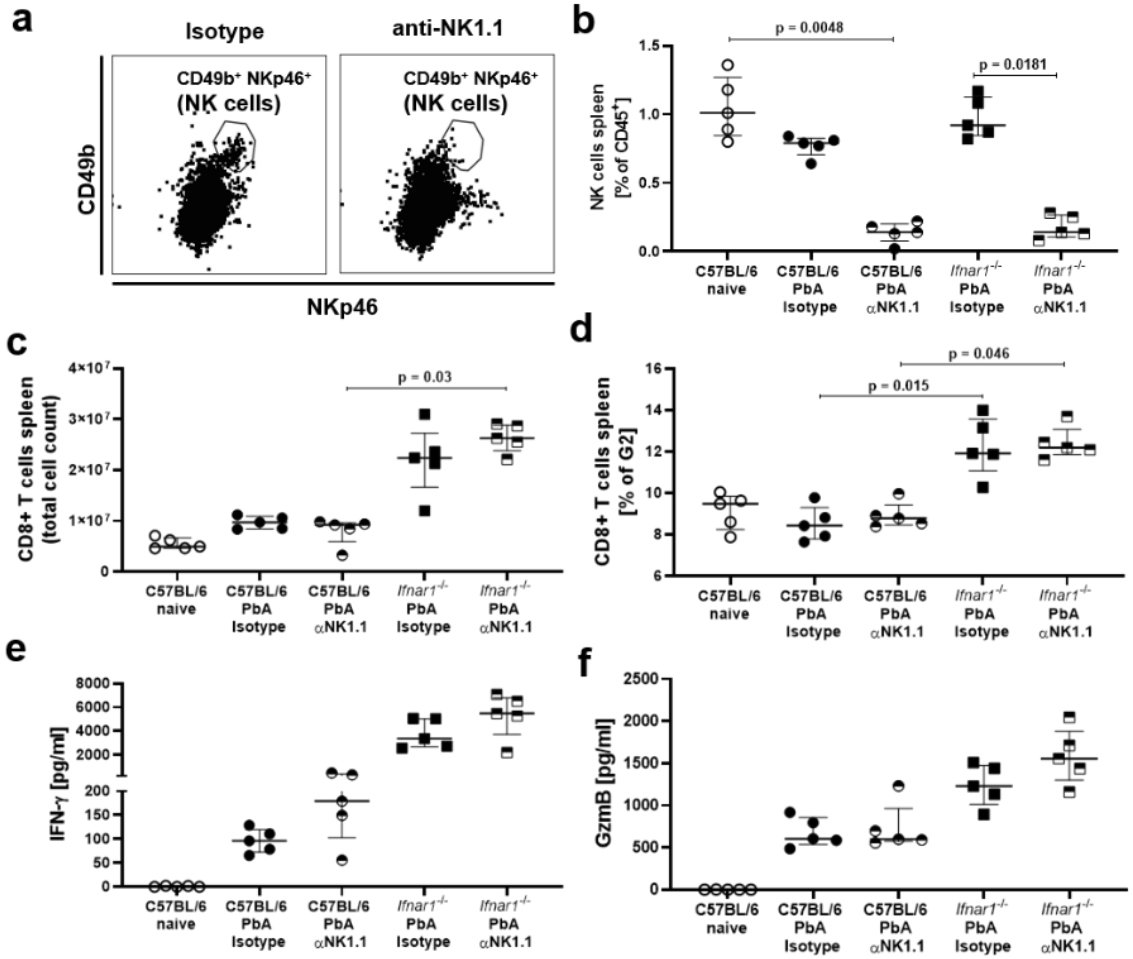

Figure 17: PbA-infected *Ifnar1*$^{-/-}$ mice still show accumulation of CD8^{+} T cells in the spleen upon NK cell depletion 6 dpi. C57BL/6 and *Ifnar1*$^{-/-}$ mice received anti-NK1.1 or isotype control on day -2, +1 and +4 around PbA infection (d0) that was performed by administering 5e+04 PbA iRBCs i. v. to the animals. After 6 days RMCBS score of each mouse as well as the parasitemia was determined and immunological analyses were performed. **(a)** Final gate of NK cells (gated on CD45^{+} cells). **(b)** Frequency [% of CD45^{+} cells] of NK cells in the spleen 6 dpi. **(c)** Total cell count of CD8^{+} T cells in the spleen 6 dpi. **(d)** Frequency [% of G2] of CD8^{+} T cells in the spleen 6 dpi. **(e)** IFN-γ level and **(f)** GzmB level in spleen cell in vitro cultures prepared 6 dpi. Bars represent the median with interquartile ranges. Data in (b-f) n = 5 per group, data from 1 experiment. Data were analysed with Kruskal-Wallis test and Dunn's post-test. A p-value below 0.05 was considered to be significant.

There was an increase in IFN-γ levels in the spleen in all groups following PbA infection (Fig. 17e). The levels of IFN-γ in the isotype controls of both WT and *Ifnar1*$^{-/-}$ mice were

comparable to the levels in the depleted mouse groups. Thus, NK cells did not appear to be significantly involved in the IFN-γ level in the spleen. Nevertheless, this could also be explained by the fact that in the absence of NK cells, other cells compensate the IFN-γ production, e.g., ILC1s and $CD8^+$ T cells. Such redundant effector mechanisms are already known in other models (Hamada *et al.* 2013). The same trend was observed for the GzmB levels (Fig. 17f).

In summary, the data suggest that NK cells are not of central importance for ECM development in WT mice, because WT mice develop ECM despite the absence of NK cells. On the other hand, NK cells are also apparently not responsible for the protection of *Ifnar1*$^{-/-}$ mice from ECM, because these mice were still protected from ECM in the absence of NK cells. Therefore, the observed difference in phenotype and functionality of NK cells isolated from the spleens of *Ifnar1*$^{-/-}$ mice compared with WT NK cells does not explain the protective mechanism.

3.2.5 *Ifnar1*$^{-/-}$ mice show a strong regulatory and type 2 immune response upon PbA infection

Previous analyses focused strongly on the inflammatory immune responses in WT and *Ifnar1*$^{-/-}$ upon PbA infection. It was therefore of interest to look more closely at possible type 2 and regulatory immune responses to obtain a complete picture of the immune response in *Ifnar1*$^{-/-}$ mice. For this purpose, Th2 cells, eosinophils, IL-10 and IL-13 levels were analyzed in the spleens.

Both PbA-infected *Ifnar1*$^{-/-}$ groups (isotype controls and NK cell depleted mice) had increased Th2 cell counts in the spleen compared to the WT mice, with the cell count in the depleted *Ifnar1*$^{-/-}$ mice being significantly higher than in the depleted WT mice ($p=0.012$) (Fig. 18a). Regarding the proportion of Th2 cells, it was observed that PbA-infected WT mice (isotype controls and NK cell depleted mice) had a lower proportion of these cells in the $CD45^+$ cells in the spleen compared to the naive control ($p=0.06$ and $p=0.0056$) (Fig. 18b). In contrast, both *Ifnar1*$^{-/-}$ groups had higher proportions of Th2 cells among $CD45^+$ cells in the spleen than the corresponding WT groups ($p=0.1148$ and $p=0.07$). Furthermore, PbA-infected *Ifnar1*$^{-/-}$ mice had a significantly higher cell count ($p=0.027$) and proportion ($p=0.038$) of eosinophils in the spleen than the PbA-infected WT mice (Fig. 18c, 18d). Thus, there was an accumulation of Th2 cells and eosinophils in the spleen of *Ifnar1*$^{-/-}$ mice upon PbA infection. Analysis of the

cytokine milieu in the spleen revealed higher IL-10 levels in the spleen of PbA-infected *Ifnar1*$^{-/-}$ mice than in PbA-infected WT mice in general (Fig. 18e). Although the depleted WT mice also showed a tendential increase in IL-10 level compared with the naive controls (p=0.067), the IL-10 levels in the isotype controls of *Ifnar1*$^{-/-}$ mice tended to be higher than in the corresponding WT isotype controls. A similar picture was seen for IL-13 levels (Fig. 18f). Again, PbA-infected *Ifnar1*$^{-/-}$ mice had higher levels than WT mice (p=0.06).

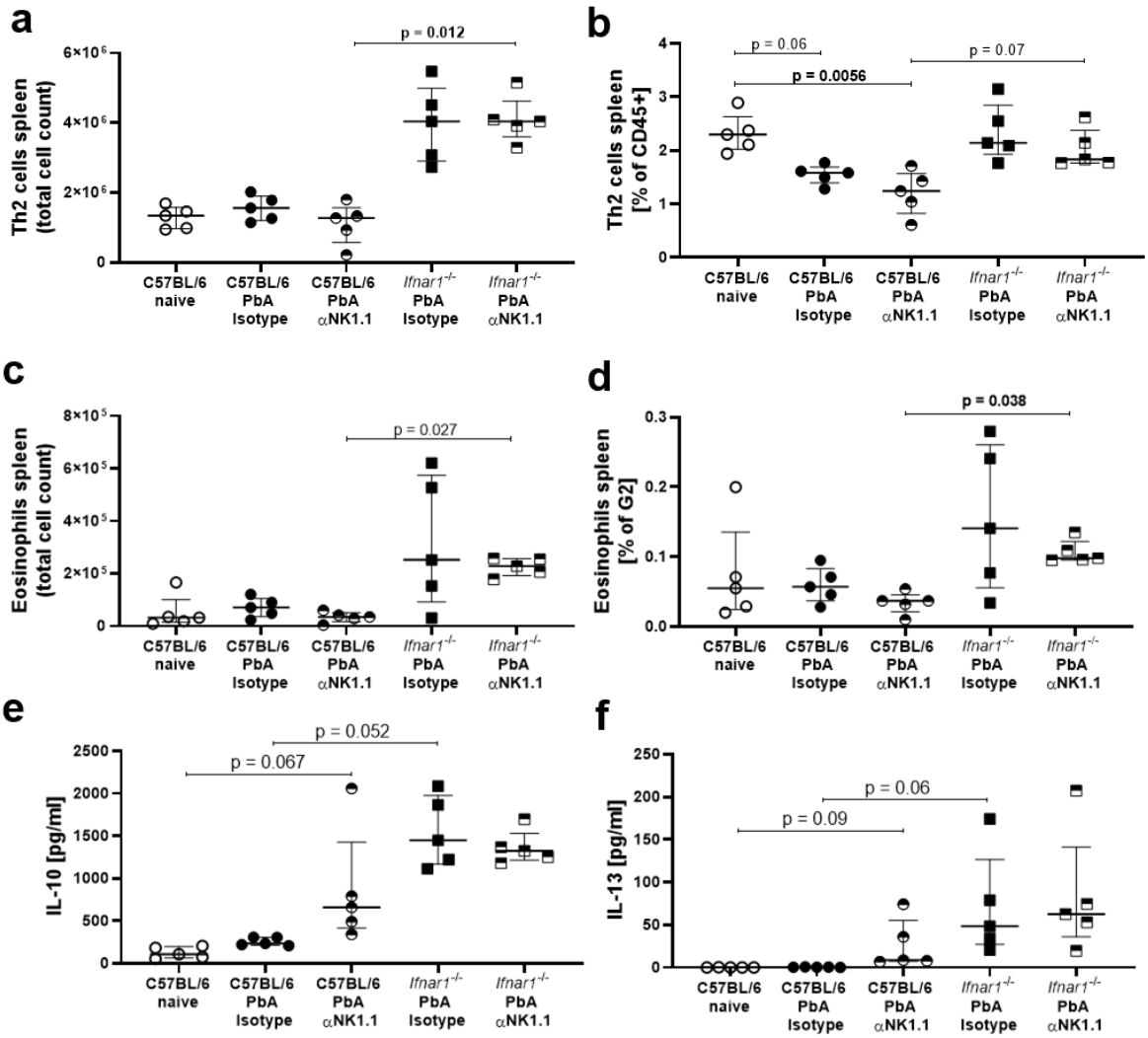

Figure 18: PbA-infected *Ifnar1*$^{-/-}$ show a strong type 2 and regulatory immune response characterized by accumulation of eosinophils in the spleen 6 dpi. C57BL/6 and *Ifnar1*$^{-/-}$ mice received 600 µg anti-NK1.1 or Isotype control on day -2, +1 and +4 around PbA infection (d0). Infection was performed by administering 5e+04 PbA iRBCs i. v. into the animals. After 6 days RMCBS score of each mouse as well as the parasitemia was determined and immunological analyses were performed. Th2 cells were characterized as CD45^{+} Lin^{+} TCRβ^{+} CD90.2^{+} GATA-3^{+}, eosinophils were characterized as CD19^{-} CD11b^{+} Ly6G^{-} Ly6C^{int-hi} siglec-F^{+}. **(a)** Total cell count of Th2 cells in the spleen 6 dpi. **(b)** Frequency [% of CD45^{+} cells] of Th2 cells in the spleen 6 dpi. **(c)** Total cell count of eosinophils in the spleen 6 dpi. **(d)** Frequency [% of G2] of eosinophils in the spleen 6 dpi. **(e)** IL-10 level in the spleen 6 dpi. **(f)** IL-13 level in the spleen 6 dpi. Bars represent the median with interquartile ranges. Data in (a-f) n = 5 per group, data from 1 experiment. Data were analysed with Kruskal-Wallis test and Dunn's post-test. A p-value below 0.05 was considered to be significant.

Thus, there is a pronounced type 2 and regulatory immune response in the *Ifnar1*$^{-/-}$ mice upon PbA infection. This could provide an explanation for the protection of the *Ifnar1*$^{-/-}$ mice from ECM development. The accumulation of eosinophils was particularly striking, as these cells are specifically induced during filarial infections and appear here as protective immune cells (Huang & Appleton 2016; Frohberger *et al.* 2019; Yasuda & Kuroda 2019). Accordingly, it was already demonstrated that a regulatory immune response induced by filariae leads to protection from ECM (Specht *et al.* 2010).

3.2.6 Depletion of eosinophils in PbA-infected *Ifnar1*$^{-/-}$ mice leads to ECM development 6 dpi

To further define the role of eosinophils in the protection of *Ifnar1*$^{-/-}$ mice from ECM development, eosinophils were depleted after PbA infection in *Ifnar1*$^{-/-}$ mice and the corresponding analyses were performed 6 dpi (Fig. 19a). In WT mice, in accordance with previous results, there was a significant reduction in the RMCBS score to a median score of less than 5 and thus ECM development in these mice (Fig. 19b). In contrast, *Ifnar1*$^{-/-}$ mice were protected from ECM as their RMCBS was nominally significantly higher than that of WT mice (p=0.004). Depletion of eosinophils led to a nominal significant reduction in RMCBS in *Ifnar1*$^{-/-}$ mice compared with non-depleted *Ifnar1*$^{-/-}$ mice (p=0.0192). Also, the median RMCBS score of the eosinophil-depleted *Ifnar1*$^{-/-}$ mice was below 10, suggesting that the first ECM symptoms were already appearing at this time point. The score approached that of WT mice, indicating equal ECM development of both groups. Parasitemia was comparable between WT PbA and *Ifnar1*$^{-/-}$ mice, confirming previous results, whereas the parasitemia of eosinophil-depleted *Ifnar1*$^{-/-}$ mice was slightly lower compared to WT mice (Fig. 19c, Scheunemann, Reichwald *et al.* submitted). Analysis of CD45^{+} immune cells isolated from the brain revealed a significant increase in the total cell count of CD45^{+} cells in PbA-infected WT mice compared to naive controls (p=0.0206), suggesting infiltration of immune cells into the brain and therefore ECM development (Fig. 19c). In *Ifnar1*$^{-/-}$ mice, this increase in total cell count was not observed compared with naive controls. However, depleted *Ifnar1*$^{-/-}$ mice showed an increased total cell count of immune cells in the brain compared with naive controls and compared with non-depleted *Ifnar1*$^{-/-}$ mice. Thus, following eosinophil depletion, there was infiltration of immune cells into the brain in the *Ifnar1*$^{-/-}$ mice, which fits to the results of the RMCBS scores. Eosinophils

therefore appear to be important mediators of the protective mechanism in *Ifnar1*$^{-/-}$ mice.

Further results concerning the role of eosinophils and regulatory immune responses in the ECM model as well as the eosinophil depletion in *Ifnar1*$^{-/-}$ mice are part of the publication that was recently submitted (Scheunemann, Reichwald *et al.* submitted).

It was further demonstrated in the associated publication that parasite-specific immune responses and basic T cell functions (IFN-γ and GzmB production and expression) were not impaired in *Ifnar1*$^{-/-}$ mice. Therefore, the protection was not caused by a limited parasite-specific immune response.

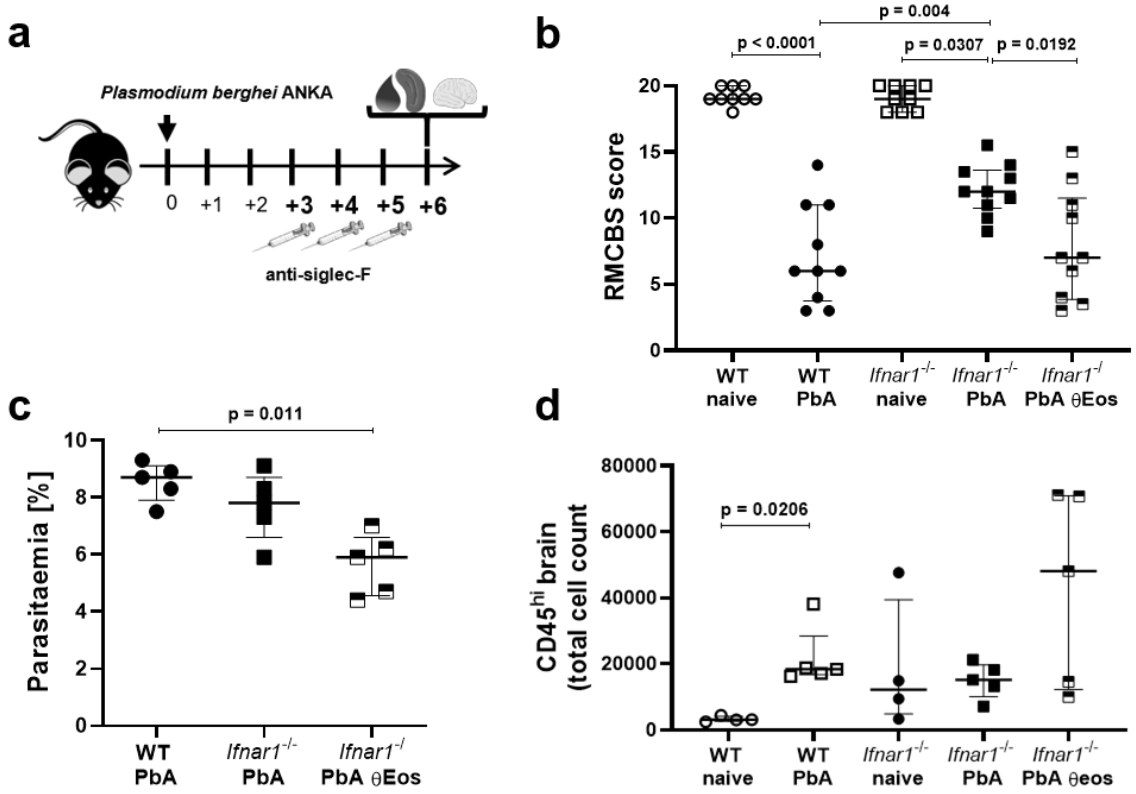

Figure 19: Depletion of eosinophils leads to ECM development in *Ifnar1*$^{-/-}$ mice 6 dpi. C57BL/6 and *Ifnar1*$^{-/-}$ mice were infected with 5e+04 PbA iRBCs i. v. *Ifnar1*$^{-/-}$ received 1.5µg/g body weight anti-siglecF i. p. on day 3, 4 and 5 post infection. After 6 days RMCBS score of each mouse as well as the parasitemia was determined. After 6 days RMCBS score of each mouse as well as the parasitemia was determined and immunological analyses were performed. **(a)** Experimental setup. **(b)** RMBCS score 6 dpi. **(c)** Parasitemia [%] 6 dpi. **(d)** Total cell count of CD45^{+} immune cells isolated from the brain 6 dpi. Bars represent the median with interquartile ranges. Data in (b) n = 9 for naive mice, n = 10 for PbA-infected mice, pooled data from 2 independent experiments experiment. Data in (c) n = 4 for naive mice, n = 5 for PbA-infected mice, data show 1 representative experiments from 2 independent experiments. Spearman's test for heteroscedasticity was performed and only data failing the heteroscedasticity were pooled. Data were analysed with Kruskal-Wallis test and Dunn's post-test. Data in (d) were additionally analyzed with Mann-Whitney test for nominal comparison of WT PbA vs. *Ifnar1*$^{-/-}$ PbA and for *Ifnar1*$^{-/-}$ PbA vs. *Ifnar1*$^{-/-}$ PbA ΦEos. A p-value below 0.05 was considered to be significant.

Also, the protection could not be explained by a lower parasitemia, as the parasitemia of *Ifnar1*$^{-/-}$ mice did not differ from that of WT mice 6 dpi. However, it has been shown that *Ifnar1*$^{-/-}$ mice have significantly higher CCL5 levels in the spleen, a chemokine that plays an important role in the migration of effector and memory T cells (Aldinucci & Colombatti 2014). These high levels of CCL5 were also shown to be mainly produced by eosinophils and CD8+ T cells and lead to the retention of CD8+ T cells in the spleens of *Ifnar1*$^{-/-}$ mice (Scheunemann, Reichwald *et al.* submitted).

Taken together, the data about the different ILC populations provide important insights into the role of ILCs in the immune response to PbA. In particular, the kinetic experiments contribute to a better understanding of the dynamics of the immune response to PbA and reveal ILCs as a component of this response. So far, such data have been lacking, as the focus has been mainly on the importance of T cells. Although ILCs were subject to changes in the ECM model, a central role of ILCs in mediating pathology in WT and protection in *Ifnar1*$^{-/-}$ mice could not be determined. In contrast, the protective effect against ECM observed in *Ifnar1*$^{-/-}$ mice was in part dependent on eosinophils.

3.3 *Litomosoides sigmodontis* – filariasis

Unlike *Plasmodium* infection, an infection with helminths in general and *L. sigmodontis* in particular is mainly characterized by a type 2 and regulatory immune response. This is accompanied by an increase of e.g. eosinophils and alternatively activated macrophages and by an increase of regulatory and type 2 cytokines especially at the site of infection (Maizels & McSorley 2016; Frohberger *et al.* 2019).

To date, there have been few studies addressing the importance of ILCs during helminth infection, which are often limited to studies on intestinal helminths such as *N. brasiliensis* and *H. polygyrus* (Oliphant *et al.* 2014; Wilhelm *et al.* 2016; Herbert *et al.* 2019; Löser *et al.* 2019). Studies in the *L. sigmodontis* model have only once been carried out so far, but the used gating strategy was not completely suitable to identify ILCs and the study did not carry out functional analyses of ILC2s (Boyd *et al.* 2015). This gap needed to be addressed in this project to determine the role of different ILC populations during *L. sigmodontis* infection.

3.3.1 BALB/c mice develop chronic *L. sigmodontis* infection whereas C57BL/6 eliminate the parasite until 70 dpi

In particular, BALB/c and C57BL/6 mice were compared in the *L. sigmodontis* model, since it is already known that BALB/c mice develop a chronic infection, whereas C57BL/6 mice efficiently eliminate the parasite shortly after the molt into adult worms (Layland *et al.* 2015). Comparison of the two strains of mice provided an opportunity to investigate the extent to which ILCs play a role in chronic infection and whether certain ILC subsets might be involved in the elimination of the parasite in C57BL/6 mice. Kinetic experiments similar to the PbA experiments were performed to show the development of ILC subsets during the course of infection.

It was confirmed that BALB/c mice develop chronic *L. sigmodontis* infection, whereas C57BL/6 almost completely eliminated the parasite by day 70 (Fig. 20a). Worm burden in both groups was comparable at 9 dpi and 30 dpi, the latter the timepoint of moulting into adult worms. At 70 dpi, C57BL/6 mice had a significantly lower worm burden than BALB/c mice ($p=0.0079$). Furthermore, the worm burden of C57BL/6 mice decreased significantly from 9 dpi to 70 dpi ($p=0.0609$) and from 30 dpi to 70 dpi ($p=0.0072$). Both male and female worms isolated from the pleural cavity on 30 dpi from C57BL/6 mice were significantly shorter than worms from BALB/c mice (Fig. 20b). This suggests that C57BL/6 mice are less susceptible to *L. sigmodontis* infection and that worm moulting is affected in these mice as well. Indeed, at this point, C57BL/6 mice still showed L4 larvae in contrast to BALB/c mice in which almost all worms were already adult at this point (data not shown).

Analysis of microfilariae over the course of infection revealed that only BALB/c mice had peripheral microfilaremia, starting at day 63, whereas C57BL/6 mice did not (Fig. 20c). The proportion of Mf^+ BALB/c mice among all BALB/c mice was approximately 40% at day 57, with 100% of BALB/c mice being Mf^+ by day 63 after infection (Fig. 20d). Thus, no complete life cycle of *L. sigmodontis* occurred in C57BL/6 mice because no microfilariae were detected and elimination of worms took place until day 70.

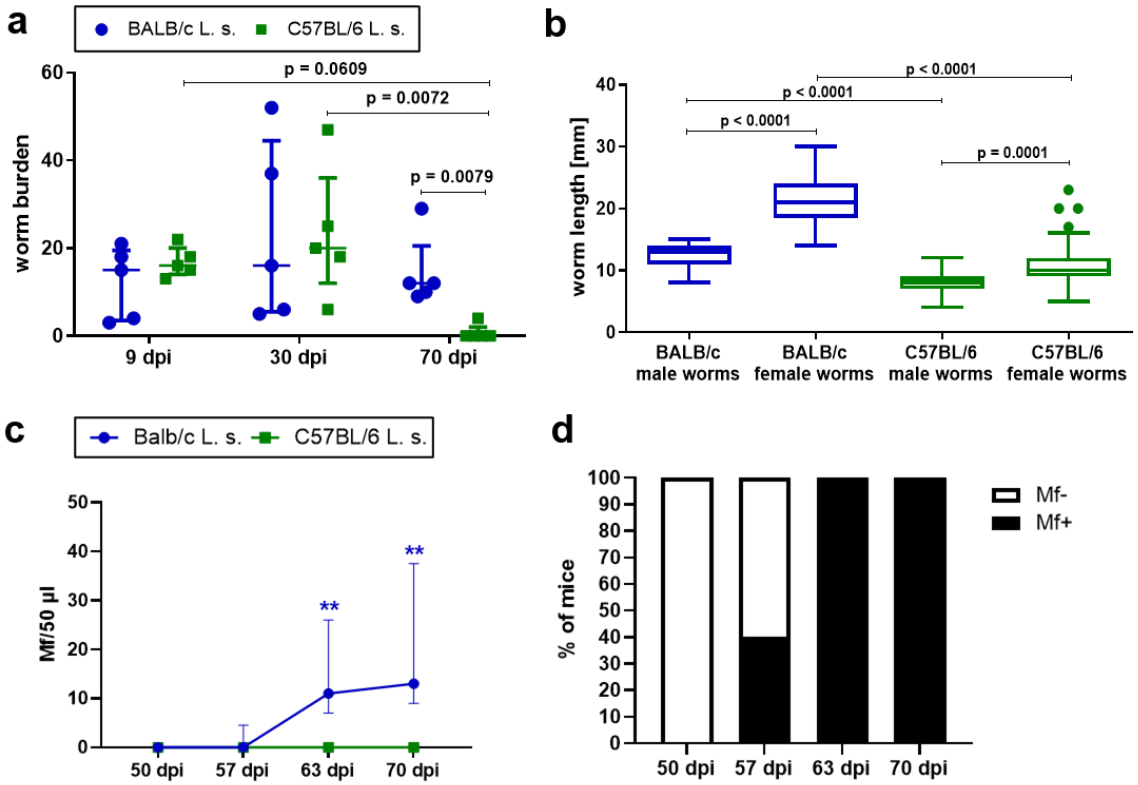

Figure 20: Chronic *L. sigmodontis* infection in BALB/c mice and elimination of the parasite in C57BL/6 mice. (a) Worm burden 9, 30 and 70 d post natural *L. sigmodontis* infection in susceptible BALB/c and semi-susceptible C57BL/6 mice. **(b)** Worm length 30 dpi. **(c)** Microfilariae (Mf) per 50µl of blood 50, 57, 63 and 70 dpi. **(d)** Percentage [% of all mice] of Mf+ and Mf- BALB/c mice 50, 57, 63 and 70 dpi. Bars represent the median with interquartile ranges. Data in (a+c+d) n = 5 per group and timepoint, data show 1 representative experiment from 2 (9 dpi) and 4 (30, 70 dpi) independent experiments. Data in (b) n = 49 worms for BALB/c female worms and C57BL/6 male worms, n = 67 worms for C57BL/6 female worms and n = 65 worms for BALB/c male worms, data show 1 representative experiment from 4 independent experiments. Data in (a+c+d) were analysed with Kruskal-Wallis test and Dunn's post-test. Data in (c) were analysed with 2-way ANOVA and Bonferroni multiple comparison test. A p-value below 0.05 was considered to be significant. **p<0.01.

Taken together previous data could be confirmed and provided a base for upcoming immunological analysis, especially for the kinetic analysis of ILC subsets during the course of *L. sigmodontis* infection.

3.3.2 ILC2s are increased during *L. sigmodontis* infection in the pleural cavity of semi-susceptible C57BL/6 mice in comparison to susceptible BALB/c mice

As a next step, kinetic analyses were performed for each ILC population to detect possible differences between C57BL/6 and BALB/c mice at various timepoints after *L. sigmodontis* infection.

There was an increase in the cell count of pleural cavity cells 9 dpi in both C57BL/6 (p=0.0881) and BALB/c mice (p=0.0248) (Fig. 21a). From 9 dpi to 30 dpi, cell numbers increased significantly in both *L. sigmodontis*-infected mouse groups compared to their

naive controls, reaching their peak at 30 dpi. At day 70 after infection, only BALB/c mice showed a significant increase in pleural cavity cells (p=0.0072). C57BL/6 mice did not show an increased cell count at this time, but it tended to be lower compared to the cell counts obtained at 30 dpi (p=0.0851). Only one C57BL/6 mouse had pleural cavity cell counts comparable to those of the BALB/c mice, but this mouse had not yet completely eliminated the infection at this timepoint. This trend of an reduction in pleural cavity cell counts from 30 dpi to 70 dpi in C57BL/6 mice was not observed in BALB/c mice. This followed the results of the worm burden, since on day 70 C57BL/6 mice effectively eliminated the infection, whereas BALB/c mice were chronically infected (Fig. 20).

The total cell count of ILC1s in the pleural cavity increased in C57BL/6 and BALB/c mice compared with naive controls already 9 dpi, reaching statistical significance for C57BL/6 mice (Fig 21b). 30 dpi, a significant increase in ILC1s was observed in both groups compared with naive controls. A different picture was seen at 70 dpi. Here, a significant increase in ILC1 cell counts occurred only in BALB/c mice compared with the naive controls (p=0.0012), with the total cell number of ILC1s of *L. sigmodontis*-infected C57BL/6 mice being significantly lower than in *L. sigmodontis*-infected BALB/c mice (p=0.0074). Furthermore, from 30 dpi to 70 dpi, there was a significant reduction in ILC1 cell numbers in the pleural cavity in *L. sigmodontis*-infected C57BL/6 mice (p=0.0004) and from 9 dpi to 70 dpi in *L. sigmodontis*-infected BALB/c mice (p=0.001). Regarding the proportions of ILC1s among all $CD45^+$ lymphocytes in the pleural cavity at day 9 and 30, no differences were detected, neither when comparing naive and *L. sigmodontis*-infected mice nor when comparing C57BL/6 and BALB/c mice. 70 dpi, a significant increase in the proportion of ILC1s occurred only in BALB/c mice compared with naive controls (p=0.0012), with the proportion of ILC1s in *L. sigmodontis*-infected BALB/c mice being significantly higher than in *L. sigmodontis*-infected C57BL/6 mice (p=0.0074).

NK cells in the pleural cavity 9 dpi showed a significant increase in total cell count in both BALB/c and C57BL/6 mice compared with naive controls (Fig. 21d). This increase was also observed at day 30 for both groups but at day 70 only in BALB/c mice. In C57BL/6 mice, the total cell count of NK cells in the pleural cavity decreased significantly from 9 dpi to 70 dpi (p=0.002) and from 30 dpi to 70 dpi (p=0.0029), with

C57BL/6 mice having significantly lower NK cell counts in the pleural cavity than BALB/c mice at day 70 after infection (p=0.0202).

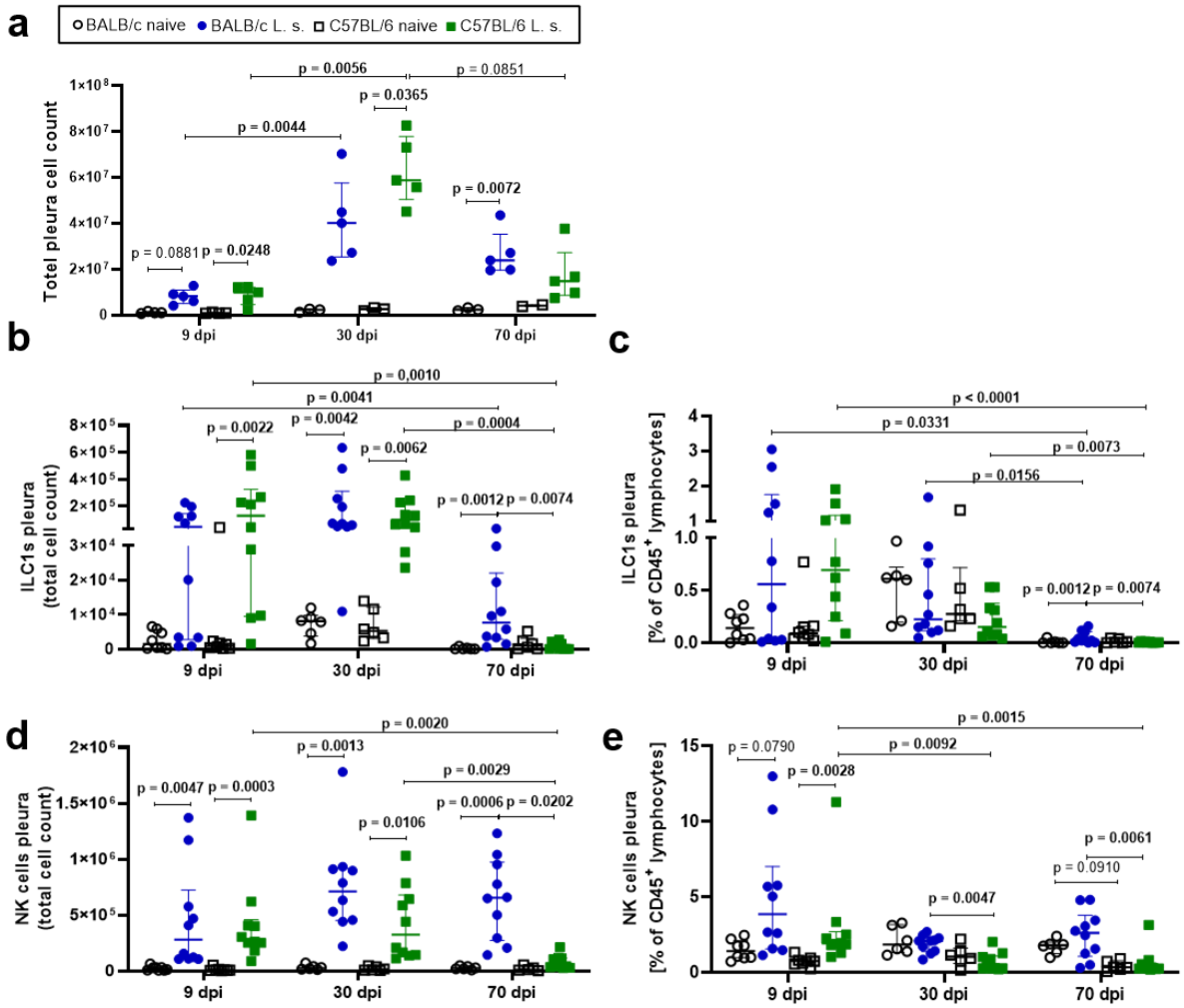

Figure 21: ILC1s and NK cells are lost in the pleural cavity of C57BL/6 mice upon elimination of *L. sigmodontis* until 70 dpi. (a) Total cell count of pleura cells 9, 30 and 70 d post natural *L. sigmodontis* infection in susceptible BALB/c and semi-susceptible C57BL/6 mice. **(b)** Total cell count of ILC1s in the pleura 9, 30 and 70 dpi. **(c)** Frequency [% of CD45$^+$ lymphocytes] of ILC1s in the pleura 9, 30 and 70 dpi. **(d)** Total cell count of NK cells in the pleura 9, 30 and 70 dpi. **(e)** Frequency [% of CD45$^+$ lymphocytes] of NK cells in the pleura 9, 30 and 70 dpi. Bars represent the median with interquartile ranges. Data in (a) n = 3 for naive mice 30 and 70 dpi, n = 4 for naive mice 9 dpi, n = 5 for all other groups 9, 30 and 70 dpi, data show 1 representative experiment from 2 independent experiments. Data in (b-e) n = 8 for naive mice 9 dpi, n = 6 for naive mice 30 and 70 dpi, n = 10 for *L. sigmodontis*-infected mice on all timepoints, pooled data from 2 independent experiments per timepoint. Spearman's for heteroscedasticity was performed and only data failing the heteroscedasticity were pooled. Data were analysed with Kruskal-Wallis test and Dunn's post-test. A p-value below 0.05 was considered to be significant.

Regarding the proportions of NK cells among all CD45$^+$ lymphocytes, an increase was observed at day 9 after infection in BALB/c (p=0.0790) and C57BL/6 (p=0.0028) (Fig. 21e). At day 30 and 70, this increase was not observed. However, *L. sigmodontis*-infected C57BL/6 mice had a significantly lower percentage of NK cells than *L. sigmodontis*-infected BALB/c mice at both time points. Furthermore, from 9 dpi to 30

dpi (p=0.0092) and 9 dpi to 70 dpi (p=0.0015), the proportion of NK cells in the pleural cavity of *L. sigmodontis*-infected C57BL/6 mice decreased significantly.

Thus, chronically infected BALB/c mice had abundant numbers of ILC1s and NK cells in the pleural cavity at day 70 after infection, whereas C57BL/6 mice had hardly any ILC1s and NK cells at the same time point.

The total cell count of ILC2s in the pleural cavity of C57BL/6 mice increased significantly 9 dpi, 30 dpi, and 70 dpi compared with naive controls (Fig. 22a). In BALB/c mice, this significant increase was also observed at day 9 and 70, and less prominent at day 30 (p=0.1249). Interestingly, in *L. sigmodontis*-infected BALB/c and C57BL/6 mice, the total cell count of ILC2s increased significantly from 9 dpi to 30 dpi, only to decrease significantly again from 30 dpi to 70 dpi. Therefore, the total cell count of ILC2s in the pleural cavity peaked 30 days after *L. sigmodontis* infection in both groups of mice. The cell count of ILC2s in 30 days *L. sigmodontis*-infected C57BL/6 mice was furthermore higher than in BALB/c mice (p=0.1436). The proportion of ILC2s among all $CD45^+$ lymphocytes in the pleural cavity increased 9 dpi in both BALB/c (p=0.0929) and C57BL/6 mice (p=0.0354) compared with naive controls (Fig. 22b). 30 days after infection, a significant increase in the proportion of ILC2s compared with naive controls was detected only in C57BL/6 mice (p<0.0001), and the proportion of ILC2s was higher in *L. sigmodontis*-infected C57BL/6 mice than in BALB/c mice (p=0.0967). The same was true 70 dpi, where the difference concerning the frequency of ILC2s between *L. sigmodontis*-infected BALB/c and C57BL/6 was significant (p=0.0051). From 9 dpi to 70 dpi (p<0.0001) and 30 dpi to 70 dpi (p=0.0376), the proportion of ILC2s among all $CD45^+$ lymphocytes in the pleural cavity decreased significantly in *L. sigmodontis*-infected BALB/c mice, whereas it increased significantly from 9 dpi to 30 dpi in C57BL/6 mice (p=0.0036) and then decreased significantly from 30 dpi to 70 dpi (p=0.0128). The peak of the proportion of ILC2s was reached on day 30 as it was observed for the total cell count as well. Thus, C57BL/6 mice showed significantly higher cell numbers and proportions of ILC2s at the site of infection than BALB/c mice, especially at day 30 after *L. sigmodontis* infection.

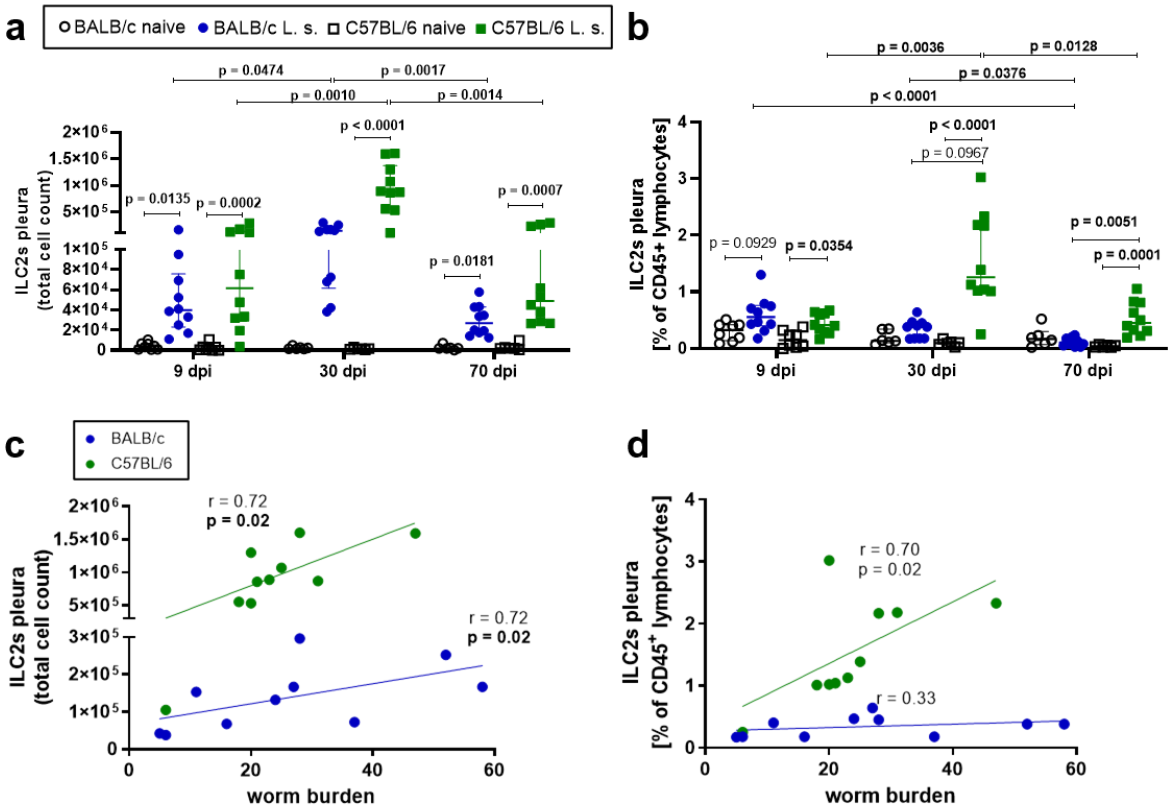

Figure 22: ILC2s are significantly increased in C57BL/6 mice upon *L. sigmodontis* infection compared to BALB/c mice and correlate with the worm burden. (a) Total cell count of ILC2s in the pleura 9, 30 and 70 d post natural *L. sigmodontis* infection in susceptible BALB/c and semi-susceptible C57BL/6 mice. **(b)** Frequency [% of CD45⁺ lymphocytes] of ILC2s in the pleura 9, 30 and 70 dpi. **(c)** Correlation of the worm burden with the total cell count of ILC2s in the pleura 30 dpi. **(d)** Correlation of the worm burden with the frequency [% of CD45⁺ lymphocytes] of ILC2s in the pleura 30 dpi. Bars represent the median with interquartile ranges. Data in (a-b) n = 8 for naive mice 9 dpi, n = 6 for naive mice 30 and 70 dpi, n = 10 for *L. sigmodontis*-infected mice on all timepoints, pooled data from 2 independent experiments per timepoint. Data in (c-d) n = 10, pooled data from 2 independent experiments. Spearman's test for heteroscedasticity was performed and only data failing the heteroscedasticity were pooled. Data were analysed with Kruskal-Wallis test and Dunn's post-test. Correlation analysis was performed by nonparametric Spearman correlation. A p-value below 0.05 was considered to be significant. An r-value of 1 represents a perfect positive correlation.

Furthermore, 30 dpi, the day of the peak of ILC2s, the total cell number of ILC2s in the pleural cavity positively correlated with the worm burden in BALB/c (r=0.72, p=0.02) and C57BL/6 mice (r=0.72, p=0.02) (Fig. 22c). The same was observed for the proportions of ILC2s in the pleural cavity of C57BL/6 mice 30 dpi (r=0.70, p=0.02) (Fig. 22d). Based on this correlation it was hypothesized that ILC2s play a central role in the immune response to *L. sigmodontis* and possibly in the elimination of the parasite in C57BL/6 mice.

The increase in ILC3 populations after *L. sigmodontis* infection in BALB/c and C57BL/6 mice tended to follow the general increase in pleural cavity cells (Fig. 23). There also was little difference between the two mouse strains and naive controls in particular

varied strongly in terms of ILC3 populations. Therefore, the ILC3s were not further investigated in the upcoming analyses.

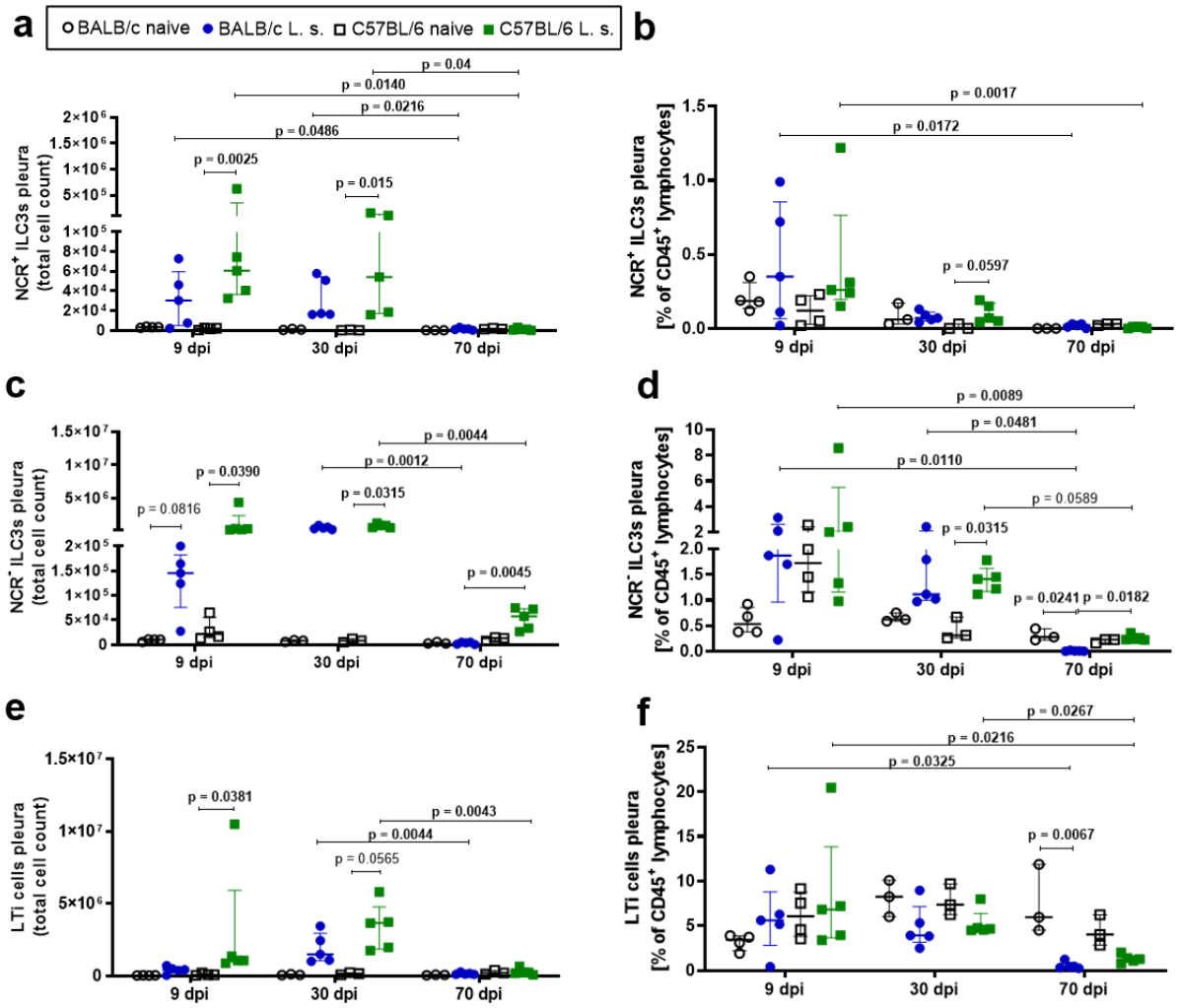

Figure 23: No significant differences in ILC3 populations between BALB/c and C57BL/6 mice during *L. sigmodontis* infection. (a) Total cell count of NCR+ ILC3s in the pleura 9, 30 and 70 d post natural *L. sigmodontis* infection in susceptible BALB/c and semi-susceptible C57BL/6 mice. **(b)** Frequency [% of CD45⁺ lymphocytes] of NCR+ ILC3s in the pleura 9, 30 and 70 dpi. **(c)** Total cell count of NCR- ILC3s in the pleura 9, 30 and 70 dpi. **(d)** Frequency [% of CD45⁺ lymphocytes] of NCR- ILC3s in the pleura 9, 30 and 70 dpi. **(e)** Total cell count of LTi cells in the pleura 9, 30 and 70 dpi. **(f)** Frequency [% of CD45⁺ lymphocytes] of LTi cells in the pleura 9, 30 and 70 dpi. Bars represent the median with interquartile ranges. Data in (a-f) n = 3-4 for naive mice 9, 30 and 70 dpi, n = 5 for L. sigmodontis-infected mice 9, 30 and 70 dpi. Data show 1 representative experiment from 2 independent experiments per timepoint. Data were analysed with Kruskal-Wallis test and Dunn's post-test. A p-value below 0.05 was considered to be significant.

The most striking differences between BALB/c and C57BL/6 mice were found with respect to ILC2s, particularly 30 dp *L. sigmodontis* infection (Fig. 24).

a

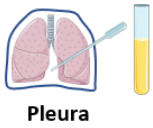

Cell counts of…	30 dpi		70 dpi	
	BALB/c	C57BL/6	BALB/c	C57BL/6
ILC1s	++	++	+	→
NK cells	+	+	+	→
ILC2s	+	++	+	++
NCR+ ILC3s	+	+	→	→
NCR- ILC3s	+	+	→	+
LTi cells	+	+	→	→

++ = strongly increased compared to naive control
\+ = increased compared to naive control
\- = decreased compared to naive control
→ = no difference to naïve control
□ = most important differences

b

Frequency of…	30 dpi		70 dpi	
	BALB/c	C57BL/6	BALB/c	C57BL/6
ILC1s	→	→	+	→
NK cells	→	→	+	→
ILC2s	→	++	→	+
NCR+ ILC3s	→	+	→	→
NCR- ILC3s	→	+	-	→
LTi cells	→	→	-	-

Figure 24: Summary of results from 30 and 70 days *L. sigmodontis*-infected C57BL/6 and BALB/c mice. Cell counts as well as frequencies of ILC1s, NK cells, ILC2s and ILC3s of 30 and 70 days *L. sigmodontis*-infected C57BL/6 and BALB/c were compared to their naive controls. ++ = strongly increased compared to naive control, + = increased compared to naive control, - = decreased compared to naive control, → = no differences to naive control. Red square = most important differences. Day 9 is not shown as the differences were minor. **(a)** Summary of the changes of ILC1, NK cell, ILC2 and ILC3 total cell counts in the pleural cavity of *L. sigmodontis*-infected C57BL/6 and BALB/c mice. (b) Summary of the changes of ILC1, NK cell, ILC2 and ILC3 frequencies in the pleural cavity of *L. sigmodontis*-infected C57BL/6 and BALB/c mice. Pictures of the lung, the pipette and the vial were taken from Servier Medical Art.

Since these cells have further been shown to be important in numerous other parasitic infectious diseases and as there was a positive correlation between ILC2 numbers and worm burden, the focus of further analyses was on the ILC2s and their involvement in the immune response to *L. sigmodontis* infection.

3.3.3 Stronger type 2 immune response in the pleural cavity of *L. sigmodontis*-infected C57BL/6 mice on day 30 compared to BALB/c mice

Not only the kinetics of different ILC populations in the pleural cavity of *L. sigmodontis* infected animals were of great interest, but also the corresponding cytokine milieu at the site of infection. Since there were significant differences between BALB/c and C57BL/6 mice, especially with regard to ILC2s, the cytokines IL-5 and IL-13 produced by ILC2s were measured by ELISA.

At day 9 post infection, there was no increase in IL-5 or IL-13 levels in the pleural cavity of *L. sigmodontis*-infected BALB/c and C57BL/6 mice compared with naive controls (Fig. 25a, 25b). 30 dpi, there was a significant increase in IL-5 ($p=0.0167$) and IL-13 ($p=0.0011$) levels in the pleural cavity only in C57BL/6 mice compared to naive controls, and the levels were also significantly higher than in *L. sigmodontis*-infected BALB/c mice. 70 dpi, IL-5 and IL-13 levels were significantly increased in both BALB/c and C57BL/6 mice compared with naive controls and *L. sigmodontis*-infected C57BL/6 mice showed slightly higher IL-5 levels than *L. sigmodontis*-infected BALB/c mice at

that timepoint (Fig. 25a). IL-5 and IL-13 levels in *L. sigmodontis*-infected C57BL/6 mice peaked at 30 dpi whereas BALB/c mice had its IL-5 peak at 70 dpi and IL-13 levels remained at a similar low range at each time point (Fig. 25b). Accordingly, C57BL/6 mice reach significantly higher levels of type 2 cytokines after *L. sigmodontis* infection than BALB/c mice and the levels peaked at day 30, at a timepoint where the highest ILC2 numbers were observed.

Since not only ILC2s produce IL-5 and IL-13, but also Th2 cells, kinetics of Th2 cells over the course of infection were additionally performed to obtain a complete picture of the type 2 immune response at the site of infection (Figs. 25c, 25d). At day 9, the Th2 cell numbers significantly increased in the pleural cavity in both BALB/c mice ($p=0.0194$) and C57BL/6 mice ($p=0.0002$) compared with naive controls, but both mouse types did not differ in this regard (Fig. 25c). At 30 dpi, an increase in Th2 cell numbers was also observed in both strains compared with naive controls, with *L. sigmodontis*-infected C57BL/6 mice having slightly higher cell numbers than *L. sigmodontis*-infected BALB/c mice ($p=0.2025$).

At day 70, in contrast to all other time points, no significant increase in Th2 cell counts was observed; here, the variance within the *L. sigmodontis*-infected groups was quite high. Over the entire course of infection, from 9 to 30 dpi, the total cell number of Th2 cells in the pleural cavity increased significantly in both *L. sigmodontis*-infected groups, to decrease significantly again from 30 dpi to 70 dpi. With regard to the proportions of Th2 cells among all $CD45^+$ lymphocytes in the pleural cavity, a significant increase was observed at 30 dpi only in *L. sigmodontis*-infected C57BL/6 mice compared with naive controls ($p=0.0313$) but not in BALB/c mice (Fig. 25d). The percentage of Th2 cells was thus significantly higher than in *L. sigmodontis*-infected BALB/c mice ($p=0.0282$).

Furthermore, Th2 cell numbers positively correlated with the ILC2 cell numbers in the pleural cavity in both 30 days *L. sigmodontis*-infected BALB/c ($r=0.87$, $p=0.002$) and C57BL/6 mice ($r=0.6$, $p=0.08$) (Fig. 25e). The same was true for the proportions of both cell types among all $CD45^+$ lymphocytes (Fig. 25f).

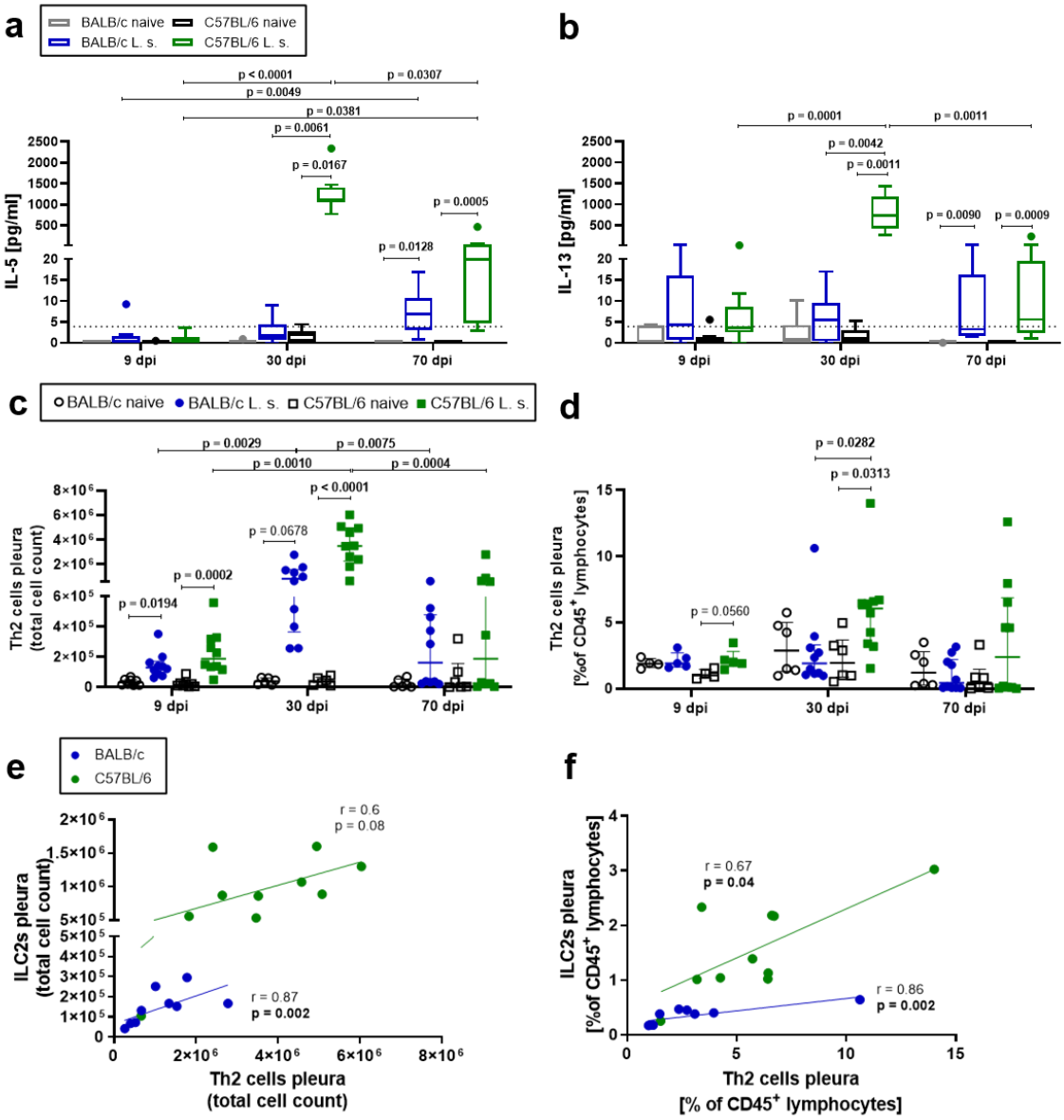

Figure 25: C57BL/6 show a significantly stronger type 2 immune response than BALB/c mice 30 dpi. **(a)** IL-5 levels in the pleura 9, 30 and 70 d post natural *L. sigmodontis* infection in susceptible BALB/c and semi-susceptible C57BL/6 mice. **(b)** IL-13 levels in the pleura 9, 30 and 70 dpi. **(c)** Total cell count of Th2 cells in the pleura 9, 30 and 70 dpi. **(d)** Frequency [% of $CD45^+$ lymphocytes] of Th2 cells in the pleura 9, 30 and 70 dpi. **(e)** Correlation of the total cell count of ILC2s in the pleura with the total cell count of Th2 cells in the pleura 30 dpi. **(f)** Correlation of the frequency of ILC2s in the pleura with the frequency of Th2 cells in the pleura 30 dpi. (a-b) show box and whiskers with Tukey. Bars in (c-f) represent the median with interquartile ranges. Data in (a-d) n = 8 for naive mice 9 dpi, n = 6 for naive mice 30 and 70 dpi, n = 10 for *L. sigmodontis*-infected mice on all timepoints, pooled data from 2 independent experiments per timepoint. Data in (e-f) n = 10, pooled data from 2 independent experiments per timepoint. Spearman's test for heteroscedasticity was performed and only data failing the heteroscedasticity were pooled. Data were analysed with Kruskal-Wallis test and Dunn's post-test. Correlation analysis was performed by nonparametric Spearman correlation. A p-value below 0.05 was considered to be significant. An r-value of 1 represents a perfect positive correlation.

Taken together, the data show a stronger type 2 immune response in C57BL/6 as a result of *L. sigmodontis* infection than in BALB/c mice, particularly at day 30, and this immune response is also more likely to be maintained in C57BL/6 mice until day 70 than in BALB/c mice.

3.3.4 ILC2s are more potent in producing IL-5 than CD4⁺ T cells in both *L. sigmodontis*-infected C57BL/6 and BALB/c mice

In particular, significant differences in IL-5 levels in the pleural cavity were detected between *L. sigmodontis*-infected BALB/c and C57BL/6 mice. Thus, it was determined which cells contribute to these high IL-5 levels in the pleural cavity and to what extent ILC2s and CD4⁺ T cells differ in their IL-5 production. Since there was little difference between the two mouse strains on day 9, the upcoming analyses focused on 30 and 70 dpi.

IL-5⁺ CD4⁺ T cells were characterized as CD45⁺ Lin⁺ CD4⁺ TCRβ⁺ IL-5⁺ and IL-5-expressing ILC2s were characterized as CD45⁺ Lin⁻ CD4⁻ TCRβ⁻ IL-33R⁺ GATA-3⁺ IL-5⁺ (Fig. 26). Importantly, bigger cells like granulocytes and monocytes were excluded in the first gate to increase the resolution in the later gates.

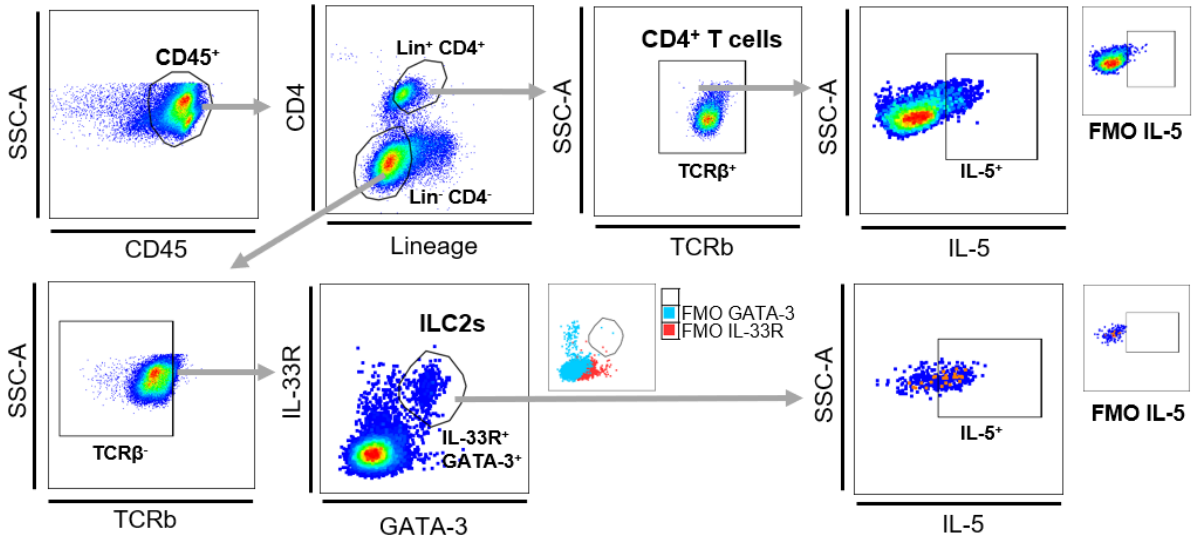

Figure 26: Gating strategy for the identification of IL-5-expressing ILC2s and T cells in the pleural cavity of *L. sigmodontis*-infected mice. The gating strategy is shown exemplarily in the pleural cavity of a *L. sigmodontis*-infected C57BL/6 mouse. The cells were gated on CD45⁺ lymphocytes whereas granulocytes and monocytes were excluded in the first gate to increase resolution. IL-5-expressing ILC2s were identified as CD45⁺ Lin⁻ TCRβ⁻ CD4⁻ IL-33R⁺ GATA-3⁺ IL-5⁺ and IL-5-expressing CD4⁺ T cells were identified as CD45⁺ Lin⁺ CD4⁺ TCRβ⁺ IL-5⁺.The gates were set by using FMOs.

On day 30 pi, there was a significantly higher total cell count of IL-5-producing ILC2s in the pleural cavity of *L. sigmodontis*-infected C57BL/6 mice compared with BALB/c mice (p=0.0068) (Fig. 27a). In contrast, at day 70, cell numbers were comparable, whereas the total cell count decreased significantly from 30 dpi to 70 dpi in C57BL/6 mice (p=0.0015). With regard to IL-5-producing CD4⁺ T cells, a similar picture emerged (Fig. 27b). Here, 30 dpi there were significantly higher total cell counts in C57BL/6 mice than in BALB/c mice (p=0.0052). Also, the cell number of IL-5⁺ CD4⁺ T cells in C57BL/6

mice decreased significantly from 30 dpi to 70 dpi (p=0.04) to a level comparable to that in BALB/c mice.

The proportion of IL-5$^+$ ILC2s among all CD45$^+$ lymphocytes was significantly higher in *L. sigmodontis*-infected C57BL/6 mice than in BALB/c mice at both day 30 and day 70 (Fig. 27c). Furthermore, the proportion of IL-5$^+$ CD4$^+$ T cells among all CD45$^+$ lymphocytes was significantly higher 30 and 70 dpi in C57BL/6 mice than in BALB/c mice (Fig. 27d). In both mouse strains, the proportion increased from 30 dpi to 70 dpi (p=0.0785 for BALB/c, p=0.040 for C57BL/6).

The percentage of ILC2s being IL-5$^+$ among all ILC2s in the pleural cavity was comparable between BALB/c and C57BL/6 mice 30 dpi (Fig 27e). Interestingly, the percentage of ILC2s among all ILC2s that are IL-5$^+$ decreased significantly in BALB/c mice from 30 dpi to 70 dpi (p=0.0079), whereas it did not decrease in the C57BL/6 mice and was thus also significantly higher than in BALB/c mice at 70 dpi (p=0.0317). The percentage of CD4$^+$ T cells producing IL-5 at day 30 was also comparable between BALB/c and C57BL/6 mice (Fig. 27f). By day 70, the percentage of IL-5$^+$ CD4$^+$ T cells among all CD4$^+$ T cells decreased significantly in BALB/c mice (p=0.0002), whereas it remained constant in C57BL/6 mice. At day 30, among the ILC2s, approximately 60% are positive for IL-5, compared to under 10% of CD4$^+$ T cells (Fig. 27e, 27f).

Consequently, especially at day 30 after *L. sigmodontis* infection, not only the number and proportion of ILC2s and Th2 cells increased, but also the number of IL-5-producing cells. Furthermore, in line with the kinetic data C57BL/6 mice also exhibited higher cell numbers and proportions of these cells compared with BALB/c mice. In chronically infected BALB/c mice fewer ILC2s and CD4$^+$ T cells appeared to remain IL-5$^+$ in comparison to C57BL/6 mice that already eliminated infection at day 70.

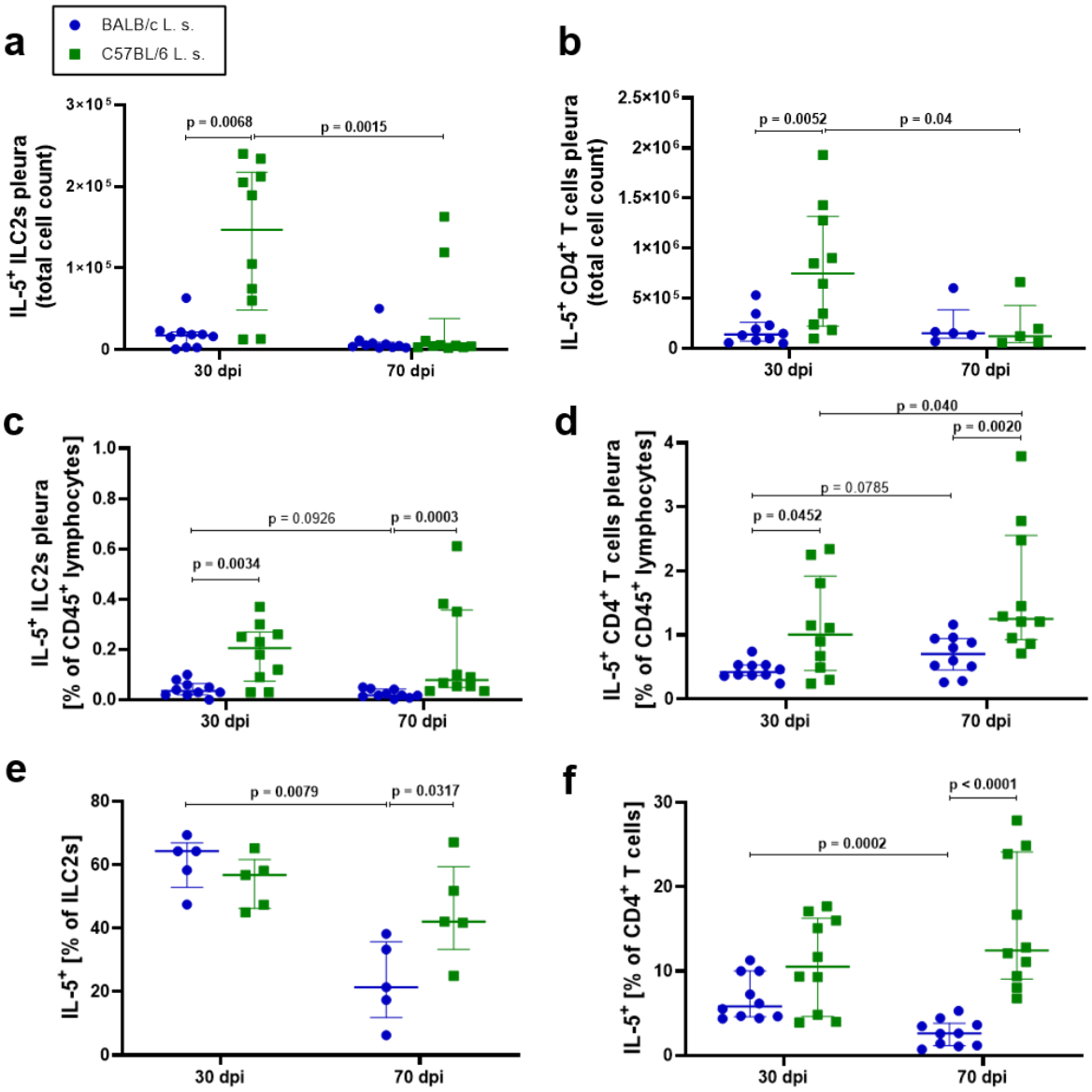

Figure 27: C57BL/6 show significantly more IL-5-expressing ILC2s and T cells upon *L. sigmodontis* infection than BALB/c mice 30 dpi. Pleural cavity cells were isolated from 30 and 70 d *L. sigmodontis* infected susceptible BALB/c and semi-susceptible C57BL/6 mice and restimulated in vitro with PMA and ionomycin in the presence of Brefeldin A and monensin. **(a)** Total cell count of IL-5-expressing ILC2s and **(b)** Total cell count of IL-5-expressing CD4$^+$ T cells. **(c)** Frequency [% of CD45$^+$ lymphocytes] of IL5-expressing ILC2s in the pleura 30 and 70 dpi. **(d)** Frequency [% of CD45$^+$ lymphocytes] of IL5-expressing CD4$^+$ T cells in the pleura 30 and 70 dpi. **(e)** Percentage [% of ILC2s] of ILC2s being IL-5$^+$ among all ILC2s in the pleura 30 and 70 dpi. **(f)** Percentage [% of CD4$^+$ T cells] of CD4$^+$ T cells being IL-5$^+$ among all CD4$^+$ T cells in the pleura 30 and 70 dpi. Bars represent the median with interquartile ranges. Data in (a-d) and (f) n = 10 per group and timepoint, pooled data from 2 independent experiments per timepoint. Data in (e) n = 5 per group and timepoint, data show 1 representative experiment from 2 independent experiments per timepoint. Spearman's test for heteroscedasticity was performed and only data failing the heteroscedasticity were pooled. Data were analysed with Mann-Whitney test to compare 2 mouse groups per timepoint and 2 timepoints per mouse group. A p-value below 0.05 was considered to be significant.

Expression analysis revealed a significantly higher IL-5 expression of ILC2s than CD4$^+$ T cells in both BALB/c (p=0.0079) and C57BL/6 mice (p=0.0079) 30 dpi (Fig. 28a). IL-5 expression of ILC2s from C57BL/6 mice tended to be lower compared with ILC2s from

BALB/c mice (p=0.09). On day 70 after *L. sigmodontis* infection, ILC2s again showed higher IL-5 expression than $CD4^+$ T cells in both BALB/c (p=0.0556) and C57BL/6 mice (p=0.0079) (Fig. 28b). Interestingly, at this time point, the ILC2s (p=0.0079) and $CD4^+$ T cells (p=0.0952) in C57BL/6 mice both showed higher IL-5 expression levels than the same cells in BALB/c mice. Accordingly, ILC2s were more potent IL-5 producers during *L. sigmodontis* infection than $CD4^+$ T cells.

The composition of IL-5 producers also showed striking differences when comparing BALB/c and C57BL/6 mice (Figs. 28c, 28d). 30 dpi, lymphoid cells, particularly in C57BL/6, emerged as dominant IL-5 sources (Fig. 28c) consisting of ILC2s and $CD4^+$ T cells, which together accounted for approximately 70% of IL-5 producers. In contrast, in BALB/c mice, the proportion of lymphoid sources was much lower with approximately 40%. Overall, the percentage of $CD4^+$ T cells (p=0.008) and ILC2s (p=0.03) among all $IL\text{-}5^+$ cells was significantly higher in C57BL/6 mice than in BALB/c mice, which had a significantly higher percentage of eosinophils among IL-5+ producers than the C57BL/6 mice (p=0.008). Other cellular sources accounted for a small proportion among all IL-5 producers. At 70 dpi, a similar picture was observed for both C57BL/6 and BALB/c mice (Fig. 28d).

Cell counts of all $IL\text{-}5^+$ cells revealed comparable total $IL\text{-}5^+$ cell counts (p=0.6905) on day 30 in BALB/c and C57BL/6 mice with again lymphoid sources being dominant (Fig. 28e). On day 70 pi, C57BL/6 mice showed significantly lower $IL\text{-}5^+$ cell numbers than BALB/c mice (p=0.0159), but interestingly, total cell numbers of $IL\text{-}5^+$ $CD4^+$ T cells and $IL\text{-}5^+$ ILC2s did not differ between the two mouse strains (Fig. 28f). This is consistent with previous data (Fig. 27). BALB/c mice only showed significantly higher cell numbers of IL-5-positive eosinophils.

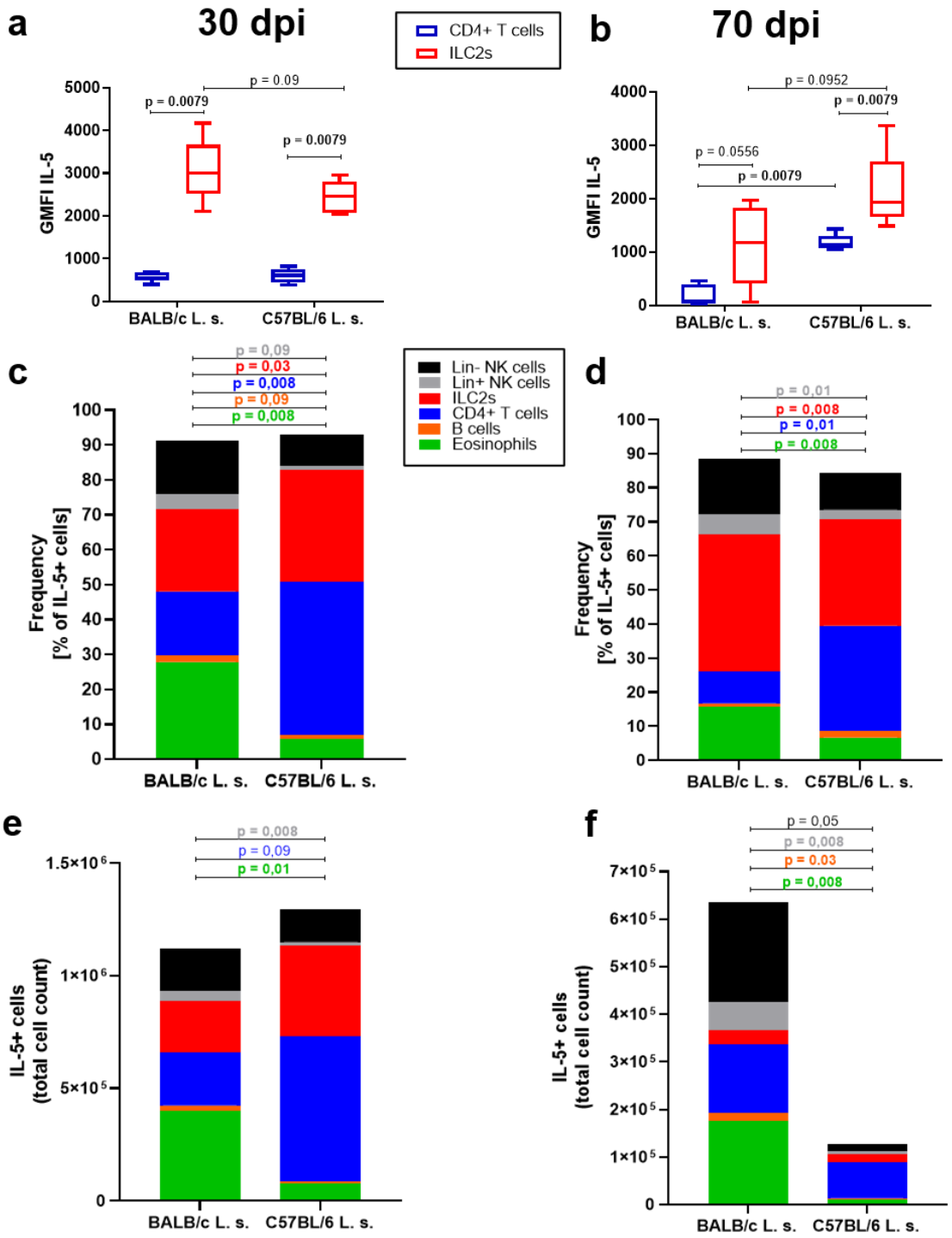

Figure 28: ILC2s are more potent in producing IL-5 than CD4⁺ T cells. Pleural cavity cells were isolated from 30 and 70 d *L. sigmodontis* infected susceptible BALB/c and semi-susceptible C57BL/6 mice and restimulated in vitro with PMA and ionomycin in the presence of Brefeldin A and monensin. **(a)** IL-5 expression level (GMFI) of ILC2s and CD4⁺ T cells in the pleura 30 d post natural *L. sigmodontis* infection in susceptible BALB/c and semi-susceptible C57BL/6 mice. **(b)** IL-5 expression level (GMFI) of ILC2s and CD4⁺ T cells in the pleura 70 dpi. **(c)** Composition of IL-5⁺ cells in the pleura 30 dpi. **(d)** Composition of IL-5⁺ cells in the pleura 70 dpi. **(e)** Stacked graph of all total cell counts of IL-5-expressing cells in the pleura 30 dpi and **(f)** 70 dpi. (a-b) show box and whiskers with Tukey. Bars in (c-f) respresent the median of each cell type. Data in (a+b+d+f) n = 5 per group and timepoint, data show 1 representative experiment from 2 independent experiments per timepoint. Data in (c+e) n = 5, data from 1 experiment. Data were analysed with Mann-Whitney test to compare 2 cell types per mouse group, 2 mouse groups per cell type in (a+b) and the 2 mouse groups in (c-f). A p-value below 0.05 was considered to be significant.

Overall, it was concluded that different cellular sources were responsible for IL-5 levels in the pleural cavity of *L. sigmodontis*-infected BALB/c and C57BL/6 mice. In particular, the differences with regard to eosinophils were striking, as they accounted for a significant proportion only in BALB/c mice. Although eosinophils generally showed higher IL-5 expression than $CD4^+$ T cells and ILC2s (data not shown), eosinophils did not emerge as a dominant source in terms of their proportion among all $IL\text{-}5^+$ cells, nor did they occur in greater cell numbers than lymphoid sources. Accordingly, they probably contributed only to a low extent to the high IL-5 levels.

3.3.5 ILC2 depletion enhances the microfilarial load in *L. sigmodontis*-infected *Rag2*$^{-/-}$ mice 63 dpi

A next step would have been to deplete ILC2s particularly in C57BL/6 mice to demonstrate their involvement in the elimination of *L. sigmodontis*. However, there is as yet no suitable antibody that exclusively depletes ILCs, since these cells share many markers with T cells and other cells (Eberl *et al.* 2015). Depletion would thus automatically lead to depletion of other cell types and distort the results. Also, it is hardly possible to deplete a certain subpopulation of ILCs without affecting other subsets, since the subpopulations also share certain markers (Serafini *et al.* 2015). Furthermore, to date, no suitable mouse line exists that lacks only ILCs and at the same time exhibits a normal phenotype in the naive state (The Jackson Laboratory 2018). Therefore, specific depletion of ILC2s was not possible at this time point. Therefore, another model was used, *Rag2*$^{-/-}$ mice lacking T and B cells. They allowed the study of the immune response by ILCs to *L. sigmodontis* in the absence of the adaptive immune system. It is already known that *Rag2*$^{-/-}$ mice that additionally lack ILCs/NK cells (*Rag2IL2γR*$^{-/-}$ mice) have a higher worm burden than C57BL/6 mice and develop chronic infections (Layland *et al.* 2015). This suggests that T and B cells are to some extent central for the elimination of the parasite in C57BL/6 mice. However, this does not clarify the specific role of ILC2s during *L. sigmodontis* infection in C57BL/6 mice, as *Rag2IL2γR*$^{-/-}$ mice also lack ILCs. Moreover, there is a very strong interaction of T cells with ILC2s (Burg *et al.* 2015, Kumar 2020). $CD4^+$ T cells require ILC2s for proliferation as well as survival and secretion of type 2 cytokines, and ILC2s require $CD4^+$ T cells to maintain their function. Therefore, it could not be determined whether ILC2s also play a role in the immune response and elimination of *L. sigmodontis*. This hypothesis was further investigated by infecting *Rag2*$^{-/-}$ mice that

lack T and B cells but still possess ILC2s with *L. sigmodontis* and depleting ILC2s by administration of anti-CD90.2 before day 30 of infection, the timepoint adult worms develop and ILC2s peak in C57BL/6 mice.

Rag2$^{-/-}$ mice had a significantly higher worm burden than C57BL/6 mice 30 dpi (p=0.0159) (Fig. 29a). Furthermore, the worms of *Rag2*$^{-/-}$ mice were significantly longer than those of C57BL/6 mice (Fig. 29b). It was observed that in C57BL/6 mice L4 larvae were still present, while in *Rag2*$^{-/-}$ mice all worms had already undergone moulting into adult worms (Fig. 29c).

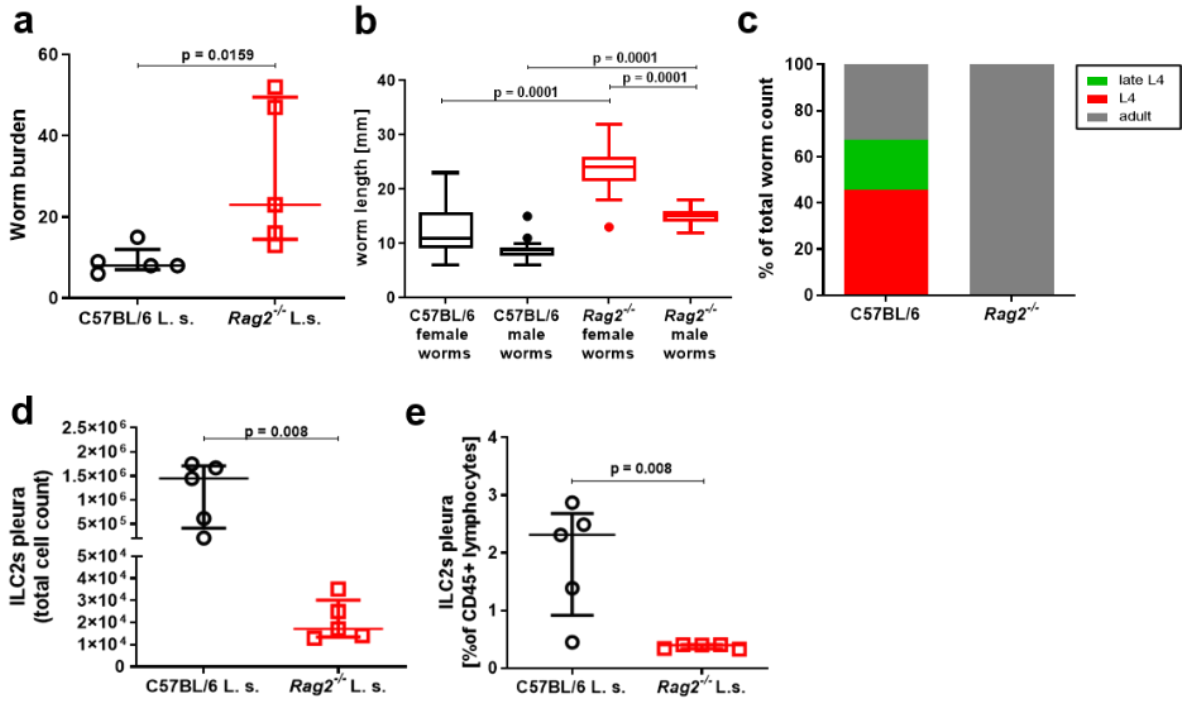

Figure 29: *Rag2*$^{-/-}$ show a significantly increased worm burden compared to C57BL/6 mice 30 dpi. **(a)** Worm burden 30 d post natural *L. sigmodontis* infection in semi-susceptible C57BL/6 mice and susceptible *Rag2*$^{-/-}$ mice. **(b)** Worm length [mm] of female and male worms 30 dpi. **(c)** Stages of worms 30 dpi. **(d)** Total cell count of ILC2s in the pleura 30 dpi. **(e)** Frequency [% of CD45+ lymphocytes] of ILC2s in the pleura 30 dpi. Bars represent the median with interquartile ranges. Data in (a+b+d+e) n = 5, data from 1 experiment. Data in (b+d) n = 18 worms for male worms of C57BL/6 mice, n = 24 worms for female worms of C57BL/6 mice, n = 57 worms for female worms of *Rag2*$^{-/-}$ mice and n = 89 worms for male worms of *Rag2*$^{-/-}$ mice, data from 1 experiment. Data in (a+b+d+e) were analysed with Mann-Whitney test, data in (b) were analysed with Kruskal-Wallis test and Dunn's post-test. A p-value below 0.05 was considered to be significant.

To define the baseline situation with regard to ILC2 cell numbers, these were analyzed in the pleural cavity of both mouse strains. Again, C57BL/6 mice showed very high ILC2 cell numbers and proportions among all CD45^{+} lymphocytes (Fig. 29d, 29e). In contrast, *Rag2*$^{-/-}$ mice had significantly fewer ILC2s in the pleural cavity, which were approximately equivalent to the numbers and frequency in chronically infected BALB/c mice.

To analyse the involvement of ILC2s in the immune response to *L. sigmodontis* in *Rag2*$^{-/-}$ mice, ILC2s were depleted just before the molt into adult worms. The corresponding analyses were performed at day 63 (Fig. 30a), a timepoint when the chronic infection is fully developed and microfilariae are produced in susceptible mouse strains, thus the cycle of *L. sigmodontis* completed.

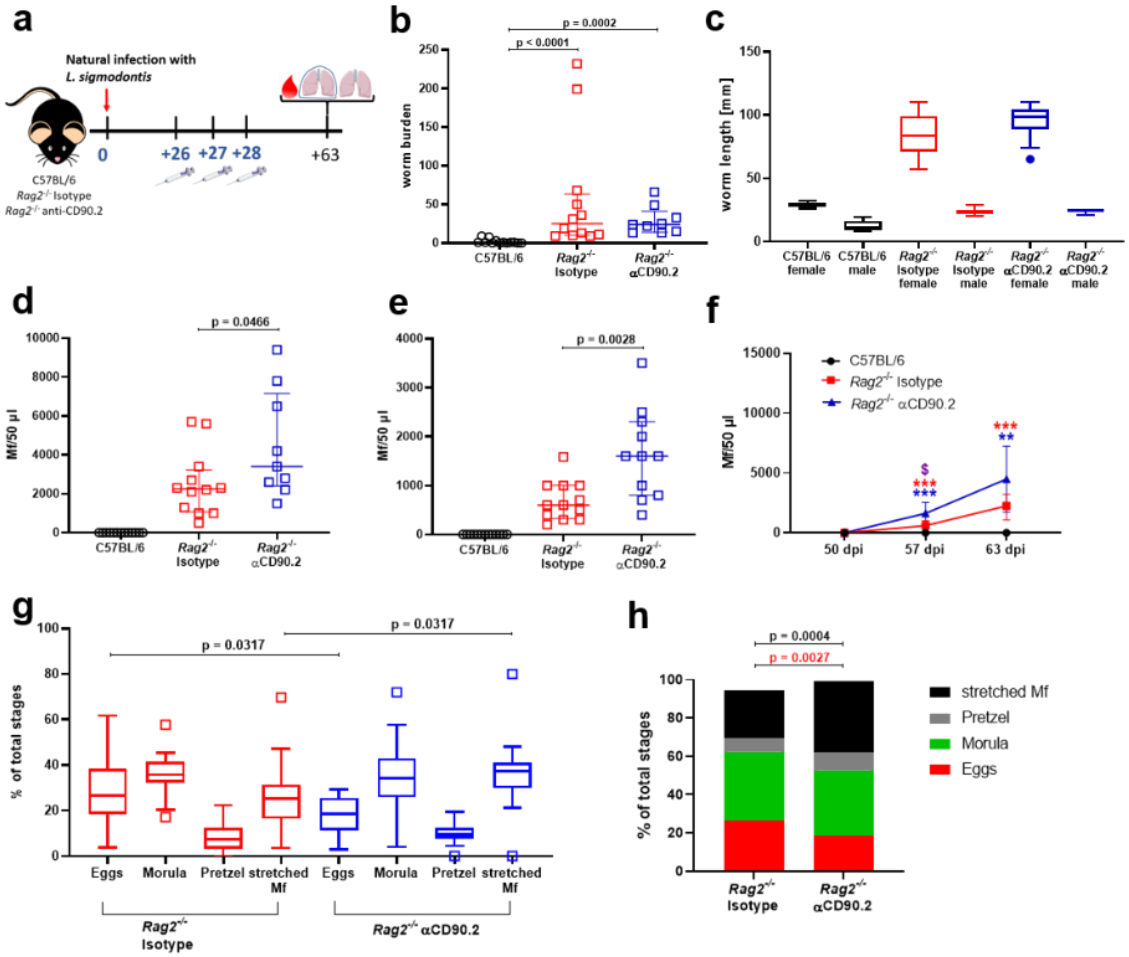

Figure 30: ILC2 depletion enhances microfilarial load in *L. sigmodontis*-infected *Rag2*$^{-/-}$ mice. (a) Experimental setup of ILC2 depletion. **(b)** Adult worm burden 63 d post natural *L. sigmodontis* infection in semi-susceptible C57BL/6 mice, susceptible *Rag2*$^{-/-}$ mice and ILC2-depleted *Rag2*$^{-/-}$ mice. **(c)** Worm length [mm] of female and male worms 63 dpi. **(d)** Microfilariae (Mf) in the blood 57 dpi. **(e)** Microfilariae (Mf) in the blood 63 dpi. **(f)** Microfilariae (Mf) in the blood over time. **(g)** Embryonic stages (egg, morula, pretzel, stretched Mf) (% of total stages) of female worms 63 dpi. **(h)** Distribution of embryonic stages (% of total stages) in female worms 63 dpi. Bars represent the median with interquartile ranges. Data in (b and d-f) n = 11-13, pooled data from 2 independent experiments. Data in (c) n = 2 worms for female worms of C57BL/6 mice, n = 6 worms for male worms of C57BL/6 mice, n = 20 worms for female worms of Isotype *Rag2*$^{-/-}$ mice and n = 20 worms for male worms of Isotype *Rag2*$^{-/-}$ mice, n = 14 for female worms of αCD90.2-treated *Rag2*$^{-/-}$ mice and n = 15 for male worms of αCD90.2-treated *Rag2*$^{-/-}$ mice, data show 1 representative experiment from 2 independent experiments. Data in (g-h) n = 25-28, data from 1 experiment. Spearman's test for heteroscedasticity was performed and only data failing the heteroscedasticity were pooled. Data in (a-c) and (g) were analysed with Kruskal-Wallis test and Dunn's post-test. Data in (d-e) were analysed with Mann-Whitney test for the comparison of Isotype Rag2$^{-/-}$ mice with αCD90.2-treated *Rag2*$^{-/-}$ mice. Data in (h) were analysed with Mann-Whitney test. Data in (f) were analysed with Mixed-effects analysis with Bonferroni test for multiple comparisons, $ = *Rag2*$^{-/-}$ Isotype vs. *Rag2*$^{-/-}$ αCD90.2. A p-value below 0.05 was considered to be significant. **p<0.01, ***p<0.0001

Rag2$^{-/-}$ mice in general exhibited a significantly increased adult worm burden in the pleural cavity at day 63 after *L. sigmodontis* infection compared with C57BL/6 mice (Fig. 30b). However, there was no difference in adult worm burden between the isotype control *Rag2*$^{-/-}$ mice and the depleted *Rag2*$^{-/-}$ mice. Also, the length of the worms did not differ between the isotype controls and the depleted *Rag2*$^{-/-}$ mice (Fig. 30c). It was concluded that depletion of ILC2s at the timepoint of the molting of L4 larvae into adult worms did not affect the subsequent adult worm burden at day 63.

Despite the absence of a phenotype in terms of the adult worm burden, a difference was observed in terms of worm progeny, the microfilariae, between the isotype controls and the depleted *Rag2*$^{-/-}$ mice. Nominal comparison of the two *Rag2*$^{-/-}$ groups revealed a significantly higher microfilarial load in the peripheral blood in depleted *Rag2*$^{-/-}$ mice compared with the isotype controls at day 57 ($p=0.0466$) (Fig. 30d) and day 63 ($p=0.0028$) (Fig. 30e) after *L. sigmodontis* infection. Furthermore, there was an increase in microfilarial load in peripheral blood during the course of infection, both in the isotype controls and in the depleted *Rag2*$^{-/-}$ mice (Fig. 30f). Consequently, depletion of ILC2s at the selected time point did not increase or decrease adult worm burden but did result in increased susceptibility of *Rag2*$^{-/-}$ mice with respect to microfilarial load.

To confirm this result, the embryogenesis in female worms in both *Rag2*$^{-/-}$ groups was analyzed at day 63 after *L. sigmodontis* infection (Fig. 30g, 30h). This should determine whether and to what extent embryogenesis within the female worms is affected by ILC2 depletion in *Rag2*$^{-/-}$ mice. The proportion of eggs among all embryonic stages was significantly lower in the depleted *Rag2*$^{-/-}$ mice than in the isotype controls ($p=0.0317$), whereas the proportion of stretched Mf among all stages was significantly higher in the depleted *Rag2*$^{-/-}$ mice compared to the isotype controls ($p=0.0317$). The proportion of all other stages was comparable between the isotype control and the depleted *Rag2*$^{-/-}$ mice. Thus, the result of the microfilarial load in peripheral blood was confirmed by the embryogenesis analysis, as female worms of depleted *Rag2*$^{-/-}$ mice had significantly more already fully developed Mf at the timepoint of *ex vivo* analysis on day 63, which later entered the peripheral blood.

As in the previously described experiments, immunological analysis was also performed during the depletion experiments in order to determine how depletion of

ILC2s at the selected time point affected, in particular, IL-5, IL-13 levels at the site of infection and the number and proportion of ILC2s at day 63. With regard to IL-5 levels in the pleural cavity, no differences were detected among all groups (Fig. 31a), so that *Rag2*$^{-/-}$ mice with and without depletion of ILC2s were capable of IL-5 production to the same extent as C57BL/6 mice. This suggests that, at least at the timepoint of analysis, T cells were not among the dominant sources of IL-5 because *Rag2*$^{-/-}$ mice lack these cells and were still able to produce comparable amounts of IL-5 as C57BL/6 mice. Although the IL-13 levels were significantly higher in C57BL/6 mice than in both *Rag2*$^{-/-}$ groups (Fig. 31b), the levels were below the detection limit, so it can only be cautiously assumed that T cells are significantly involved in the IL-13 levels at the site of infection. Analysis of the ILC2s was intended to show the extent to which depletion of these cells at the chosen time point affected the number of these cells at the time of analysis, since it was expected that they would arise again by day 63, as depletion was maintained for only 3 days. Although there was a significantly higher number of ILC2s in the pleural cavity of C57BL/6 mice compared with both *Rag2*$^{-/-}$ groups (Fig. 31c), there was no difference between the two *Rag2*$^{-/-}$ groups. The same was true for the proportion of ILC2s among all CD45^{+} lymphocytes (Fig. 31d). From these data and the cytokine data, it was concluded that the type 2 immune response in *Rag2*$^{-/-}$ mice following *L. sigmodontis* infection was generally impaired, except with respect to the production of IL-5, and depletion of ILC2s had no further negative or positive effect on this immune response in *Rag2*$^{-/-}$ mice.

To analyze the type 2 immune response in more detail, IL-5 producers were examined in the depletion experiments as well. Only C57BL/6 mice had appreciable numbers of IL-5-producing ILC2s at day 63 after *L. sigmodontis* infection (Fig. 32a, 32b), whereas very low numbers of IL-5-producing ILC2s were detected in both *Rag2*$^{-/-}$ groups. This was in line with the results of general ILC2 counts. Within the ILC2s, a significantly higher proportion was IL-5 positive in C57BL/6 mice than in the two *Rag2*$^{-/-}$ groups (Fig. 32c), in which only approximately 10% of the ILC2s produced IL-5. Furthermore, IL-5 expression by ILC2s was significantly higher in C57BL/6 mice than in depleted *Rag2*$^{-/-}$ mice ($p=0.0002$) (Fig. 32d). These results confirmed the impaired type 2 immune response in *Rag2*$^{-/-}$ mice in general and the fact that depletion of ILC2s had no further effect on this immune response at least at day 63 after *L. sigmodontis* infection.

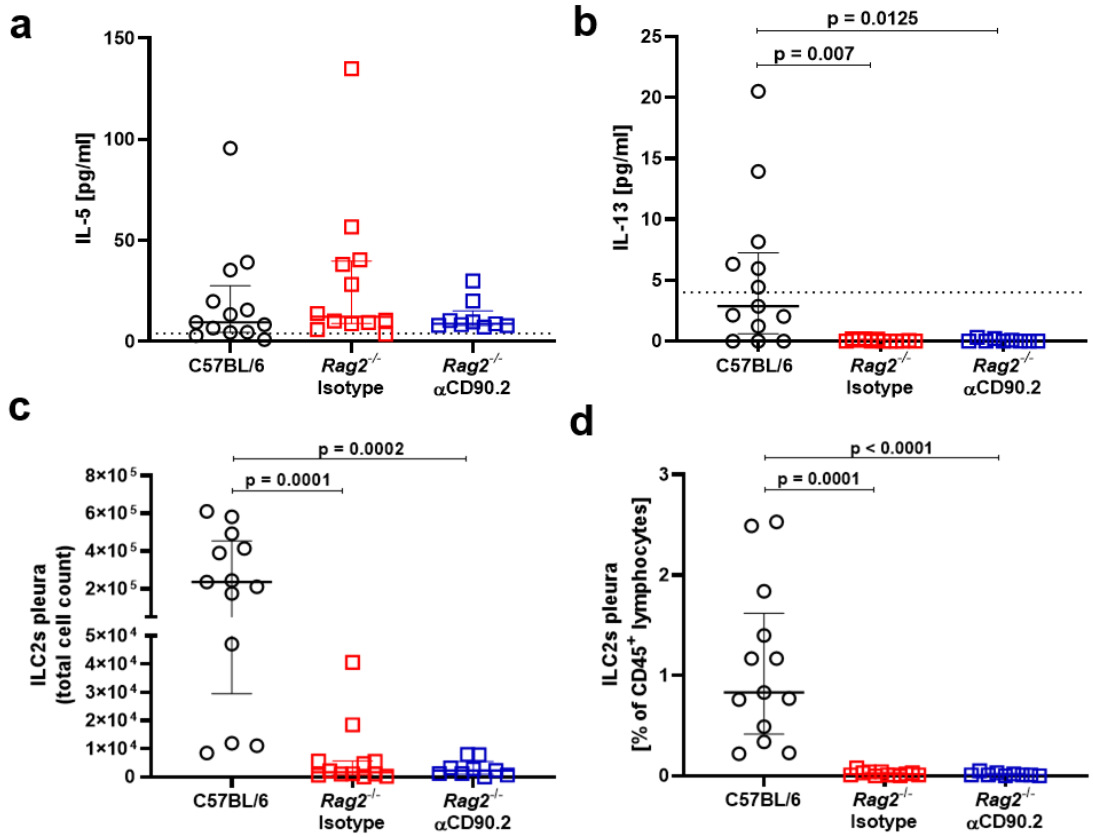

Figure 31: Limited type 2 immune response in *Rag2*$^{-/-}$ mice 63 dpi. (a) IL-5 levels and **(b)** IL-13 levels in the pleura 63 d post natural *L. sigmodontis* infection in semi-susceptible C57BL/6 mice, susceptible *Rag2*$^{-/-}$ mice and ILC2-depleted *Rag2*$^{-/-}$ mice. **(c)** Total cell count of ILC2s in the pleura 63 dpi. **(d)** Frequency [% of CD45^{+} lymphocytes] of ILC2s in the pleura 63 dpi. Bars represent the median with interquartile ranges. Data in (a-d) n = 11-13, pooled data from 2 independent experiments. Spearman's test for heteroscedasticity was performed and only data failing the heteroscedasticity were pooled. Data in (a-d) were analysed with Kruskal-Wallis test and Dunn's post-test. A p-value below 0.05 was considered to be significant.

Furthermore, the composition of IL-5 producers was examined (Fig. 32e, 32f). Here, in both *Rag2*$^{-/-}$ groups, ILC2s, despite their low numbers, were shown to be the dominant IL-5 source, as they accounted by trend for a higher proportion of all IL-5-positive cells in the isotype controls than in the C57BL/6 mice (p=0.0556) and for a significantly higher proportion in depleted *Rag2*$^{-/-}$ mice compared with C57BL/6 mice (p=0.0211) (Fig. 32e). Other sources, such as eosinophils, accounted for a similar proportion of IL-5 producers among all groups. The impaired type 2 immune response was further shown by the addition of total cell counts of IL-5 producers (Fig. 32f), as C57BL/6 mice in general had more IL-5-positive cells than the two *Rag2*$^{-/-}$ groups (p=0.05). However, because the IL-5 levels in the pleural cavity were comparable among all groups, it was assumed that the IL-5 levels in *Rag2*$^{-/-}$ mice, given the low number of IL-5-producing ILC2s and the low IL-5 expression, were probably caused by increased IL-5 expression by other cell types (e.g. eosinophils).

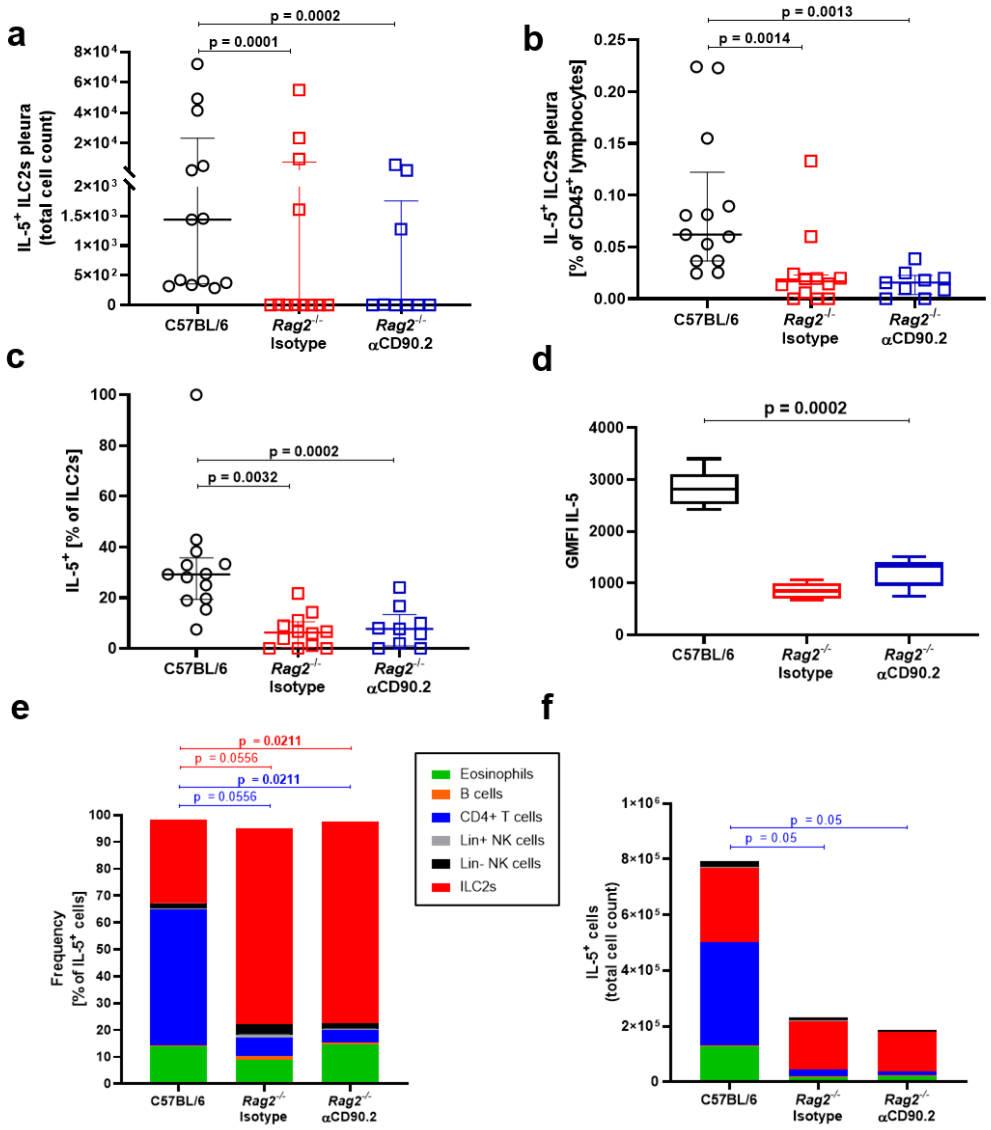

Figure 32: *L. sigmodontis*-infected *Rag2*$^{-/-}$ mice show a weaker type 2 immune response than C57BL/6 mice 63 dpi. (a) Total cell count of IL-5-expressing ILC2s in the pleura 63 d post natural *L. sigmodontis* infection in semi-susceptible C57BL/6 mice, susceptible *Rag2*$^{-/-}$ mice and ILC2-depleted *Rag2*$^{-/-}$ mice. **(b)** Frequency [% of CD45^{+} lymphocytes] of IL5-expressing ILC2s in the pleura 63 dpi. **(c)** Percentage [% of ILC2s] of ILC2s being IL-5+ among all ILC2s in the pleura 63 dpi. **(d)** IL-5 expression level (GMFI) of ILC2s 63 dpi. **(e)** Composition of IL-5+ cells in the pleura 63 dpi. **(f)** Stacked graph of all total cell counts of IL-5-expressing cells in the pleura 63 dpi. Bars in (a-c) represent the median with interquartile ranges. (d) shows box and whiskers with Tukey. Bars in (e-f) represent the median of each cell type. Data in (a-f) n = 11-13 per group, pooled data from 2 independent experiments. Spearman's test for heteroscedasticity was performed and only data failing the heteroscedasticity were pooled. Data in (a-f) were analysed with Kruskal-Wallis test and Dunn's post-test. A p-value below 0.05 was considered to be significant.

Since differences between isotype controls and depleted *Rag2*$^{-/-}$ mice were detected with regard to microfilariae and microfilariae are associated with an enhanced type 1 immune response (Hübner *et al.* 2008), IFN-γ-producing ILCs and IFN-γ levels at the site of infection were analyzed during the depletion experiments (Fig. 33) as a final step to determine whether an enhanced type 1 immune response could be observed due to the increased microfilarial load.

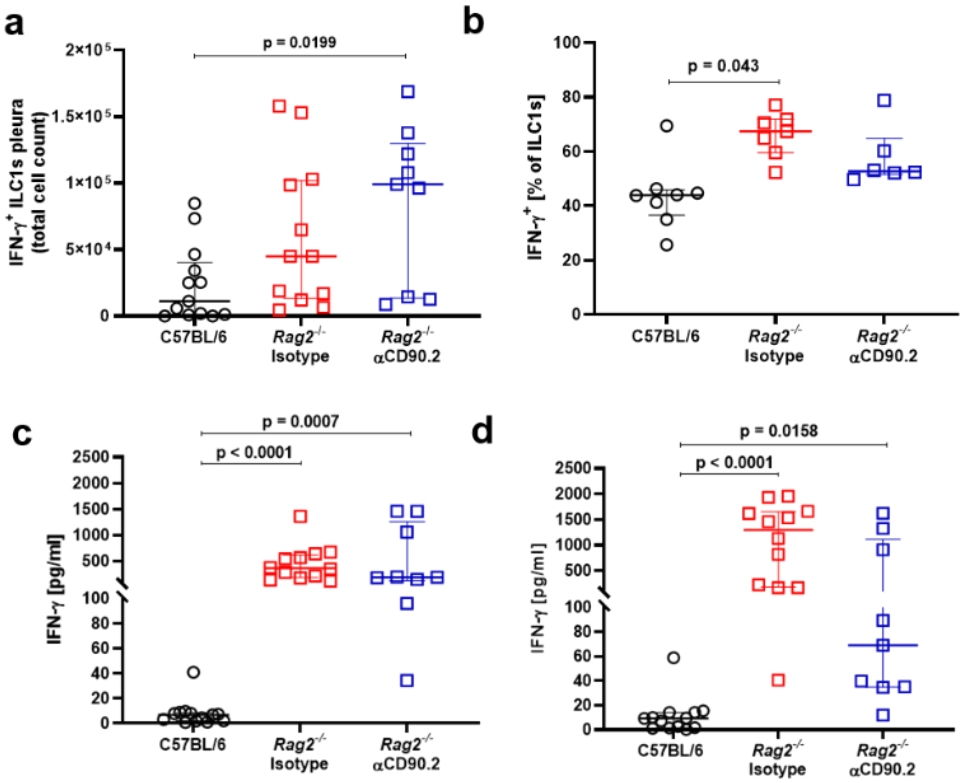

Figure 33: Enhanced type 1 immune response in *L. sigmodontis*-infected *Rag2*$^{-/-}$ mice. (a) Total cell count of IFN-γ-expressing ILC1s in the pleura 63 d post natural *L. sigmodontis* infection in semi-susceptible C57BL/6 mice, susceptible *Rag2*$^{-/-}$ mice and ILC2-depleted *Rag2*$^{-/-}$ mice. **(b)** Frequency [% of CD45^{+} lymphocytes] of IFN-γ-expressing ILC1s in the pleura 63 dpi. **(c)** IFN-γ level produced by stimulated pleura cells. **(d)** IFN-γ level in the pleura 63 dpi. Bars in (a-c) represent the median with interquartile ranges. Data in (a-d) n = 11-13 per group, pooled data from 2 independent experiments. Spearman's test for heteroscedasticity was performed and only data failing the heteroscedasticity were pooled. Data were analysed with Kruskal-Wallis test and Dunn's post-test. A p-value below 0.05 was considered to be significant.

The number of IFN-γ-producing ILC1s was significantly higher in depleted *Rag2*$^{-/-}$ mice than in C57BL/6 mice (p=0.0199) 63 days after *L. sigmodontis* infection (Fig. 33a). The proportion of ILC1s that were IFN-γ-positive was significantly higher in isotype *Rag2*$^{-/-}$ mice than in C57BL/6 mice (p=0.043) (Fig. 30b), with 50% to 70% of ILC1s being positive for IFN-γ in *Rag2*$^{-/-}$ mice and only slightly more than 40% in C57BL/6 mice. IFN-γ production by pleural cavity cells was significantly higher in both *Rag2*$^{-/-}$ groups than in C57BL/6 mice (Fig. 33c) but comparable between both *Rag2*$^{-/-}$ groups. IFN-γ levels in the pleural cavity 63 dpi were also significantly higher in both *Rag2*$^{-/-}$ groups compared with C57BL/6 mice (Fig. 33d), with isotype controls showing slightly higher, although not significantly, IFN-γ levels than depleted *Rag2*$^{-/-}$ mice. Overall, it was concluded that *Rag2*$^{-/-}$ mice generally showed a significantly stronger type 1 immune response after *L. sigmodontis* infection than C57BL/6 mice. However, depletion of ILC2s at the selected time point did not further enhance or dampen this immune response, although the microfilariae load would have suggested this.

4. Discussion

ILCs have only recently been identified as a distinct immune cell population. They are increasingly coming into the focus of infection research because they are found in almost all tissues (Elemam *et al.* 2017) and in particular, their function in barrier immunity has already been widely demonstrated (Kim *et al.* 2017). However, ILCs are not only involved in barrier immunity, but also are part of the complex immune cell network within the organs and often act here as links between other immune cells, especially those of the adaptive immunity, e. g. T cells (Burg *et al.* 2015). They contribute to immune homeostasis, produce effector molecules and are even capable of antigen presentation (Oliphant *et al.* 2014).

Although ILCs are a relatively rare cell population compared to e.g. T cells they are found enriched in various tissues, e.g. ILC2s are enriched in the lung (Artis & Spits 2015). Accordingly, they could represent central components of the immune response in the corresponding tissue. Their role is therefore characterized in various infectious diseases in order to contribute to a better understanding of the corresponding immune responses and disease pathogenesis. In the present thesis, extensive kinetic analyses were performed concerning the different subsets of ILCs in two different parasitic infectious disease models, the *P. berghei* ANKA mouse model for ECM in C57BL/6 WT mice and the *L. sigmodontis* model for filariasis. Both infections trigger completely differently directed immune responses in their host. While malaria is mainly characterized by an inflammatory response (Belachew 2018), worm infections lead to a type 2 immune response (Babu & Nutman 2014). The involvement of ILCs in both immune responses is therefore of particular interest, as ILCs are either protective or detrimental depending on the infection. For example, in the *N. brasiliensis* model, they are responsible for the expulsion of the parasite (Bouchery *et al.* 2015), but during *Salmonella* infection they lead to immunopathology (Elemam *et al.* 2017). Thus, this study provides interesting insights into the differential involvement of ILCs in immune responses to two completely different parasites.

4.1 Challenges in analyzing ILCs via flow cytometry

As mentioned earlier, ILCs are a rather rare immune cell type, at least when compared to T or B cells. Thus, they do not occur in high numbers, which leads to some challenges during flow cytometric analysis. The most important one, which also had to

be overcome in the context of this thesis, was to identify them unambiguously in different organs (here the brain, the spleen and the pleural cavity) so that they can be detected in subsequent functional analyses. Although markers, that can be used in flow cytometric analysis, exist for ILCs (Serafini *et al.* 2015), these markers are often also found on or in T cells or other immune cells. E.g. T cells are positive for CD90.2 just like ILC2s (Haeryfar & Hoskin 2004) and Th2 cells, like ILC2s, are positive for the transcription factor GATA-3 (Sasaki *et al.* 2013). Thus, in the analysis, as a first step it is important to gate out all non-ILCs, which is possible with the help of the lineage cocktail that includes antibodies against T cells, B cells, myeloid cells and erythroid cells (Biolegend 2018b). Frequently, ILCs are then further gated as $CD127^+$ and differentiated by their transcription factors T-bet, GATA-3 and RORγt (Nagakumar *et al.* 2016; Zhong *et al.* 2016; Dutton *et al.* 2017; Abidi *et al.* 2020).

However, based on the data shown here, it was observed that despite a prior characterization of lineage-negative cells, there are still numerous non-ILCs remaining in the subsequent gates, which consequently end up skewing the results by suggesting there are more ILCs than there actually are. Contamination of gates with T cells was previously observed, although prior differentiation into lineage-negative and lineage-positive cells was performed (Burkhard *et al.* 2014). General contamination of the following gates is seen in the gating strategies shown here as well, as in the Lin^- $TCR\beta^-$ gate some cells were included in further analysis that were later shown to have no other ILC markers and thus must be excluded from the analysis. For the reliability of the data, it was decided in this study to use more markers for the identification of each ILC subset in order to ensure that all detected cells can be unambiguously defined as ILCs. However, this decision was accompanied by other challenges, as the use of more markers within one flow cytometric panel increases the risk of resolution loss. This loss of resolution is less problematic for cell populations that are found in large quantities, as distinct populations can often be still found (Cossarizza *et al.* 2019). For ILCs, which are present only in small numbers depending on the organ, the loss of resolution has a much stronger effect, since here often only a few cells remain, for which a clear signal is important.

Therefore, in the present study, it was decided not to analyze all ILC subsets in one panel, but to analyze each subpopulation in a separate panel. This minimized the loss of resolution while allowing more markers to be integrated for each subset. However,

this had the disadvantage of not analyzing the subsets in parallel in one panel, which is why no compositional analyses of the ILCs in the individual organs were shown in the present study. Nevertheless, the advantages of the single panels outweighed the disadvantages, as they made the data robust and reproducible. Thus, this work provides not only insights into ILC subsets during parasitic infections, but also detailed and robust gating strategies for each ILC subset.

4.2 ILC1s/NK cell infiltration into the brain during ECM

Cerebral malaria is one of the most serious complications of *P. falciparum* infection (Schiess *et al.* 2020). In particular, children under five years of age are at risk of developing this complication (Centers for Disease Control and Prevention 2020b). To better understand the pathology mechanisms behind this disease, there is a well-established mouse model, in which C57BL/6 mice are infected with *Plasmodium berghei* ANKA (PbA) that develop symptoms corresponding to those of human cerebral malaria (de Souza *et al.* 2010; Ghazanfari *et al.* 2018).

However, the comparability of the model with the human situation is not fully given, because until today it is questionable to what extent *P. berghei*-infected erythrocytes can adhere to the endothelial cells of the brain and thus sequestration of the erythrocytes occurs during ECM (Craig *et al.* 2012). The ability to sequester is an important property of *P. falciparum* and thus of human CM (Pasternak & Dzikowski 2009; Deroost *et al.* 2016; Belachew 2018). Although there are first indications of a possible sequestration of *P. berghei*-infected erythrocytes (El-Assaad *et al.* 2013), the general dogma is that there is no active sequestration of erythrocytes during ECM, but only an accumulation (Cabrales *et al.* 2010) and simultanous infiltration of immune cells, which has also been observed in human CM (Dorovini-Zis *et al.* 2011; Hochman *et al.* 2015). In addition, the model used here is an artificial infection, since the liver phase is skipped. Furthermore, an immune response to the parasite does not occur in the skin as in the natural infection. This could also have an impact on the outcome of the infection. Nevertheless, *P. berghei* is a well-suited model to better understand the pathogenesis of CM. Even if sequestration of infected erythrocytes does not occur, the infiltration of immune cells that ultimately causes pathology is comparable to human CM and results in severe neurological symptoms. When interpreting the results, it must

be kept in mind, as with all mouse models, that the transferability to the human situation is not completely given.

There is so far only one study that observed an involvement of especially ILC2s in the protection from ECM (Besnard *et al.* 2015). There, IL-33 that was administered to WT mice and led to protection from ECM through expansion of ILC2s that start to produce type 2 cytokines and lead to polarization of alternatively activated macrophages and finally expansion of regulatory T cells. Regulatory T cells in turn dampen the type 1 immune response, which plays an important role in the pathogenesis of ECM (Besnard *et al.* 2015). However, another report demonstrated a detrimental role of the IL-33/ST2 pathway, as ST2-deficient mice were protected from ECM and pathogenic T cell immune responses in the brain depended on IL-33/ST2 signaling (Palomo *et al.* 2015). ILC2s appear to play a mediating role, as their response to IL-33 administration provides the basis for the expansion of other immune cells at least in the study by Besnard et al. It is already well known that IL-33 leads to the expansion of ILC2s (Artis & Spits 2015; Eberl *et al.* 2015; Serafini *et al.* 2015; Stier *et al.* 2018). However, detailed analyses of all ILC populations during the course of PbA infection have been lacking (Palomo *et al.* 2017) and the question has been raised whether ILC2s might also mediate the apparent protection against ECM in *Ifnar1*$^{-/-}$ mice or whether other cells are in focus. Also, there have been few data on inflammatory ILC1s in the ECM model. Only in non-lethal *P. chabaudi chabaudi* AS infection a decrease of ILC1s in the spleen and liver was detected (Ng *et al.* 2018). This was also found during *P. falciparum* infection in human blood. The NK cells, on the other hand, were investigated in more detail concerning their involvement in ECM pathogenesis (Burrack *et al.* 2019) but depending on the used depletion antibody the outcome was different as use of anti-asialo GM1 antibody led to ECM protection in WT mice (Hansen *et al.* 2007), but anti-NK1.1 did not (Yañez *et al.* 1996). Importantly, anti-asialo GM1 does affect other cells populations, not only NK cells, e.g. basophils (Nishikado *et al.* 2011), macrophages and CD8^{+} T cells (Burrack *et al.* 2019).

The first aim of this project was therefore to analyze all three ILC subsets over the course of infection in C57BL/6 WT mice in comparison to an ECM-protected mouse strain (*Ifnar1*$^{-/-}$ mice) to get an overview over the dynamics of ILC populations during PbA infection and to see whether mice protected from ECM display differences in ILC subsets hinting at an involvement of these cells in the protected phenotype. Afterwards

functional analyses and depletion experiments were performed to demonstrate a presumed involvement of specific subsets, here NK cells.

First, previous data were confirmed in this study showing that *Ifnar1*$^{-/-}$ mice are protected from ECM (Ball *et al.* 2013; Palomo *et al.* 2013). However, these studies also indicate that *Ifnar1*$^{-/-}$ mice are only partially protected, often develop ECM later or die of hyperparasitemia if infection continues/persists (Ball & Gonçalves 2010). Although no survival experiments were performed for this thesis, it was observed that some *Ifnar1*$^{-/-}$ mice indeed had a lower RMCBS score after PbA infection than other *Ifnar1*$^{-/-}$ mice of the same experiment. As the score in *Ifnar1*$^{-/-}$ remained above 10 and ECM is not assumed until the score is below 5, the *Ifnar1*$^{-/-}$ mice were considered protected in this thesis. This is supported by the cellular infiltrates which were present to a much lesser extent in the brains of PbA-infected *Ifnar1*$^{-/-}$ mice, which in contrast were clearly increased in PbA-infected WT mice. This phenomenon has already been observed in other ECM-protected mouse strains (Kuehlwein *et al.* 2020). However, the increased cell numbers could be explained by the fact that migration of immune cells towards the brain also occurs in the *Ifnar1*$^{-/-}$ mice, but the BBB is still intact (Scheunemann, Reichwald et al. submitted) and the detected cells therefore reside upstream of the BBB and only later, when the non-protected *Ifnar1*$^{-/-}$ mice develop ECM, infiltrate into the brain.

Furthermore, for the first time, ILC1s were identified among the cells in the brain during ECM in WT mice. Previously, this was only shown for NK cells (Burrack *et al.* 2019). Although NK cells are also among the ILC1s, the analyses shown here allowed a distinction between cytotoxic NK cells and non-cytotoxic, inflammatory ILC1s. This is particularly interesting because ILC1s are potent IFN-γ producers (Serafini *et al.* 2015) and IFN-γ plays a central role in the pathology of ECM (Rudin *et al.* 1997; Villegas-Mendez *et al.* 2017). Although the extent to which ILC1s contribute to IFN-γ levels in the brain was not examined in detail here, the question was where these ILC1s originate, since ILCs are generally referred to as tissue-resident (Gasteiger *et al.* 2015) and thus cannot be assumed to actively migrate into the brain from other tissues. However, recent studies also show a different picture, demonstrating that ILCs have a certain migratory potential (Dutton *et al.* 2019; Willinger 2019). It is therefore possible that they indeed actively migrate into the brain or that they are ILC1s of the central

nervous system, which are also present in the naive state and could proliferate as a result of infection (Romero-Suárez *et al.* 2019).

Since ILC1s, like NK cells, were found in low numbers in the brain samples compared with $CD8^+$ T cells, which have already been shown to play a crucial role during ECM (Belnoue *et al.* 2002; Howland *et al.* 2015; Ghazanfari *et al.* 2018), and also during human CM (Riggle *et al.* 2020), the question was to what extent they might be involved here at all and whether their presence merely represents an indirect effect resulting from the general infiltration of immune cells into the brain. However, the NK cells showed a 10-fold higher GzmB expression in the brain than the $CD8^+$ T cells. GzmB, just like IFN-γ, belongs to the pathology-mediating effector molecules during ECM (Haque *et al.* 2011b), so that it could be assumed that at least the NK cells, despite their low numbers, might as well contribute to pathology development. To further investigate this hypothesis, functional analyses were performed with NK cells isolated from WT and *Ifnar1*$^{-/-}$ mice to determine possible functional and phenotypic differences.

4.3 ILC subset dynamics in the spleen of PbA-infected mice

In addition to the brain, the immune response in the spleen is of central importance during ECM, as not only infected erythrocytes are recycled here, but the immune system also comes into contact with high amounts of parasite antigen, which in turn has an impact on the outcome of infection (Del Portillo *et al.* 2012). Previous studies showed that there is a migration of $CD8^+$ T cells from the spleen to the brain in WT mice (Belnoue *et al.* 2008), whereas ECM-protected *Ifnar1*$^{-/-}$ mice show accumulation or retention of these cells (Scheunemann, Reichwald et al. submitted). This phenomenon appears to be a central aspect of the protective mechanism, as depletion of $CD8^+$ T cells prevents ECM in WT mice (Belnoue *et al.* 2002). Nevertheless, depletion of other cells, e.g. $Ly6C^{hi}$ monocytes (Schumak *et al.* 2015), also leads to protection of WT mice. Therefore, it is likely that the pathology of ECM is a multifactorial process that depends on many different cell types and mechanisms and not only on $CD8^+$ T cells as suggested by the depletion experiments. GzmB and perforin have also been characterized as essential for ECM development, since mice lacking GzmB (Haque *et al.* 2011b) or perforin (Nitcheu *et al.* 2003) are protected from ECM. Given that in addition to $CD8^+$ T cells a NK cells produce both IFN-γ and GzmB (Serafini *et al.* 2015) and ILC1s are also IFN-γ producers (Artis & Spits 2015) it was of particular

interest to look more closely at the ILC subsets in the spleen and determine how these cells change during the course of infection. There have been no extensive studies on this to date, except for the one performed during non-lethal *P. chabaudi chabaudi* infection in the blood (Ng *et al.* 2018). Those new analysis should provide hints for a possible involvement of ILCs in the immune response and possibly also in the protection against ECM.

Importantly, differences in splenic ILC subsets between WT and *Ifnar1*$^{-/-}$ mice usually did not appear until day 5 or 6, suggesting that differences develop just before ECM onset and that it must be a relatively rapid process as it is already known for human CM where the disease rapidly develops (Mishra & Newton 2009). This is supported by the fact that the severe neurological symptoms observed in WT mice usually develop within a few hours on day 6 and that these mice experience a rapid decline of their health condition. Furthermore, the T cells have been shown to still be in the spleen on day 5 and then appear to receive a signal on day 6 that causes them to leave the spleen to the brain in WT mice. This is not observed for *Ifnar1*$^{-/-}$ mice, as they do show retention of CD8^{+} T cells in the spleen, no infiltration of these cells in the brain and no neurological symptoms as indicated earlier. Analysis of ILC1s and NK cells revealed no differences between WT and *Ifnar1*$^{-/-}$ mice with respect to ILC1s 6 dpi, neither in total cell count nor in the proportion of these cells among all immune cells in the spleen. An involvement of ILC1s in the immune response to PbA in general cannot be completely excluded, as ILC1s, just like CD8^{+} T cells, produce IFN-γ (Elemam *et al.* 2017), which has already been characterized as a central effector molecule during ECM (Cabantous *et al.* 2005; King & Lamb 2015; Villegas-Mendez *et al.* 2017). As no detailed analysis of IFN-γ production in ILC1s was performed in this thesis, it cannot be excluded that ILC1s differ functionally between WT and *Ifnar1*$^{-/-}$ mice. However, the most striking differences between the two mouse strains were detected with respect to the NK cells. Because significantly more NK cells were detected in the spleens of *Ifnar1*$^{-/-}$ mice at day 6 in the study presented here and these cells apparently infiltrated into the brain in the WT mice, NK cells seemed to show the same phenomenon as CD8^{+} T cells by which they migrate from the spleen towards the brain (Belnoue *et al.* 2008). Therefore, the next analyses focused on NK cells, their functional properties in WT and *Ifnar1*$^{-/-}$, and on how depletion of these cells affects ECM development in WT mice and protection against ECM in *Ifnar1*$^{-/-}$ mice.

4.4 No central role of NK cells in ECM development or ECM protection

The basis for the functional analyses was that the type I interferon receptor (IFNAR) on NK cells negatively regulates their IFN-γ production (Lee *et al.* 2019). Although this was a study with viral infection, it nevertheless showed that NK cells might differ in function when comparing WT and *Ifnar1*$^{-/-}$ mice. In particular, the possible influence on IFN-γ production was interesting, as this cytokine plays a crucial role during ECM (Villegas-Mendez *et al.* 2017). Accordingly, it would have been expected that due to the absence of the type I interferon receptor in *Ifnar1*$^{-/-}$ mice, NK cells produce higher levels of IFN-γ. However, the opposite was observed, as NK cells of PbA-infected *Ifnar1*$^{-/-}$ mice were less activated than those of PbA-infected WT mice and produced less IFN-γ. Those discrepancies can be due to the different immune responses elicited to viruses and *Plasmodium*. Although viruses and plasmodia both induce strong inflammatory immune responses (Rouse & Sehrawat 2010; Belachew 2018), they are completely different. In *Ifnar1*$^{-/-}$ mice, PbA infection appears to result in regulation of NK cell function. Since the naive NK cells show no differences in activity and production of effector molecules, the observed differences only occur with infection and the NK cells of *Ifnar1*$^{-/-}$ mice are therefore not less active from the beginning. The signal cascade downstream of the IFNAR provides a possible explanation for this, as the absence of IFNAR prevents the detection of interferons that ultimately lead to transcription of ISGs, which in turn encode factors for further immune responses (McNab *et al.* 2015). This could have an impact on the ability of NK cells to produce effector molecules while limiting their activity. And since naive NK cells are not exposed to interferon, due to the specific pathogen-free environment for the animals, the differences only occur with infection and the subsequent release of type 1 interferons due to PbA infection (He *et al.* 2020).

Certainly, the data presented here are limited by the cell number, the stimulus used (IL-15 in this case), and the incubation times. These parameters were chosen following the study by Lee et al. 2019, however, a different stimulus such as IL-12 instead of IL-15 could have different effects on NK cells than observed here since at least in the human situation IL-12 and IL-15 derived by dendritic cells have distinct roles in NK cell activation (Ferlazzo *et al.* 2004). Because many cytokines are secreted during infectious diseases in a specific time course, the choice of the time point of analysis is of key importance. Certain cytokines might not have been produced after the 24h

chosen here or might already be degrading since some cytokines do have a relatively short half-life (Whiteside 1994). As NK cells are ILCs, they do respond within a few hours (Serafini *et al.* 2015) and 24 h of stimulation was chosen. The activity of NK cells was determined in this thesis using the two NK cell receptors NK1.1 and NKp46, which belong to the activating receptors (Joshi & Lang 2013; Glasner *et al.* 2018). Additional activation markers for NK cells are CD27 and CD69 (Fogel *et al.* 2013), but these were not examined here. Based on the presented functional data, it was concluded that NK cells from PbA-infected WT and *Ifnar1*$^{-/-}$ mice are different and *Ifnar1*$^{-/-}$ NK cells are less activated and produce fewer effector molecules, raising the question whether this fact might be part of the protective mechanism of these mice.

To address this question, the next step was to deplete NK cells in both WT and *Ifnar1*$^{-/-}$ mice. NK cells were already depleted in *P. berghei*-infected WT mice, but different outcomes were observed depending on the antibody used. Use of anti-asialo GM1 (Hansen *et al.* 2007) protected WT mice from ECM, whereas anti-NK1.1 did not (Yañez *et al.* 1996). Importantly, anti-asialo GM1 also affects other cells, e.g. basophils (Nishikado *et al.* 2011), macrophages and CD8^{+} T cells (Burrack *et al.* 2019). This clearly could have an effect on the outcome of infection since ECM development is a very complex process that involves many different immune cells. Such experiments have not yet been performed for *Ifnar1*$^{-/-}$ mice. The depletion of NK cells here using the anti-NK1.1 antibody did not protect the WT mice against ECM, confirming the results of Yañez et al., but also did not worsen RMCBS scores. No effect was detected in the *Ifnar1*$^{-/-}$ mice either. From this, it was concluded that NK cells are not involved in the pathology of ECM in WT mice nor in the protection against ECM in the *Ifnar1*$^{-/-}$ mice. Nevertheless, it is interesting that they infiltrate into the brain in WT mice. Possibly, this is an indirect effect due to the general infiltration of immune cells into the brain of WT mice during PbA infection. Here, just as in the spleen, they could be involved in the immune response, e.g. by producing IFN-γ and GzmB, but are not among the central pathology-mediating cells. NK cells are furthermore found enriched in the liver (Jiao *et al.* 2016) and also play a significant role here in the control of liver-stage *Plasmodium* infection (Roland *et al.* 2006). However, the liver phase was skipped in the model presented here and thus future studies should consider the natural *Plasmodium* infection to determine whether the NK cells are central in the liver phase and thereby influence ECM development and protection in *Ifnar1*$^{-/-}$ mice.

4.5 Protective type 2 and regulatory immune responses in ECM

As ILC1s and NK cells did not play a central role in the ECM model, type 2 and regulatory immune responses were additionally investigated. These have already been characterized as protective in other parasitic diseases, but mainly during helminth infections (Babu & Nutman 2014; Frohberger *et al.* 2019). In contrast, the immune response to *Plasmodium* infection is mainly characterized as a type 1 inflammatory response (Belachew 2018). It is the balance and intensity of the inflammatory immune response that plays a critical role in the severity of malaria disease, because a strong immune response to *Plasmodium* facilitates parasite elimination, but exacerbated inflammatory immune responses are detrimental to the host (Deroost *et al.* 2016). Since *Ifnar1*$^{-/-}$ mice are protected from ECM, the question was whether type 2 and regulatory immune responses contribute to protection by limiting the inflammatory response.

Indeed, type 2 and regulatory immune responses were enhanced in *Ifnar1*$^{-/-}$ mice, characterized by significantly higher numbers of Th2 cells, eosinophils, and high levels of IL-10 and IL-13 compared with WT mice, which had no IL-10 and IL-13 in the spleen and showed hardly any eosinophils and Th2 cells in the spleen. It was therefore hypothesized that these immune responses mediate protection against ECM in *Ifnar1*$^{-/-}$ mice. However, despite the strong type 2 immune response in *Ifnar1*$^{-/-}$ mice, no major differences in ILC2 cell numbers were detected. Although *Ifnar1*$^{-/-}$ mice showed significantly more ILC2s in the spleen on day 6 after infection than WT mice, this was due to the splenomegaly that was observed in these animals. The proportion of ILC2s among all immune cells was comparable between WT and *Ifnar1*$^{-/-}$ mice. In contrast, frequencies of eosinophils and Th2 cells were increased in spleens of PbA-infected *Ifnar1*$^{-/-}$ mice. Thus, in *Ifnar1*$^{-/-}$ mice, the type 2 immune response at least in the spleen appears to be mediated by Th2 cells rather than ILC2s. It was hypothesized that ILCs may play a role only in the first hours after infection, because they respond within a few hours after infection, whereas the adaptive immune system is activated only later in the course of infection. However, in the absence of functional analyses for ILC2s, their involvement cannot be conclusively assessed, in particular not in genetically deficient *Ifnar1*$^{-/-}$ mice where it is challenging to specifically deplete ILC2s, as to date no suitable antibodies exist that do not also affect other immune cells as well. Since ILC2s and T cell share many markers (Artis & Spits 2015), antibodies to deplete ILCs

often affect T cells which would lead to protection due to the central importance of T cells during an ECM and thus does not show the importance of ILCs alone. It is however possible that ILC2s are involved to some extent in the induction of a type 2 immune milieu via the production of IL-5 and IL-13.

Given the increase of eosinophils in *Ifnar1*$^{-/-}$ mice, eosinophils were analyzed in a focused manner in the course of ECM, since eosinophils have already been characterized as central mediators of the protective immune response in many parasitic helminth infections (Huang & Appleton 2016; Frohberger *et al.* 2019). Eosinophils have also been suggested to play a role in the immune response during malaria in humans (Kurtzhals *et al.* 1998). Moreover, they have become a focus of immunological studies in general, as they have been shown to have many specific functions (Rosenberg *et al.* 2013; Ehrens *et al.* 2021). Thus, they are also of interest for the model shown here and were specifically depleted in *Ifnar1*$^{-/-}$ mice to determine whether these mice subsequently develop ECM. Indeed, *Ifnar1*$^{-/-}$ mice developed ECM on day 6 after PbA infection when eosinophils were depleted. It was concluded that eosinophils are central for the protection of *Ifnar1*$^{-/-}$ mice from ECM. Preliminary data from our lab indicated that this is mediated by chemokines produced by eosinophils, in particular CCL5/RANTES (Scheunemann, Reichwald et al. submitted). Here, *Ifnar1*$^{-/-}$ mice were found to have increased levels of CCL5 in the spleen, a chemokine responsible for the migration of T cells (Crawford *et al.* 2011), which was greatly increased in the brains of WT mice compared with *Ifnar1*$^{-/-}$ mice. Given that cells follow the concentration gradient of chemokines (Hughes & Nibbs 2018), it can be speculated that CD8^{+} T cells migrate from the spleen to the brain in WT mice, where CCL5 was elevated, whereas they remain in the spleen in *Ifnar1*$^{-/-}$ mice, where CCL5 concentration was elevated. Eosinophils were characterized as major producers of this chemokine, and they also showed the highest expression of CCL5. However, further analyses need to be performed here, focusing not only on the depletion of eosinophils, but also on the use of eosinophil-deficient mice (e.g. dblGATA or PHIL mice). However, the genetic background of the animals is problematic here, as dblGATA mice are so far only available on BALB/c background and BALB/c mice do not develop ECM (Gun *et al.* 2014). Future experiments should therefore focus on the use of PHIL mice that are on C57BL/6 background (Lee *et al.* 2004; Jacobsen *et al.* 2014) in this model to investigate in more detail the role of eosinophils in ECM.

Overall, it was concluded from the results presented here that ILCs do not have a decisive influence on ECM development or on protection against ECM. Although ILCs were detected in the brain and there was also an increase in ILC populations in the spleen as a result of infection, NK cells showed functional differences, which were subsequently shown not to be essential for ECM development. The question remains to what extent ILC1s contribute to pathology in the brain, since they were detected there and could produce effector molecules. There is also the question of whether ILC2s actually play no role in the immune response in the spleen, as functional analyses would have been required for this. Despite these remaining questions, the data presented here provide for the first time a complete overview of the development of ILC populations during PbA infection in ECM-susceptible WT mice and ECM-protected *Ifnar1*$^{-/-}$ mice and contribute significantly to our understanding the immunological processes during ECM in mice.

Importantly, type 2 and regulatory immune response, especially eosinophils, were shown to contribute to the protective effect in *Ifnar1*$^{-/-}$ mice.

4.6 Strain-dependent susceptibility to *L. sigmodontis* infection

In the *L. sigmodontis* model, it was confirmed that BALB/c mice develop chronic infection with release of microfilariae into the peripheral blood, while C57BL/6 mice are only semi-susceptible, as the adult worms are eliminated before the onset of microfilaremia. This was consistent with previous results showing the lower susceptibility of C57BL/6 mice (Babayan *et al.* 2003; Layland *et al.* 2015; Finlay & Allen 2020). These strain-dependent differences in susceptibility have already been demonstrated in other parasitic infection models. Depending on the model, either one strain or the other had an advantage. In the ECM model, it is the BALB/c mice that are protected from ECM, whereas the C57BL/6 mice develop ECM (Gun *et al.* 2014). However, strain differences have also been observed in other helminth infections, such as intestinal helminths, where the adult worm burden of *Strongyloides ratti* is higher in C57BL/6 mice than in BALB/c mice (Dawkins *et al.* 1980; Hartmann *et al.* 2021). In the *H. polygyrus* model, C57BL/6 mice are also completely susceptible, whereas BALB/c mice are only partially susceptible (Filbey *et al.* 2014). The site of infection seems to play a role in the susceptibility of certain strains, since in intestinal helminth infections the BALB/c mice are more resistant, whereas in *L. sigmodontis*, which lives in the

pleural cavity, the C57BL/6 mice are semi-susceptible. This phenomenon of strain-dependent susceptibility can be further explained by a different immune system due to the obvious genetic differences. Apparently, during *L. sigmodontis* infection, a milieu develops in the C57BL/6 mice that results in the worms not being able to complete their life cycle, i.e. not producing microfilariae and even being completely eliminated by day 70, whereas in BALB/c mice they survive and produce offspring. This milieu was investigated in detail in the present thesis with regard to the possible involvement of ILCs. ILC2s have already been identified as important protective mediators in several models using intestinal helminths. In the *N. brasiliensis* model IL-13-producing ILC2s interact with CD4+ T cells to activate M2 macrophages leading to larvae killing (Bouchery *et al.* 2015). Amphiregulin produced by ILC2s is important for the immune response to *T. muris* (Zaiss *et al.* 2006), whereas IL-33 leads to the expansion of ILC2s during *S. venezuelensis* infection (Yasuda *et al.* 2012). Such analyses have been largely lacking for *L. sigmodontis*. Although there is one study that has already demonstrated an increase in ILC2s during *L. sigmodontis* infection (Boyd *et al.* 2015), it did not contain enough markers to uniquely identify ILC2s and no functional analyses were performed. Therefore, the aim of this work was first to establish kinetics of all ILC populations during *L. sigmodontis* infection and compare them between BALB/c and C57BL/6 mice to determine which ILC population may play a role in the immune response in both strains and the elimination of *L. sigmodontis* in C57BL/6 mice.

4.7 ILC2s and type 2 immune responses in *L. sigmodontis* infection

For the first time, kinetics of all ILC populations over the course of *L. sigmodontis* infection were elaborated, providing first hints for the involvement of specific ILC populations in the immune response to *L. sigmodontis*. It was observed that during infection not only adaptive immune cells and myeloid cells infiltrate the site of infection, the pleural cavity, but also a large number of ILC subsets. In particular, significant differences in ILC2 cell numbers were observed between chronically infected BALB/c mice and semi-susceptible C57BL/6 mice, as the latter had significantly more ILC2s in the pleural cavity than the BALB/c mice at both day 30 and day 70. This was unexpected since C57BL/6 are thought to tend to a more prominent type 1 immune response whereas BALB/c mice are characterized as a rather type 2-dominated mouse strain (Mills *et al.* 2000). This is further underlined by the fact that C57BL/6 mice also had significantly more Th2 cells at the same time, which positively correlated with ILC2

cell counts. The strong increase in ILC2s was also observed by Boyd et al. 2015, but with the already mentioned limitations concerning the gating strategy. Furthermore, in the present thesis it is shown that worm counts positively correlate with ILC2 counts at day 30 post infection. This correlation could indicate either that more ILC2s lead to a higher worm burden or that more worms lead to more ILC2s in the pleural cavity. The second explanation is much more likely here because ILC2s have already been characterized as protective in other helminth infections (Bouchery *et al.* 2015; Meiners *et al.* 2020). Furthermore, depletion of ILC2s in the present study resulted in increased susceptibility of *Rag2*$^{-/-}$ mice to *L. sigmodontis* infection, suggesting a protective function of ILC2s. Importantly, this correlation was observed for the first time in the *L. sigmodontis* model, and the data presented here helps to refute the previously held view of type-2 dominated BALB/c and type-1 dominated C57BL/6 mice, as here clearly C57BL/6 mice had more ILC2s and Th2 cells than BALB/c mice and this probably explains their lower susceptibility. Indeed, strong type 2 immune responses are considered protective in other models and during *L. sigmodontis* infection (Volkmann *et al.* 2003; Anthony *et al.* 2007; Ajendra *et al.* 2014; Frohberger *et al.* 2019). This is supported by the very strong type 2 immune response in *L. sigmodontis*-infected C57BL/6 mice, characterized by significantly higher IL-5 and IL-13 levels in the pleural cavity compared with BALB/c mice, which showed only low production of these cytokines. BALB/c mice showed detectable IL-5 and IL-13 levels only at a later time point of infection (70 dpi), where the adult worm burden starts to decline in this strain as well. It was also interesting to observe that the type 2 immune response in C57BL/6 mice was still present at day 70, thus after elimination of the worm infection. Since IL-5 in particular has already been characterized as a key protective effector molecule during *L. sigmodontis* infection (Martin *et al.* 2000; Frohberger *et al.* 2019), the question was which cells contribute to these very high IL-5 levels and whether ILC2s play a crucial role here, since they are capable of IL-5 production (Serafini *et al.* 2015).

First, it was observed that C57BL/6 not only have more ILC2s in the pleural cavity, but also more IL-5-producing ILC2s. These are maintained just like the IL-5 levels at day 70. While the ILC2s of C57BL/6 maintained their IL-5 expression until day 70, it was lost in the BALB/c mice, where fewer ILC2s were IL-5-positive than at day 30. In addition, it was interesting to observe that more ILC2s than T cells were IL-5-positive and ILC2s generally had a higher IL-5 expression than T cells. Thus, it was concluded

that ILC2s are more potent IL-5 producers than T cells in the context of *L. sigmodontis* infection. Also, ILC2s of C57BL/6 mice were more potent in producing IL-5 than ILC2s of BALB/c mice at day 70 pi, again confirming that the type 2 immune response is maintained in C57BL/6 mice at day 70, even though they no longer had worms at that time. Analysis of the composition of IL-5 producers revealed substantial differences between BALB/c and C57BL/6 mice, as lymphoid sources were dominant in the latter, whereas eosinophils contributed in BALB/c mice. Interestingly, C57BL/6 mice had significantly lower total cell counts of IL-5-positive cells on day 70, but were still able to maintain high IL-5 levels in the thoracic cavity.

4.8 ILC2s inhibit *L. sigmodontis* microfilaremia

Specific depletion of ILC2s in C57BL/6 mice to demonstrate their involvement in adult worm elimination in these mice is, to date, not possible, as there is no antibody that specifically depletes ILCs because ILCs share many markers with T cells and other cells (Serafini *et al.* 2015). ILC subsets among themselves also share many markers. To date, at least for the model presented here, there is no suitable mouse strain that lacks ILCs. Therefore, the *Rag2*$^{-/-}$ C57BL/6 model was chosen. These mice lack T and B cells (The Jackson Laboratory 2021) but still have ILCs and allow analysis of the immune response to *L. sigmodontis* in the absence of the adaptive immune system.

L. sigmodontis infection of *Rag2*$^{-/-}$ mice resulted in a significantly higher worm burden at day 30 and day 63 compared with C57BL/6 mice, with microfilariae in the peripheral blood from day 57, as is also seen in BALB/c mice. Also, it is already known that animals that additionally lack NK cells (*Rag2IL2γR*$^{-/-}$ mice) develop chronic infection (Layland *et al.* 2015). Results from the current thesis may suggest that ILCs do not play an essential role in the elimination of adult worms in C57BL/6 mice, since *Rag2*$^{-/-}$ mice still possess ILC2s – however at lower numbers compared to semi-susceptible C57BL/6 mice - but develop chronic *L. sigmodontis* infection. However, T cells and ILC2s undergo a strong interaction that is essential for the maintenance and function of both cell populations (Kumar 2020), which could impact the susceptibility to *L. sigmodontis*. Thus, immune responses must always be interpreted within a complex network of immune cells, as many signalling pathways build on each other, are interdependent, and cells always influence each other (Batista & Dustin 2013). Thus, although T and B cells are obviously essential for C57BL/6 mice to eliminate infection,

this does not mean that ILC2s are not also involved. Indeed, the absence of T cells may have reduced their functionality to such an extent that they are no longer able to support the elimination of worms in the C57BL/6 mice. In this context it was investigated if specific ILC2 depletion in *Rag2*$^{-/-}$ mice at a time when molting into the adult worms was occurring and ILC2 cell counts reached their peak influences susceptibility to *L. sigmodontis* infection. ILC2-depleted *Rag2*$^{-/-}$ mice had a comparable worm burden compared to the isotype controls 63 dpi, indicating no impact of ILC2 depletion (during the moult into adult worms) on the adult worm burden. However, depletion of ILC2s significantly increased the microfilarial load in *Rag2*$^{-/-}$ mice compared with the isotype controls. Thus, depletion of ILC2s in T and B cell-deficient *Rag2*$^{-/-}$ mice, did increase the susceptibility of *Rag2*$^{-/-}$ mice to *L. sigmodontis* infection and ILC2s control microfilarial load in T and B cell-deficient *Rag2*$^{-/-}$ mice. One possible explanation would be that depletion of ILC2s favours adult worm development and embryogenesis, leading to an enhanced microfilariae release. Alternatively, depletion of ILC2s at the chosen time point may later allow more microfilariae to enter the blood from the pleural cavity. To test the latter hypothesis, an analysis of microfilariae in the pleural cavity at different time points could be done. Furthermore, intra-thoracic administration of microfilariae and subsequent analysis of microfilariae counts in the peripheral blood could also provide hints at the underlying mechanism. However, embryogenesis results demonstrated that ILC2 depletion facilitated adult worm fertility, indicating that this is the mechanism that led to the observed higher microfilariae load in ILC2-depleted *Rag2*$^{-/-}$ mice.

In addition to the parasitological parameters, immunological analyses were performed to define the effect of ILC2 depletion on the immune response in *Rag2*$^{-/-}$ mice. Interestingly, little effect was seen at 63 dpi. Although *Rag2*$^{-/-}$ generally had a limited type 2 immune response due to the absence of Th2 cells and concomitant lower ILC2 numbers, it is likely that ILC2s can compensate for the functions of Th2 cells to some extent, so that limited type 2 immunity is still observed. Interestingly, ILC2s indeed seem to partially take over some of the functions of T cells, as shown by the analysis of IL-5 producers. ILC2s were the dominant source of IL-5 in *Rag2*$^{-/-}$ mice and compensated the proportion of T cells among the IL-5 producers in C57BL/6 mice.

Because microfilariae are associated with a type 1 inflammatory immune response (Hübner *et al.* 2008), it was reasonable to assume that the increased microfilarial load

due to ILC2 depletion in *Rag2*$^{-/-}$ mice would also lead to an increased type 1 immune response. Surprisingly, this was not the case. Although *Rag2*$^{-/-}$ mice in general showed an increased inflammatory immune response, at least with respect to IFN-γ levels, there was no difference between the isotype controls and the depleted *Rag2*$^{-/-}$ mice. However, because only the local immune response was examined here and not the systemic one, no conclusion can be drawn as to whether this is generally the case. It is likely that more inflammatory markers are found in serum that is in direct contact with the microfilariae.

Overall, the data clearly indicate an involvement of ILC2s in the protective type 2 immune response during *L. sigmodontis* infection in C57BL/6 mice and further demonstrate that they are responsible for controlling microfilarial load in the absence of T and B cells. Since microfilariae are the filarial stage in human onchocerciasis that can lead to severe pathology, it is of great interest that ILC2s appear to play a role in minimizing the microfilariae burden.

4.9 Summary & Outlook

In summary, the work presented in this thesis provides a robust gating strategy for the identification and characterization of the individual ILC subsets (ILC1s, NK cell subsets, ILC2s, ILC3 subsets) in different organs, with particular emphasis on uniqueness. It provides detailed characterization at maximum resolution. Moreover, it can be applied to many different organs and allowed the generation of reliable data.

In the ECM model, a detailed analysis of the individual ILC subsets over the course of infection was performed for the first time, not only in the spleen, which is one of the most important organs in the immune response to PbA, but also in the brain, where the pathology originates. Here, for the first time, ILC1s were detected among the infiltrating cells. Furthermore, NK cells were identified as potential mediators of the immune response and pathology and studied in detail with respect to their functional properties in ECM-susceptible WT mice and ECM-protected *Ifnar1*$^{-/-}$ mice. It was noticed that the NK cells of *Ifnar1*$^{-/-}$ were significantly less activated than those of WT mice and also produced fewer effector molecules. However, depletion of NK cells in WT and *Ifnar1*$^{-/-}$ did not alter the outcome of ECM. Importantly, a strong type 2 and regulatory immune response was detected in *Ifnar1*$^{-/-}$ mice, which was particularly dependent on eosinophils. Eosinophils were subsequently identified as central

mediators of protection in the *Ifnar1*$^{-/-}$ mice. Although no involvement of ILCs was demonstrated on the basis of the studies performed here, they provide important insights into the development of ILC populations during PbA infection and put the focus on the type 2 immune responses for further analyses. Future analyses should focus in particular on the importance of ILC2s, since no functional analyses were performed for them here, and they are known to interact closely with eosinophils (Jacobsen *et al.* 2019). In particular, their influence on eosinophils in *Ifnar1*$^{-/-}$ mice would be of great interest.

Comparing chronically *L. sigmodontis*-infected BALB/c mice with semi-susceptible C57BL/6 mice, a strong type 2 immune response in C57BL/6 mice including increased ILC2 cell numbers and high levels of type 2 cytokines (IL-5 and IL-13) were observed. These type 2 cytokines were largely produced by ILC2s, which had higher IL-5 expression than Th2 cells. Furthermore, cells in BALB/c mice were less potent in producing IL-5 than cells in C57BL/6 mice. Thus, it was assumed that ILC2s not only play a role during intestinal helminth infections during the immune response, but also during extraintestinal filarial infection. Depleting ILC2s in mice lacking T and B cells on a semi-susceptible C57BL/6 background did not lead to higher worm burdens compared to isotype controls, but depleted *Rag2*$^{-/-}$ mice had significantly increased microfilarial burdens. Future studies should further aim to elucidate the mechanism behind the apparent control of microfilariae by ILC2s and their specific role in microfilariae- and L3-induced pathology, especially in the lung, influencing the migration of the L3 and microfilariae.

Overall, the presented work contributes decisively to a better understanding of the functions of ILCs during parasitic infectious diseases and, in particular, highlights their importance during filarial infections. Although ILCs are among the rare immune cells, they are of great importance for the immune response and are therefore certainly not only of interest in parasitic infectious diseases. They often serve as a first line of defense against invading pathogens, as they are enriched at barrier sites and can respond rapidly to the pathogen here. Similarly, in the later course of an infection they are central mediators of the immune responses, especially ILC2s have emerged within this work as important components that are able to influence the outcome of an infection, even if the mechanism behind it still needs to be elucidated. Developments

in depletion antibodies and the generation of ILC-deficient mice will contribute significantly to a better understanding of immune responses by ILCs in the future.

References

Abidi, A., Laurent, T., Bériou, G., Bouchet-Delbos, L., Fourgeux, C., Louvet, C., Triki-Marrakchi, R., Poschmann, J., Josien, R. & Martin, J. (2020) Characterization of Rat ILCs Reveals ILC2 as the Dominant Intestinal Subset. *Frontiers in Immunology* **11**, 255.

Ajendra, J., Specht, S., Neumann, A.-L., Gondorf, F., Schmidt, D., Gentil, K., Hoffmann, W. H., Taylor, M. J., Hoerauf, A. & Hübner, M. P. (2014) ST2 deficiency does not impair type 2 immune responses during chronic filarial infection but leads to an increased microfilaremia due to an impaired splenic microfilarial clearance. *PloS one* **9** (3), e93072.

Aldinucci, D. & Colombatti, A. (2014) The inflammatory chemokine CCL5 and cancer progression. *Mediators of Inflammation* **2014**, 292376.

Allen, J. E. & Maizels, R. M. (2011) Diversity and dialogue in immunity to helminths. *Nature Reviews Immunology* **11** (6), 375–388.

Alvar, J., Alves, F., Bucheton, B., Burrows, L., Büscher, P., Carrillo, E., Felger, I., Hübner, M. P., Moreno, J., Pinazo, M.-J., Ribeiro, I., Sosa-Estani, S., Specht, S., Tarral, A., Wourgaft, N. S. & Bilbe, G. (2020) Implications of asymptomatic infection for the natural history of selected parasitic tropical diseases. *Seminars in Immunopathology* **42** (3), 231–246.

Amani, V., Vigário, A. M., Belnoue, E., Marussig, M., Fonseca, L., Mazier, D. & Rénia, L. (2000) Involvement of IFN-gamma receptor-medicated signaling in pathology and anti-malarial immunity induced by *Plasmodium berghei* infection. *European journal of immunology* (30(6)), 1646–1655.

Anthony, R. M., Rutitzky, L. I., Urban, J. F., Stadecker, M. J. & Gause, W. C. (2007) Protective immune mechanisms in helminth infection. *Nature Reviews Immunology* **7** (12), 975–987.

Artis, D. & Spits, H. (2015) The biology of innate lymphoid cells. *Nature* **517** (7534), 293–301.

Autino, B., Noris, A., Russo, R. & Castelli, F. (2012) Epidemiology of malaria in endemic areas. *Mediterranean Journal of Hematology and Infectious Diseases* **4** (1), e2012060.

Babayan, S., Ungeheuer, M.-N., Martin, C., Attout, T., Belnoue, E., Snounou, G., Rénia, L., Korenaga, M. & Bain, O. (2003) Resistance and susceptibility to filarial infection with *Litomosoides sigmodontis* are associated with early differences in parasite development and in localized immune reactions. *Infection and immunity* **71** (12), 6820–6829.

Babu, S. & Nutman, T. B. (2014) Immunology of lymphatic filariasis. *Parasite Immunology* **36** (8), 338–346.

Bal, S. M., Golebski, K. & Spits, H. (2020) Plasticity of innate lymphoid cell subsets. *Nature reviews. Immunology*.

Ball, E. & Gonçalves, C. P. (2010) Uncovering the role of IFNAR1 in experimental cerebral malaria. *Malaria Journal* **9** (S2), 1.

Ball, E. A., Sambo, M. R., Martins, M., Trovoada, M. J., Benchimol, C., Costa, J., Antunes Gonçalves, L., Coutinho, A. & Penha-Gonçalves, C. (2013) IFNAR1 controls progression to cerebral malaria in children and CD8+ T cell brain pathology in *Plasmodium berghei*-infected mice. *Journal of immunology (Baltimore, Md. 1950)* (190(10)), 5118–5127.

Bando, J. K. & Colonna, M. (2016) Innate lymphoid cell function in the context of adaptive immunity. *Nature immunology* **17** (7), 783–789.

Barrera, V., Haley, M. J., Strangward, P., Attree, E., Kamiza, S., Seydel, K. B., Taylor, T. E., Milner, D. A., Craig, A. G. & Couper, K. N. (2019) Comparison of CD8+ T Cell Accumulation in the Brain During Human and Murine Cerebral Malaria. *Frontiers in Immunology* **10**.

Barrow, A. D. & Colonna, M. (2018) Innate lymphoid cell sensing of tissue vitality. *Current opinion in immunology* **56**, 82–93.

Batista, F. D. & Dustin, M. L. (2013) Cell:cell interactions in the immune system. *Immunological reviews* **251** (1), 7–12.

Belachew, E. B. (2018) Immune Response and Evasion Mechanisms of *Plasmodium falciparum* Parasites. *Journal of immunology research* **2018**, 6529681.

Belnoue, E., Kayibanda, M., Vigario, A. M., Deschemin, J.-C., van Rooijen, N., Viguier, M., Snounou, G. & Rénia, L. (2002) On the pathogenic role of brain-sequestered alphabeta CD8+ T cells in experimental cerebral malaria. *Journal of immunology (Baltimore, Md. 1950)* **169** (11), 6369–6375.

Belnoue, E., Potter, S. M., Rosa, D. S., Mauduit, M., Grüner, A. C., Kayibanda, M., Mitchell, A. J., Hunt, N. H. & Rénia, L. (2008) Control of pathogenic CD8+ T cell migration to the brain by IFN-gamma during experimental cerebral malaria. *Parasite immunology* **30** (10), 544–553.

Berbudi, A., Ajendra, J., Wardani, A. P. F., Hoerauf, A. & Hübner, M. P. (2016) Parasitic helminths and their beneficial impact on type 1 and type 2 diabetes. *Diabetes/metabolism research and reviews* **32** (3), 238–250.

Besnard, A.-G., Guabiraba, R., Niedbala, W., Palomo, J., Reverchon, F., Shaw, T. N., Couper, K. N., Ryffel, B. & Liew, F. Y. (2015) IL-33-mediated protection against experimental cerebral malaria is linked to induction of type 2 innate lymphoid cells, M2 macrophages and regulatory T cells. *PLoS Pathogens* **11** (2), e1004607.

Biolegend (2018a) APC anti-mouse Ly-6A/E Sca-1 Antibody anti-Ly-6A/E - E13-161.7. https://www.biolegend.com/en-us/products/apc-anti-mouse-ly-6a-e-sca-1-antibody-3897. Accessed 4/4/2018.

Biolegend (2018b) Pacific Blue anti-mouse Lineage Cocktail. https://www.biolegend.com/en-gb/products/pacific-blue-anti-mouse-lineage-cocktail-7765. Accessed 9/19/2018.

Bouchery, T., Kyle, R., Camberis, M., Shepherd, A., Filbey, K., Smith, A., Harvie, M., Painter, G., Johnston, K., Ferguson, P., Jain, R., Roediger, B., Delahunt, B., Weninger, W., Forbes-Blom, E. & Le Gros, G. (2015) ILC2s and T cells cooperate to ensure maintenance of M2 macrophages for lung immunity against hookworms. *Nature communications* **6**, 6970.

Boyd, A., Killoran, K., Mitre, E. & Nutman, T. B. (2015) Pleural cavity type 2 innate lymphoid cells precede Th2 expansion in murine *Litomosoides sigmodontis* infection. *Experimental parasitology* **159**, 118–126.

Brown, H., Rogerson, S., Taylor, T., Tembo, M., Mwenechanya, J., Molyneux, M. & Turner, G. (2001) Blood-brain barrier function in cerebral malaria in Malawian children. *The American journal of tropical medicine and hygiene* **64** (3-4), 207–213.

Bryceson, A. D., Warrell, D. A. & Pope, H. M. (1977) Dangerous reactions to treatment of onchocerciasis with diethylcarbamazine. *British Medical Journal* **1** (6063), 742–744.

Buerfent, B. C., Gondorf, F., Wohlleber, D., Schumak, B., Hoerauf, A. & Hübner, M. P. (2015) *Escherichia coli*-induced immune paralysis is not exacerbated during chronic filarial infection. *Immunology* **145** (1), 150–160.

Burg, N. von, Turchinovich, G. & Finke, D. (2015) Maintenance of Immune Homeostasis through ILC/T Cell Interactions. *Frontiers in Immunology* **6**, 416.

Burkhard, S. H., Mair, F., Nussbaum, K., Hasler, S. & Becher, B. (2014) T cell contamination in flow cytometry gating approaches for analysis of innate lymphoid cells. *PloS one* **9** (4), e94196.

Burrack, K. S., Hart, G. T. & Hamilton, S. E. (2019) Contributions of natural killer cells to the immune response against *Plasmodium*. *Malaria Journal* **18** (1), 321.

Cabantous, S., Poudiougou, B., Traore, A., Keita, M., Cisse, M. B., Doumbo, O., Dessein, A. J. & Marquet, S. (2005) Evidence that interferon-gamma plays a protective role during cerebral malaria. *The Journal of infectious diseases* **192** (5), 854–860.

Cabrales, P., Zanini, G. M., Meays, D., Frangos, J. A. & Carvalho, L. J. M. (2010) Murine cerebral malaria is associated with a vasospasm-like microcirculatory dysfunction, and survival upon rescue treatment is markedly increased by nimodipine. *The American journal of pathology* **176** (3), 1306–1315.

Capobianchi, M. R., Uleri, E., Caglioti, C. & Dolei, A. (2015) Type I IFN family members: similarity, differences and interaction. *Cytokine & growth factor reviews* **26** (2), 103–111.

Carroll, R. W., Wainwright, M. S., Kim, K.-Y., Kidambi, T., Gómez, N. D., Taylor, T. & Haldar, K. (2010) A rapid murine coma and behavior scale for quantitative assessment of murine cerebral malaria. *PloS one* (5(10)).

Centers for Disease Control and Prevention (2018a) How Can Malaria Cases and Deaths Be Reduced? https://www.cdc.gov/malaria/malaria_worldwide/reduction/index.html. Accessed 1/20/2021.

Centers for Disease Control and Prevention (2018b) Lymphatic Filariasis. https://www.cdc.gov/parasites/lymphaticfilariasis/. Accessed 2/3/2021.

Centers for Disease Control and Prevention (2018c) Lymphatic Filariasis - Disease. https://www.cdc.gov/parasites/lymphaticfilariasis/disease.html. Accessed 8/1/2019.

Centers for Disease Control and Prevention (2018d) Lymphatic Filariasis - Treatment. https://www.cdc.gov/parasites/lymphaticfilariasis/treatment.html. Accessed 2/3/2021.

Centers for Disease Control and Prevention (2019a) Lymphatic Filariasis - Biology. https://www.cdc.gov/parasites/lymphaticfilariasis/biology.html. Accessed 2/3/2021.

Centers for Disease Control and Prevention (2019b) Lymphatic Filariasis - Epidemiology & Risk Factors. https://www.cdc.gov/parasites/lymphaticfilariasis/epi.html. Accessed 8/1/2019.

Centers for Disease Control and Prevention (2019c) Onchocerciasis. https://www.cdc.gov/parasites/onchocerciasis/. Accessed 2/3/2021.

Centers for Disease Control and Prevention (2019d) Onchocerciasis - Biology. https://www.cdc.gov/parasites/onchocerciasis/biology.html. Accessed 2/4/2021.

Centers for Disease Control and Prevention (2019e) Onchocerciasis - Epidemiology & Risk Factors. https://www.cdc.gov/parasites/onchocerciasis/epi.html. Accessed 2/3/2021.

Centers for Disease Control and Prevention (2019f) Onchocerciasis - Prevention & Control. https://www.cdc.gov/parasites/onchocerciasis/prevent.html. Accessed 2/3/2021.

Centers for Disease Control and Prevention (2020a) CDC - Malaria - About Malaria - Biology. https://www.cdc.gov/malaria/about/biology/index.html. Accessed 7/17/2020.

Centers for Disease Control and Prevention (2020b) CDC - Malaria - About Malaria - Disease. https://www.cdc.gov/malaria/about/disease.html. Accessed 7/17/2020.

Centers for Disease Control and Prevention (2020c) Impact of Malaria. https://www.cdc.gov/malaria/malaria_worldwide/impact.html. Accessed 1/20/2021.

Centers for Disease Control and Prevention (2020d) Lymphatic Filariasis - Prevention & Control. https://www.cdc.gov/parasites/lymphaticfilariasis/prevent.html. Accessed 2/3/2021.

Centers for Disease Control and Prevention (2020e) Parasites - About Parasites. https://www.cdc.gov/parasites/about.html. Accessed 2/3/2021.

Centers for Disease Control and Prevention (2020f) Where Malaria Occurs. https://www.cdc.gov/malaria/about/distribution.html. Accessed 1/20/2021.

Chaplin, D. D. (2010) Overview of the immune response. *The Journal of allergy and clinical immunology* **125** (2 Suppl 2), S3-23.

Chen, Q., Amaladoss, A., Ye, W., Liu, M., Dummler, S., Kong, F., Wong, L. H., Loo, H. L., Loh, E., Tan, S. Q., Tan, T. C., Chang, K. T. E., Dao, M., Suresh, S., Preiser, P. R. & Chen, J. (2014) Human natural killer cells control *Plasmodium falciparum* infection by eliminating infected red blood cells. *Proceedings of the National Academy of Sciences* **111** (4), 1479–1484.

Chu, C., Moriyama, S., Li, Z., Zhou, L., Flamar, A.-L., Klose, C. S. N., Moeller, J. B., Putzel, G. G., Withers, D. R., Sonnenberg, G. F. & Artis, D. (2018) Anti-microbial Functions of Group 3 Innate Lymphoid Cells in Gut-Associated Lymphoid Tissues Are Regulated by G-Protein-Coupled Receptor 183. *Cell reports* **23** (13), 3750–3758.

Colebunders, R., Hendy, A., Mokili, J. L., Wamala, J. F., Kaducu, J., Kur, L., Tepage, F., Mandro, M., Mucinya, G., Mambandu, G., Komba, M. Y., Lumaliza, J. L., van Oijen, M. & Laudisoit, A. (2016) Nodding syndrome and epilepsy in onchocerciasis endemic regions: comparing preliminary observations from South Sudan and the Democratic Republic of the Congo with data from Uganda. *BMC research notes* **9**, 182.

Collins, J. W., Keeney, K. M., Crepin, V. F., Rathinam, V. A. K., Fitzgerald, K. A., Finlay, B. B. & Frankel, G. (2014) Citrobacter rodentium: infection, inflammation and the microbiota. *Nature reviews. Microbiology* **12** (9), 612–623.

Cossarizza, A., Chang, H.-D. & Radbruch, A. et al. (2019) Guidelines for the use of flow cytometry and cell sorting in immunological studies (second edition). *European journal of immunology* **49** (10), 1457–1973.

Craig, A. G., Grau, G. E., Janse, C., Kazura, J. W., Milner, D., Barnwell, J. W., Turner, G. & Langhorne, J. (2012) The role of animal models for research on severe malaria. *PLOS Pathogens* **8** (2), e1002401.

Crawford, A., Angelosanto, J. M., Nadwodny, K. L., Blackburn, S. D. & Wherry, E. J. (2011) A role for the chemokine RANTES in regulating CD8 T cell responses during chronic viral infection. *PLOS Pathogens* **7** (7), e1002098.

Cuff, A. O. & Male, V. (2017) Conventional NK cells and ILC1 are partially ablated in the livers of Ncr1iCreTbx21fl/fl mice. *Wellcome Open Research* **2**, 39.

Dawkins, H., Grove, D. I., Dunsmore, J. D. & Mitchell, G. F. (1980) *Strongyloides ratti*: Susceptibility to infection and resistance to reinfection in inbred strains of mice as assessed by excretion of larvae. *International Journal for Parasitology* **10** (2), 125–129.

de Souza, B. J. & Riley, E. M. (2002) Cerebral malaria: the contribution of studies in animal models to our understanding of immunopathogenesis. *Microbes and Infection* **4** (3), 291–300.

de Souza, J. B., Hafalla, J. C., Riley, E. M. & Couper, K. N. (2010) Cerebral malaria: why experimental murine models are required to understand the pathogenesis of disease. *Parasitology* (137), 755–772.

Debrah, A. Y., Mand, S., Marfo-Debrekyei, Y., Batsa, L., Pfarr, K., Buttner, M., Adjei, O., Buttner, D. & Hoerauf, A. (2007) Macrofilaricidal effect of 4 weeks of treatment with doxycycline on *Wuchereria bancrofti. Tropical medicine & international health TM & IH* **12** (12), 1433–1441.

Del Portillo, H. A., Ferrer, M., Brugat, T., Martin-Jaular, L., Langhorne, J. & Lacerda, M. V. G. (2012) The role of the spleen in malaria. *Cellular microbiology* **14** (3), 343–355.

Deroost, K., Pham, T.-T., Opdenakker, G. & van den Steen, P. E. (2016) The immunological balance between host and parasite in malaria. *FEMS microbiology reviews* **40** (2), 208–257.

Diefenbach, A. (2013) Innate lymphoid cells in the defense against infections. *European journal of microbiology & immunology* **3** (3), 143–151.

Dorovini-Zis, K., Schmidt, K., Huynh, H., Fu, W., Whitten, R. O., Milner, D., Kamiza, S., Molyneux, M. & Taylor, T. E. (2011) The neuropathology of fatal cerebral malaria in malawian children. *The American journal of pathology* **178** (5), 2146–2158.

Drake, L. Y., Iijima, K. & Kita, H. (2014) Group 2 innate lymphoid cells and CD4+ T cells cooperate to mediate type 2 immune response in mice. *Allergy* **69** (10), 1300–1307.

Dutton, E. E., Camelo, A., Sleeman, M., Herbst, R., Carlesso, G., Belz, G. T. & Withers, D. R. (2017) Characterisation of innate lymphoid cell populations at different sites in mice with defective T cell immunity. *Wellcome Open Research* **2**, 117.

Dutton, E. E., Gajdasik, D. W., Willis, C., Fiancette, R., Bishop, E. L., Camelo, A., Sleeman, M. A., Coccia, M., Didierlaurent, A. M., Tomura, M., Pilataxi, F., Morehouse, C. A., Carlesso, G. & Withers, D. R. (2019) Peripheral lymph nodes contain migratory and resident innate lymphoid cell populations. *Science immunology* **4** (35).

Ebbo, M., Crinier, A., Vély, F. & Vivier, E. (2017) Innate lymphoid cells: major players in inflammatory diseases. *Nature reviews. Immunology* **17** (11), 665–678.

Eberl, G., Colonna, M., Di Santo, J. P. & McKenzie, A. N. J. (2015) Innate lymphoid cells. Innate lymphoid cells: a new paradigm in immunology. *Science (New York, N.Y.)* **348** (6237), aaa6566.

Edwards, C. L., Best, S. E., Gun, S. Y., Claser, C., James, K. R., Oca, M. M. de, Sebina, I., Rivera, F. d. L., Amante, F. H., Hertzog, P. J., Engwerda, C. R., Renia, L. & Haque, A. (2015) Spatiotemporal requirements for IRF7 in mediating type I IFN-dependent susceptibility to blood-stage *Plasmodium* infection. *European journal of immunology* **45** (1), 130–141.

Ehrens, A., Lenz, B., Neumann, A.-L., Giarrizzo, S., Reichwald, J. J., Frohberger, S. J., Stamminger, W., Buerfent, B. C., Fercoq, F., Martin, C., Kulke, D., Hoerauf, A. & Hübner, M. P. (2021) Microfilariae Trigger Eosinophil Extracellular DNA Traps in a Dectin-1-Dependent Manner. *Cell reports* **34** (2), 108621.

El-Assaad, F., Wheway, J., Mitchell, A. J., Lou, J., Hunt, N. H., Combes, V. & Grau, G. E. R. (2013) Cytoadherence of *Plasmodium berghei*-infected red blood cells to murine brain and lung microvascular endothelial cells in vitro. *Infection and immunity* (81(11)), 3984–3991.

Elemam, N. M., Hannawi, S. & Maghazachi, A. A. (2017) Innate Lymphoid Cells (ILCs) as Mediators of Inflammation, Release of Cytokines and Lytic Molecules. *Toxins* **9** (12).

Engwerda, C. R., Beattie, L. & Amante, F. H. (2005) The importance of the spleen in malaria. *Trends in Parasitology* (21(2)), 75–80.

Favre, N., Da Laperousaz, C., Ryffel, B., Weiss, N. A., Imhof, B. A., Rudin, W., Lucas, R. & Piguet, P. F. (1999) Role of ICAM-1 (CD54) in the development of murine cerebral malaria. *Microbes and Infection* (1(12)), 961–968.

Ferlazzo, G., Pack, M., Thomas, D., Paludan, C., Schmid, D., Strowig, T., Bougras, G., Muller, W. A., Moretta, L. & Münz, C. (2004) Distinct roles of IL-12 and IL-15 in human natural killer cell activation by dendritic cells from secondary lymphoid organs. *Proceedings of the National Academy of Sciences of the United States of America* **101** (47), 16606–16611.

Filbey, K. J., Grainger, J. R., Smith, K. A., Boon, L., van Rooijen, N., Harcus, Y., Jenkins, S., Hewitson, J. P. & Maizels, R. M. (2014) Innate and adaptive type 2 immune cell responses in genetically controlled resistance to intestinal helminth infection. *Immunology and cell biology* **92** (5), 436–448.

Finlay, C. M. & Allen, J. E. (2020) The immune response of inbred laboratory mice to *Litomosoides sigmodontis*: a route to discovery in myeloid cell biology. *Parasite immunology*, e12708.

Fisher Scientific (2017) eBioscience™ Mouse IFN gamma ELISA Ready-SET-Go!™ Kit. https://www.fishersci.com/shop/products/mouse-ifn-gamma-elisa-ready-set-go-kit-3/p-7091935. Accessed 8/23/2017.

Flores-Borja, F., Irshad, S., Gordon, P., Wong, F., Sheriff, I., Tutt, A. & Ng, T. (2016) Crosstalk between Innate Lymphoid Cells and Other Immune Cells in the Tumor Microenvironment. *Journal of immunology research* **2016**, 7803091.

Fogel, L. A., Sun, M. M., Geurs, T. L., Carayannopoulos, L. N. & French, A. R. (2013) Markers of nonselective and specific NK cell activation. *Journal of immunology (Baltimore, Md. 1950)* **190** (12), 6269–6276.

Frohberger, S. J., Ajendra, J., Surendar, J., Stamminger, W., Ehrens, A., Buerfent, B. C., Gentil, K., Hoerauf, A. & Hübner, M. P. (2019) Susceptibility to *L. sigmodontis* infection is highest in animals lacking IL-4R/IL-5 compared to single knockouts of IL-4R, IL-5 or eosinophils. *Parasites & vectors* **12** (1), 248.

Gad, A., Ali, S., Zahoor, T. & Azarov, N. (2018) Case Report: A Case of Severe Cerebral Malaria Managed with Therapeutic Hypothermia and Other Modalities for Brain Edema. *The American journal of tropical medicine and hygiene* **98** (4), 1120–1122.

Gasteiger, G., Fan, X., Dikiy, S., Lee, S. Y. & Rudensky, A. Y. (2015) Tissue residency of innate lymphoid cells in lymphoid and nonlymphoid organs. *Science (New York, N.Y.)* **350** (6263), 981–985.

Gasteiger, G. & Rudensky, A. Y. (2014) Interactions between innate and adaptive lymphocytes. *Nature reviews. Immunology* **14** (9), 631–639.

Gazzinelli, R. T., Kalantari, P., Fitzgerald, K. A. & Golenbock, D. T. (2014) Innate sensing of malaria parasites. *Nature Reviews Immunology* (14), 744–757.

Geiger, T. L. & Sun, J. C. (2016) Development and maturation of natural killer cells. *Current opinion in immunology* **39**, 82–89.

Germain, R. N. & Huang, Y. (2018) ILC2s - resident lymphocytes pre-adapted to a specific tissue or migratory effectors that adapt to where they move? *Current opinion in immunology* **56**, 76–81.

Ghazanfari, N., Mueller, S. N. & Heath, W. R. (2018) Cerebral Malaria in Mouse and Man. *Frontiers in Immunology* **9**, 157.

Glasner, A., Levi, A., Enk, J., Isaacson, B., Viukov, S., Orlanski, S., Scope, A., Neuman, T., Enk, C. D., Hanna, J. H., Sexl, V., Jonjic, S., Seliger, B., Zitvogel, L. & Mandelboim, O. (2018) NKp46 Receptor-Mediated Interferon-γ Production by Natural Killer Cells Increases Fibronectin 1 to Alter Tumor Architecture and Control Metastasis. *Immunity* **48** (1), 107-119.e4.

Guimont-Desrochers, F. & Lesage, S. (2013) Revisiting the Prominent Anti-Tumoral Potential of Pre-mNK Cells. *Frontiers in Immunology* **4**, 446.

Gun, S. Y., Claser, C., Tan, K. S. W. & Rénia, L. (2014) Interferons and Interferon Regulatory Factors in Malaria. *Mediators of Inflammation* (2014(1)), 1–21.

Haeryfar, S. M. M. & Hoskin, D. W. (2004) Thy-1: more than a mouse pan-T cell marker. *Journal of immunology (Baltimore, Md. 1950)* **173** (6), 3581–3588.

Hamada, H., Bassity, E., Flies, A., Strutt, T. M., Garcia-Hernandez, M. d. L., McKinstry, K. K., Zou, T., Swain, S. L. & Dutton, R. W. (2013) Multiple redundant effector mechanisms of CD8+ T cells protect against influenza infection. *Journal of immunology (Baltimore, Md. 1950)* **190** (1), 296–306.

Hansen, D. S., Bernard, N. J., Nie, C. Q. & Schofield, L. (2007) NK cells stimulate recruitment of CXCR3+ T cells to the brain during *Plasmodium berghei*-mediated cerebral malaria. *Journal of immunology (Baltimore, Md. 1950)* **178** (9), 5779–5788.

Haque, A., Best, S. E., Ammerdorffer, A., Desbarrieres, L., Oca, M. M. de, Amante, F. H., Labastida Rivera, F. de, Hertzog, P., Boyle, G. M., Hill, G. R. & Engwerda, C. R. (2011a) Type I interferons suppress $CD4^+$ T-cell-dependent parasite control during blood-stage *Plasmodium* infection. *European journal of immunology* **41** (9), 2688–2698.

Haque, A., Best, S. E. & Montes de Oca, M. et al. (2014) Type I IFN signaling in CD8- DCs impairs Th1-dependent malaria immunity. *The Journal of clinical investigation* **124** (6), 2483–2496.

Haque, A., Best, S. E., Unosson, K., Amante, F. H., Labastida, F. de, Anstey, N. M., Karupiah, G., Smyth, M. J., Heath, W. R. & Engwerda, C. R. (2011b) Granzyme B expression by CD8+ T cells is required for the development of experimental cerebral malaria. *Journal of Immunology* (186(11)), 6148–6156.

Hartmann, W., Blankenhaus, B., Brunn, M.-L., Meiners, J. & Breloer, M. (2021) Elucidating different pattern of immunoregulation in BALB/c and C57BL/6 mice and their F1 progeny. *Scientific Reports* **11** (1), 1536.

He, X., Xia, L., Tumas, K. C., Wu, J. & Su, X. (2020) Type I Interferons and Malaria: A Double-Edge Sword Against a Complex Parasitic Disease. *Frontiers in Cellular and Infection Microbiology* **10**, 594621.

Herbert, D. R., Douglas, B. & Zullo, K. (2019) Group 2 Innate Lymphoid Cells (ILC2): Type 2 Immunity and Helminth Immunity. *International journal of molecular sciences* **20** (9).

Hochman, S. E., Madaline, T. F., Wassmer, S. C., Mbale, E., Choi, N., Seydel, K. B., Whitten, R. O., Varughese, J., Grau, G. E. R., Kamiza, S., Molyneux, M. E., Taylor, T. E., Lee, S., Milner, D. A. & Kim, K. (2015) Fatal Pediatric Cerebral Malaria Is Associated with Intravascular Monocytes and Platelets That Are Increased with HIV Coinfection. *mBio* **6** (5), e01390-15.

Hoerauf, A. (2008) Filariasis: new drugs and new opportunities for lymphatic filariasis and onchocerciasis. *Current opinion in infectious diseases* **21** (6), 673–681.

Hoerauf, A., Mand, S., Volkmann, L., Büttner, M., Marfo-Debrekyei, Y., Taylor, M., Adjei, O. & Büttner, D. W. (2003) Doxycycline in the treatment of human onchocerciasis: kinetics of *Wolbachia* endobacteria reduction and of inhibition of embryogenesis in female *Onchocerca* worms. *Microbes and Infection* **5** (4), 261–273.

Hoerauf, A., Pfarr, K., Mand, S., Debrah, A. Y. & Specht, S. (2011) Filariasis in Africa--treatment challenges and prospects. *Clinical microbiology and infection the official publication of the European Society of Clinical Microbiology and Infectious Diseases* **17** (7), 977–985.

Howland, S. W., Claser, C., Poh, C. M., Gun, S. Y. & Rénia, L. (2015) Pathogenic $CD8^+$ T cells in experimental cerebral malaria. *Seminars in Immunopathology* (37), 221–231.

Huang, L. & Appleton, J. A. (2016) Eosinophils in Helminth Infection: Defenders and Dupes. *Trends in Parasitology* **32** (10), 798–807.

Huang, Q., Seillet, C. & Belz, G. T. (2017) Shaping Innate Lymphoid Cell Diversity. *Frontiers in Immunology* **8**, 1569.

Huang, Y., Mao, K. & Germain, R. N. (2018) Thinking differently about ILCs-Not just tissue resident and not just the same as CD4 + T-cell effectors. *Immunological Reviews* **286** (1), 160–171.

Hübner, M. P., Layland, L. E. & Hoerauf, A. (2013) Helminths and their implication in sepsis – a new branch of their immunomodulatory behaviour? *Pathogens and Disease* **69** (2), 127–141.

Hübner, M. P., Pasche, B., Kalaydjiev, S., Soboslay, P. T., Lengeling, A., Schulz-Key, H., Mitre, E. & Hoffmann, W. H. (2008) Microfilariae of the filarial nematode *Litomosoides sigmodontis* exacerbate the course of lipopolysaccharide-induced sepsis in mice. *Infection and immunity* **76** (4), 1668–1677.

Hübner, M. P., Torrero, M. N., McCall, J. W. & Mitre, E. (2009) *Litomosoides sigmodontis*: A simple method to infect mice with L3 larvae obtained from the pleural space of recently infected jirds (*Meriones unguiculatus*). *Experimental parasitology* **123** (1), 95–98.

Hughes, C. E. & Nibbs, R. J. B. (2018) A guide to chemokines and their receptors. *The Febs Journal* **285** (16), 2944–2971.

Ignacio, A., Breda, C. N. S. & Camara, N. O. S. (2017) Innate lymphoid cells in tissue homeostasis and diseases. *World journal of hepatology* **9** (23), 979–989.

Jacobsen, E. A., Lee, N. A. & Lee, J. J. (2014) Re-defining the unique roles for eosinophils in allergic respiratory inflammation. *Clinical and experimental allergy journal of the British Society for Allergy and Clinical Immunology* **44** (9), 1119–1136.

Jacobsen, E. A., Lesuer, W. E., Nazaroff, C. D., Ochkur, S. I., Doyle, A. D., Wright, B. L., Rank, M. A. & Lee, J. J. (2019) Eosinophils Induce Recruitment and Activation of ILC2s. *Journal of Allergy and Clinical Immunology* **143** (2), AB289.

Jiao, Y., Huntington, N. D., Belz, G. T. & Seillet, C. (2016) Type 1 Innate Lymphoid Cell Biology: Lessons Learnt from Natural Killer Cells. *Frontiers in Immunology* **7**, 426.

Joshi, S. K. & Lang, M. L. (2013) Fine tuning a well-oiled machine: Influence of NK1.1 and NKG2D on NKT cell development and function. *International immunopharmacology* **17** (2), 260–266.

Kakooza-Mwesige, A. (2017) Unravelling the mysterious onchocerciasis-nodding syndrome link: new developments and future challenges. *Annals of Translational Medicine* **5** (24), 486.

Kalantari, P. (2018) The Emerging Role of Pattern Recognition Receptors in the Pathogenesis of Malaria. *Vaccines* **6** (1).

Kim, J., Kim, G. & Min, H. (2017) Pathological and therapeutic roles of innate lymphoid cells in diverse diseases. *Archives of pharmacal research* **40** (11), 1249–1264.

King, C. L., Suamani, J., Sanuku, N., Cheng, Y.-C., Satofan, S., Mancuso, B., Goss, C. W., Robinson, L. J., Siba, P. M., Weil, G. J. & Kazura, J. W. (2018) A Trial of a Triple-Drug Treatment for Lymphatic Filariasis. *The New England journal of medicine* **379** (19), 1801–1810.

King, T. & Lamb, T. (2015) Interferon-γ: The Jekyll and Hyde of Malaria. *PLoS Pathogens* (11(10)).

Knipper, J. A., Ivens, A. & Taylor, M. D. (2019) Helminth-induced Th2 cell dysfunction is distinct from exhaustion and is maintained in the absence of antigen. *PLoS neglected tropical diseases* **13** (12), e0007908.

Kolbaum, J., Tartz, S., Hartmann, W., Helm, S., Nagel, A., Heussler, V., Sebo, P., Fleischer, B., Jacobs, T. & Breloer, M. (2012) Nematode-induced interference with the anti-*Plasmodium* CD8+ T-cell response can be overcome by optimizing antigen administration. *European journal of immunology* **42** (4), 890–900.

Krabbendam, L., Bal, S. M., Spits, H. & Golebski, K. (2018) New insights into the function, development, and plasticity of type 2 innate lymphoid cells. *Immunological Reviews* **286** (1), 74–85.

Kuehlwein, J. M., Borsche, M., Korir, P. J., Risch, F., Mueller, A.-K., Hübner, M. P., Hildner, K., Hoerauf, A., Dunay, I. R. & Schumak, B. (2020) Protection of Batf3-deficient mice from experimental cerebral malaria correlates with impaired cytotoxic T-cell responses and immune regulation. *Immunology* **159** (2), 193–204.

Kumar, V. (2020) Innate lymphoid cell and adaptive immune cell cross-talk: A talk meant not to forget. *Journal of leukocyte biology*.

Kurtzhals, J. A., Reimert, C. M., Tette, E., Dunyo, S. K., Koram, K. A., Akanmori, B. D., Nkrumah, F. K. & Hviid, L. (1998) Increased eosinophil activity in acute *Plasmodium falciparum* infection--association with cerebral malaria. *Clinical and experimental immunology* **112** (2), 303–307.

Layland, L. E., Ajendra, J., Ritter, M., Wiszniewsky, A., Hoerauf, A. & Hübner, M. P. (2015) Development of patent *Litomosoides sigmodontis* infections in semi-susceptible C57BL/6 mice in the absence of adaptive immune responses. *Parasites & vectors* **8**, 396.

Lee, A. J., Mian, F., Poznanski, S. M., Stackaruk, M., Chan, T., Chew, M. V. & Ashkar, A. A. (2019) Type I Interferon Receptor on NK Cells Negatively Regulates Interferon-γ Production. *Frontiers in Immunology* **10**.

Lee, J. J., Dimina, D., Macias, M. P., Ochkur, S. I., McGarry, M. P., O'Neill, K. R., Protheroe, C., Pero, R., Nguyen, T., Cormier, S. A., Lenkiewicz, E., Colbert, D., Rinaldi, L., Ackerman, S. J., Irvin, C. G. & Lee, N. A. (2004) Defining a link with asthma in mice congenitally deficient in eosinophils. *Science* **305** (5691), 1773–1776.

López, C., Yepes-Pérez, Y., Hincapié-Escobar, N., Díaz-Arévalo, D. & Patarroyo, M. A. (2017) What Is Known about the Immune Response Induced by *Plasmodium vivax* Malaria Vaccine Candidates? *Frontiers in Immunology* **8**, 126.

Löser, S., Smith, K. A. & Maizels, R. M. (2019) Innate Lymphoid Cells in Helminth Infections-Obligatory or Accessory? *Frontiers in Immunology* **10**, 620.

Mackenzie, C. D., Behan-Braman, A., Hauptman, J. & Geary, T. (2017) Assessing the Viability and Degeneration of the Medically Important Filarial Nematodes. In: Shah, M. M. & Mahamood, M. (eds.) *Nematology - Concepts, Diagnosis and Control*. InTech.

Maizels, R. M., Balic, A., Gomez-Escobar, N., Nair, M., Taylor, M. D. & Allen, J. E. (2004) Helminth parasites--masters of regulation. *Immunological Reviews* **201**, 89–116.

Maizels, R. M. & McSorley, H. J. (2016) Regulation of the host immune system by helminth parasites. *The Journal of allergy and clinical immunology* **138** (3), 666–675.

Mand, S., Büttner, D. W. & Hoerauf, A. (2008) Bancroftian filariasis--absence of *Wolbachia* after doxycycline treatment. *The American journal of tropical medicine and hygiene* **78** (6), 854–855.

Mand, S., Debrah, A. Y., Klarmann, U., Batsa, L., Marfo-Debrekyei, Y., Kwarteng, A., Specht, S., Belda-Domene, A., Fimmers, R., Taylor, M., Adjei, O. & Hoerauf, A. (2012) Doxycycline improves filarial lymphedema independent of active filarial infection: a randomized controlled trial. *Clinical infectious diseases an official publication of the Infectious Diseases Society of America* **55** (5), 621–630.

Martin, C., Le GOFF, L., Ungeheuer, M. N., Vuong, P. N. & BAIN, O. (2000) Drastic reduction of a filarial infection in eosinophilic interleukin-5 transgenic mice. *Infection and immunity* **68** (6), 3651–3656.

Mavoungou, E., Held, J., Mewono, L. & Kremsner, P. G. (2007) A Duffy binding-like domain is involved in the NKp30-mediated recognition of *Plasmodium falciparum*-parasitized erythrocytes by natural killer cells. *The Journal of infectious diseases* **195** (10), 1521–1531.

McNab, F., Mayer-Barber, K., Sher, A., Wack, A. & O'Garra, A. (2015) Type I interferons in infectious disease. *Nature Reviews Immunology* **15** (2), 87–103.

McSorley, H. J., Hewitson, J. P. & Maizels, R. M. (2013) Immunomodulation by helminth parasites: defining mechanisms and mediators. *International Journal for Parasitology* **43** (3-4), 301–310.

Meiners, J., Reitz, M., Rüdiger, N., Turner, J.-E., Heepmann, L., Rudolf, L., Hartmann, W., McSorley, H. J. & Breloer, M. (2020) IL-33 facilitates rapid expulsion of the parasitic nematode *Strongyloides ratti* from the intestine via ILC2- and IL-9-driven mast cell activation. *PLOS Pathogens* **16** (12), e1009121.

Mills, C. D., Kincaid, K., Alt, J. M., Heilman, M. J. & Hill, A. M. (2000) M-1/M-2 macrophages and the Th1/Th2 paradigm. *Journal of immunology (Baltimore, Md. 1950)* **164** (12), 6166–6173.

Mishra, S. K. & Newton, C. R. J. C. (2009) Diagnosis and management of the neurological complications of falciparum malaria. *Nature reviews. Neurology* **5** (4), 189–198.

Miu, J., Mitchell, A. J., Müller, M., Carter, S. L., Manders, P. M., McQuillan, J. A., Saunders, B. M., Ball, H. J., Lu, B., Campbell, I. L. & Hunt, N. H. (2008) Chemokine Gene Expression during Fatal Murine Cerebral Malaria and Protection Due to CXCR3 Deficiency. *The Journal of Immunology* (180(2)), 1217–1230.

Montes de Oca, M., Engwerda, C. & Haque, A. (2013) *Plasmodium berghei* ANKA (PbA) infection of C57BL/6J mice: a model of severe malaria. *Methods in molecular biology (Clifton, N.J.)* **1031**, 203–213.

Monticelli, L. A., Sonnenberg, G. F., Abt, M. C., Alenghat, T., Ziegler, C. G. K., Doering, T. A., Angelosanto, J. M., Laidlaw, B. J., Yang, C. Y., Sathaliyawala, T., Kubota, M., Turner, D., Diamond, J. M., Goldrath, A. W., Farber, D. L., Collman, R. G., Wherry, E. J. & Artis, D. (2011) Innate lymphoid cells promote lung-tissue homeostasis after infection with influenza virus. *Nature immunology* **12** (11), 1045–1054.

Muhsin, M., Ajendra, J., Gentil, K., Berbudi, A., Neumann, A.-L., Klaas, L., Schmidt, K. E., Hoerauf, A. & Hübner, M. P. (2018) IL-6 is required for protective immune responses against early filarial infection. *International Journal for Parasitology* **48** (12), 925–935.

Nagakumar, P., Denney, L., Fleming, L., Bush, A., Lloyd, C. M. & Saglani, S. (2016) Type 2 innate lymphoid cells in induced sputum from children with severe asthma. *The Journal of allergy and clinical immunology* **137** (2), 624-626.e6.

Neill, D. R. & Fallon, P. G. (2017) Innate lymphoid cells and parasites: ancient foes with shared history. *Parasite immunology*.

Ng, S. S. & Engwerda, C. R. (2018) Innate Lymphocytes and Malaria - Players or Spectators? *Trends in Parasitology*.

Ng, S. S., Souza-Fonseca-Guimaraes, F. & Rivera, F. d. L. et al. (2018) Rapid loss of group 1 innate lymphoid cells during blood stage *Plasmodium* infection. *Clinical & translational immunology* **7** (1), e1003.

Nishikado, H., Mukai, K., Kawano, Y., Minegishi, Y. & Karasuyama, H. (2011) NK cell-depleting anti-asialo GM1 antibody exhibits a lethal off-target effect on basophils in vivo. *Journal of immunology (Baltimore, Md. 1950)* **186** (10), 5766–5771.

Nitcheu, J., Bonduelle, O., Combadiere, C., Tefit, M., Seilhean, D., Mazier, D. & Combadiere, B. (2003) Perforin-dependent brain-infiltrating cytotoxic CD8+ T lymphocytes mediate experimental cerebral malaria pathogenesis. *Journal of immunology (Baltimore, Md. 1950)* (170(4)), 2221–2228.

Nutman, T. B., Kumaraswami, V. & Ottesen, E. A. (1987) Parasite-specific anergy in human filariasis. Insights after analysis of parasite antigen-driven lymphokine production. *Journal of Clinical Investigation* **79** (5), 1516–1523.

Oakley, M. S., Sahu, B. R., Lotspeich-Cole, L., Solanki, N. R., Majam, V., Pham, P. T., Banerjee, R., Kozakai, Y., Derrick, S. C., Kumar, S. & Morris, S. L. (2013) The transcription factor T-bet regulates parasitemia and promotes pathogenesis during *Plasmodium berghei* ANKA murine malaria. *Journal of immunology (Baltimore, Md. 1950)* **191** (9), 4699–4708.

Oliphant, C. J., Hwang, Y. Y., Walker, J. A., Salimi, M., Wong, S. H., Brewer, J. M., Englezakis, A., Barlow, J. L., Hams, E., Scanlon, S. T., Ogg, G. S., Fallon, P. G. & McKenzie, A. N. J. (2014) MHCII-mediated dialog between group 2 innate lymphoid cells and CD4(+) T cells potentiates type 2 immunity and promotes parasitic helminth expulsion. *Immunity* **41** (2), 283–295.

Ortego, J., La Poza, F. de & Marín-López, A. (2014) Interferon α/β receptor knockout mice as a model to study bluetongue virus infection. *Virus research* **182**, 35–42.

Palomo, J., Fauconnier, M., Coquard, L., Gilles, M., Meme, S., Szeremeta, F., Fick, L., Franetich, J.-F., Jacobs, M., Togbe, D., Beloeil, J.-C., Mazier, D., Ryffel, B. & Quesniaux, V. F. J. (2013) Type I interferons contribute to experimental cerebral malaria development in response to sporozoite or blood-stage *Plasmodium berghei* ANKA. *European journal of immunology* (43(10)), 2683–2695.

Palomo, J., Quesniaux, V., Togbe, D., Reverchon, F. & Ryffel, B. (2017) Unravelling the Roles of Innate Lymphoid Cells in Cerebral Malaria Pathogenesis. *Parasite immunology*.

Palomo, J., Reverchon, F., Piotet, J., Besnard, A.-G., Couturier-Maillard, A., Maillet, I., Tefit, M., Erard, F., Mazier, D., Ryffel, B. & Quesniaux, V. F. J. (2015) Critical role of IL-33 receptor ST2 in experimental cerebral malaria development. *European journal of immunology* **45** (5), 1354–1365.

Pasternak, N. D. & Dzikowski, R. (2009) PfEMP1: an antigen that plays a key role in the pathogenicity and immune evasion of the malaria parasite *Plasmodium falciparum*. *The International Journal of Biochemistry & Cell Biology* **41** (7), 1463–1466.

PATH's Malaria Vaccine Initiative (2015) Life cycle of the malaria parasite. https://www.malariavaccine.org/malaria-and-vaccines/vaccine-development/life-cycle-malaria-parasite. Accessed 1/20/2021.

R&D Systems (2017) Mouse CCL5/RANTES DuoSet ELISA. https://www.rndsystems.com/products/mouse-ccl5-rantes-duoset-elisa_dy478. Accessed 8/23/2017.

Rénia, L., Howland, S. W., Claser, C., Charlotte Gruner, A., Suwanarusk, R., Hui Teo, T., Russell, B. & Ng, L. F. P. (2012) Cerebral malaria: Mysteries at the blood-brain barrier. *Virulence* **3** (2), 193–201.

Riggle, B. A., Manglani, M., Maric, D., Johnson, K. R., Lee, M.-H., Neto, O. L. A., Taylor, T. E., Seydel, K. B., Nath, A., Miller, L. H., McGavern, D. B. & Pierce, S. K. (2020) CD8+ T cells target cerebrovasculature in children with cerebral malaria. *The Journal of clinical investigation* **130** (3), 1128–1138.

Risch, F., Ritter, M., Hoerauf, A. & Hübner, M. P. (2021) Human filariasis-contributions of the *Litomosoides sigmodontis* and *Acanthocheilonema viteae* animal model. *Parasitology research*.

Roland, J., Soulard, V., Sellier, C., Drapier, A.-M., Di Santo, J. P., Cazenave, P.-A. & Pied, S. (2006) NK cell responses to *Plasmodium* infection and control of intrahepatic parasite development. *Journal of immunology (Baltimore, Md. 1950)* **177** (2), 1229–1239.

Romero-Suárez, S., Del Rio Serrato, A., Bueno, R. J., Brunotte-Strecker, D., Stehle, C., Figueiredo, C. A., Hertwig, L., Dunay, I. R., Romagnani, C. & Infante-Duarte, C. (2019) The Central Nervous System Contains ILC1s That Differ From NK Cells in the Response to Inflammation. *Frontiers in Immunology* **10**, 2337.

Rosenberg, H. F., Dyer, K. D. & Foster, P. S. (2013) Eosinophils: changing perspectives in health and disease. *Nature Reviews Immunology* **13** (1), 9–22.

Rouse, B. T. & Sehrawat, S. (2010) Immunity and immunopathology to viruses: what decides the outcome? *Nature Reviews Immunology* **10** (7), 514–526.

Rudin, W., Favre, N., Bordmann, G. & Ryffel, B. (1997) Interferon-gamma is essential for the development of cerebral malaria. *European journal of immunology* (27(4)), 810–815.

Saint André, A. v., Blackwell, N. M., Hall, L. R., Hoerauf, A., Brattig, N. W., Volkmann, L., Taylor, M. J., Ford, L., Hise, A. G., Lass, J. H., Diaconu, E. & Pearlman, E. (2002) The role of endosymbiotic *Wolbachia* bacteria in the pathogenesis of river blindness. *Science* **295** (5561), 1892–1895.

Sarkar, S. & Bhattacharya, P. (2008) Cerebral malaria caused by *Plasmodium vivax* in adult subjects. *Indian journal of critical care medicine peer-reviewed, official publication of Indian Society of Critical Care Medicine* **12** (4), 204–205.

Sasaki, T., Onodera, A., Hosokawa, H., Watanabe, Y., Horiuchi, S., Yamashita, J., Tanaka, H., Ogawa, Y., Suzuki, Y. & Nakayama, T. (2013) Genome-Wide Gene Expression Profiling Revealed a Critical Role for GATA3 in the Maintenance of the Th2 Cell Identity. *PloS one* **8** (6), e66468.

Schiess, N., Villabona-Rueda, A., Cottier, K. E., Huether, K., Chipeta, J. & Stins, M. F. (2020) Pathophysiology and neurologic sequelae of cerebral malaria. *Malaria Journal* **19** (1), 266.

Schofield, L. & Grau, G. E. (2005) Immunological processes in malaria pathogenesis. *Nature reviews. Immunology* **5** (9), 722–735.

Schumak, B., Klocke, K., Kuepper, J. M., Biswas, A., Djie-Maletz, A., Limmer, A., van Rooijen, N., Mack, M., Hoerauf, A. & Dunay, I. R. (2015) Specific depletion of Ly6C(hi) inflammatory monocytes prevents immunopathology in experimental cerebral malaria. *PloS one* **10** (4), e0124080.

Sebina, I. & Haque, A. (2018) Effects of type I interferons in malaria. *Immunology* **155** (2), 176–185.

Sebina, I., James, K. R., Soon, M. S. F., Fogg, L. G., Best, S. E., Labastida Rivera, F. de, Montes de Oca, M., Amante, F. H., Thomas, B. S., Beattie, L., Souza-Fonseca-Guimaraes, F., Smyth, M. J., Hertzog, P. J., Hill, G. R., Hutloff, A., Engwerda, C. R. & Haque, A. (2016) IFNAR1-Signalling Obstructs ICOS-mediated Humoral Immunity during Non-lethal Blood-Stage Plasmodium Infection. *PLOS Pathogens* **12** (11), e1005999.

Serafini, N., Vosshenrich, C. A. J. & Di Santo, J. P. (2015) Transcriptional regulation of innate lymphoid cell fate. *Nature reviews. Immunology* **15** (7), 415–428.

Sharma, S., DeOliveira, R. B., Kalantari, P., Parroche, P., Goutagny, N., Jiang, Z., Chan, J., Bartholomeu, D. C., Lauw, F., Hall, J. P., Barber, G. N., Gazzinelli, R. T., Fitzgerald, K. A. & Golenbock, D. T. (2011) Innate immune recognition of an AT-rich stem-loop DNA motif in the Plasmodium falciparum genome. *Immunity* (35(2)), 194–207.

Sierro, F. & Grau, G. E. R. (2019) The Ins and Outs of Cerebral Malaria Pathogenesis: Immunopathology, Extracellular Vesicles, Immunometabolism, and Trained Immunity. *Frontiers in Immunology* **10**, 830.

Simonsen, P. E., Fischer, P. U., Hoerauf, A. & Weil, G. J. (2013) The Filariases. *Manson's Tropical Diseases: Twenty-Third Edition*, 737-765.e5.

Specht, S., Ruiz, D. F., Dubben, B., Deininger, S. & Hoerauf, A. (2010) Filaria-induced IL-10 suppresses murine cerebral malaria. *Microbes and Infection* **12** (8-9), 635–642.

Specht, S., Taylor, M. D., Hoeve, M. A., Allen, J. E., Lang, R. & Hoerauf, A. (2012) Over expression of IL-10 by macrophages overcomes resistance to murine filariasis. *Experimental parasitology* **132** (1), 90–96.

Spits, H., Artis, D., Colonna, M., Diefenbach, A., Di Santo, J. P., Eberl, G., Koyasu, S., Locksley, R. M., McKenzie, A. N. J., Mebius, R. E., Powrie, F. & Vivier, E. (2013) Innate lymphoid cells--a proposal for uniform nomenclature. *Nature reviews. Immunology* **13** (2), 145–149.

STEMCELL Technologies Inc. (2020) EasySep™ Mouse NK Cell Isolation Kit. https://www.stemcell.com/easysep-mouse-nk-cell-isolation-kit.html. Accessed 9/23/2020.

Stier, M. T., Zhang, J., Goleniewska, K., Cephus, J. Y., Rusznak, M., Wu, L., van Kaer, L., Zhou, B., Newcomb, D. C. & Peebles, R. S. (2018) IL-33 promotes the egress of group 2 innate lymphoid cells from the bone marrow. *The Journal of Experimental Medicine* **215** (1), 263–281.

Swanson, P. A., Hart, G. T., Russo, M. V., Nayak, D., Yazew, T., Peña, M., Khan, S. M., Janse, C. J., Pierce, S. K. & McGavern, D. B. (2016) CD8+ T Cells Induce Fatal Brainstem Pathology during Cerebral Malaria via Luminal Antigen-Specific Engagement of Brain Vasculature. *PLOS Pathogens* **12** (12), e1006022.

Symowski, C. & Voehringer, D. (2017) Interactions between Innate Lymphoid Cells and Cells of the Innate and Adaptive Immune System. *Frontiers in Immunology* **8**, 1422.

Tamarozzi, F., Halliday, A., Gentil, K., Hoerauf, A., Pearlman, E. & Taylor, M. J. (2011) Onchocerciasis: the role of Wolbachia bacterial endosymbionts in parasite biology, disease pathogenesis, and treatment. *Clinical Microbiology Reviews* **24** (3), 459–468.

Taylor, M. D., Harris, A., Nair, M. G., Maizels, R. M. & Allen, J. E. (2006) F4/80+ alternatively activated macrophages control CD4+ T cell hyporesponsiveness at sites peripheral to filarial infection. *Journal of immunology (Baltimore, Md. 1950)* **176** (11), 6918–6927.

Taylor, M. D., van der Werf, N., Harris, A., Graham, A. L., Bain, O., Allen, J. E. & Maizels, R. M. (2009) Early recruitment of natural CD4+ Foxp3+ Treg cells by infective larvae determines the outcome of filarial infection. *European journal of immunology* **39** (1), 192–206.

Taylor, M. D., van der Werf, N. & Maizels, R. M. (2012) T cells in helminth infection: the regulators and the regulated. *Trends in immunology* **33** (4), 181–189.

Taylor, M. J., Hoerauf, A. & Bockarie, M. (2010) Lymphatic filariasis and onchocerciasis. *The Lancet* **376** (9747), 1175–1185.

The Jackson Laboratory (2018) B6C3Fe a/a-Rorα ko - staggerer. https://www.jax.org/strain/000237. Accessed 2/16/2018.

The Jackson Laboratory (2021) B6.Cg-Rag2<tm1.1Cgn>/J. https://www.jax.org/strain/008449. Accessed 4/22/2021.

Twum-Danso, N. A. Y. (2003) *Loa loa* encephalopathy temporally related to ivermectin administration reported from onchocerciasis mass treatment programs from 1989 to 2001: implications for the future. *Filaria Journal* **2 Suppl 1** (Suppl 1), S7.

Vigário, A. M., Belnoue, E., Cumano, A., Marussig, M., Miltgen, F., Landau, I., Mazier, D., Gresser, I. & Rénia, L. (2001) Inhibition of *Plasmodium yoelii* blood-stage malaria by interferon alpha through the inhibition of the production of its target cell, the reticulocyte. *Blood* **97** (12), 3966–3971.

Villegas-Mendez, A., Strangward, P., Shaw, T. N., Rajkovic, I., Tosevski, V., Forman, R., Muller, W. & Couper, K. N. (2017) Gamma Interferon Mediates Experimental Cerebral Malaria by Signaling within Both the Hematopoietic and Nonhematopoietic Compartments. *Infection and Immunity* **85** (11).

Vivier, E., Artis, D., Colonna, M., Diefenbach, A., Di Santo, J. P., Eberl, G., Koyasu, S., Locksley, R. M., McKenzie, A. N. J., Mebius, R. E., Powrie, F. & Spits, H. (2018) Innate Lymphoid Cells: 10 Years On. *Cell* **174** (5), 1054–1066.

Volkmann, L., Bain, O., Saeftel, M., Specht, S., Fischer, K., Brombacher, F., Matthaei, K. I. & Hoerauf, A. (2003) Murine filariasis: interleukin 4 and interleukin 5 lead to containment of different worm developmental stages. *Medical microbiology and immunology* **192** (1), 23–31.

Walzer, T. & Vivier, E. (2011) G-protein-coupled receptors in control of natural killer cell migration. *Trends in immunology* **32** (10), 486–492.

Whiteside, T. L. (1994) Cytokines and cytokine measurements in a clinical laboratory. *Clinical and Diagnostic Laboratory Immunology* **1** (3), 257–260.

Wilhelm, C., Harrison, O. J., Schmitt, V., Pelletier, M., Spencer, S. P., Urban, J. F., Ploch, M., Ramalingam, T. R., Siegel, R. M. & Belkaid, Y. (2016) Critical role of fatty acid metabolism in ILC2-mediated barrier protection during malnutrition and helminth infection. *The Journal of Experimental Medicine* **213** (8), 1409–1418.

Willinger, T. (2019) Metabolic Control of Innate Lymphoid Cell Migration. *Frontiers in Immunology* **10**, 2010.

World Health Organization (2000) Severe falciparum malaria. World Health Organization, Communicable Diseases Cluster. *Transactions of the Royal Society of Tropical Medicine and Hygiene* **94 Suppl 1**, S1-90.

World Health Organization (2015) *Global technical strategy for malaria, 2016-2030*. Global Malaria Programme, World Health Organization, Geneva, Switzerland.

World Health Organization (2017) *Guideline – Alternative mass drug administration regimens to eliminate lymphatic filariasis*. WORLD HEALTH ORGANIZATION, Geneva.

World Health Organization (2019) *WORLD MALARIA REPORT 2019*. WORLD HEALTH ORGANIZATION, [S.l.].

World Health Organization (2020a) Fact sheet about Malaria. https://www.who.int/news-room/fact-sheets/detail/malaria. Accessed 1/20/2021.

World Health Organization (2020b) Top 10 causes of death. https://www.who.int/gho/mortality_burden_disease/causes_death/top_10/en/. Accessed 7/17/2020.

World Health Organization (2021a) Epidemiology. https://www.who.int/lymphatic_filariasis/epidemiology/en/. Accessed 9/22/2020.

World Health Organization (2021b) Global Programme to Eliminate Lymphatic Filariasis. https://www.who.int/lymphatic_filariasis/elimination-programme/en/. Accessed 2/3/2021.

World Health Organization (2021c) Lymphatic filariasis. https://www.who.int/news-room/fact-sheets/detail/lymphatic-filariasis. Accessed 2/3/2021.

World Health Organization (2021d) Onchocerciasis (river blindness). https://www.who.int/news-room/fact-sheets/detail/onchocerciasis. Accessed 2/3/2021.

Yañez, D. M., Manning, D. D., Cooley, A. J., Weidanz, W. P. & van der Heyde, H. C. (1996) Participation of lymphocyte subpopulations in the pathogenesis of experimental murine cerebral malaria. *Journal of immunology (Baltimore, Md. 1950)* **157** (4), 1620–1624.

Yasuda, K. & Kuroda, E. (2019) Role of eosinophils in protective immunity against secondary nematode infections. *Immunological medicine*, 1–8.

Yasuda, K., Muto, T., Kawagoe, T., Matsumoto, M., Sasaki, Y., Matsushita, K., Taki, Y., Futatsugi-Yumikura, S., Tsutsui, H., Ishii, K. J., Yoshimoto, T., Akira, S. & Nakanishi, K. (2012) Contribution of IL-33-activated type II innate lymphoid cells to pulmonary eosinophilia in intestinal nematode-infected mice. *Proceedings of the National Academy of Sciences* **109** (9), 3451–3456.

Zaiss, D. M., Yang, L., Shah, P. R., Kobie, J. J., Urban, J. F. & Mosmann, T. R. (2006) Amphiregulin, a TH2 cytokine enhancing resistance to nematodes. *Science* **314** (5806), 1746.

Zaiss, D. M. W., Gause, W. C., Osborne, L. C. & Artis, D. (2015) Emerging functions of amphiregulin in orchestrating immunity, inflammation, and tissue repair. *Immunity* **42** (2), 216–226.

Zhong, C., Cui, K., Wilhelm, C., Hu, G., Mao, K., Belkaid, Y., Zhao, K. & Zhu, J. (2016) Group 3 innate lymphoid cells continuously require the transcription factor GATA-3 after commitment. *Nature immunology* **17** (2), 169–178.

Scientific Contributions

Published Paper during PhD

A. Ehrens, B. Lenz, AL. Neumann, S. Giarrizzo, **J. J. Reichwald**, S. J. Frohberger, W. Stamminger, B. C. Buerfent, F. Fercoq, C. Martin, D. Kulke, A. Hoerauf and M. P. Huebner. **Microfilariae trigger eosinophil extracellular DNA traps in a Dectin-1-dependent manner.** – *Cell Reports (2021)*

Submitted

J. F. Scheunemann, **J. J. Reichwald,** P. J. Korir, J. M. Kuehlwein, LM. Jenster, C. Hammerschmidt-Kamper, M. D. Lewis, K. Klocke, M. P. Borsche, K. E. Schmidt, C. Soun, S. Thiebes, A. Limmer, D. Engel, AK. Mueller, A. Hoerauf, M. P. Hübner, B. Schumak. **Eosinophils suppress the migration of T cells into the brain of *Plasmodium berghei*-infected *Ifnar1*$^{-/-}$ mice and protect them from experimental cerebral malaria**. *(submitted 2021)*

Under preparation

J. J. Reichwald, AL. Neumann, F. Risch, S. J. Frohberger, J. F. Scheunemann, A. Ehrens, W. Strutz, A. Hörauf, B. Schumak, M. P. Hübner**. ILC2s control microfilaremia during *Litomosoides sigmodontis* infection**.

Acknowledgements

First of all, I would like to thank the director of our institute, Prof. Dr. Achim Hörauf, for the opportunity to do my PhD thesis at the Institute of Medical Microbiology, Immunology and Parasitology at the University Hospital Bonn.

My thanks also go to Prof. Dr. Sven Burgdorf for agreeing to be my second supervisor and to PD Dr. Gerhild van Echten-Deckert and Prof. Dr. Ulrike Thoma for their willingness for joining the examination committee board.

Many thanks go to Prof. Dr. Marc P. Hübner, who accepted me halfway through my doctoral thesis in his research group and has supervised me excellently ever since. He always had an open ear also and gave me the feeling that I was doing a good job. He was always available for the discussion of my results and provided suggestions for further analyses as well as helpful and fast feedback concerning any kind of writing tasks.

I would also like to thank Dr. Beatrix Schumak for supervising me so wonderfully during my master thesis, her good advices and for giving me the opportunity to continue with my PhD thesis in her group afterwards. Even after she left the institute, she was always available and could be relied on for feedback and ideas.

I would further like to thank Johanna Scheunemann, with whom I carried out the many malaria experiments together and from which a joint publication resulted. Thanks to the perfect collaboration with her, the long lab days were only half as bad and we always had fun and pleasure working together. For me, she has become an important support in the daily laboratory and office routine, with whom I had a lot of fun and funny evenings away from work. I would also like to thank Frederic Risch, who helped me with my *L. sigmodontis* experiments, especially with the infections, and who was always available for a spontaneous discussion about my latest data. He also provided an entertaining working atmosphere with his funny jokes. Furthermore, I would like to thank all the other members of the group who were always helpful, critically discussed my data with me, supported me especially in the daily tasks in the animal house and made sure that the fun was not neglected. Therefore, special thanks go to Dr. Alexandra Ehrens, Dr. Indulekha Karunakaran, Dr. Stefan J. Frohberger, Anna-Lena Neumann, Benjamin Lenz, Marianne Koschel, Martina Fendler and Wiebke Strutz. Thank you for the wonderful time!

I would also like to thank all the other members of the Institute (AG Layland/Ritter, AG Pfarr and AG Adjobimey) for the very positive working atmosphere, the support when sometimes one or the other antibody was missing, the collaborations and the live discussions during our seminars. I also want to thank the secretary of the institute.

Special thanks also go to the Jürgen Manchot Foundation, which supported me for 3 years with a PhD scholarship.

Finally, my special thanks go to my family, first of all to my loving husband Pascal, who was always by my side during all these years, encouraged me to continue on my way to the PhD, picked me up from the institute even at night and provided me with a warm meal afterwards despite the late hour. He was a huge support on difficult days and has also ensured that a successful day was celebrated. I would also like to thank my parents and my siblings, who supported me in every way and also always believed that I would succeed on this path.